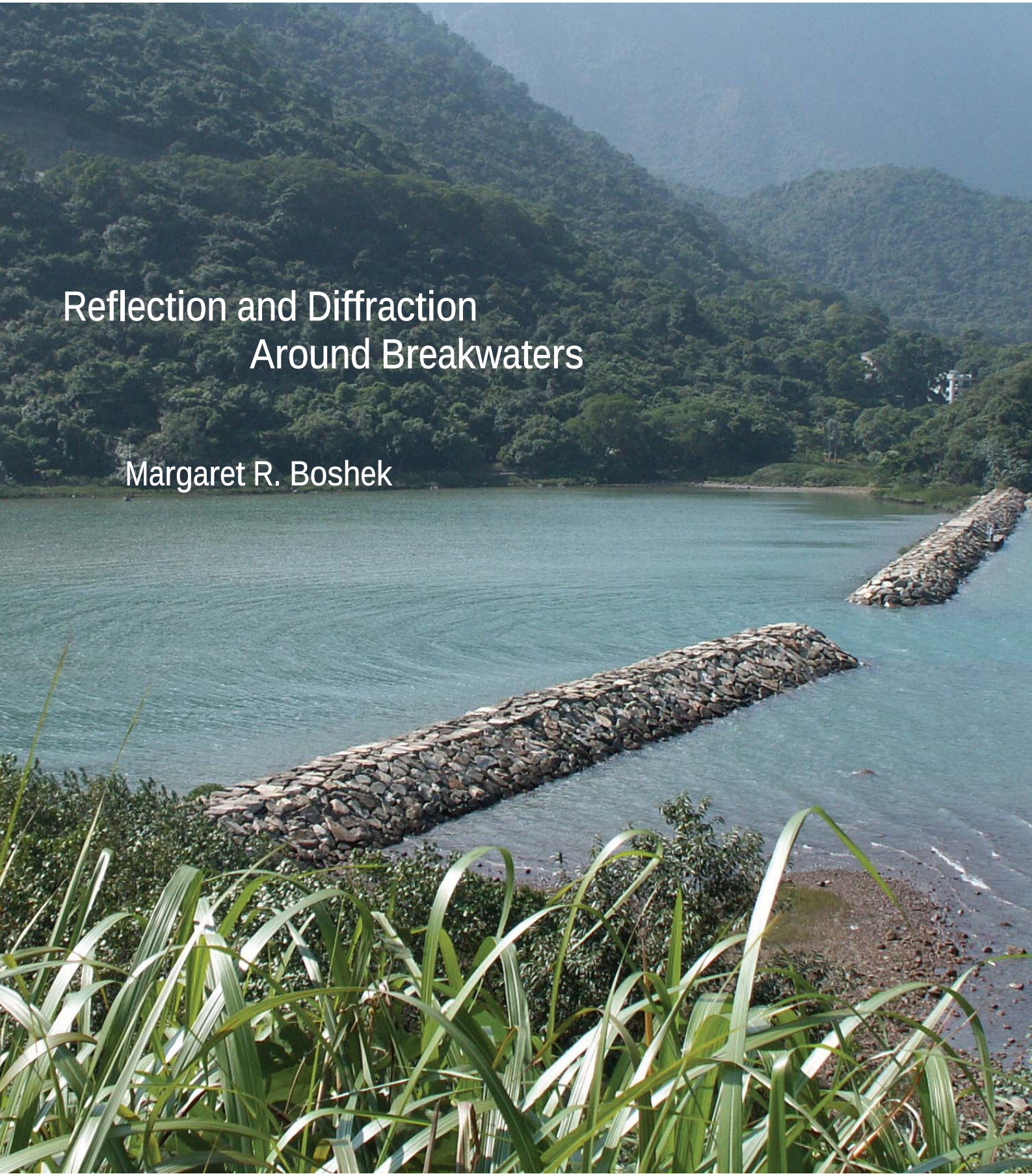

Reflection and Diffraction Around Breakwaters

Margaret R. Boshek

CoMEM

Faculty of Civil Engineering and Geosciences

TU Delft

Delft University of Technology

Preface

This thesis concludes the Master of Science curriculum of the CoMEM program of the Faculty of Civil Engineering and Geosciences at Delft University of Technology, The Netherlands.

I would like to thank the members of my graduation committee for their comments and suggestions over the course of this study. Their insight has been invaluable to my understanding and education. Individually, I would like to thank: Marcel J.F. Stive for being the most positive and upbeat member of my team. His confidence in my work helped me get over my doubts; Henk Jan Verhagen for being one of the most amazingly smart and helpful people I know and responding to all my emails no matter how late at night I send them; Gerbrant van Vledder for putting up with my sometimes circular questions and being my SWAN guru; and Judith van Os for getting me on the right path with PHAROS while making every aspect easy to understand and for giving up some of her free time to be on my committee.

Furthermore, I would like to thank Marcel Zijlema for stepping in as SWAN guru when Gerbrant wasn't available. Lenie Wasmus for being a fantastic cheerleader and occasional slave driver. Inge and Chantel for fearlessly navigating multiple schedules and still finding time to fit me in. My fellow CoMEM partners, Chris, Sid, and Andi for the lunches, coffee breaks, and friendship that kept me sane. The people of the CoMEM and Erasmus Mundus programs for making these past two years of phenomenal education possible. And of course Sanne for helping me out when I needed it most and being supportive every minute of every day.

Finally, I would like to thank my friends and family for their support.

Margaret R. Boshek
June 2009

Reflection and Diffraction Around Breakwaters

Margaret R. Boshek

Faculty of Civil Engineering and Geosciences
Delft University of Technology, Delft, The Netherlands

June 2009

Prof. dr. ir. M.J.F. Stive – Coastal Engineering, TUDelft
Ir. Henk Jan Verhagen – Coastal Engineering, TUDelft
Dr. ir. G.P. van Vledder – Fluid Mechanics, TUDelft
Ir. J. Van Os – Deltares

Abstract

Diffraction diagrams are frequently utilized by engineers within the feasibility and early design phases of a project. These helpful graphics, based on directional spreading and wavelength, can be used for a number of layouts and angles of incidence. In spite of the tendency to design breakwaters for the fullest dissipation of wave energy, current diffraction diagrams in use are for full reflection. They have a very strict view of the breakwaters themselves; solely an infinitely thin, fully reflecting, vertical breakwater without any transmission or overtopping. This study focuses on the changes to the diffraction patterns once construction aspects related to breakwater reflection are considered.

The alteration to diffraction coefficients due to wave spectra variations, both directional and frequency, is examined through the use of theory and advanced modeling systems. It is found that the directional spectrum causes large changes while frequency variation is negligible. This primary driving component is than related to breakwater layout and incident angles.

A study of literature related to breakwater reflection is used in advanced computer models to determine where and how much this characteristic contributes to the diffraction pattern. Two separate types of models, phase-resolving and phase-averaging, are used to test breakwater reflection in diffraction modeling. This comparison confirms theoretical assumptions, finds possible faults in current diffraction diagrams, and creates new questions about breakwater tip physics.

The full analysis shows that breakwater reflectivity causes little change to the diffraction pattern beyond the area closest to the breakwater. The areas of greatest influence are located at the breakwater tips, which can be associated with reflection off the breakwater's front face, and along the leeside of the breakwater, which can be attributed to the absorption of the leeside's reduced reflectivity. Therefore, the need for new, updated diffraction diagrams based on reflectivity is unnecessary.

As a secondary objective of this study, the usefulness of using the SWAN modeling program for diffraction studies was examined. This topic is of importance as SWAN is an efficient alternative to more computationally intensive modeling programs. In addition, it is a free software which is universally available. Believed to be incapable of computing rapidly changing wave environments near breakwaters or in harbor situations, SWAN performed diffraction remarkably well for broad directional waves. More narrow directionally spread waves had good accuracy throughout with only minor scaling differences. SWAN, within this study, was unable to replicate the effects of reflection on both sides of a breakwater and therefore was not used for the primary objective.

TABLE OF CONTENTS

Abstract……i
Table of Contents……ii
List of Tables……iv
List of Figures……v

PART I: INTRODUCTION

Chapter 1. Introduction 2
1.1. Problem Description 2
1.2. Objectives 3
1.3. Problem Approach 3

PART II: DIFFRACTION

Chapter 2. Diffraction Theory 6
2.1. Theoretical Background 6
2.2. Spatial Variation due to Reflective Structures 7
2.3. Additional Driving Forces of Diffraction 12
2.3.1. Wave Characteristics 13
2.3.1.1. Regular vs. Irregular 13
2.3.1.2. Directional and Frequency Spectrums 14
2.3.2. Construction Aspects 14
2.3.2.1. Layout 15
2.3.2.2. Wave Diffraction of Oblique Incidence 17
2.3.2.3. Transmission 18

Chapter 3. Diffraction Diagrams 20
3.1. Application for Design 22

PART III: MODELING

Chapter 4. Models 24
4.1. Phase-Resolving vs. Phase-Averaged 24
4.2. Universal Model Setup 25
4.2.1. Wave Characterization 25
4.2.2. Universal Model Inputs 26
4.2.3. Model Grid 27
4.3. Reference Cases 27

Chapter 5. PHAROS 28
5.1. Model Setup 28
5.1.1. Layout 28
5.1.2. Wave Characteristics 29
5.1.3. PHAROS Limitations to Study 31
5.2. Interpretation of Model Results 32
5.2.1. Reflection Effects 33
5.2.2. Composite Breakwaters 34

5.2.3. Angle of incidence 36
5.2.4. Directional and Frequency Spreading 37
5.2.5. Gap Entrance Amplification 39
5.2.6. Large Gaps 39
5.2.7. Breakwater Tip Effects 40
5.3. Model Evaluation 41

Chapter 6. SWAN 42
6.1. Model Inputs 42
6.1.1. Layout 43
6.1.2. Wave Characteristics 44
6.2. Sensitivity Analysis of Grid and Model Conditions 44
6.2.1. Directional Resolution 45
6.2.2. Spatial Resolution 46
6.2.3. Computational Area 47
6.2.4. Smoothing 47
6.2.5. Diffraction & Obstacle Reflection 48
6.2.6. Final Model Setup 50
6.3. SWAN Limitations to Study 50
6.4. Interpretation of SWAN Reflection 51
6.5. Model Evaluation 53

Chapter 7. Comparison of Theory and Model Results 54
7.1. Regular Wave Theory 54
7.2. Irregular Wave Theory 56
7.2.1. Comparison between PHAROS and SWAN 56
7.2.2. Comparison of Diffraction Coefficients 59
7.2.2.1. PHAROS Comparison to Theory 61
7.2.2.2. SWAN Comparison to Theory 61

PART IV: CONCLUSIONS & RECOMMENDATIONS

Chapter 8. Modeling Conclusions 64

Chapter 9. Importance of the Reflection Coefficient 66

Chapter 10. Application and Relevance 66

Chapter 11. Recommendations 67

REFERENCES 68

APPENDIX A: Sommerfeld Solution for Wave Diffraction
APPENDIX B: Select Wiegel Diffraction Diagrams, 1962
APPENDIX C: Goda Diffraction Diagrams, 1978
APPENDIX D: PHAROS Model Results
APPENDIX E: SWAN Model Results
APPENDIX F: SWAN Input File

List of Tables:

Table 2-1: Deviation angle of diffracted waves through a breakwater gap for obliquely incident waves (Goda, 2000) *18*
Table 4-1: Wave Characterization within Models *26*
Table 4-2: Standard modeling Inputs *26*
Table 5-1: PHAROS Model Inputs *31*
Table 6-1: SWAN Wave Characteristics Inputs *44*
Table 6-2: SWAN Final Layout Inputs *50*

List of Figures:

Figure 2-1: Wave passing through a slit and bending into the shadow zone 6
Figure 2-2: Definition sketch for Sommerfeld Solution (Daemrich, 1978)..... 7
Figure 2-3: Partial wave fields according to Sommerfeld solution (Daemrich, 1978) .. 8
Figure 2-4: Tip diffraction definition sketch (Silvester, 1968) 9
Figure 2-5: K for all incident angles with or without reflection (Silvester, 1968) 10
Figure 2-6: Definition Sketch for Mitsui Solution 11
Figure 2-7: Comparison of Diffraction Coefficient K' for Multiple Theories (Daemrich, 1978)..... 11
Figure 2-8: Weighting Factor F_r for second term of Sommerfeld solution for various degrees of reflection (Daemrich, 1978) 12
Figure 2-9: Breakwater Gap Diffraction..... 16
Figure 2-10: Determining Effective Gap Width, B'..... 17
Figure 2-11: Effective Gap Width due to Oblique Angle Deviation 18
Figure 3-1: Diffraction diagram of regular wave at a 90° angle (Wiegel, 1962)..... 20
Figure 3-2: Diffraction diagrams of irregular waves at a breakwater gap, B/L = 2 (Goda, 1978)..... 21
Figure 3-3: Comparison of Regular and Irregular Wave Diffraction..... 22
Figure 4-1: Wrapped Normal and Mitsuyasu Directional Spreading Functions (Briggs, 1995)..... 26
Figure 5-1: Direction Spreading Representation In PHAROS..... 30
Figure 5-2: Cumulative Jonswap Spectrum in PHAROS 31
Figure 5-3: PHAROS model Layouts and Boundary Conditions..... 32
Figure 5-4: Portion of Diffraction Coefficient, K', attributed to Reflection..... 34
Figure 5-5: Effects related to non-uniform breakwaters, Swell Waves 35
Figure 5-6: Effects related to non-uniform breakwaters, Wind Waves..... 36
Figure 5-7: Oblique Angle influence on Reflective Effects..... 37
Figure 5-8: Effect of directional spreading..... 38
Figure 5-9: Effect of frequency spreading 38
Figure 5-10: Diffraction of B/L = 8 for Broad Spectrum Waves (wind type)..... 40
Figure 5-11: Breakwater Tip Enhancement..... 40
Figure 6-1: SWAN model Layouts and Boundary Conditions 43
Figure 6-2: Directional Resolution Comparison in SWAN..... 46
Figure 6-3: Spatial Resolution Check, Swell waves..... 47
Figure 6-4: Use of Smoothing..... 47
Figure 6-5: Study of Reflection within SWAN..... 49
Figure 6-6: Instability of Small Gap Sizes Within SWAN 51
Figure 6-7: Difference of wave height due to reflection coefficients in SWAN..... 52
Figure 7-1: PHAROS vs. Regular Wave Theory: Semi-infinite Breakwater..... 55
Figure 7-2: PHAROS vs. Regular Wave Theory: Breakwater Gap B/L=2 56
Figure 7-3: Wave Build-up in Gap Diffraction..... 57
Figure 7-4: Comparison between SWAN & PHAROS model outputs..... 58
Figure 7-5: Diffraction Diagrams for Various Methods, Breakwater Gap B/L = 2 59
Figure 7-6: Diffraction Diagrams for Various Methods, Semi-Infinite Breakwater 60

PART I: Introduction

Chapter 1. Introduction

Wave diffraction is the phenomenon in which water waves bend around objects and propagate into a sheltered area at a different angle than the original wave train. This action is of high concern to designers of ports and harbors whom use breakwaters as barriers to protect the interior from damaging wave energy. Diffraction is also of interest to engineers designing shore stabilization systems in how they will affect the sediment transport. By understanding the mechanics of wave diffraction, a designer can properly prevent diffracted wave energy from causing significant agitation within the shadow zone.

Wave diffraction has been of interest for a number of years. Sommerfeld's solution, based on optics, was shown to also apply to water waves by Penny & Price (1952). This paper ignited many studies into the characteristics of diffraction when applied to the tumultuous ocean. An inventory of theses papers and their findings prove that diffraction is sensitive to a number of variables. However, by knowing key characteristics that most highly affect diffraction, one can define, within a degree of accuracy, the general diffraction pattern one can expect.

1.1. Problem Description

Preliminary research has suggested that previous studies into wave diffraction have assumed a perfect, reflective breakwater. More typical situations in the design and construction of ports and harbors utilize energy absorbing materials, such as rubble or armor units to avoid enhanced turbulence close to the breakwaters. This is even more prevalent for harbor entrances where boater safety is a concern.

It is theorized that the amount of reflection from the structure directly affects how much energy is diffracted around the tip of the breakwater into the shadow zone. This means that current diffraction diagrams, which are based off a fully reflective breakwater, are conservative in their predictions when applied to an partially absorbent breakwater.

The only way to properly define a diffraction pattern at any given real world location is to model the situation using advanced, time-consuming models. Typically, the time required to properly run such a model and the combined cost of the software as well as the cost of the model operator, is greater than a budget allowed for a feasibility study. As such, generalized wave diffraction diagrams, such as those created by Wiegel and Goda, are commonly used in feasibility studies for the design and construction of offshore structures. Both engineers, using similar restrictions and breakwater layouts, based their research solely on the variations of the ocean environment. Unfortunately, as both sets of diagrams are limited by their scope of research, they contain error.

Following Goda's work, much advancement has been made in the understanding of how diffraction is affected not only by the ocean environment but also by the characteristics of the object by which the wave energy is diffracted around. As of yet, these modifications have not been presented pictorially.

While there are many variables what will alter diffraction, this study will focus primarily on the effect of reflection on the diffraction pattern around breakwaters and through breakwater gaps. Other influences, such as transmission, will be briefly discussed but not included in the model studies.

1.2. Objectives

The main objective of this study is to investigate the influence of breakwater reflection on water wave diffraction. As a secondary objective, SWAN, a freely available nearshore wave modeling program, will be tested in its ability to perform diffraction around obstacles.

1.3. Problem Approach

To achieve these objectives, the following tasks shall be performed:

- Perform a literature study on water wave diffraction
- Research specific driving forces related to breakwater reflection coefficient.
- Obtain knowledge on driving forces and sensitivities in wave diffraction study
- Discuss how wave environment and breakwater construction influence diffraction
- Research methods used by authors of currently available wave diffraction diagrams
- Define set of modeling inputs which reflect classic computations for each utilized computational model
- Perform study and comparison of PHAROS and SWAN models
- Attempt to replicated diffraction coefficient diagrams developed from theory with the assistance of state-of-the-art computer modeling systems
- Assess if model results, particularly those of SWAN, are comparable to analytical solutions
- Determine causes for dissimilarities between model outputs and theory
- Evaluate usefulness of model(s) for diffraction studies
- Perform additional diffraction studies using breakwaters with variable reflection coefficients
- Discuss effects of breakwater reflection coefficients on diffraction patterns

PART II: Diffraction

Chapter 2. Diffraction Theory

Wave diffraction is defined as the bending of wave energy around an obstacle. Unlike particles which continue in a straight line, waves will bend into an area behind the obstacle called the “shadow zone.” The diffracted waves contain less energy than the originally supplied waves as it is distributed throughout the shadow zone. Depending on the object with which the waves collide and at what angle, the wave energy will react differently. Additionally, the resultant diffracted energy is a function of the original wave’s wavelength.

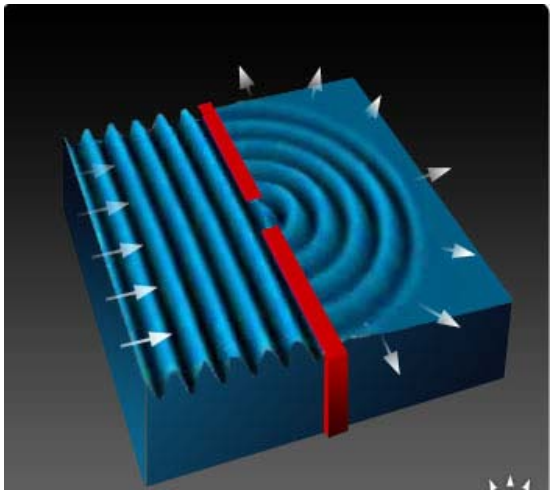

Figure 2-1: Wave passing through a slit and bending into the shadow zone

2.1. Theoretical Background

Diffracted wave height within the shadow zone can be estimated using the Sommerfeld (1896) solution of optical diffraction which is based on velocity potential theory. This solution applies to all wave physics such as light, sound, and electromagnetic waves. Sommerfeld’s solution was later modified for water waves by Penny & Price (1952).

The Sommerfeld solution is given as the following (for symbols see Figure 2-2):

$$F(r,\theta) = f(\sigma)e^{-ikr\cos(\theta-\theta_o)} + f(\sigma')e^{-ikr\cos(\theta+\theta_o)} \tag{1.1}$$

Where: $\sigma = 2\sqrt{\frac{kr}{\pi}}\sin\left(\frac{\theta-\theta_o}{2}\right)$ (1.2)

$$\sigma' = -2\sqrt{\frac{kr}{\pi}}\sin\left(\frac{\theta+\theta_o}{2}\right) \tag{1.3}$$

$$f(\sigma) = \frac{1+i}{2}\int_{-\infty}^{\sigma} e^{-i\pi t^2/2}dt \tag{1.4}$$

$$f(\sigma') = \frac{1+i}{2}\int_{-\infty}^{\sigma'} e^{-i\pi t^2/2}\,dt \qquad (1.5)$$

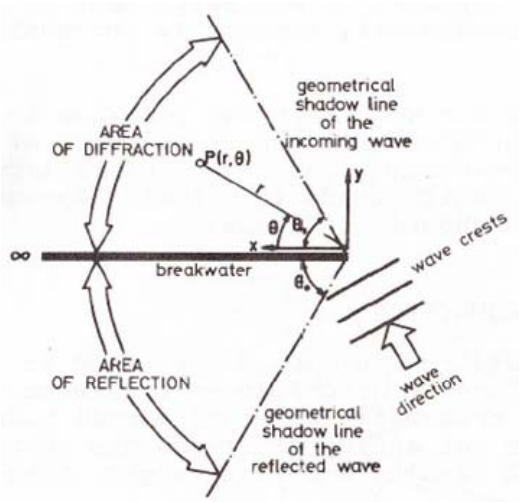

Figure 2-2: Definition sketch for Sommerfeld Solution (Daemrich, 1978)

The diffraction heights of irregular sea waves should be computed as follows by introduction of the directional wave spectrum, $S(f,\theta)$:

$$(K_d)_{eff} = \left[\frac{1}{m_0}\int_0^{\infty}\int_{\theta\min}^{\theta\max} S(f,\theta)K_d^2(f,\theta)\,d\theta\,df\right]^{1/2} \qquad (1.6)$$

$(K_d)_{eff}$ = diffraction coefficient of random sea waves

$K_d(f,\theta)$ = diffraction coefficient of component (regular) waves with frequency f and direction θ

m_0 = integral of the directional spectrum

$$S(f,\theta) = S(f)G(\theta \mid f) \qquad (1.7)$$

$S(f)$ = frequency spectral density function

$G(\theta \mid f)$ = directional spreading function or directional distribution

2.2. Spatial Variation due to Reflective Structures

The available diffraction diagrams produced by Wiegel and Goda assume a thin, fully reflecting breakwater. In many cases where breakwaters are used to shelter lee areas from wave attack, this is not the case. Breakwaters constructed of rubble material or interlocking armor units have become commonplace in coastal engineering and harbor design. The added benefit of using these types of armor is that it partially absorbs wave energy which reduces the wave height adding effect created by reflection off of the breakwater. This is very beneficial in harbor design as the structure does not cause unwanted turbulence in either the entrance channel or within the harbor.

Despite the tendency to design breakwaters for the greatest dissipation of waves, diffraction theory currently in use is based upon 100% reflection.

Classically, diffraction calculations are based on the Sommerfeld solution which is mathematically exact for fully-reflecting, thin walls. When breakwaters are constructed with reduced reflecting front sides, channels, or guildwalls, a modified equation must be used. However, any modification of this solution makes it no longer mathematically exact. Only the total solution of the equation fulfills the boundary conditions.

By considering the two terms of the Sommerfeld equation of wave diffraction behind a semi-infinite breakwater separately, the influence of both the incident wave and the reflected wave can be evaluated. The first term represents the fraction of diffracted wave height resulting from the incident wave while the second term represents the fraction attributed to reflected wave energy. For 100% reflection, the two terms are added together to give the diffraction coefficient. For partial reflection, the second term must be reduced proportional to the degree of reflection.

$$K' = \left|F\left(r,\theta\right)\right| = \text{incident term + reflected term} \tag{1.8}$$

$$F\left(r,\theta\right) = f\left(\sigma\right)e^{-ikr\cos\left(\theta-\theta_o\right)} + f\left(\sigma'\right)e^{-ikr\cos\left(\theta+\theta_o\right)} \tag{1.9}$$

According to the laws of geometrical optics, each term represents part of the wave field around the breakwater. It consists of a straight-crested wave field and a circular scatter wave field. The scatter wave field is influenced by the breakwater itself causing phase shifts. However, it should be noted that by simplifying the procedure of calculation for water waves to laws of geometrical optics introduces error. This error is expected to reduce when directional spreading characteristics of irregular waves are used.

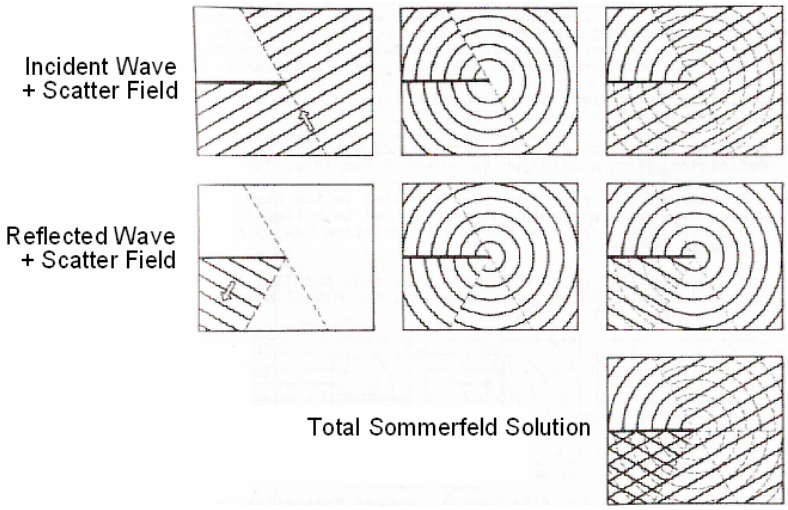

Figure 2-3: Partial wave fields according to Sommerfeld solution (Daemrich, 1978)

As expressed by the Sommerfeld solution, some of the energy reflected and scattered off of the breakwater will also diffract into the harbor basin along with the incident

waves and contribute to the overall diffraction coefficient. These waves pass through an angle equivalent to 360°-2θ. Outside the shadow zone, the interaction of the incident waves and the reflected waves creates a short crested system which is detailed in Carr and Stelzriede (1951).

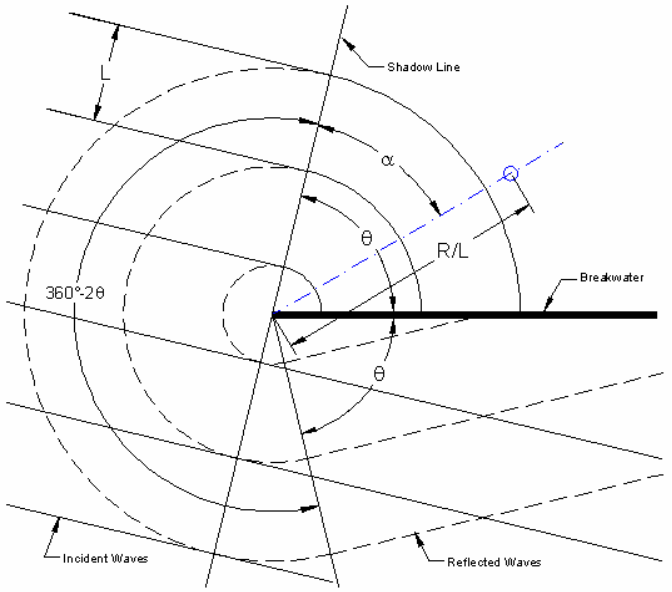

Figure 2-4: Tip diffraction definition sketch (Silvester, 1968)

It can be accepted that the contribution of diffracted reflection waves is small within the shadow zone, however, it is not insignificant for fully reflective breakwaters. In the direct leeside of the breakwater, the reflected and incident components are found to each be 50% of the total wave height. This is significant when the reflected component may not exist at all due to proper dissipation.

However, care should be taken using these principles when the breakwater is not uniformly constructed. Theories are not specific about further modifications due to non-uniform breakwaters. Breakwaters with reflective leesides will allow the diffracted wave energy to travel further along the interior of the breakwater. Breakwaters with absorbent leesides will further dampen the energy as it runs along the breakwater creating a calmer environment within its vicinity.

Figure 2-5 was presented by Silvester (1968). It shows that the incident wave component is only dependant upon the angle away from the shadow line. Conversely, the reflected wave component increases with increased distance away from the shadow line; climaxing along the leeside of the breakwater. This graphic is only valid for fully reflecting breakwater. Breakwaters with reduced reflection can be calculated by introducing a weighting factor discussed later in the chapter.

For example: for a wave with θ=70° and a location of R/L=10, α=30°

K(incident) = 0.1

360°-2θ+α=250° -> K(reflected) = 0.03

K(incident) + K(reflected) = K(100% reflection) = 0.13

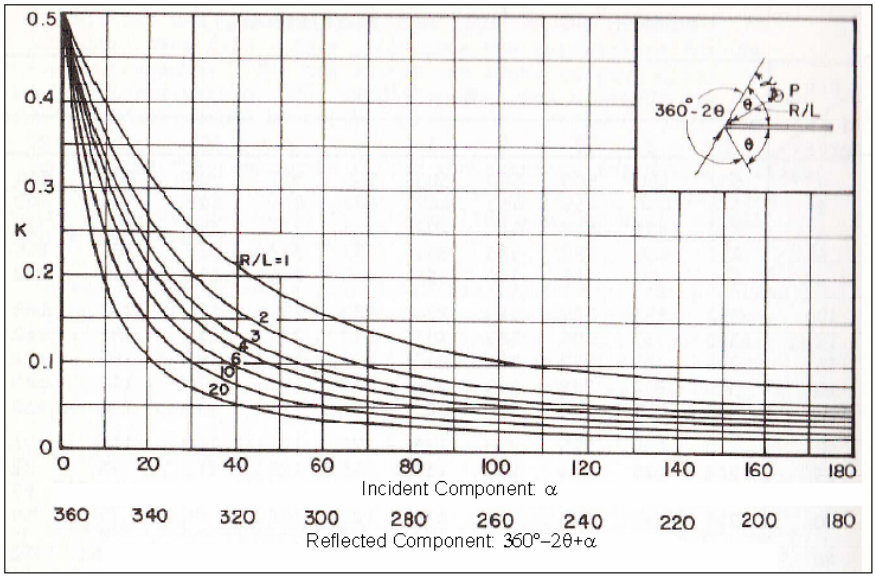

Figure 2-5: K for all incident angles with or without reflection (Silvester, 1968)

Figure 2-5 shows that the effects of reflected wave diffraction are greatest at the breakwater tip and along the leeside of the breakwater. Further inside the shadow area, reflected wave height is insignificant compared to the incident wave height.

Hydraulic model tests were performed and reported by Daemrich (1978) using absorbent materials along the breakwater front side to prevent reflection effects. This theoretically eliminates the second term of the Sommerfeld solution reducing it to the "simplified solution." However, while performing the model tests, he found that along the leeside of the breakwater, where the wave heights should theoretically be zero, they reached considerable values. This difference is attributed to the breakdown of the Sommerfeld solution once reduced reflection is introduced.

Another way to determine the influence of reflected wave diffraction is to effectively remove its presents by introducing guildwalls normal from the tip of the breakwater. It should be noted that this approach will only work for regular waves running parallel to the guild wall effectively removing reflection. Mitsui (1967) studied this approach and came up with the Mitsui solution for wedges; a 90° wedge being a guildwall. Daemrich found that the Mitsui solution for wedges with wave direction parallel to one wall in the region of diffraction is very similar to the solution for non-reflecting breakwaters and therefore can be used as a good approximation.

The Mitsui solution for a rectangular wedge or guildwall is given below. The solution must be halved for wave propagation directions parallel to one wall.

$$F(\rho,\theta)_{v=\frac{2}{3}\pi} = \frac{4}{3}J_o(\rho) + \frac{8}{3}\sum_{n=1}^{\infty} e^{in\pi/3} J_{2n/3}(\rho)\cos\frac{2}{3}n\alpha\cos\frac{2}{3}n\theta$$

with

$J_o(\rho), J_{2n/3}(\rho) =$ Bessel functions, first kind (1.10)

$\rho = \text{kr} = \frac{2\pi}{\text{L}} r$

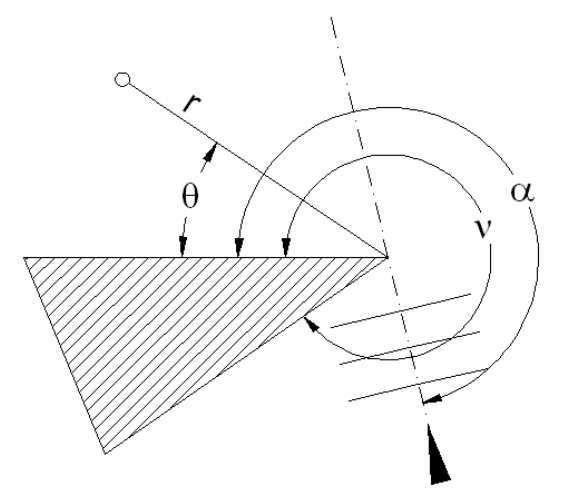

Figure 2-6: Definition Sketch for Mitsui Solution

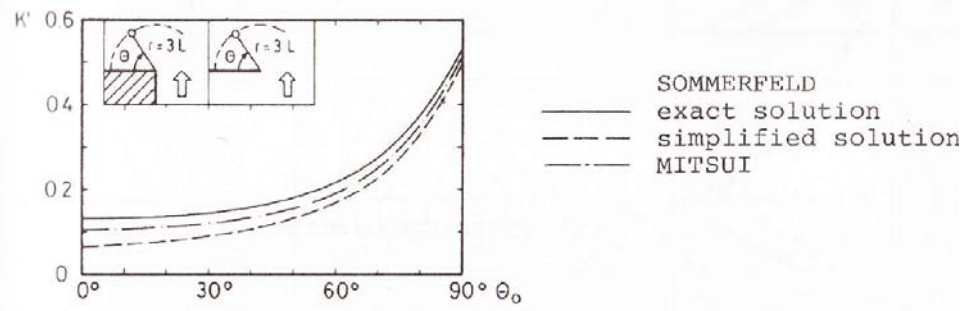

Figure 2-7: Comparison of Diffraction Coefficient K' for Multiple Theories (Daemrich, 1978)

In Figure 2-7, can be seen that the Mitsui solution is typically greater than the simplified solution but less than the total Sommerfeld solution. Therefore, it can be approximated by introducing a weighting factor to the second term of the Sommerfeld solution which is dependant on the wave direction, θ.

Daemrich found the only way to theoretically represent a non-reflective breakwater while fulfilling the boundary condition was to assume that while the reflected wave is dissipated by the absorbent breakwater, the pertinent scattered wave system must still react in accordance to a fully-reflecting breakwater. Using that idea, he came up with the following weighting factors, F_r.

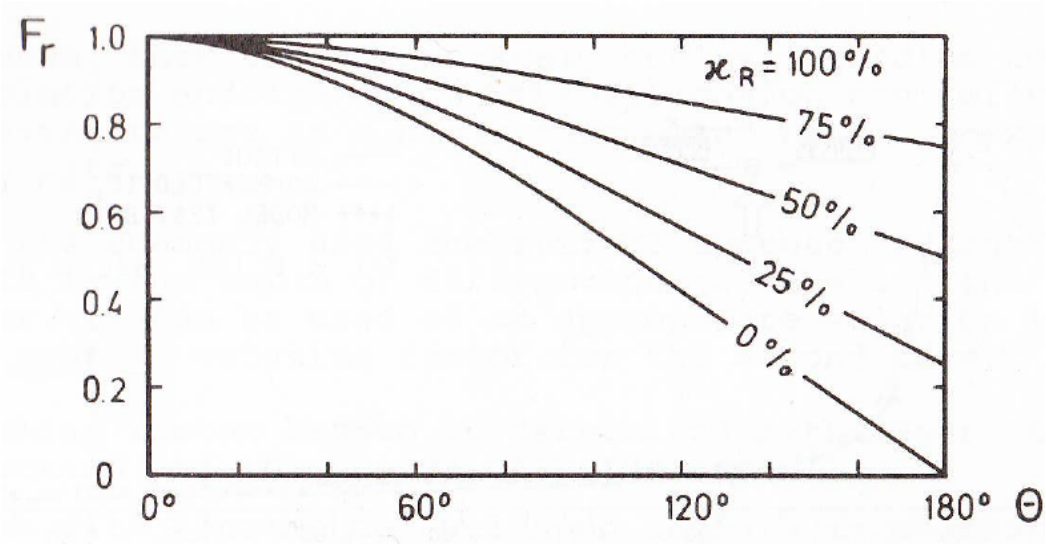

Figure 2-8: Weighting Factor F_r for second term of Sommerfeld solution for various degrees of reflection (Daemrich, 1978)

$$F_d(r,\alpha,f,\theta) = F_{id}(r,\alpha,f,\theta) + F_r F_{rd}(r,\alpha,f,\theta) \quad (1.11)$$

where: F_r denotes the weighting factor

As can be seen Figure 2-8, taking the second term as zero for non-reflecting breakwaters, as suggested by Silvester, is incorrect. While non-reflective breakwaters absorb the would-be reflected wave energy, wave scatter still exists and contributes to the overall height of the diffracted wave.

It should be noted that F_r does not contain any information related to phase (except when F_r=1 or 0) and therefore the equation remains an approximation.

Revisiting the example given above while using this new weighting factor, provides a more realistic diffraction coefficient:

Example: for a wave with θ=70° and a location of R/L=10, α=30°

K(incident) = 0.1 (from Figure 2-5)

360°-2θ+α=250° -> K(reflected) = 0.03 (from Figure 2-5)

K(incident) + K(reflected) = K(100% reflection) = 0.13

K(50% reflection, F_r =0.88) = 0.126

K(0% reflection, F_r =0.73) = 0.122

2.3. Additional Driving Forces of Diffraction

Many variables manipulate the outcome of a diffraction pattern. Due to this, only advanced modeling can accurately describe a diffraction pattern at any area of

concern. That said, knowing what variables play leading roles in diffraction can help an engineer roughly define the diffraction pattern at any given area. Doing this can aid in early design and feasibility studies. The following sections define some of the key variables that strongly influence wave diffraction.

2.3.1. Wave Characteristics

Any good coastal engineering project will start with a wave analysis. In the engineering and construction of structures and layouts for longevity, strength, and extreme events, engineers will often define a "design wave." This wave, which is derived from regular wave theory, is a representative regular wave which has properties believed to be equivalent to those of an irregular sea. Some less experienced engineers will use this wave to determine diffraction through the use of regular wave diffraction theory. This can lead to damaging agitation within the shadow zone on a daily basis.

The correct application of diffraction into a design requires knowledge of not only the extreme wave characteristics but of the full irregular wave seas which can occur regularly. In some cases, it is the daily and seasonal storm values that create the greatest wave penetration and not the design wave values chosen for strength analysis.

While all wave fields are unique, this study will concentrate on the basic distinctions between wave types. Diffraction behavior is similar within these distinctions and therefore their effects represent a good estimation for early design.

2.3.1.1. Regular vs. Irregular

In the study of wave movement, waves can be classified into two groups: regular and irregular waves.

Regular
Regular waves, waves with a single period and direction, are the basis of complex ocean environments. They are the simplest wave forms and are therefore used as a starting point of most wave theories. Through the understanding of diffraction of a single, regular wave, the diffraction environment created from a myriad of waves within an ocean climate can be more accurately estimated.

Irregular
Ocean waves are random phenomena whose exact state cannot be predicted. They are the combination of an ever changing series of regular wave fields. The combination of these wave fields is what we commonly refer to as irregular waves. Irregular waves contain directional and/or frequency spreading. The absence of both spreading types is a regular wave.

Due to the complex nature of irregular waves, engineers frequently use a "regular wave concept" which relates regular wave theory to irregular waves. This concept is founded on the basis of one single regular wave which has properties believed to be

equivalent to those of an irregular sea. Linear transfer functions are used to accurately predict important statistical properties, such as significant and maximum values of waves. For these predictions, the wave energy distribution over the directions and frequencies should be known. These values of an equivalent regular wave are then used as the design values for calculations related to motion and forces such as diffraction. Of course, this concept has its shortcomings as it does not explicitly consider probabilistic characteristics of sea waves.

For the purpose of determining diffraction around a breakwater in a real world application, irregular waves should always be used. However, the use of regular waves is beneficial when working in a laboratory setting or when analysis of specific wave processes are desired. By removing the added complexity of irregular wave fields, the physics of singular wave motion can be more easily understood.

2.3.1.2. Directional and Frequency Spectrums

Directional Spreading
Ocean waves are tumultuous, traveling in many directions at the same time. The range of propagation directions is in relation to the generating force. For example, waves generated by wind have large directional spreading while swell waves, generated by offshore storms, have a more defined direction. Uni-directional waves travel in only one direction though can contain wave trains of various periods.

Directional spreading has a large influence on the effects of diffraction. The more spread out a wave field is, the more quickly the wave energy is dampened within a short distance. On the other hand, more focused waves, such as swell and uni-directional waves, travel farther behind the breakwater without significant dampening effects. Knowing what type of waves are present at a given location will aid in developing protection suitable to the degree of directional spread.

Frequency Spreading
In addition to directional spreading, irregular waves typically display some type of frequency spreading. Frequency spreading is the range of various wave periods represented in a wave field. Again, wind-generated waves will have a larger range of frequency spreading than swell type waves. Monochromatic waves only have one frequency and wavelength though they can propagate in many directions. It is found that frequency spreading does not have a strong influence on diffraction effects.

Both directional spreading and frequency spreading are examined further in section 5.2.4.

2.3.2. Construction Aspects

In conjunction with how the wave environment will affect diffraction, the layout of breakwaters and how they are constructed heavily influence the tranquility on their leeside. Breakwaters are built for a variety of purposes and, as such, there are many methods of construction. Layout and construction are driven not only by the ocean environment but also by regulations, permits, cost restrictions, material restrictions,

purpose, crest height, and many other variables. All of these aspects must be kept in mind when designing the layout for a harbor or breakwater.

Previously published diffraction diagrams are generated using an infinitely thin, vertical, fully reflecting breakwater. In modern practice, fully reflecting breakwaters are rarely used within harbor construction. Reflection off the interior walls of a harbor would cause unwanted resonance which can be damaging to vessels and mooring lines as well as dangerous for boater navigation. Reflective breakwaters also cause amplified wave heights in front of the breakwater which is a hazard to vessels traveling in this region. For those reasons, energy absorbing materials, such as rubble or concrete armor units, are generally preferred over vertical walls. Of course, this has its exceptions. Deep water is prohibitive to the use of rubble mound breakwaters which are both large and costly. In these instances, monolithic walls or vertical sided cassions are employed to reduce the structures footprint and overall cost.

Another issue which frequently occurs in breakwater/harbor construction is non-uniformity. Harbor developers who want to utilize all available footprint for usable, and therefore revenue generating, dockage space, prefer to use vertical interior walls. This means that the exterior of the harbor is constructed with energy absorbing materials, such as rubble, while the interior is vertical faced. This type of structure represents a composite breakwater which can not be correctly defined by either fully reflecting diffraction characteristics or fully absorbing diffraction characteristics. Composite breakwaters will be briefly discussed in section 5.2.2.

The following subsections will discuss a few of the design variables which affect diffraction. Because there are numerous variables which contribute to diffraction effects and harbor agitation, only a limited number are discussed here.

2.3.2.1. Layout

Breakwaters, both detached and shore-connected, have been used extensively to protect harbors and small craft marinas from unwanted wave agitation. The position in which these breakwaters are placed greatly affects the functionality of the interior basin. Many layouts can be constructed within a given footprint but it is the layout which has the most benefits and the least drawbacks which is truly the best design. Using structure layouts determined by extreme analysis, the layout should also be tested for daily, seasonal, and annual events against their allowable agitation levels and modified if necessary.

An engineer should design a breakwater layout with primary consideration for the wave environment and the purpose for which the breakwater is being built. If the breakwater is part of a harbor, then vessel approach and maneuverability are of great importance. If the breakwater is designed as part of a shore protection system, the distance from shore as well as the littoral movement is of prime concern. Knowing how diffraction effects will help or hinder the breakwater's primary purpose will dictate how best to position the layout.

Diffraction around structures can be classified in one of three layout groups: semi-infinite breakwater, breakwater gap, or detached breakwater. For this study, only two layouts were studied; semi-infinite breakwaters and breakwater gaps. These two layout groups were also chosen for study by Wiegel and Goda. Comparisons between these studies will be presented later in this report.

Classically, the simplest approach for estimating wave diffraction is to consider regular waves in constant deep water incident against a thin straight, vertical breakwater. Though this setup is improbable in real application, its analysis aids in the generation of more complex diffraction analyses.

Semi-infinite breakwater layouts, which consist of a single breakwater, diffract wave energy around its tip into the shadow zone, which is not directly effected by wave propagation. Waves which do not impact the breakwater flow unhindered pass the breakwater causing elevated wave heights outside the breakwater's shadow zone.

Breakwater gap layouts consist of two breakwaters which are separated by an open space. Wave energy flows through this gap and is diffracted into both shadow zones behind the breakwaters. The distance at which diffraction occurs is a function of the gap width and the wave characteristics. When the gap size is only a few wavelengths wide, all wave energy behind the breakwaters is diffused. Even the wave energy which flows directly between the breakwater gap loses height as the energy spreads into the shadow zone. This idea is presented pictorially in Figure 2-9.

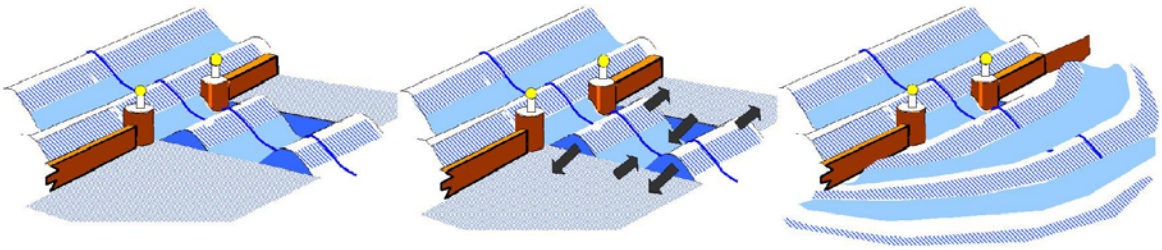

Figure 2-9: Breakwater Gap Diffraction

Exact theoretical solutions exist for both layouts. Semi-infinite breakwaters are well defined by Noble (1988) and for infinitely long solid breakwaters with a gap, the exact solution was presented by Carr and Stelzriede (1952).

In many cases, breakwaters will not be constructed along a straight line. Regardless of this, a straight line between breakwater tips is called its gap width, B. Often, however, waves will approach the breakwater gap at oblique angles. When this occurs, an effective gap width, B', is used. An 'effective gap' is what the wave would "see" as it propagates between the two breakwaters. It is found by determining the gap between the two breakwaters as if the wave was propagating normal through the gap width.

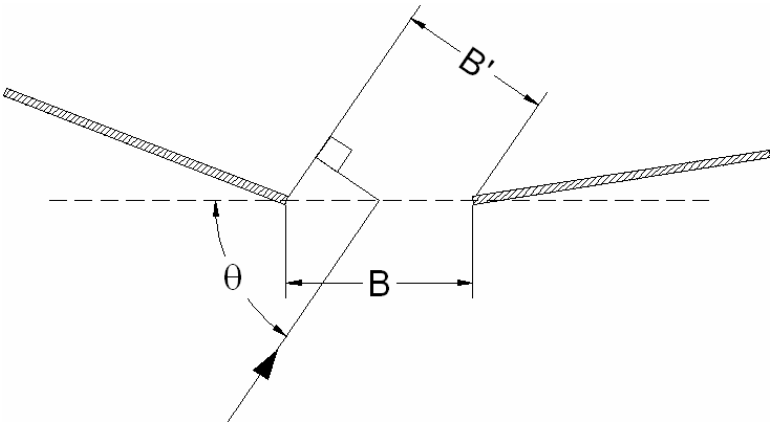

Figure 2-10: Determining Effective Gap Width, B'

2.3.2.2. Wave Diffraction of Oblique Incidence

Diffraction is affected by the angle at which the wave train impacts the structure. In most cases, waves will arrive at a breakwater at an oblique angle. This is an angle other than normal to either the semi-infinite breakwater or to the breakwater gap. When this is the case, more wave energy will be concentrated in the general direction of incidence.

In the case of wave diffraction by a semi-infinite breakwater, an approximate representation of wave diffraction can be made by rotating the axis of the breakwater in the diffraction diagrams for normal incidence while keeping the wave direction and the coordinate axes at their original positions (Goda, 2000). This method is most accurate when the angle between the propagation ray and the breakwater is greater than 45°. For principle wave approach angles less than 45° from the breakwater, error is introduced and in which case, this technique is not recommended.

For waves propagating through a breakwater gap, a different technique should be used. It is important to recognize that the axis of the deepest penetrating diffracted waves through a gap does not run parallel to the incident wave angle. This axis deviates slightly toward the line normal to the breakwater gap. This deviation angle is dependant on the angle of approach relative to the breakwater gap, the effective gap width, and the wave characteristics. Goda developed the list of deviation angles based on the analysis of several diffraction diagrams for obliquely incident waves given in Table 2-1.

Goda defined a wave environment based on the maximum directional concentration parameter, s_{max}, which is related to the wave steepness. From this parameter, he could differentiate wind-type waves from swell-type waves as stated below. S_{max} can be assumed to increase as the wave steepness decreases.

$$s_{\max} = \begin{cases} 10: \text{ for wind waves} \\ 75: \text{ for swell with medium to long decay distance} \end{cases}$$

It should be stated that this parameter, s_{max}, is not used in the following modeling analyses, though, as it will be shown, it can closely be related to the wave environments chosen for this study.

Table 2-1: Deviation angle of diffracted waves through a breakwater gap for obliquely incident waves (Goda, 2000)

s_{max}	B/L	Deviation angle Δθ			
		θ=15°	θ=30°	θ=45°	θ=60°
10	1.0	37°	28°	20°	11°
	2.0	31°	23°	17°	10°
	4.0	26°	19°	15°	10°
75	1.0	26°	15°	10°	6°
	2.0	21°	11°	7°	4°
	4.0	15°	6°	4°	2°

Because the angle of deepest penetration deviates from the angle of incident wave propagation, the effective gap width also changes. An example of how this changes the effective gap width is shown in Figure 2-11.

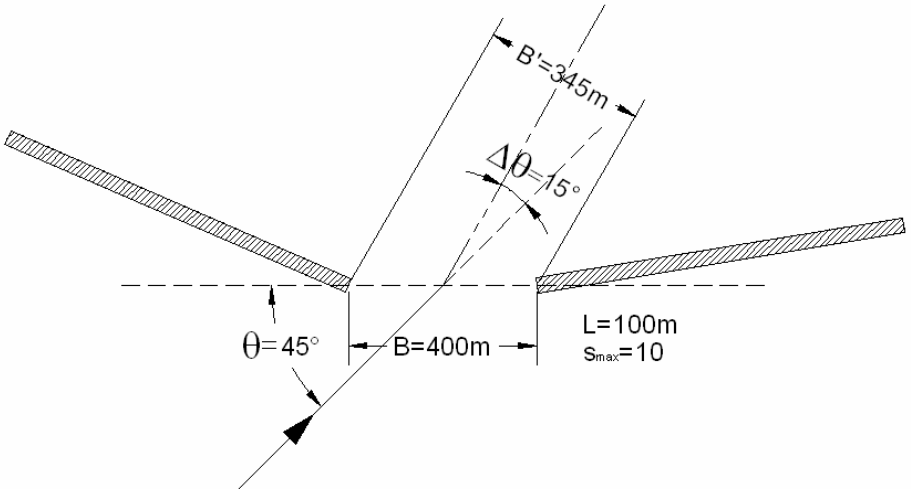

Figure 2-11: Effective Gap Width due to Oblique Angle Deviation

As shown, the majority of diffracted wave energy travels in relation to the angle of incidence. Therefore, when designing obstacles or breakwaters to create tranquil waters, it is best to angle the structure appropriately for maximum sheltering. By working with angled diffraction effects, the designer can effectively maximize the breakwater footprint and lower the overall cost of construction.

2.3.2.3. Transmission

Although not fully explored in this report, the issues of transmission and overtopping are major contributors to shadow zone agitation. In addition to diffracted wave effects, transmission allows wave energy to travel through or over the breakwater and into the shadow zone. The transmission coefficient is a function of permeability, wave overtopping, and breakwater geometry. It should be kept in mind that permeability will

effect both the transmission and reflection coefficients and in turn effect the diffraction coefficient. The general effect of transmission is a decrease in diffraction effects.

Beyond breakwaters, many sheltered regions plagued by small period wind waves use floating wave attenuators. From a physics standpoint, these systems react similarly to porous breakwaters with wave energy transmission. In addition to transmission, diffraction takes place at the float's edges adding to the wave energy in the leeside. However, the contribution of diffracted wave energy will be greatest at a distance away from the attenuator. The region directly behind the breakwater/attenuator will be most greatly affected by the transmitted wave energy.

Chapter 3. Diffraction Diagrams

Diffraction diagrams are generalized graphics depicting contours of diffraction coefficients. A diffraction coefficient is defined as the ratio of the diffracted wave height to the incident wave height and is presented mathematically as:

$$K_d = \frac{H_d}{H_i} \tag{1.12}$$

The first collection of diffraction diagrams were created by Wiegel based on the exact theory of the diffraction of linear water waves by a semi-infinite breakwater. These drawings, which included incident angles between 0° and 90°, were very useful to engineers whom, at the time, may not have had the aid of computer modeling. Wiegel prepared his diagrams based on regular waves with constant period and a single directional component incident against a thin, straight, fully reflecting semi-infinite breakwater. In addition, he also represented gap diffraction diagram originally created by Johnson (1952). One such diagram by Wiegel, is shown in Figure 3-1. These diagrams have been used extensively in the past and are still represented in engineering manuals.

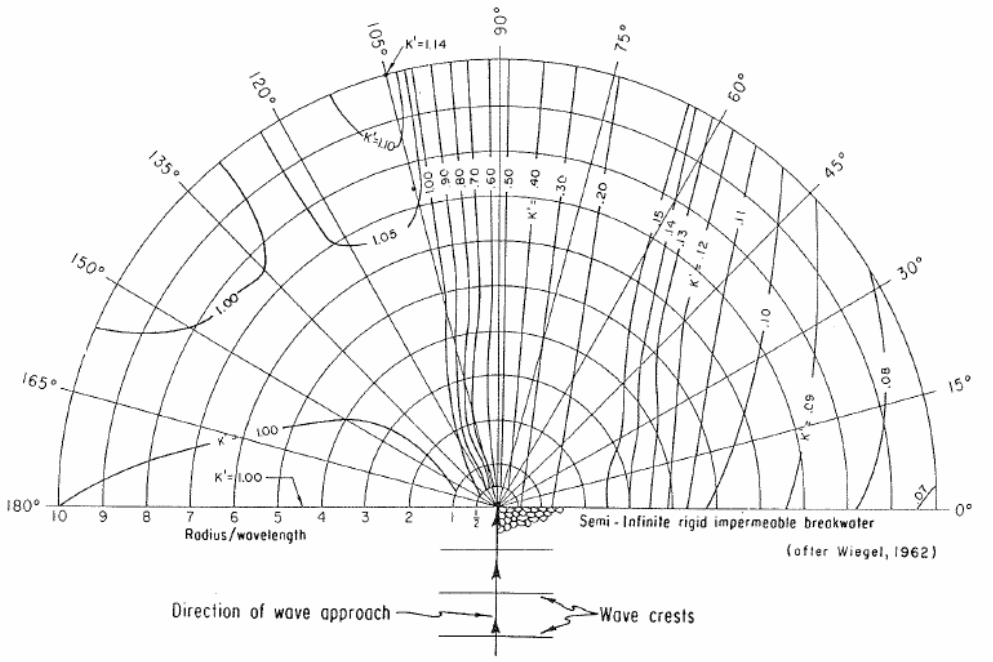

Figure 3-1: Diffraction diagram of regular wave at a 90° angle (Wiegel, 1962)

As knowledge of diffraction grew, these classical diagrams were replaced by diffraction diagrams making use of directional and frequency spreading wave characteristics. The most commonly used set of irregular wave diffraction diagrams were produced by Goda (1978). It was recognized that a real ocean environment is tumultuous and is made up of many regular wave layers traveling at different heights and directions, with different periods. Goda's study focused on both wind generated

waves with large directional spreading and short attenuation lengths and swell waves with small directional spreading and long attenuation lengths.

As shown by Goda (1985), the use of traditional regular wave diffraction diagrams for real irregular ocean waves with directional and frequency spreading typically results in considerable underestimation of the wave energy within the shadow zone. A more comprehensive and general approach, in which a directional spectrum is used to estimate the diffracted wave energy, was first presented by Mobarek and Wiegel (1966) and later put into useful diagrams by Goda (1978). Using the Sommerfeld solution, many uni-directional wave components, in total representing the directional wave spectrum, are combined. The directional wave spectrum is presented in equation (1.7).

The direction spectrum used within Goda's diffraction diagrams is a combination of the Bretschneider-Mitsuyasu frequency spectrum and the Mitsuyasu-type spreading function. Goda produced two different diffraction diagrams based on the range of the directional spectrum; narrow banded spectrums represented swell-type waves (s_{max}=75) and broad banded spectrums represented wind generated seas (s_{max}=10). Goda used 10 frequency intervals and 20 to 36 directional intervals of equal spacing ($\Delta\theta$ = 9° to 5°) for the integrations in the directional wave spectrum equation.

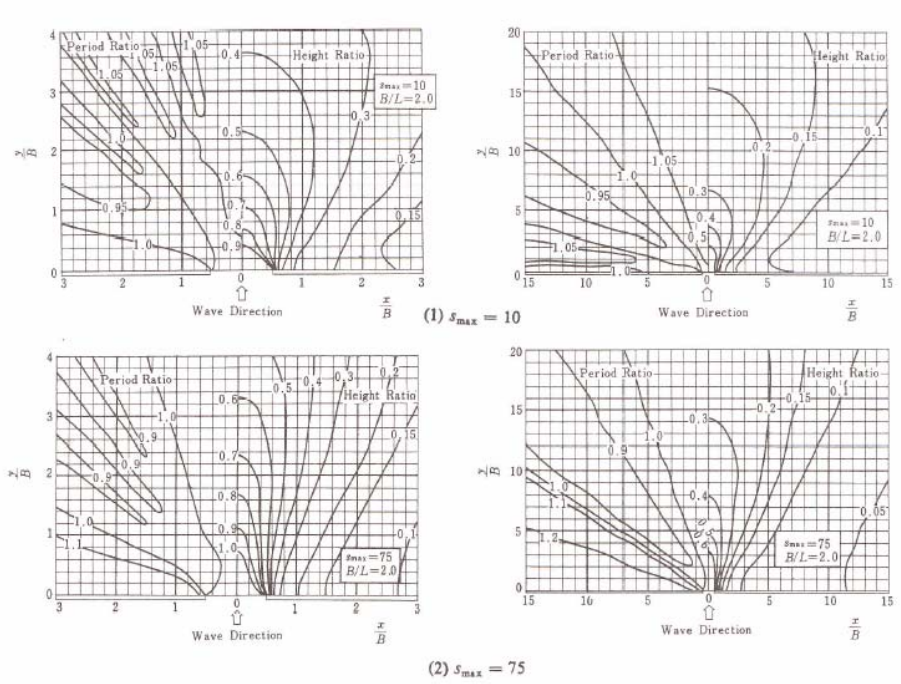

Figure 3-2: Diffraction diagrams of irregular waves at a breakwater gap, B/L = 2 (Goda, 1978)

An example of the irregular wave diffraction diagrams created by Goda is shown in Figure 3-2. His diagrams depicted variations in wave period as well as changes in wave height. He found that the diffraction of irregular waves, particularly those with frequency dependant directional spreading, illustrated changes in wave period in addition to wave period.

Figure 3-3 is a comparison graphic between the two wave types of diffraction. It shows the significant difference between regular wave diffraction diagrams and irregular diffraction diagrams for broadly directional spread waves through a breakwater gap of B/L = 2. It is easily visible that for areas outside of direct penetration, regular wave diffraction coefficients are much lower than their equivalent irregular wave value. Application of regular wave theory for this case would result in underestimation of the wave height.

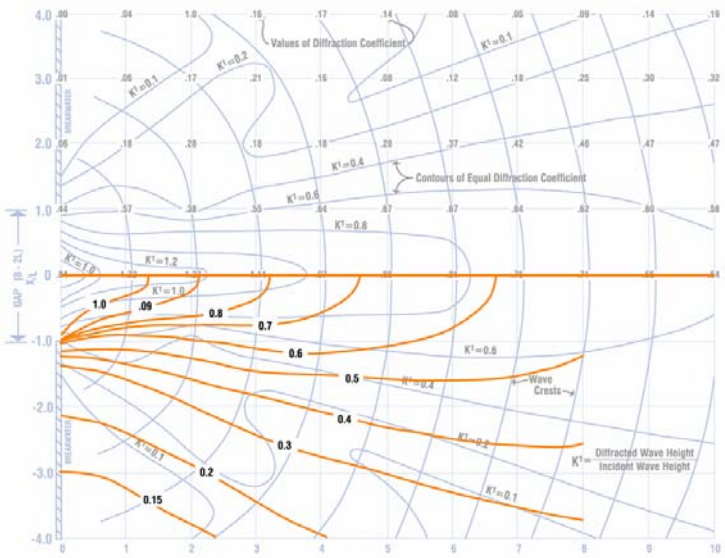

Figure 3-3: Comparison of Regular and Irregular Wave Diffraction

From the creation of irregular diffraction diagrams, Goda found that "in terms of spectral density, the theory of regular wave diffraction yields only 3% of the observed value (Goda, 1978)." This can lead to grievous errors when regular wave diffraction diagrams are used for irregular seas.

Additional analytical diffraction diagrams by Wiegel and Goda can be found in the appendix.

3.1. Application for Design

It should be noted that direct application of any diffraction diagram to real situations for the purpose of final design is not recommended. This practice can lead to erroneous results. Diffraction studies presented herein as well as the diagrams presented by Wiegel and Goda were not generated based on theory and not real scenarios. To ensure diffraction diagrams are based solely on diffraction, effects from bottom friction, refraction, and wave breaking were removed from the analysis. In real situations, these processes will effect the diffraction outcome.

Diffraction diagrams should only be used by engineers in feasibility studies and preliminary stages of design. For realistic, location specific diffraction patterns, engineers are encouraged to employ the use of advanced computer models which capture the many aspects of diffraction.

PART III: Modeling

Chapter 4. Models

4.1. Phase-Resolving vs. Phase-Averaged

Many computational models which study ocean processes are available on the market today. Knowing which model will be most beneficial to a task can be an obstacle in itself. However, making the correct choice of model can save an engineer both time and energy by avoiding unnecessary computing time.

A fundamental criterion for classifying models is based on the rate of spatial evolution of the wave field. This is determined by the intensity of the processes causing the change. From this standpoint, two main families of models exist; those dealing with rapidly changing waves (phase-resolving models) and those dealing with slowly changing waves (phase-averaged models). Each type of model approaches the problem and computes it differently.

Phase-averaged models, which are more efficient, are well suited for processes which have weak variations over the scale of a wavelength. They deal with averaged properties, using kinematic propagation equations expressed in terms of such concepts as wave number, group velocity, wave rays, etc. and an energy balance equation in one form or another (Battjes, 1994).

Phase-resolving models can accurately model local properties which vary strongly within a small scale. They consist of equations describing the immediate state of motion, either in the time domain or in the frequency domain. Phase-resolving models are so computationally intensive that, for most practical applications, they are considered necessary only in the near field of wave-structure interaction. There are three main types of phase-resolving models that can be classified by their foundation equations: boundary integral, mild-slope equation, and Boussinesq.

The spectral wave action balance equation, a phase-averaged property, contains all the necessary information to predict the most important dynamic and probabilistic properties of the local wave field. However, strong processes, such as wave diffraction, and rapidly changing bathymetry require the intensity of a phase-resolving model to capture all instantaneous processes.

The phase-averaged model is best suited to wind driven waves with large directional spreading. Because it is based on spectral wave action, it is unable to accurately represent regular or unidirectional waves. Phase-resolving models, on the other hand, can accurately represent these simple waveforms. In diffraction, phase-resolving models will produce better simulations than phase-averaged models for regular waves whereas the difference may hardly be noticeable for irregular wind waves.

There will always be a need for separate phase-averaged and phase-resolving models. The preference is to use the minimum number of models needed to give an acceptable simulations without additional cost or effort. From this standpoint, the

choice of model depends on the desired research and the complexity of the environment.

In this study, one of each model type were chosen to model reflection and diffraction around breakwaters. PHAROS is a phase-resolving model of the mild-slope equation type which is available for purchase through Deltares. In contrast, SWAN is a phase-averaged model which is freely available for download through Delft University of Technology. From an academic standpoint, PHAROS will be used to test the accuracy of the SWAN models for diffraction.

4.2. Universal Model Setup

To ensure that all model studies were as consistent as possible, some universal settings were introduced. Variables that differ between models are so noted within their sections.

Some basic assumptions were made for the modeling of diffraction: (1) uniform depth of water throughout which is considered "deep" by all input waves. (2) breakwaters are considered as thin in respect to the wavelength. (3) small amplitude waves in keeping with linear theory. (4) breakwater is considered solid and infinitely high to prohibit transmission or overtopping. (5) breakwater is considered to be uniform construction.

4.2.1. Wave Characterization

Three types of waves were studied in this report: regular waves, swell-type waves, and wind-type waves. Original works by Wiegel concentrated on regular waves. Goda recognized that ocean waves are more realistic wave forms and was the first to plot what he defined as 'swell waves' and 'wind waves'. These types of waves contain both directional and frequency spreading. Since these waves represent a full range of wave types, they were the base cases chosen for study within this report.

Goda used a spreading parameter, s_{max}, based on a spectrum definition by Mitsuyasu (1975) to describe the degree of directional spreading of a wave group. Unfortunately, neither model used in this study used this variable. Kuik (1988) developed relations between the classification of wave and the degree of directional spreading. He specified that swell waves relate to a wrapped normal spreading parameter of $\sigma = 10°$ and wind waves relate to a wrapped normal spreading parameter of $\sigma = 30°$. A study performed by Briggs (1995) related these two parameters in Figure 4-1. As shown, these two parameters are very similar.

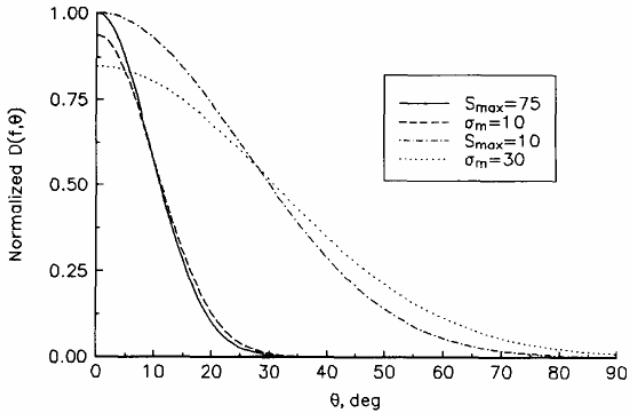

Figure 4-1: Wrapped Normal and Mitsuyasu Directional Spreading Functions (Briggs, 1995)

Both models used in this study defined wave characteristics slightly differently. Therefore, inputs specific to each model will be presented in the following chapters. Table 4-1 describes the main characteristics of these wave types.

Table 4-1: Wave Characterization within Models

	Directional Spread (deg)	Frequency Spreading	
			Jonswap Gamma
Regular	1°	No	-
Swell Irregular	10°	Yes	10
Wind Irregular	30°	Yes	3.3

4.2.2. Universal Model Inputs

As the purpose of the modeling in this report is to study diffraction, other nearshore processes, such as refraction, must be removed from the analysis. This was achieved by setting the modeling depth to 500m and the primary direction of wave propagation set normal to shore. The bottom was also specified as flat and frictionless to avoid influencing the wave characteristics. While this is an unrealistic setup for real-world design, the models will not be contaminated with unwanted ocean processes.

To standardize the modeling, a set of wave characteristics were established. For ease of transition between incident wave height and diffraction coefficient, the significant wave height was set as Hs=1m. Additionally, for ease of transition between the final diffraction diagrams and associated wavelength, a wavelength of L=100m was chosen which conveniently gives a wave period of Tp=8s in deepwater. These variables were set for all modeling runs to maintain consistency.

Table 4-2: Standard modeling Inputs

Standard	Hs (m)	Tp (s)	Depth (m)	L (m)
Inputs	1.0	8.0	500	100

For ease of creating dimensionless diffraction diagrams from the model runs, each breakwater segment within the model domain was given a length of 10L. Additionally, computational area of all layouts was set in increments of wavelength.

4.2.3. Model Grid

Defining the computational grid is one of the most important aspects of computer modeling. A correctly defined mesh should be small enough that it can capture rapidly changing local properties yet large enough to avoid unnecessary computing time. In some cases, the size of the mesh can significantly alter the outcome of a model.

To properly define a wave, literature suggests a minimum of 8 points per wavelength are needed. Less than this amount will not correctly define the wave shape. Therefore, it is generally a good idea to make the grid as fine as the model can handle and computation time will allow. On the other hand, when large areas are defined, it is advisable to use a mesh which decreases in size toward the area of interest. This will reduce computation time while concentrating on the specifics near the investigation site.

The model grids within PHAROS and SWAN are defined differently. As a phase-resolving model, PHAROS is capable of creating a very fine mesh which conforms to the criteria of 8 points per wavelength (though additional grid points are preferable, this number was chosen for computation time constraints). Its grid is unstructured and therefore the size of each element varies throughout the grid. For fine meshes based on reduced wave periods associated with spectral modeling, computation time grew exponentially.

Simple, structured grids were used within SWAN. The size of the computational area as well as the spatial resolution required repetitive testing to attain a stable model output. Guidelines for this testing are presented in the chapter on SWAN. Due to restrictions related to fine grids, spatial resolution was limited to less than 8 points per wavelength. As SWAN is a phase-averaging model, this should not significantly impact the integrity of the output data.

4.3. Reference Cases

The two prior sets of diffraction diagrams created by Wiegel and Goda were used as reference cases within this study. To ensure the models were running properly and providing the desired condition, it was first imperative to attempt to replicate these diagrams. As diffraction diagrams are intended to be universally applicable, the author's choice of wave criteria is unimportant. Comparison between the analytical cases and the modeled outputs can be found in Chapter 7.

Chapter 5. PHAROS

"PHAROS (Program for HARbour OScillations) is an integrated system for modeling wave propagation into harbors and around coastal structures." It was developed by the Delft Hydraulics department of Deltares and is commercially available for purchase.

The PHAROS model is a phase-resolving model based on the mild-slope equation. The mild-slop equation is elliptic in its complete form, requiring boundary conditions along the entire curve encompassing the computational domain and the simultaneous solution of the wave field in all interior points. The mild-slope equation is given by:

$$\nabla\bullet\left(cc_g\nabla\phi\right)+2i\omega\vec{U}\bullet\nabla\phi+\left(k^2cc_g+\omega^2-\omega_r^2+i\omega\nabla\bullet\vec{U}\right)\phi=-i\omega_rW\phi \qquad (1.13)$$

For more details about the theoretical background of PHAROS, one is referred to Chapter 9 in the PHAROS user manual.

Due to the linear assumption used by PHAROS, the wave motion is described as a sum of monochromatic uni-directional wave components that can be calculated independently over both the directional and frequency spectrum. This requires a huge computation which can be time consuming on slower computers.

Typical to mild-slope equation models, effects of wind input, whitecapping, and quadruplet interactions are not represented in PHAROS. These processes are, however, available in the phase-averaged model, SWAN, though are not an integral aspect of this study.

PHAROS was chosen for this study due to its advance modeling capabilities. The model is capable of modeling both wave diffraction around breakwaters and reflection effects with multiple wave inputs. For this study, PHAROS version 9.10 was used for all model runs.

5.1. Model Setup

The PHAROS model has an easy to use graphical interface. In conjunction with the users manual, setting up a model within PHAROS is not very difficult. More information on how the PHAROS model is set up beyond the purpose of this report can be found in the user manual.

5.1.1. Layout

As stated previous, PHAROS requires boundary conditions along the entire domain. There are only three options for the boundary elements of the grid in PHAROS: wave entrance, reflection boundary, or transmission boundary. This means that coastlines and imaginary exit boundaries must be specified as reflection boundaries. To remove

effects from reflection, a zero reflection coefficient can be specified. For a reflection boundary to perform accurately, the correct incident angle must be specified. Estimating the incident angle can be tricky when diffraction effects change the travel angle. The best way to combat this is to break the boundary into segments based on the angle at which the wave will impact. However, when the travel angles in an area of interest are very diverse, either due to diffraction effects or directional spreading, the correct angles of incidence can be very hard to specify.

Computational grids were generated using both the semi-infinite and breakwater gap layouts. To avoid the necessary input of a reflection angle along the 'wave exit' boundary, the leeside of the gap model layout was constructed as a semi-circle. As the waves through a gap spread radially, this ensure all exiting waves would collide with the boundary at near normal. Layouts for the semi-infinite breakwater remained rectangular and multiple iterations were carried out to ensure the correct reflection angles for the boundary were chosen. However, this does remain a possible source of error.

5.1.2. Wave Characteristics

PHAROS has the ability to model both regular and irregular waves with variable directional and frequency spreading parameters. For this study, three types of waves were modeled within PHAROS: regular waves, narrow banded irregular waves (swell waves), and broad banded irregular waves (wind waves). These wave types were modeled through three computation modules offered in the PHAROS model. They are named 'long crested', 'directional spreading', and 'spectral'. For additional information on each module and its capabilities beyond those used in this study, the reader is referred to the PHAROS user manual.

Long Crested
The long crested wave option models simple regular waves. Regular waves are the basis of complex wave fields. The outputs from long crested model runs will be compared to Wiegel's analytical diffraction diagrams in Chapter 7.

Directional Spreading
The directional spreading option allows the user to input a single wave height over a range of directions. The user must specify directional intervals which properly represent the distribution function. To aid the user in specifying the correct number of directional intervals, PHAROS has a built in distribution function graphic which shows the weighted factors for each direction. A correctly defined distribution spectrum should have descending weighting factors from the primary direction of propagation and cover the entire distribution.

The distribution shape is based on the specification of the power *m* within the directional spreading function. This variable controls the width of the distribution based on the directional spreading. A list of these values can be found in the PHAROS manual. For the broad spectrum wind waves with directional spreading around 30°, an *m* value of 2 was used. For the narrow spectrum swell waves with directional spreading around 10°, an *m* value of 30 was used.

As each direction represents a weighted portion of the spectrum, it is best to make the directional intervals as small as possible. However, this causes a long computation time as the PHAROS program will perform separate, long crested calculations for each of the directions specified. Therefore, for the narrow spectrum 'swell' waves, a resolution of 5° increments was chosen. Since the broad spectrum 'wind' waves cover a larger range of directions, the spacing intervals were increased to 10°. Figure 5-1 is a copy of the distribution function graphic used in this study for broad spectrum waves.

The full range of entrance directions used are presented in Table 5-1.

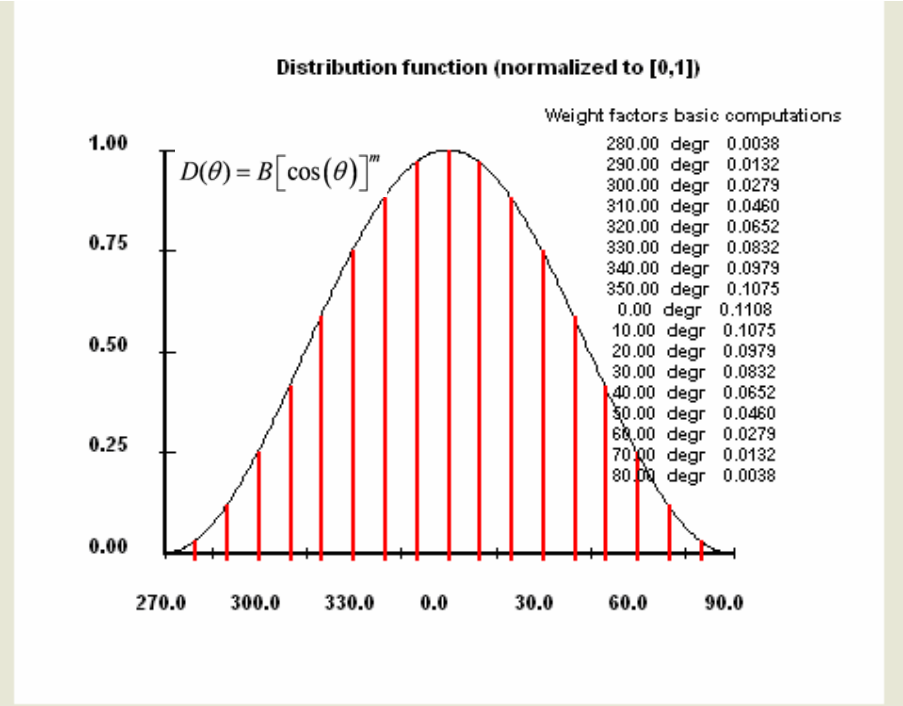

Figure 5-1: Direction Spreading Representation In PHAROS

Spectral

True sea waves consist of both directional and frequency spreading. Both of these processes are captured in the spectral modeling option in PHAROS. The only difference between the directional spreading module and the spectral module is the inclusion of frequency spreading. Therefore, for this study, the directional inputs used in the direction spreading modeling were copied into the spectral module.

It should be noted that spectral model runs require long computational time dependent on the number of directions and frequencies specified (i.e. total number of runs will be the number of directions multiplied by the number of frequencies.) An agreement should be made between proper spectrum representation, allowable computation time, and available memory.

PHAROS uses the Jonswap frequency spectrum for spectral modeling. Its peakedness is determined by the peak enhancement factor, γ, value. From literature, this value was chosen as γ=3.3 for fully developed wind seas and γ=10 for swell-type seas.

The spectral module also includes a distribution viewer to assist the user in choosing representative discrete wave periods. This viewer depicts the user entered directional intervals in relation to the spectrum distribution. This viewer also shows the user that the information is entered and read properly by the system.

It was suggested that to properly define the frequency spectrum (and avoid errors created by poor representation) at least 5 discrete wave periods should be chosen. These wave periods can easily be chosen by consulting the cumulative Jonswap spectrum option included in the viewer. Here, the wave periods associated with percentage representations of the spectrum are provided based on the user specified peak frequency and the Jonswap peakedness parameter. Figure 5-2 shows and example of the broad wind-type spectrum and the five discrete wave periods used to accurately represent this spectrum.

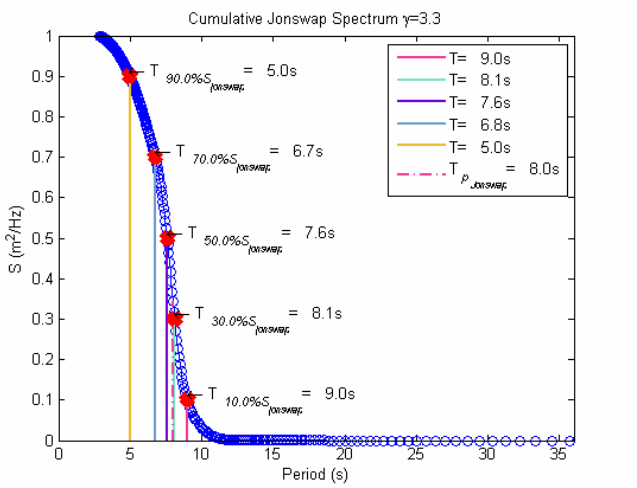

Figure 5-2: Cumulative Jonswap Spectrum in PHAROS

Table 5-1 provides all of the inputs used for the modeling performed in PHAROS.

Table 5-1: PHAROS Model Inputs

			General Parameters					Entrance Parameters		Directional Spread/Spectral Parameters		
Wave Type	PHAROS Run Type	Repres-entation	Hs (m)	Tp (s)	Main Dir	Discrete Wave Periods (s)		Incident Wave Directions	Degree Increments	Directional Spreading Function [m]	Directional Spreading	Jonswap Spectrum Gamma Peakedness
						Frequency Range (90% to 10%)	Number of Frequencies					
Regular	Long-Crested	Regular	1	8	0°	-	-	0°	-	-	-	-
Irregular	Directional	Swell	1	8	0°	-	-	-25° to 25°	5°	30	10.2°	-
	Spreading	Wind	1	8	0°	-	-	-80° to 80°	10°	2	31.5°	-
Irregular	Spectral	Swell	1	8	0°	6.1 to 8.7	5	-25° to 25°	5°	30	10.2°	10
		Wind	1	8	0°	5.0 to 9.0	5	-80° to 80°	10°	2	31.5°	3.3

5.1.3. PHAROS Limitations to Study

Although the PHAROS modeling system is highly efficient at modeling diffraction, it does posses some limitations which are prohibitive from emulating a true situation. These limitations are listed here as they can be sources for error. However, for the scope of this work, their hindering effect was minimal.

Unlike the other model system chosen for this study, PHAROS does not include an input for the energy source from wind. This is typical for mild-slope phase-resolving models though its absence could cause incorrect estimations within large scale harbors. Additional energy supply from wind sources would push the diffracted wave energy farther into the harbor allowing larger diffraction coefficients to exists further behind the breakwater(s).

Another issue which may be a source for error was the difficulty of specifying absorbent boundaries. As the boundary requires an impact angle to calculate the degree of reflection, false estimations could result in incorrect reflection of wave energy. This issue was solved in the breakwater gap model runs by creating a semi circular rear boundary as the wave trains will tend to spread circularly through the gap. However, this option could not be used in modeling of the semi-infinite breakwater. In the end, the boundary in the lee adjacent to the breakwater was separated into segments and reflective angles were specified for each segment for each regular wave. This became a long, iterative process for directionally spread wave types. Review of the semi-infinite model output found in the appendix show some reflective error in the bottom right corner where a reflective boundary meets a wave entrance boundary. After many iterations, this small error was deemed unavoidable.

5.2. Interpretation of Model Results

This section contains observations and discussions of the PHAROS model outputs. Comparisons between this model and diffraction theory or the SWAN modeling results is discussed in Chapter 7. Additional PHAROS model outputs that are not specifically shown in this section can be found in the appendix.

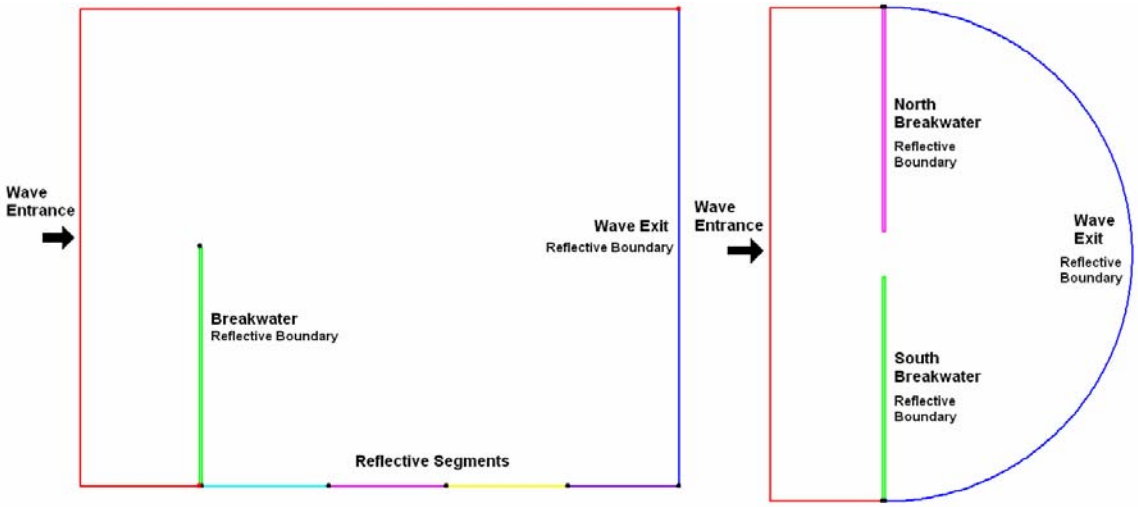

Figure 5-3: PHAROS model Layouts and Boundary Conditions

5.2.1. Reflection Effects

Reflection coefficients for the breakwater(s) were adjusted to test the contribution of structure reflection to the overall diffraction patterns. This test was conducted for both normal incident waves and obliquely incident waves. The results of normally incident waves against a semi-infinite breakwater are presented in Figure 5-4. Each column represents a different wave type and each row represents the height difference between the titled reflections. This type of figure was created by the subtraction of two separate computations with varied breakwater reflection coefficients. In this figure, it is shown that the difference between modeling with and without reflection is concentrated at the breakwater tips, and along the leeside of the breakwater. However, this plot difference shows more than just effects related to the reflection of the breakwater's front face. The absorption by the back of the breakwater is not directly related to the reflected wave energy that is diffracted from the front of the breakwater. These effects are also included in this difference plot and the difference can not be attributed to reflection off the front of the breakwater alone. Irregardless, these differences can be expected to occur when breakwaters are constructed uniformly with absorbent materials verses reflective walls.

It is also shown in this figure that for semi-infinite breakwater layouts, the concentration of reflection related wave height is located directly behind the length of the breakwater. In fact, in all wave cases, the area within three wavelength of the lee of the breakwater is affected by at least an additional $K'_{reflection} = 0.03$ which can be attributed to reflection off the front of the breakwater and absorption by the leeside. Also, the area of influence from reflection is greater for regular and narrow directionally spread waves than for broad directionally spread waves.

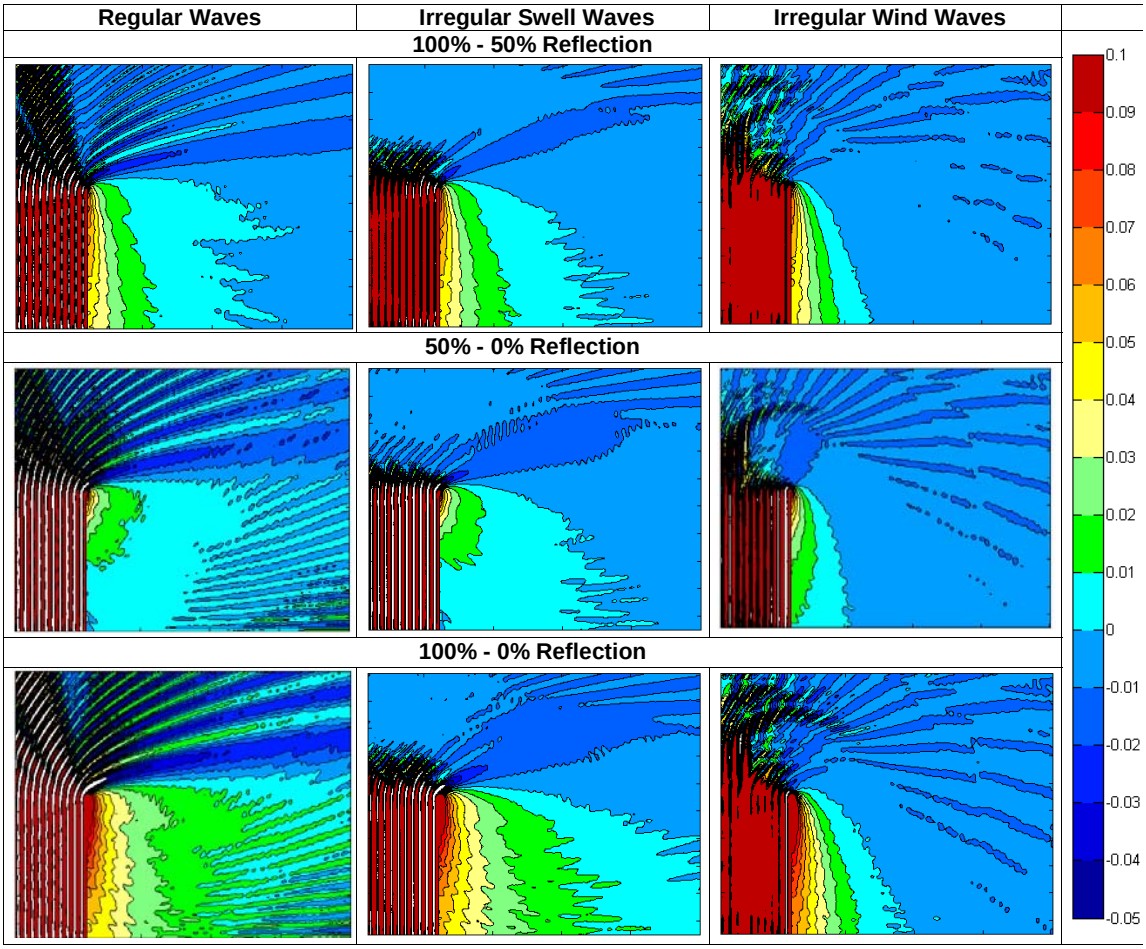

Figure 5-4: Portion of Diffraction Coefficient, K', attributed to Reflection

5.2.2. Composite Breakwaters

Currently, available diffraction diagrams and theory do not discuss the changes to diffraction patterns based on non-uniform breakwaters. As composite type breakwaters are occasionally used in practice, their analysis is of importance. In theory, energy dissipation by an absorbent uniform breakwater should occur on both the front and leesides. As the incident and reflected wave energy and associated scatter bends around the breakwater tip, it should dissipate along the absorbent material on the leeside of the breakwater. Figure 5-5 examines these effects as modeled by PHAROS for 'swell-type' waves at a propagation angle of 90° through a gap B/L =2.

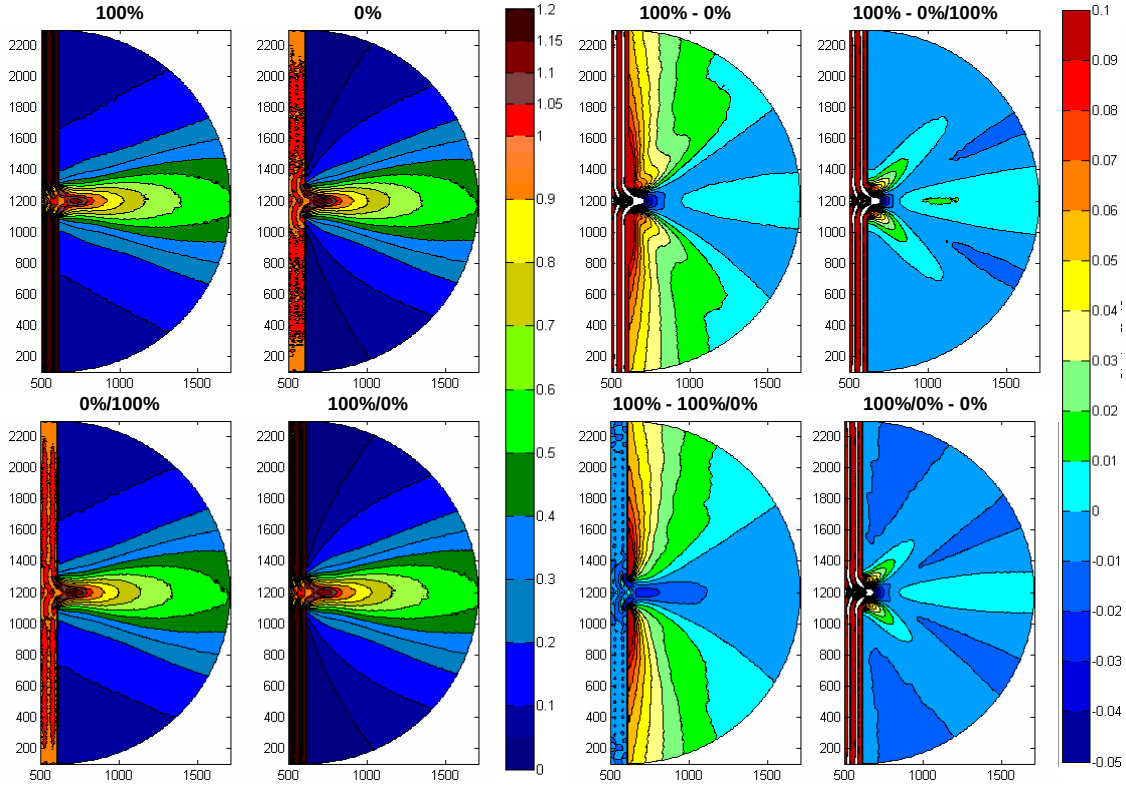

Figure 5-5: Effects related to non-uniform breakwaters, Swell Waves

On the left side of Figure 5-5 four cases of breakwater reflection are shown. Two uniformly constructed breakwaters are represented at the top with extremes of full reflection and full absorption. Below are two composite breakwaters with one side constructed fully reflective and the other is fully absorptive. The first number in the title represents the reflection coefficient of the front face of the breakwater and the second number represents the reflection coefficient of the leeside. On the right side of the figure, the subtracted differences between these computations is represented. Cases of higher reflective front cases were always used as the dominate in subtraction as shown in the titles. Therefore, any darker blue areas, which represent negative values, show concentrations were the less reflective breakwater actually has greater diffracted wave height.

This figures shows a very interesting behavior. First to notice is the cases of '100% - 0%/100%' and '100%/0% - 0%' which related to the amount of reflected energy passing through the gap. Visual, the individually related cases shown on the left side of the graphic look very similar, however, the difference plots show a different story. It is easily seen that the highest concentration of reflection-related wave energy is located at the breakwater tips. However, a majority of the remainder of the graphic is shown as having a negative difference (i.e. the case with full reflection off the front side has lower diffraction wave height at these locations than the case with an absorbent front face.) The reason for these difference, which in some cases can be as great at -0.02 are not immediately known and further investigation into this phenomenon is suggested.

The cases ‘100% - 0%’ and ‘100% - 100%/0%’ relate to the absorption of the leeside of the breakwater due to its reflection coefficient. As expected, this effect is greatest in the area immediately closest to the breakwater and causes very large diffraction coefficient differences. This suggests that the reflective coefficient of the leeside of the breakwater as more influence on the diffraction contours than the reflection of the front face. This implications is of great interest to harbor designers who design the interior of harbors with vertical walls to increase the useable footprint.

An interesting visual observation shows that if the difference cases of ‘100% - 0%/100%’, which shows front face reflection effects, and ‘100% - 100%/0%’, which shows leeside reflection effects are added together, they effectively equal the ‘100% - 0%’ case. This shows that the effects of breakwaters are a combination of both processes.

Figure 5-6 shows the same analysis for wind waves. The findings presented for swell-type waves are also visible for this type of wave however their intensity is lessened. This shows, once again, that reflection effects are greater for narrow directional waves versus broad directional waves.

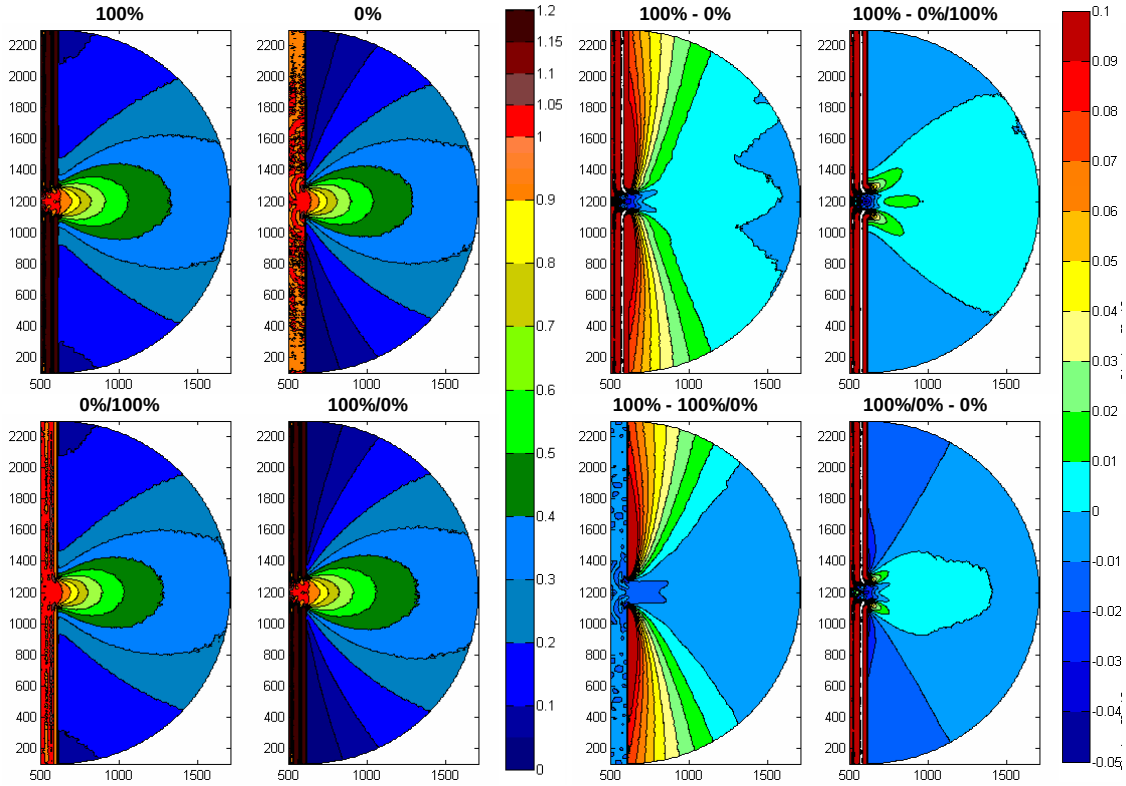

Figure 5-6: Effects related to non-uniform breakwaters, Wind Waves

5.2.3. Angle of incidence

In Chapter 2, the importance of the angle of incidence was discussed. Goda recognized that the direction of greatest penetration by an oblique waves through a gap deviated toward the gap’s normal. Table 2-1 provides some of these angle

deviations based on the degree of directional spreading and incident angle. This theory was tested through the use of PHAROS. In Figure 5-7, a 45° incident angle wave is diffracted through a gap width of B/L = 2 for a swell-type wave (s_{max}=75). From the figure, the deepest penetration angle is approximately 52° from the breakwater. This translates to an angle deviation of approximately 7° which is precisely the amount suggested by Goda. Further angular testing was not performed with PHAROS though improvement and enhancement of Goda's table would be beneficial.

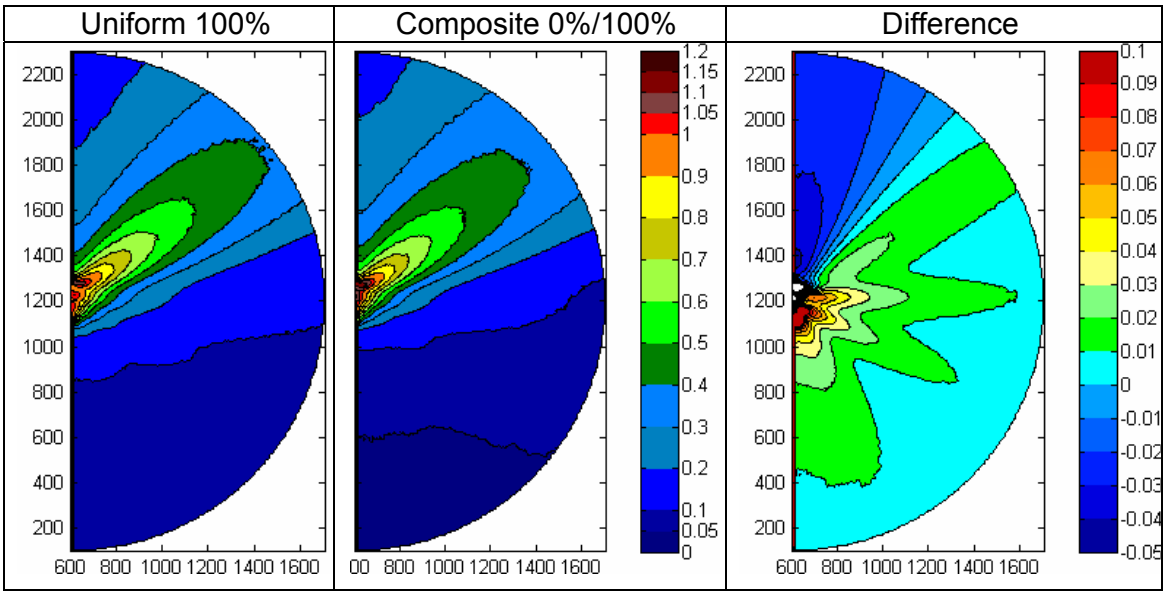

Figure 5-7: Oblique Angle influence on Reflective Effects

Through the combined study of angle of incidence and composite breakwaters, it was found that the angle of incidence also affected the diffraction effects from reflectivity. Visual inspection of normal wave incidence, shown in Figure 5-5, showed little difference between fully reflecting uniform breakwaters and composite breakwaters with fully absorbent front faces and fully reflective leesides. Even their plotted differences showed concentrated energy differences only near the breakwater tips. However, examination of the same cases for oblique angles of 45° revealed a different story. Reflection effects are strongest around the south breakwater and propagate farther within the shadow zone than for the normal incident case. This outcome is suggested by theory in Figure 2-5 developed by Silvester, 1968.

5.2.4. Directional and Frequency Spreading

Figure 5-8 and Figure 5-9 show the effect of the wave spectrum upon the diffraction coefficient. Both figures depict a breakwater gap with a opening of B/L = 2 for normal incident waves with a peak angle of approach of 90°. In Figure 5-8, the effect of directional spreading is examined. The diagram on the left shows regular waves with a single direction of propagation. The diagram on the right depicts irregular waves with 160° of directional spread. The difference between the diffraction patterns is very apparent thus proving that directional spreading is very important in the diffraction of waves.

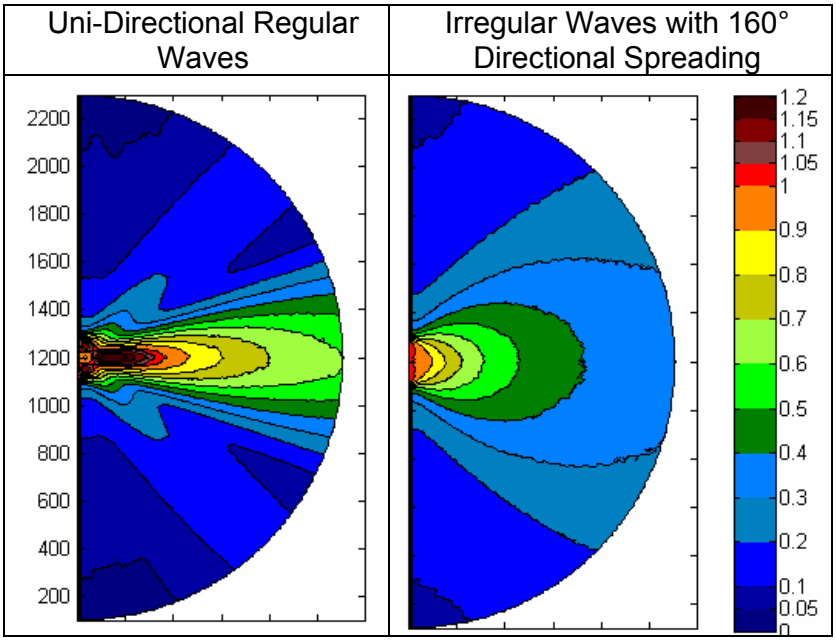

Figure 5-8: Effect of directional spreading

Figure 5-9 focuses on the effect of frequency spreading on wave diffraction. The left diagram shows uni-frequency irregular waves with directional spreading. The center diagram shows irregular waves of multiple frequencies also with directional spreading. The difference is graphed in the right diagrams. These diagrams show the largest difference between the two model runs is roughly 0.015m which could be considered insignificant in terms of the total diffraction coefficient. This indicates that frequency spreading is not very important in the diffraction of random waves. This finding is supported by Goda (1978) whom found in an analytical approach that the inclusion of frequency spreading caused a small scaling difference to the resultant diffraction coefficient diagram.

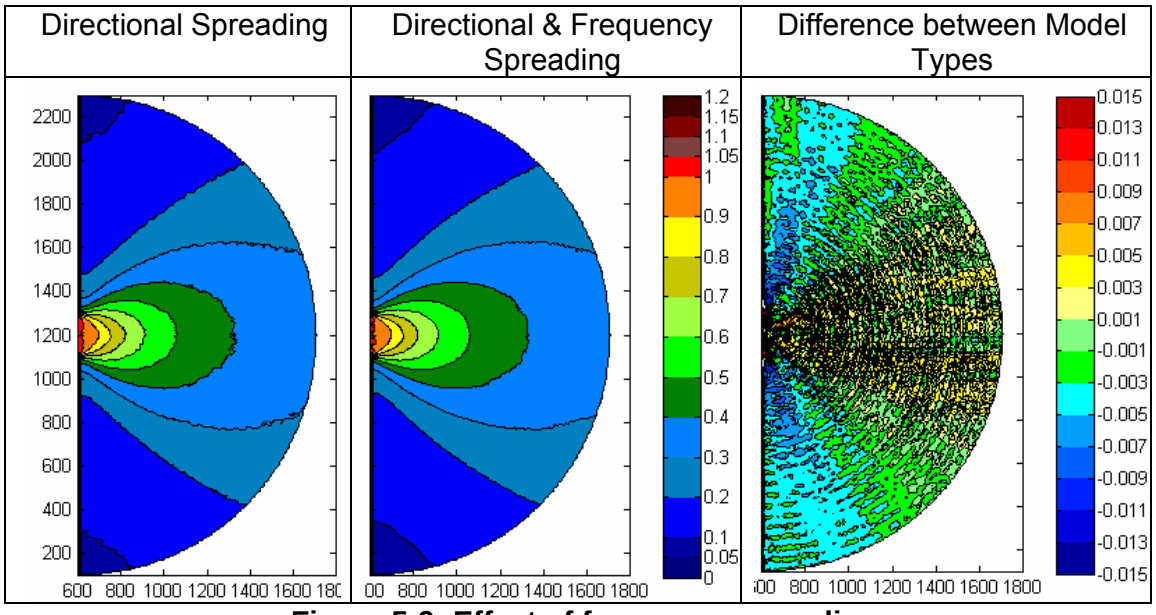

Figure 5-9: Effect of frequency spreading

While spectral modeled waves are arguable more realistic to true wave environments, the time and computer memory required to run such cases is great. For situations where this is not an issue, it is suggested to run spectral models to obtain more precise behavior. However, as this was not the case for this study, and because in this particular case the difference between a computation with and without frequency spreading was shown to be relatively small, further spectral modeling was not performed.

5.2.5. Gap Entrance Amplification

It can be observed for the cases related to narrow directional spreading (regular waves and swell-type irregular waves), the wave energy penetrates more deeply into the breakwater gap than those related to broad directional spreading. This can be seen in Figure 5-8. In addition, the wave energy converges violently in the direction of propagation behind the two breakwaters for wave fields of narrow directional spreading. This is due to the two separate diffraction effects taking place at the tip of both breakwaters. For this reason, harbor designers should be cautious in regions where swell is a regular occurrence. This convergence could cause navigation hazards for vessels traveling between the breakwaters.

5.2.6. Large Gaps

It was formerly believed that designing breakwater gaps larger than B/L = 5 would result in deep wave penetration and that the two breakwaters would react separately as two semi-infinite breakwaters. However, broad range directionally spread waves experience diffraction effects at shorter distances behind the breakwaters. Gaps as large as B/L = 8 still show reasonable diffraction coefficients within the shadow zone. The implications of this is that breakwater geometry should be based on the harder-to-diffract, swell-type waves.

For example: typical wind-type wave - T_{wind}=3s , L_o =14m , Dir = 0°
Swell-type wave - T_{swell}=12s , L_o = 224m , Dir = 0°

Gap Entrance: 112m
B/L_{wind}=8
B/L_{swell}=0.5

Diffraction Coefficient at point 224m behind gap:
K'_{wind}= 0.65
K'_{swell}= 0.5

While the diffraction coefficient for the wind-type waves is greater, swell waves can grow larger in amplitude than wind waves. All of these aspects should be kept in mind when designing breakwater layouts.

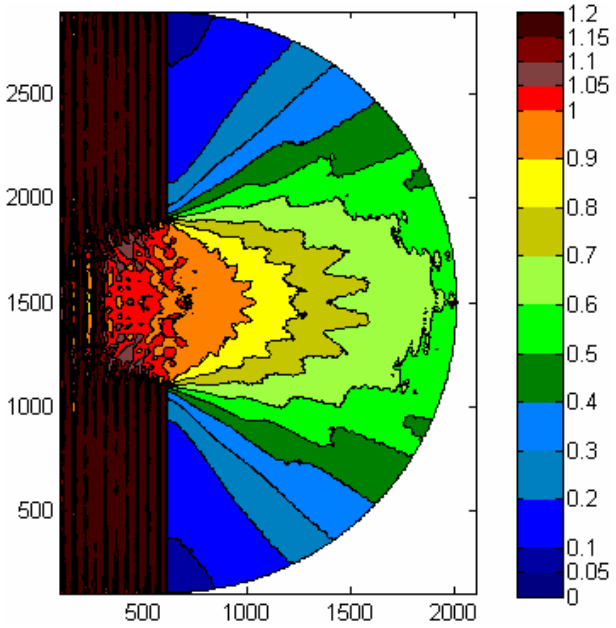

Figure 5-10: Diffraction of B/L = 8 for Broad Spectrum Waves (wind type)

5.2.7. Breakwater Tip Effects

From review of literature, the wave environment near the tip of a breakwater is very dynamic with many processes occurring at the same time. Because of this, modeling of this sensitive area can form interesting results. Figure 5-11 shows three plots created for semi-infinite breakwaters with varied reflection coefficients and normal wave incidence from swell-type waves. As shown, an anomaly in the form of a wave height amplification has occurred near the breakwater tip. This area of increased height is only occasionally represented in published diffraction graphics (not those produced by Goda). Furthermore, it appears to grow in size as the reflection coefficient decreases. The reasons for this are not immediately known and time restrictions did not allow for further research. While it could be the manifestation of a error within the model, its presence was found in an exaggerated form in additional model runs for regular waves. This leads to the understanding that it is somehow related to the degree of directional spreading. Further study into the probability of this reaction as well as breakwater tip dynamics are recommended as further study.

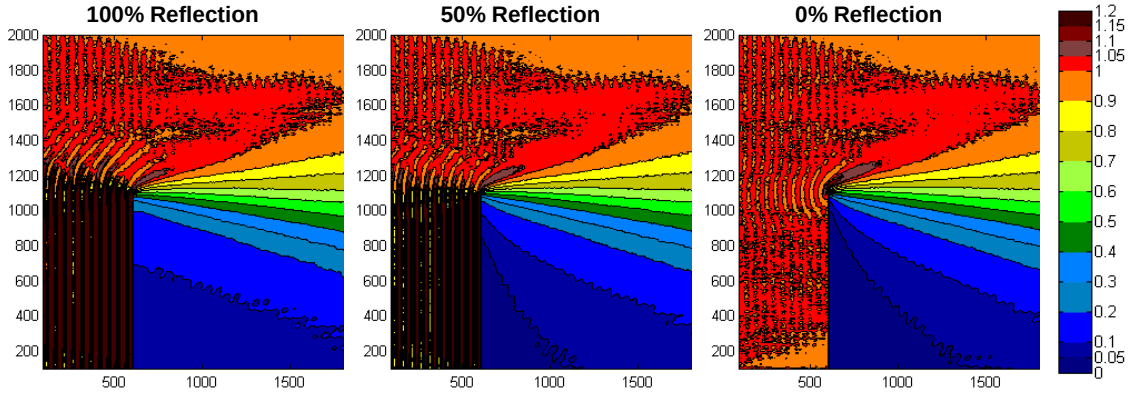

Figure 5-11: Breakwater Tip Enhancement

5.3. Model Evaluation

Overall, PHAROS was very effective in modeling diffraction effects with variable reflection coefficients. The model outputs compared to analytical solutions, which will be discussed more in Chapter 7, appear to have good congruency. Additionally, the model's graphical interface made setting up the model very easy and efficient. The user manual is well written and correspondence from Deltares about problems or bugs was quickly returned and always effective. The only hindrances in using PHAROS for this study were commented on in the model limitations section which did not significantly detract from the study or the findings.

Chapter 6. SWAN

SWAN (Simulating Waves Nearshore) is a universally available free software for the modeling of nearshore waves available for download over the internet. It is being continuously developed through Delft University of Technology and new releases and versions are made available regularly. Many research institutes, consultants, and government agencies worldwide have taken advantage of this model for a variety of purposes.

The SWAN model is a phase-averaged model which uses the wave action balance equation with sources and sinks to compute the evolution of the wave environment in time and space. The action balance equation is given by:

$$\frac{\partial N}{\partial t}+\frac{\partial\left(c_x N\right)}{\partial x}+\frac{\partial\left(c_y N\right)}{\partial y}+\frac{\partial\left(c_\sigma N\right)}{\partial \sigma}+\frac{\partial\left(c_\theta N\right)}{\partial \theta}=\frac{S}{\sigma} \tag{1.14}$$

For more details into SWAN's computation of diffraction, one is referred to SWAN's Scientific/Technical documentation.

SWAN's user manual suggests that diffraction modeling can only be conducted in a restricted sense. To avoid the rather complicated, and time consuming, computing effort of diffraction in arbitrary geophysical conditions, the diffraction in SWAN is handled by a phase-decoupled refraction-diffraction approximation which is described in Holthuijsen (2003). However, this approach does not properly model diffraction characteristics in harbors or in front of reflecting obstacles which are the subjects of interest in this report. In fact, in both the user manual and the technical documentation, it is explicitly stated that diffraction in SWAN should not be used when modeling a harbor study or if the reflection coefficient is significant off an obstacle. Then again, a study performed by Alkyon Hydraulic Consultancy & Research (Enet, 2006) found good agreement between SWAN diffraction outputs and analytical solutions for a semi-infinite breakwater for various wave types.

SWAN was chosen for this study due to its universal availability. Even though user documentation suggests that SWAN is not capable of replicating analytical results due to the manner in which it computes diffraction, an independent study has suggested otherwise. Its capabilities with both diffraction and reflection-driven diffraction are examined within this report. For this study, SWAN version 40.72 was used for all model runs.

6.1. Model Inputs

The SWAN model consists solely of a computational processor. It does not include any pre or post processing systems though they can be (and have been) programmed through mathematical software such as matlab. Delft3D contains pre and post processing graphical interfaces for SWAN but they are not considered part of the

program itself. These graphical interfaces are the only cost to the program. The processor itself is freely available. The code can be programmed to output blocks or tables which can be read by a number of mathematical programs to give pictorial representations without the use of expensive post processing programs. To run the entire model, a user must write an input file with a variety of commands. All commands are listed and described in the SWAN user manual. The input file used in this study is included in the appendix.

6.1.1. Layout

To investigate the performance of SWAN to effectively model diffraction, two simple layouts were chosen: a single semi-infinite breakwater and a breakwater gap. These layouts are typically used in diffraction studies. The bathymetry was specified as flat and deep. Deep water was used to remove the effects associated with refraction and depth related dissipation. Additional dissipation effects such as whitecapping, wind growth, and wave breaking were omitted.

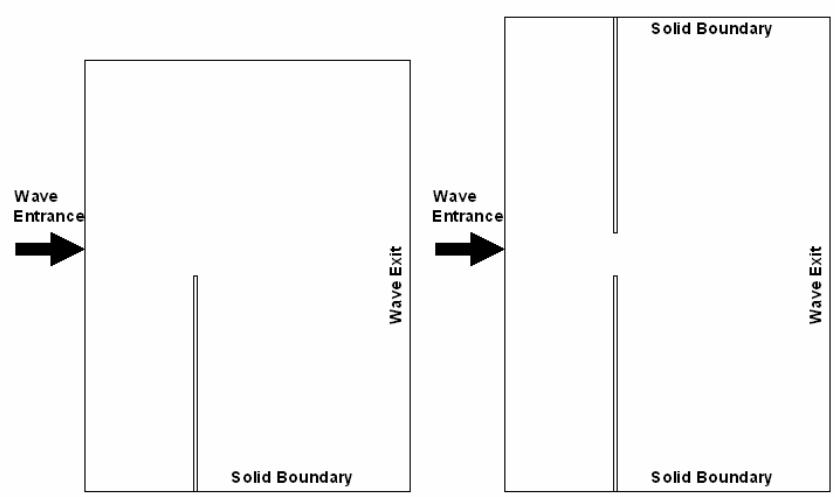

Figure 6-1: SWAN model Layouts and Boundary Conditions

For both semi-infinite and gap breakwater layouts, a simple rectangular grid was specified. To allow the wave environment to normalize before encountering the obstacle, the breakwater was positioned after an open space of five wavelength. As SWAN can run into instability problems with large computational areas, the leeside of the breakwater was restricted to ten wavelengths. The y-axis of the layout varied by the size of the breakwater gap always allowing for ten wavelength long breakwaters on either side of the gap opening (e.g. B/L=2, y-axis=22L). The semi-infinite layout consisted of a single, ten wavelength long breakwater with an open space of ten wavelength above.

Boundaries behind the obstacles, including the wave exit boundary, were removed from the boundary specifications. By removing these edges, SWAN interprets them as either fully absorbing edges or imaginary exit boundaries. In either case, this is an improvement versus the PHAROS model that required a reflective coefficient and

angle of incident for all boundaries that weren't either classified as wave entrances or transmission boundaries.

As SWAN can only handle reflection effects on one side of a single obstacle (breakwater), two separate obstacles on adjacent grid points were specified. Despite possible error introduction at the open-ended tip, this represents a thin breakwater. The reflection coefficients can either be specified as equal on both sides for uniform breakwaters or unmatched for composite-type breakwaters. No transmission effects were analyzed within this study.

SWAN can easily become unstable due to large computational areas or an excessive number of grid points. Therefore, restrictions to the grid layout are described in section 6.2.

6.1.2. Wave Characteristics

SWAN is a fully spectral model and therefore unable to represent regular or monochromatic waves effectively. Therefore, for this study, diffraction within SWAN was researched using narrow banded spectral waves similar to swell-type waves and broad banded spectral waves similar to wind-generated waves.

The universal case used in this study includes the modeling of a wave with a peak period (Tp) of 8s in a water depth of 500m. This translates to a wavelength approximately equal to 100m. The entrance boundaries were specified by a Jonswap-shaped frequency spectrum with peakedness of $\gamma = 3.3$ for wind waves and $\gamma = 10$ for swell waves. The SWAN manual suggests a directional resolution of $\Delta\theta = 10°$ for wind waves to speed up the computation process. However, using a finer resolution will better define the directional spectrum and smooth the output contour lines. The directional resolution for both cases was specified as $\Delta\theta = 2°$. This theory was tested and presented within the model interpretations section 6.2.1.

Table 6-1: SWAN Wave Characteristics Inputs

Name	Spectrum	Directional Spreading [σ]	Directional Resolution [Δθ]	Jonswap Gamma	Frequency Range	
					low (Hz)	high (Hz)
Swell	Narrow	10°	2°	10	0.04	1.00
Wind Waves	Broad	30°	2°	3.3	0.04	1.00

6.2. Sensitivity Analysis of Grid and Model Conditions

Without proper programming, diffraction computations in SWAN often become unstable or fail to converge. To properly program SWAN to model diffraction, multiple time consuming performance checks are required to ensure the model converges and remains stable. These performance checks focus primarily on the computational grid size, spatial resolution, use of smoothing, inclusion of reflection, and the requirement to include diffraction.

A good performance check of SWAN's ability to model diffraction (though without the inclusion of reflection coefficients) was performed and documented by Alkyon (Enet, 2006). Guidance for model construction was taken from this report as well as the model input scripts used and provided by Gerbrant van Vledder.

- The main conclusions of this performance check were (Enet, 2006):

- Stable results can be found when the dimensionless parameter L/Δs is smaller than 3.5;
- Stable results can be found when the size of the computational domain is less than 65 by 65 grid points;
- Too much smoothing degrades the results since the diffraction parameter becomes meaningless;
- The effect of directional spreading reduces the importance of diffraction;
- The practical limits are independent of water depth

However, Alkyon's report was created testing the performance of the 40.51 version of SWAN. Since this report utilizes the most up-to-date version of SWAN, version 40.72, a quick sensitivity study of these findings was performed.

While the Alkyon study was used as a benchmark for the modeling within this report, a few deviations from their programming was made to accommodate the purpose of this study. The deviations recognized in the programming included:

- Water depth used within Alkyon report was specified as 10m which represents 'transitional' theory. Water depth for this study is 500m which represents "deep water" theory.
- Breakwaters within Alkyon report are specified as singular and non-reflective. Breakwaters in this study have variable reflective properties.
- Spectral direction in the Alkyon study are specified as covering a 'Sector' from 270° to 90°. For reflective structures in SWAN, full 'Circle' spectral directions must be specified.
- In the Alkyon study, a narrow banded Gaussian-shaped frequency spectrum with a width of 0.01 Hz was used for all wave types irregardless of directional spreading. To remain consistent with previous modeling and analytical methodology, both swell and wind waves were defined with a Jonswap-shaped spectrum and representative peakedness parameters.
- In the Alkyon study, the only process which is excluded in the programming is quadruplet interactions. To ensure dissipation effects were omitted, this study additionally excluded whitecapping, breaking, and wind growth.

6.2.1. Directional Resolution

Unlike the PHAROS modeling system, SWAN includes a simple input parameter which specifies the directional resolution within the computational grid. In PHAROS, the user must manually enter directional components and check if they correctly represent the distribution function. With SWAN, the user can easily specify the

directional resolution with a singular data entry which represents the number of directional segments calculated over the domain.

In PHAROS, by reducing the directional resolution and increasing the number of directions studied, the computation time increases. Because of this, coarse resolutions of $\Delta\theta = 5°$ for swell-type waves and $\Delta\theta = 10°$ for wind waves were used. However, it was suggested that using a finer resolution would create a cleaner output.

The SWAN manual suggests using a directional resolution of $\Delta\theta = 2°$ for swell-type waves with $\sigma = 10°$ and $\Delta\theta = 10°$ for wind waves with $\sigma = 30°$. The suggested wind wave resolution matches that used in PHAROS. However, the outputs created in PHAROS with this resolution showed wavy lines instead of smooth contours. Since specifying the directional resolution within SWAN is very easy and the model runs more quickly than PHAROS, a quick sensitivity was performed on the directional resolution of wind waves.

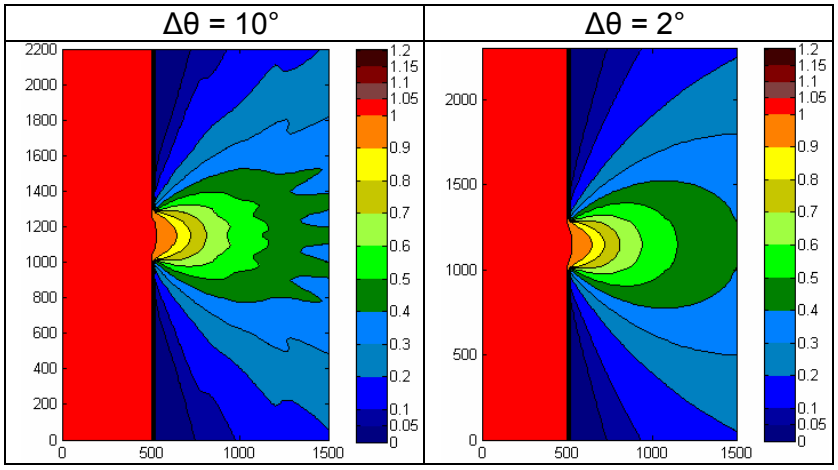

Figure 6-2: Directional Resolution Comparison in SWAN

It can be easily observed in Figure 6-2 that the finer directional resolution of $\Delta\theta = 2°$ smoothes out the representative contours lines depicting the diffraction coefficient. Because the difference in computation time was determined to be acceptable, all further computations of wind waves used $\Delta\theta = 2°$.

6.2.2. Spatial Resolution

SWAN computations of diffraction can easily become unstable if the grid is too fine. A quick study of swell waves revealed the model was stable for a spatial resolution of $L/\Delta s = 4$ grid points per wavelength. At $L/\Delta s = 5$, an instability form near the breakwater tip.

As previously discussed, to properly define a wavelength and retain its properties, eight points along that wavelength are needed. This suggests that due to spatial restrictions, errors may be introduced from the lack of clear wave definition.

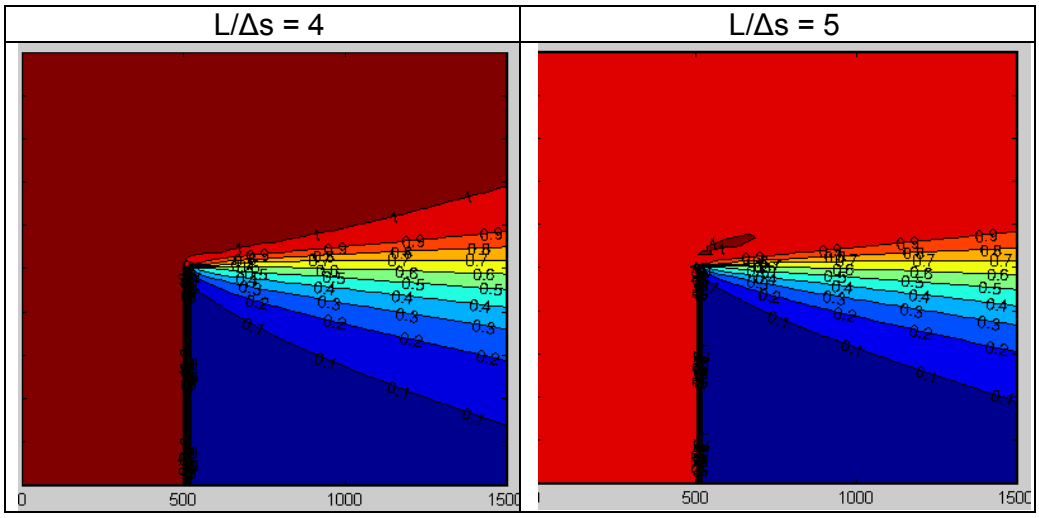

Figure 6-3: Spatial Resolution Check, Swell waves

6.2.3. Computational Area

The Alkyon study concluded that the computational area did not have limitation on the computational area for waves with directional spreading greater than σ = 10° (swell-type waves). As both waves analyzed with this model have equal to or greater directional spreading than this amount, the original layout description given in section 6.1.1 does not require alteration.

6.2.4. Smoothing

By including smoothing in the commands, all grid points exchange energy with their neighbors. This removes any wiggles in geographic space. The Alkyon report found that smoothing was only beneficial for incident waves with large directional spreading.

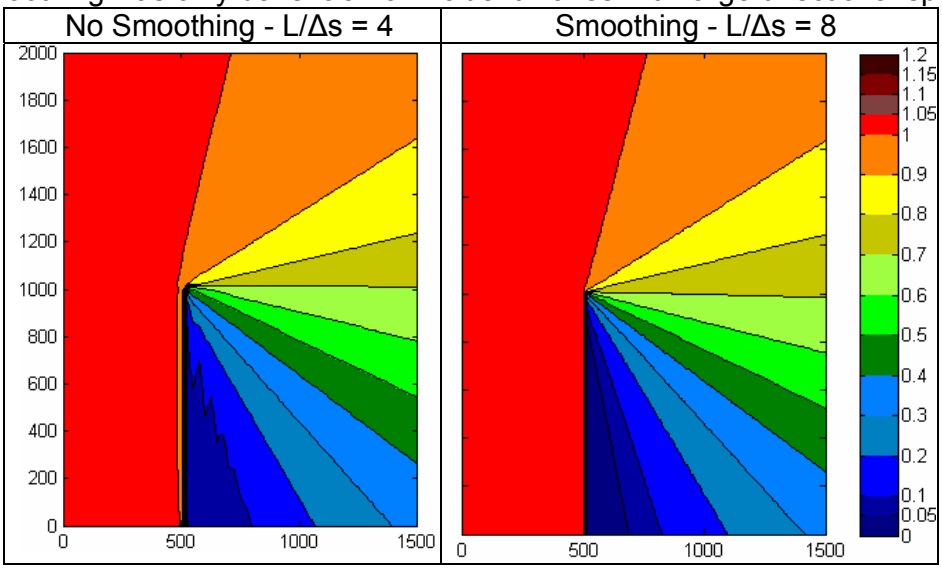

Figure 6-4: Use of Smoothing

The addition of smoothing enables stable results with a finer spatial resolution. For these reasons, smoothing was added to the wind wave models. The result of this smoothing and grid refinement is shown above.

While it was found that the wind wave case remained stable with spatial refinement at the desired L/Δs = 8, the difference between computed diffraction values with L/Δs = 5 was very small. In the interest of shortening computation time, the wind waves were computed with L/Δs = 5.

6.2.5. Diffraction & Obstacle Reflection

The argument as to whether to include diffraction within the commands is often debated. The Alkyon study concluded that for cases with narrow directional spectra, diffraction concluded in more realistic results when turned on. Wide directional spectra, on the other hand, perform better in the area away from the breakwater with the diffraction turned off. However, in the area nearest the leeside of the breakwater, the wide directional spectra performed better with the inclusion of diffraction.

It is the opinion of the author that the procedure suggested within the Alkyon report is somewhat questionable with many variables altered between the comparison cases which does not aid in pinpointing where the difference is occurring. It is obvious that further investigation should be carried out on this topic.

Within this study, many iterative processes were made to obtain the most realistic representation of breakwater diffraction around a reflective breakwater. These iterative processes included variations of obstacle specifications, reflective coefficients, smoothing functions, and inclusion of diffraction. Additionally, each of these variables require different values between modeling wind waves and swell waves.

Theory states that in addition to reflected waves off the front face of the breakwater, associated scatter also forms. In attempt to replicate this effect in SWAN, the default reflection processes which indicates the reflection angle to be equal to the incident angle was changed to diffused reflection. This implies that in addition to the primary reflected wave, the effects are scattered over the reflection angle.

Figure 6-5 shows the diffraction coefficient diagram and normalized 2D spectral plots at points located on either side of a semi-infinite breakwater for wind waves. The titles correspond to the inclusion of diffraction as well as whether the reflection coefficient was specified as 100% (‘ON”) or 0% (‘OFF’). These spectral plots tell an interesting story about what is occurring behind the breakwater.

When diffraction is turned off, as is shown in Case C., the wave spectrum on the leeside of the breakwater travels parallel to the breakwater and is not influenced by its reflective status. Conversely, when the diffraction is turned on, as in Cases A. and B., the wave spectrum passes the tip and continues to diffract around until the wave ray reverses direction back toward the breakwater. It then is either reflected or absorbed based on the reflection coefficient. This case most closely represents diffraction characteristics. It appears from this analysis that by removing diffraction from the computation, the wave energy does not change direction against the leeside of the breakwater as expected.

When reflection effects are turned on, reflected scatter can be seen in the normalized 2D spectrum at locations (460,1200) and (460,1500). This suggests that SWAN is properly modeling the reflective scatter property off the front obstacle.

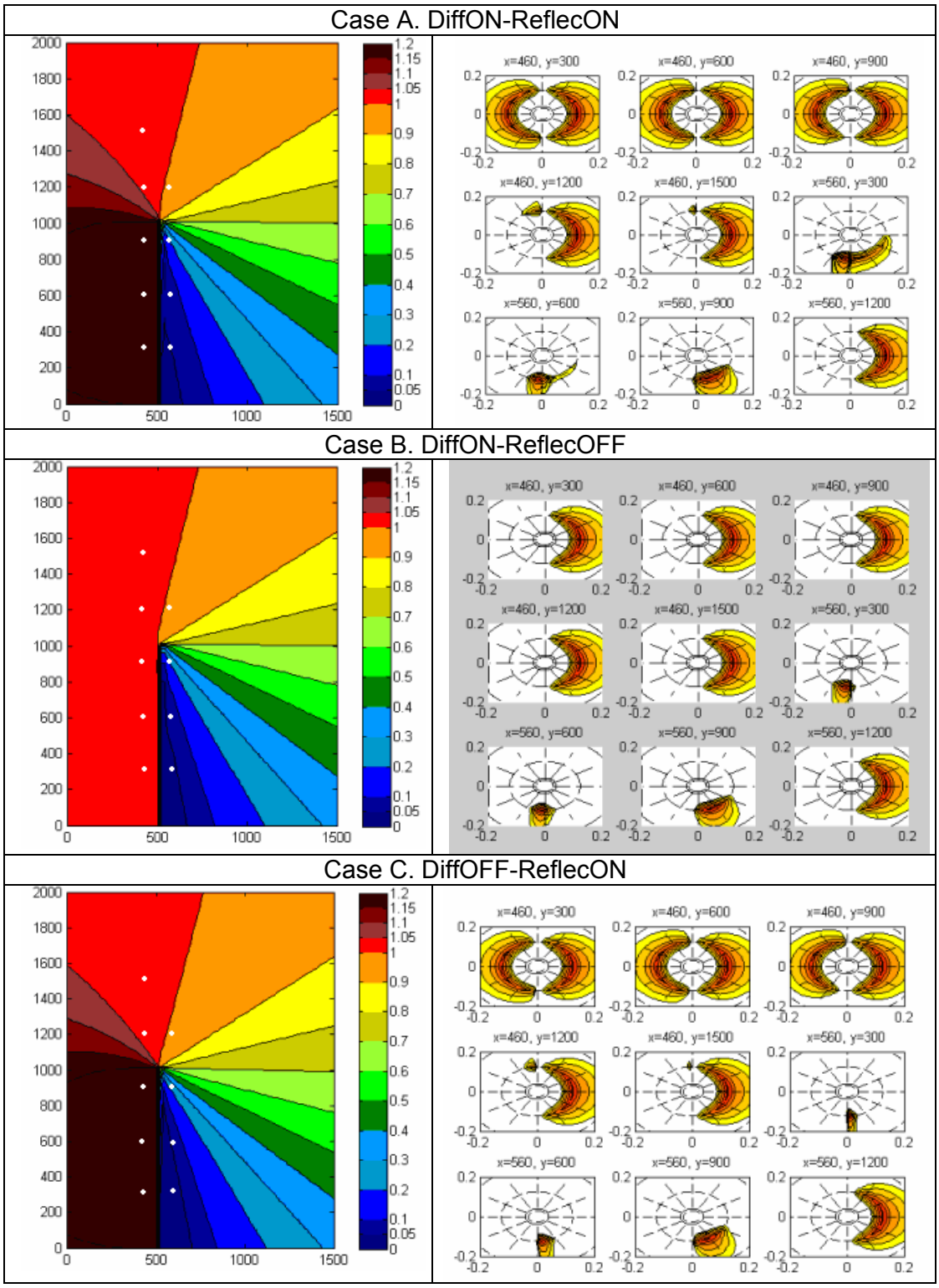

Figure 6-5: Study of Reflection within SWAN

6.2.6. Final Model Setup

The final model setup based on the performance check conducted for version 40.72 of SWAN and used within this study is detailed in the table below.

Table 6-2: SWAN Final Layout Inputs

		Grid Size			Computational Area			
Layout	Wave Type	x-axis (L)	y-axis (L)	Spatial Resolution	x-axis (grid pnts)	y-axis (grid pnts)	Diffraction	Smoothing
Semi - Infinite	Swell	15	20	4	60	80	ON	OFF
Semi - Infinite	Wind	15	20	5	75	100	OFF	ON
Gap = 1L	Swell	15	21	4	60	84	ON	OFF
Gap = 1L	Wind	15	21	5	75	105	OFF	ON
Gap = 2L	Swell	15	22	4	60	88	ON	OFF
Gap = 2L	Wind	15	22	5	75	110	OFF	ON
Gap = 4L	Swell	15	24	4	60	96	ON	OFF
Gap = 4L	Wind	15	24	5	75	120	OFF	ON

6.3. SWAN Limitations to Study

As a phase-averaged model, some limitations to the study of diffraction and reflection arise when using SWAN. Typically, the use of phase-averaged models for harbor modeling has led to erroneous results. Beyond the instability limitations described in the previous section, additional limitations were encountered that proved to be prohibitive in this study.

SWAN is a fully spectral model. Because of this, modeling simple regular waves was not possible. SWAN is, however, capable of modeling uni-directional irregular waves. As PHAROS was not capable of modeling this wave type as well as the lack of theory pertaining to these waves, they were not used within this study. Therefore, the only two wave types modeled by SWAN included the narrow directionally spread swell waves and the broad directional spread wind waves.

Due to the spatial resolution restrictions in SWAN, modeling breakwater gaps smaller than 2L resulted in unstable or non-converging runs. As stated previous, typical model simulations suggest a minimum of 8 points per wavelength. However, because SWAN is a phase-averaged model which accommodates only weak variations over the scale of a wavelength, it becomes unstable when the resolution is too fine. Unfortunately, this restriction also causes significant instability problems with gap openings below two wavelength. For broad directional spectrum wind waves, as stated earlier, the spatial resolution could increase up to at least $L/\Delta s = 8$ by turning off diffraction effects and add in smoothing. By doing this, some of the instability shown in the 'wind' figures below was removed. However, this is not an option for narrow directional spectrum swell waves.

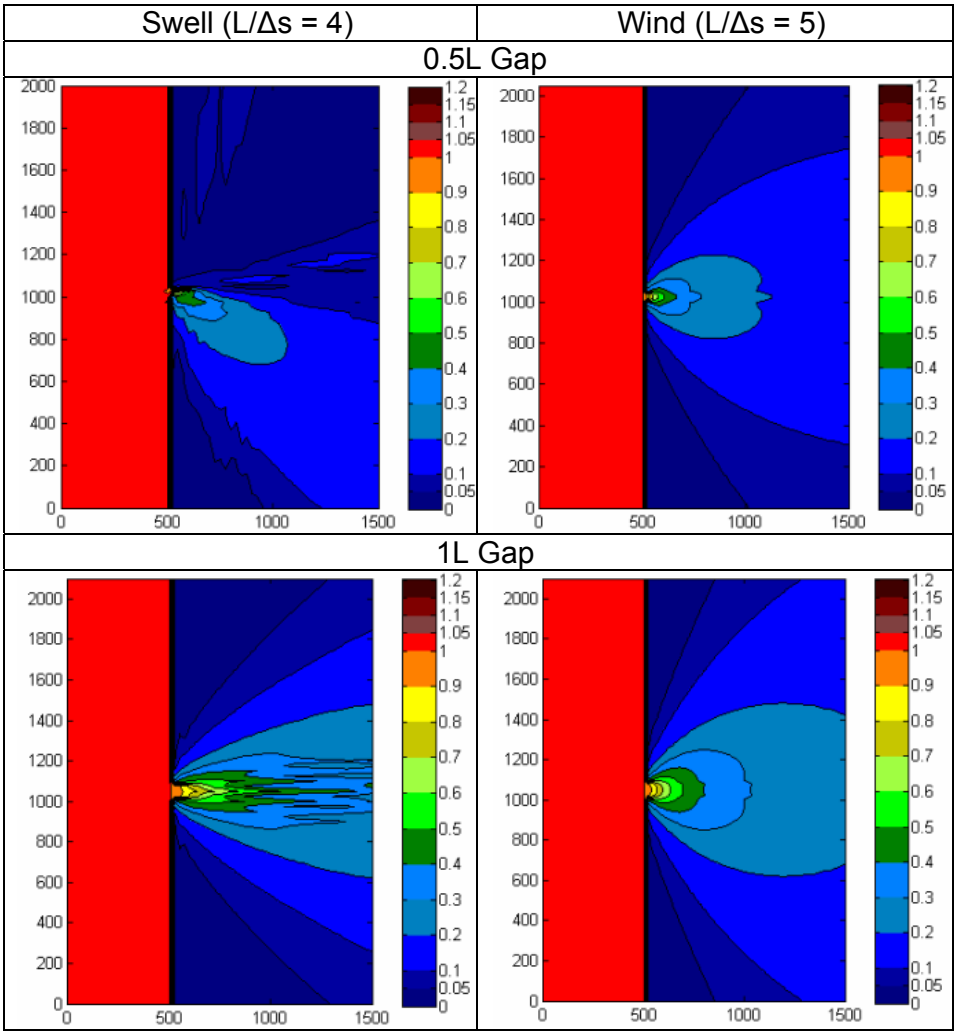

Figure 6-6: Instability of Small Gap Sizes Within SWAN

6.4. Interpretation of SWAN Reflection

From the analytical understanding of diffraction, the reflection effects are strongest near the breakwater tip and along the leeside of the breakwater. A visual inspection of the cases presented in Figure 6-5 does not reveal any significant difference in the breakwater lee are between Case A, which is fully reflective, and Case B, which is fully absorbent. A difference plot between the two confirms this assumption shown in Figure 6-7. Also in this figure, a closer inspection around the tip shows inconsistencies. From the input commands, the obstacles have been positioned on adjacent grid points at x=500 and x=520 though tip effects appear to take place beyond the obstacle edge. The reasons for this remain unknown.

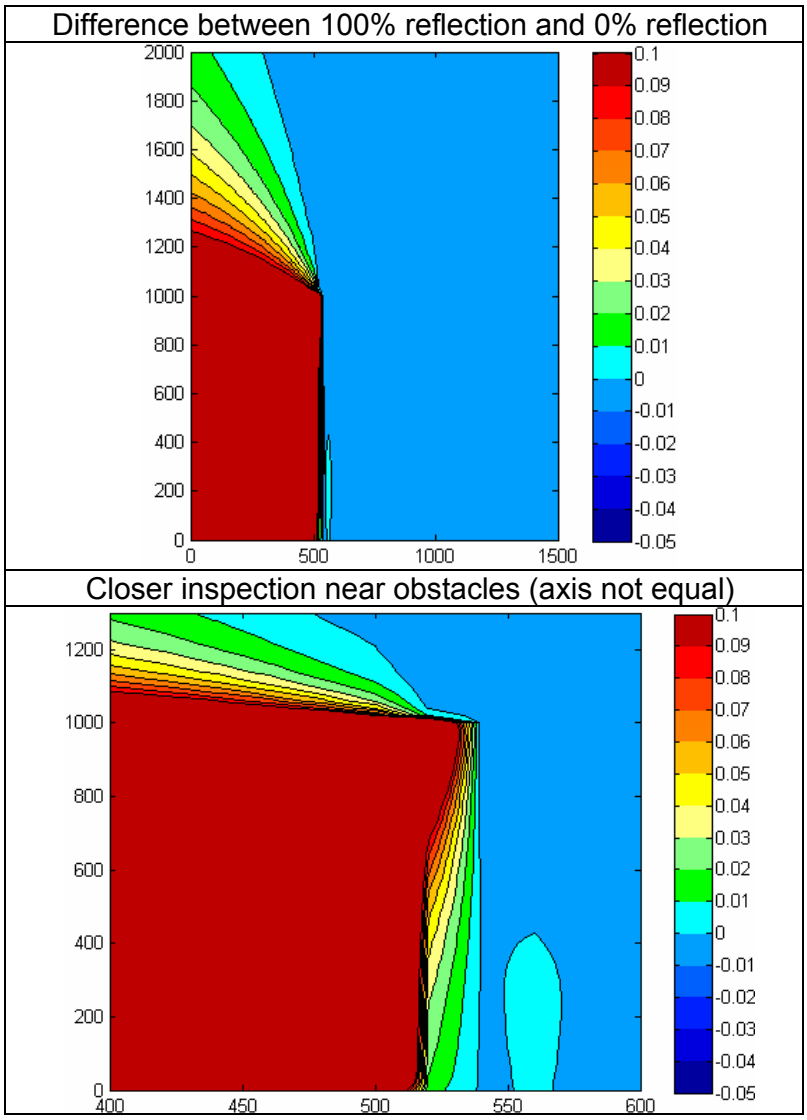

Figure 6-7: Difference of wave height due to reflection coefficients in SWAN

As discussed in section 6.2, the use of reflection on breakwaters coupled with diffraction is tricky in SWAN. Within this study, determining the proper setup to replicate diffraction effects with reflection was not achieved. The expected reflection related diffraction effects are not apparent within any of the model outputs. As such, and after extensive study, the attempt to model and analyze diffraction effects due to variable reflection coefficients in SWAN was abandoned. The diffraction approximation of the model without reflection will be compared with analytical results.

Additional study into this topic is recommended to improve the criteria for use of reflective structures for diffraction purposes within SWAN. This may only be attained with further programming and/or refining of the model itself.

6.5. Model Evaluation

Because of the lack of a preprocessing interface, SWAN is not a 'user friendly' program. The proper use of this program requires extensive reference to the user manual as well as a user whom is willing to perform numerous iterations to check and eliminate sensitivities. Occasionally, these sensitivities can lead to instabilities which are unavoidable in harbor modeling.

For this study however, SWAN performed surprisingly well for a process its user manual states it can not perform. Of course, this statement comes with restrictions. The attempted modeling of breakwater reflection in relation to diffraction proved unsuccessful as the user manual predicted. However, a visual inspection between the analytically produced diffraction diagrams of Goda and the SWAN output, which is discussed in the following Chapter 7, reveals good congruency for wind waves and reasonable results for swell waves when allowances for the absence of reflection effects are made. Even though the SWAN computational output for diffraction is only an approximation, there is much to learn from its results. While a deviation between analytical diffraction patterns and the SWAN outputs was evident, due to its wide availability, the use of SWAN for diffraction effects in feasibility modeling and even early design stages is encouraged.

There is no doubt that SWAN, to an inexperienced user, is much more difficult to operate than other commercially available modeling programs with pre- and post-processing. With that in mind, SWAN is universally available to everyone without cost and is capable of modeling a variety of subjects with good accuracy. Taking time to learn the model and perform sensitivity runs to hone the model are well worth the effort.

Chapter 7. Comparison of Theory and Model Results

Before the analyzes of reflection effects on diffraction could be performed, the selected models were tested with a set of criteria similar to those used to create the analytical diffraction diagrams of Wiegel and Goda. In the case of SWAN, this calibration study was also performed to evaluate the models ability to perform diffraction behind an obstacle with varied wave characteristics.

The universal wave criteria chosen at the beginning of this study was specifically selected to allow for easy transition into dimensionless diffraction diagrams. A wave height of 1m was chosen so that the modeled diffracted wave heights would also represent the dimensionless diffraction coefficient, $K' = H_d/H_i$. Additionally, a peak period of 8s translates to a deepwater wavelength of 100m. These values were used when scaling the original model outputs to the dimensionless diffraction pattern diagrams.

A more thorough examination between the model generated diffraction graphics and the analytical diagrams could be achieved by recreating the analytical diagrams through the calculations used to create them. This, however, was not performed as it was not the main focus of this study. Therefore, only visual inspections were performed.

As a note, care should be taken when using the diffraction diagrams published by Goda. In them, he references his axes for the semi-infinite layout in terms of wavelength. However, in his breakwater gap layouts, he references his axes in terms of gap width. As both these conventions are dimensionless, this change does not effect the layout of the diffraction pattern though it can cause confusion for the user. For this study, all layouts and associated diffraction patterns are based on dimensions of wavelength.

7.1. Regular Wave Theory

Diffracted regular waves were first plotted by Wiegel. These waves represent only one part of a real wave field and rarely exist in nature. As it has already been discussed, the use of regular wave diffraction diagrams for irregular seas can cause large errors. Surprisingly, many engineering publications still reproduce these diagrams without reference to the errors they can cause in real sea applications.

It is understood that the method used by Wiegel to generate his diagrams is derived from methodology published by Carr and Stelzriede (1951). A single wave height, period, and direction of propagation are used to define the wave field. A similar method is performed by the PHAROS model.

Since SWAN is fully a spectral model, it is unable to reproduce regular waves accurately. Therefore, only PHAROS was calibrated for this wave type. As the

breakwaters within Wiegel's diffraction diagram are specified as fully reflective, only the cases with 100% reflection were used in this comparison.

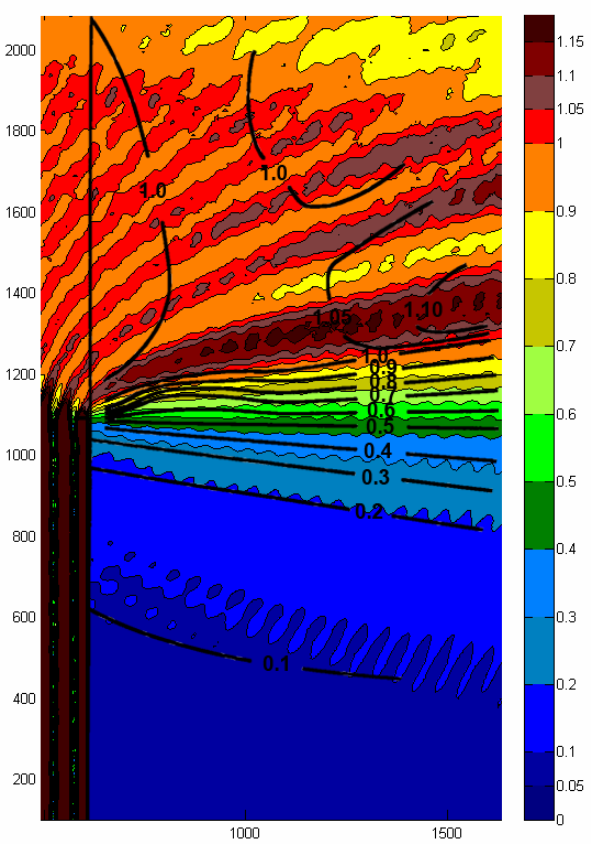

Figure 7-1: PHAROS vs. Regular Wave Theory: Semi-infinite Breakwater

Figure 7-1 shows the relation between Wiegel's 90° (normal to breakwater) diffraction diagram published in 1962. The similarity between the two graphics is very good with only slight deviations below K' = 1.0. Above this threshold, there is no indication of the additional diffraction contours Wiegel indicates.

Figure 7-2 depicts excellent likeness between the analytical diffraction coefficient contours for a breakwater gap by Wiegel and that generated by PHAROS. The largest deviations from theory occurs within the vicinity of breakwater gap entrance. Here, the contours do not match up as well as farther from the breakwaters. However, the deviation is slight and as the diagrams as well as the model are both approximations, insignificant. Though not easily visible in this figure, the highest diffraction coefficient within theory is K' = 1.2 which is also recorded in the analytical diagram.

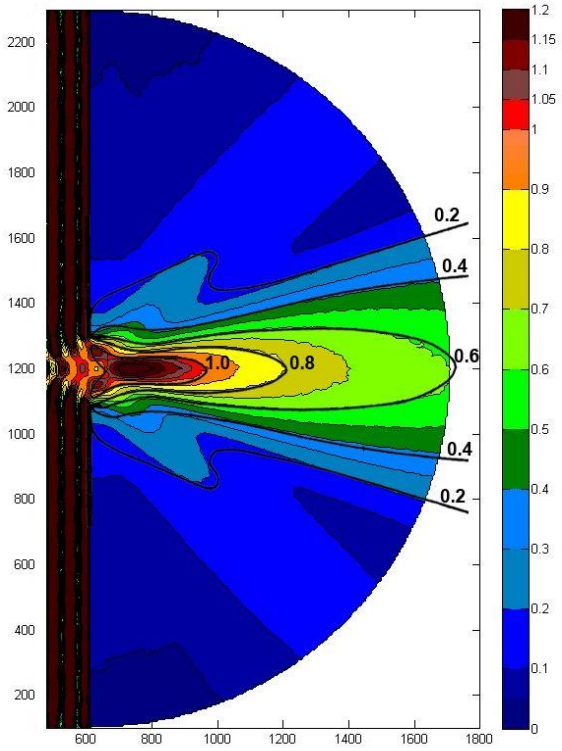

Figure 7-2: PHAROS vs. Regular Wave Theory: Breakwater Gap B/L=2

7.2. Irregular Wave Theory

Though Goda was not the first to implement irregular seas into diffraction theory, he was the first to publish a set of irregular diffraction diagrams in 1978. His diagrams made a differentiation between wind generated waves which have a broad directional spectrum and swell-type waves which are more narrowed. These waves behave very differently than regular waves which is reflected in their diffraction patterns. In the following subsections, comparisons will be made between the models and the analytical diagrams.

7.2.1. Comparison between PHAROS and SWAN

From an academic standpoint, PHAROS is considered a more accurate model when modeling diffraction around obstacles. As PHAROS is a phase-resolving model, this simulation is precisely the type of problem the system was designed for.

One difference between the two models is the computation type. As discussed previously, all PHAROS models of irregular wave type were performed with only directional spreading. This was done to reduce the computation time and memory. When tested, there was little difference between models run with frequency spreading and models run without. SWAN, on the other hand, includes frequency spreading in all model runs. From theory testing performed by Goda, a small scaling difference is possible and should be taken account for within the comparison.

Because SWAN is unable to reproduce reflection effects as they pertain to diffraction, the following comparison between the models will only consist of fully absorbent breakwaters.

One thing to notice in Figure 7-3, SWAN does not calculate wave build-up within the breakwater gap. This build-up can be very detrimental in design for vessel navigation and therefore its absence from SWAN should be noted. As it pertains to this study, the area behind the breakwater gap is of particular interest in the analyzes of reflection effects. However, as it was already determined that SWAN does not accurately represent reflection off an obstacle with diffraction, its absence is not detrimental to the study.

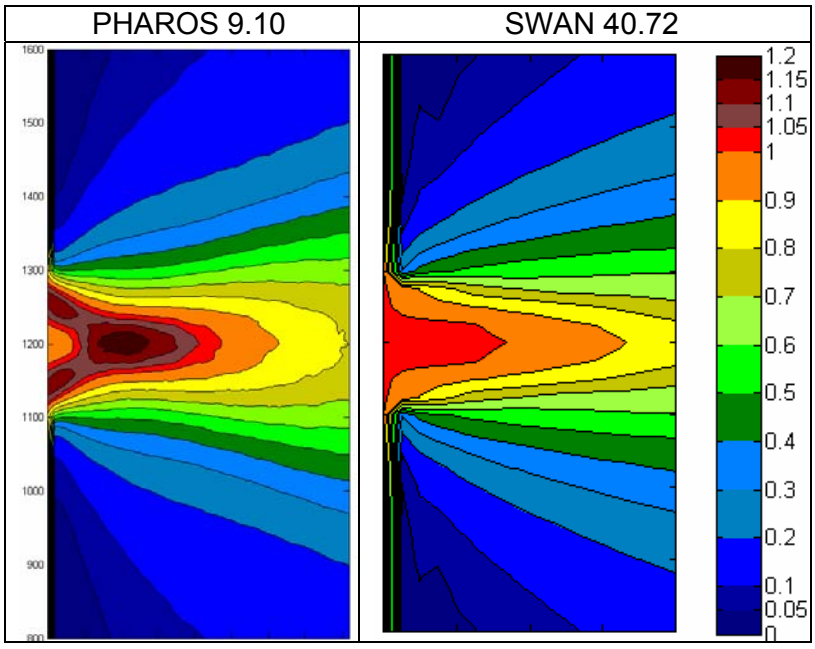

Figure 7-3: Wave Build-up in Gap Diffraction

A few of the comparisons between PHAROS and SWAN are shown in Figure 7-4. Additional model runs can be compared in the appendix. From the visual inspection, it can be concluded that there is very good agreement between the models. So much so that the comparison between wind waves for a breakwater gap of B/L = 2 is almost spot on. The greatest visual deviation is in the modeling of swell waves. As one can see, the lower diffraction coefficient contours differ between the two models and the central, upper contours have slightly different scaling. However, as SWAN is not recommended for diffraction around obstacles, these are excellent results. They show that SWAN is modeling diffraction comparatively to the phase-resolving model, PHAROS.

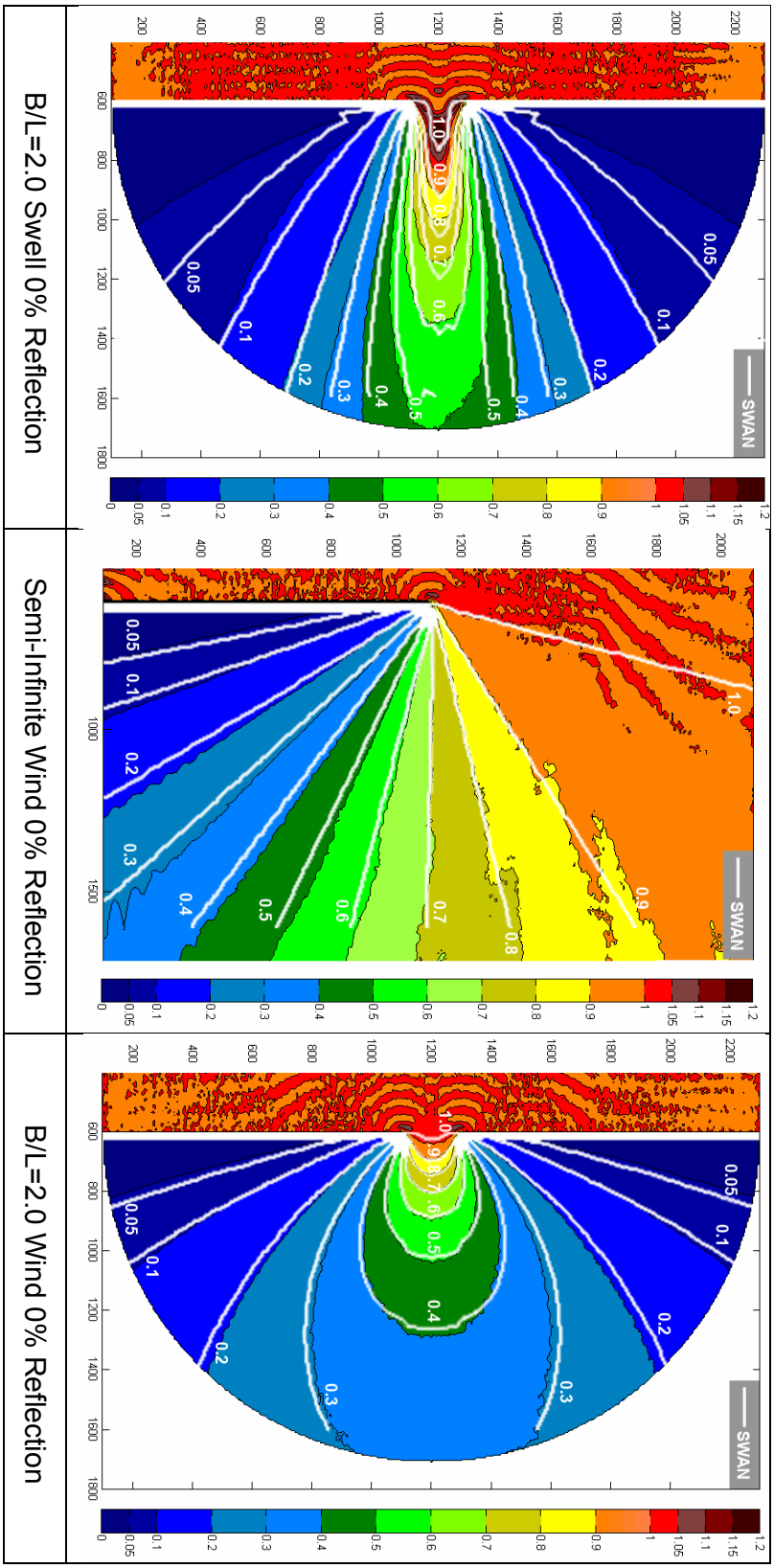

Figure 7-4: Comparison between SWAN & PHAROS model outputs

7.2.2. Comparison of Diffraction Coefficients

The following figures compare the two model outputs with the analytical diagrams created by Goda. Additional comparisons can be found in the appendix.

PHAROS, as a phase-resolving model with the capability of replicating effects due to reflection, should have good resemblance to irregular wave diffraction theory. Minor deviations can be explained by differences in model and analytical setup conditions.

Unfortunately, this study was unable to replicate structure reflection effects with diffraction properly in SWAN. Due to this, only model runs using non-reflective, uniform breakwaters were performed. The analytical diffraction diagrams which the SWAN outputs are compared to below utilized a fully reflective breakwater. This should cause significant differences in the lee area behind the breakwater were reflection effects are greatest. This difference will be more prominent within the figures depicting narrow directional spreading as the effects from reflection penetrate farther inside the shadow zone than for broad directionally spread waves.

Figure 7-5 and Figure 7-6 depict both random sea narrow directional and broad directional waves of normal incidence on various layouts. The background graphic was generated using PHAROS and the contour lines for both Goda's analytical diagrams as well as SWAN outputs are overlaid in contrasting colors. The contour lines for PHAROS and Goda are based on a fully reflective breakwater while the SWAN contours were generated based on a non-reflective breakwater.

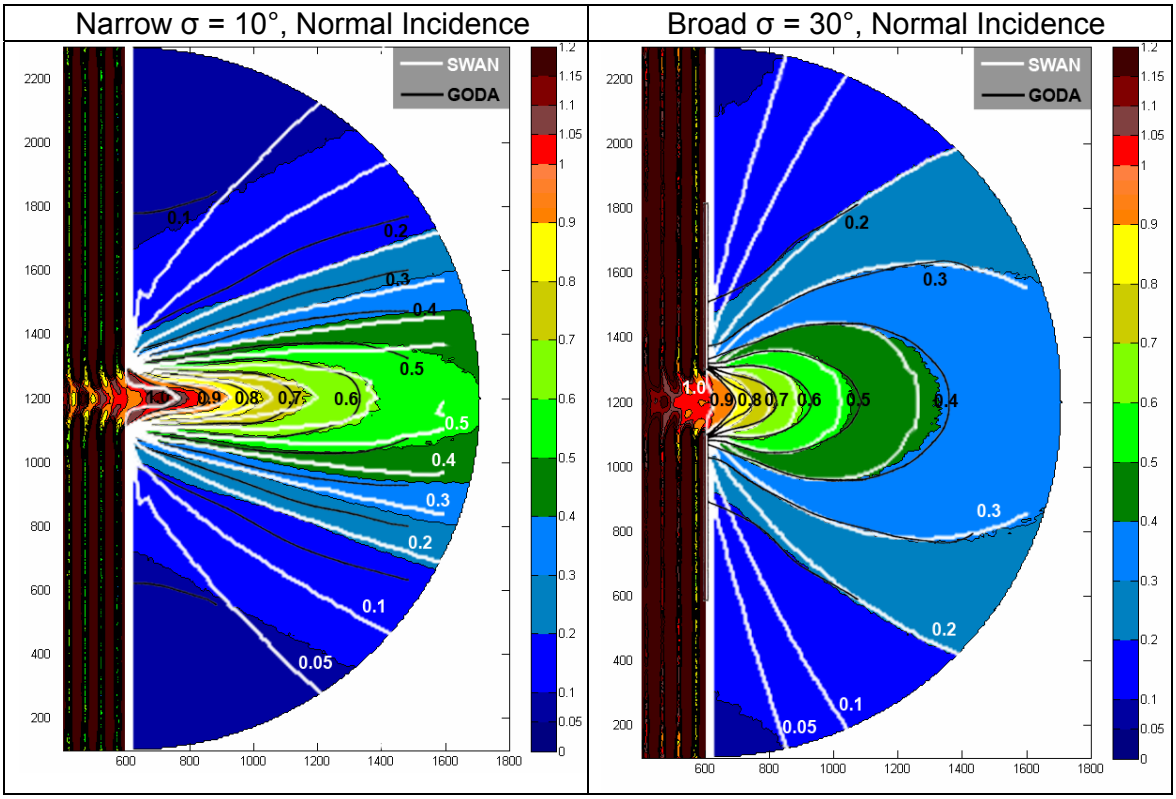

Figure 7-5: Diffraction Diagrams for Various Methods, Breakwater Gap B/L = 2

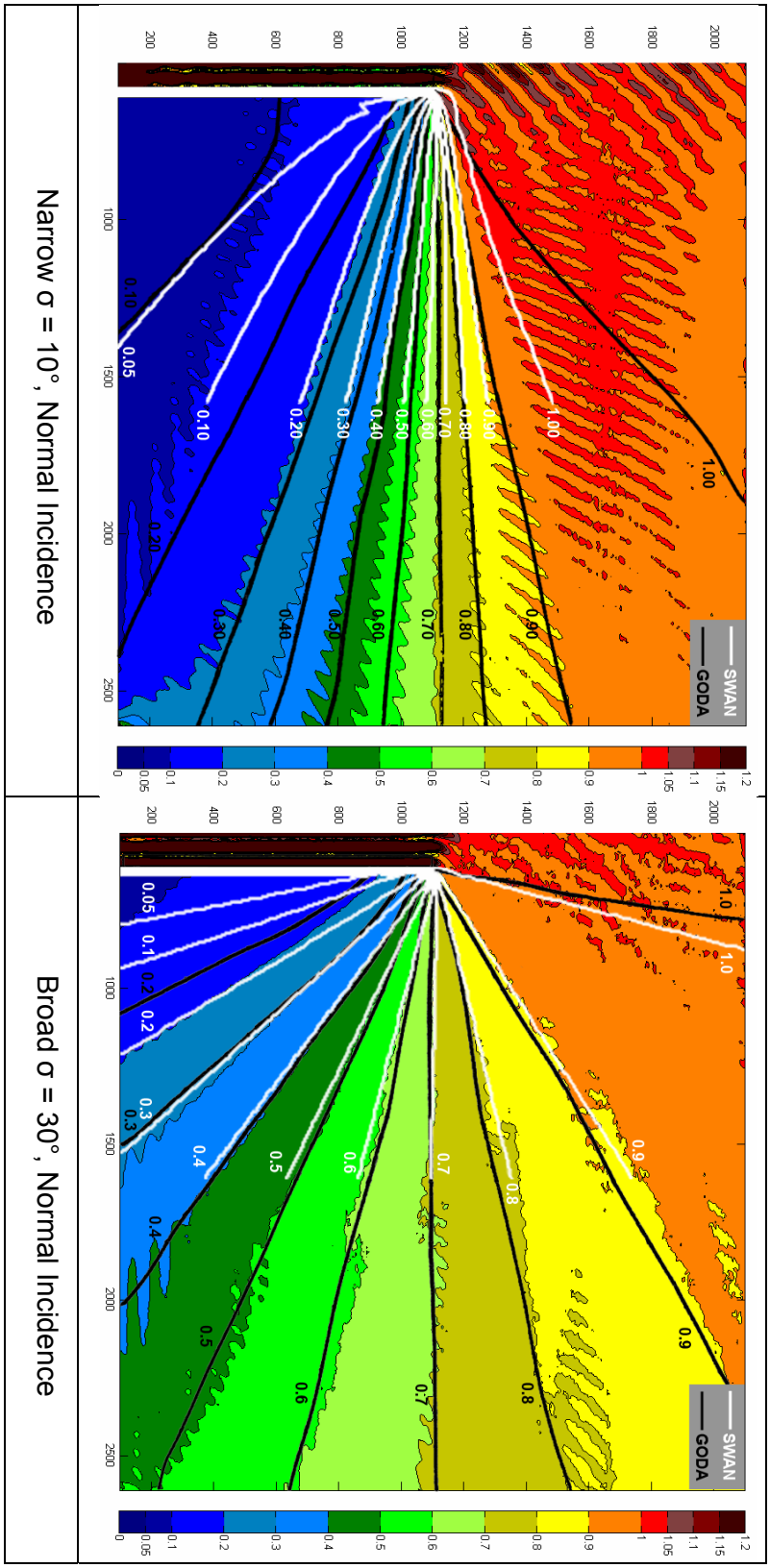

Figure 7-6: Diffraction Diagrams for Various Methods, Semi-Infinite Breakwater

7.2.2.1. PHAROS Comparison to Theory

Visual inspection of the PHAROS generated diffraction coefficients versus Goda's analytically developed contours reveals good congruency. The similarity is greater for broadly directional waves than narrow directional waves. In Figure 7-6 and Figure 7-5 Broad σ = 30°, the contours lines of PHAROS and Goda match very well. The only slight exception would be for the K'=0.2 contour for the semi-infinite breakwater layout. However, as expressed earlier, the area directly behind a breakwater has been hard to represent exactly with theory.

In Figure 7-6 Narrow σ = 10°, good compatibility exists for contours K'=0.6-0.9. However, above and below this range the deviation increases. While the contour lines appear to match nicely, Goda's analytically produced contour lines are actual a full tenth of a coefficient greater then those estimated by PHAROS. The effect is also seen to a much lesser extent in Figure 7-5 Narrow σ = 10°.

One possible source for error could be the resolution of the user inputs in PHAROS. As the operator must enter in details for ever direction specified, in an effort to minimize computing time and man-hours, this directional resolution was increased. Goda, within his analysis, used "summations over 10 frequency intervals and 20 to 36 directional intervals of equal spacing (Goda, 2000)." This is slightly finer than the 5 frequency intervals and 11 to 17 directional intervals used in this study.

7.2.2.2. SWAN Comparison to Theory

Scaling deviations between SWAN and theory are expected due to the absence of reflection effects within SWAN. However, the general shape of the contours should resemble those of theory.

As with the PHAROS outputs, the similarity between SWAN and Goda is stronger for broadly direction waves than for narrow directional waves. This is also expected as SWAN performs better in the subject of diffraction around obstacles when the wave direction is more broad. Reviewing the diffraction contours for Broad σ = 30° in Figure 7-5 and Figure 7-6, there is little deviation between theory beyond a small scaling effect that can be attributed to reflection effects.

Although there is a greater difference between the contours in Figure 7-5 Narrow σ = 10°, again this can be explained by scaling effects attributed to reflection. However, as with the PHAROS results, there is a great deviation between contours in Figure 7-6 Narrow σ = 10°. Interestingly, throughout all comparisons, the data produced by SWAN and PHAROS are much more comparable. As both models predict similar diffraction patterns, this could be attributed to similarity in the equations each uses to compute diffraction effects or could indicate a small error in Goda's analytical diagrams.

Overall, comparison between the SWAN outputs and Goda's analytical approach revealed good congruency with only significant differences in the area directly behind the breakwater. However, as reflection accounts for only a small part of the diffraction

coefficient, SWAN's approximation provides a good representation of diffraction characteristics.

PART IV: Conclusions & Recommendations

Chapter 8. Modeling Conclusions

Reflection

The effect of reflection coefficient on the pattern of diffraction coefficients was examined with the PHAROS model. These tests, which were performed with varied layout, wave characteristics, and oblique angles concluded that reflection effects are responsible for a small part of the overall diffraction coefficient. The portion of diffraction attributed to reflection is greatest at the breakwater tip and along the lee of the breakwater. However, as testing was performed primarily with uniform breakwaters, the diffraction coefficient differences directly against the leeside of the breakwater can also be attributed to the absorptive nature of the breakwater itself which can be highly influential itself.

Testing was also conducted on non-uniform breakwaters with reflective front faces and absorptive leesides and vise versa. Currently available diffraction diagrams to not consider these construction aspects and therefore their study is of interest. Additionally, these tests show how the reflective nature of each side of the breakwater contribute to diffraction separately. From these tests, it was concluded that the reflection coefficient caused significantly more agitation and farther penetration within a breakwater gap when the wave approached from an oblique angle versus approaching normal to the breakwater.

It was found that effects due to the reflection coefficient concentrate in a different direction than the incident wave when angles approach a breakwater at an oblique angle. This can be explained by theory which states that reflected waves diffract around the breakwater in a circular pattern which means it will diffract over 180°.

Model testing on reflection coefficients of 1.0 (full reflection), 0.5 (50% reflection), and 0.0 (full absorption) showed that the relationship between reflection and diffraction coefficient. This testing showed that the influence of reflection is more widespread for narrow directional waves versus broad directional waves.

Wave Characteristics

Studies of irregular waves, first presented pictorially by Goda (1978), were retested using advanced models in this study. They confirmed that the use of regular wave diffraction patterns for the use of irregular seas lead to significant errors. Despite this, regular wave diffraction patterns are still represented in engineering text without mention to their erroneous use in ocean application.

Testing of the directional spreading and frequency spreading were performed. It was found the directional spreading had a large effect on the diffraction pattern while frequency spreading made little to no difference. This finding is supported by Goda whom tested this analytically. This has great significance for regions which are plagued by narrow directionally spread swell-type waves which penetrate deeply behind the breakwater. Wind-generated waves with broad directional spreading are experience diffraction effects quickly and dissipate quickly within the shadow zone.

A commonly accepted rule-of-thumb is that breakwater gaps larger than B/L = 5 do not effectively diffract waves and can be considered at two separate semi-infinite breakwaters. However, through testing and because diffraction effects are greater for wind seas, breakwater gaps of B/L = 8 still showed applicability to design with strong diffraction associated with gap diffraction still occurring.

SWAN Model Testing

A secondary objective to this thesis was the analysis of the application of diffraction in the modeling system SWAN. This was of interest and importance because SWAN, as a universally available free software, is utilized by engineers worldwide for a variety of engineering problems. However, due to the type of model it is and the equations and assumptions used to perform diffraction, it is not recommended for structure or harbor interaction. Irregardless of this, some success has been achieved in modeling diffraction and further studies were recommended.

SWAN required a large sensitivity study prior to running model cases of interest to this thesis. Multiple model runs are required as SWAN frequently becomes unstable for diffraction in harbor and obstacle applications. This sensitivity study revealed that some aspects, such as the spatial resolution, have improved with the new version release. It also showed that using smoothing for broad directional spread wind waves allowed the spatial resolution to increase and the model outputs to create more precise contour lines.

The issue of turning on the diffraction command within the commands was of question. This test was coupled with a test to determine how the model represented a uniform, reflective breakwater. After an analysis which checked the spectral plots at points in front of and behind the breakwater, it was determined that without turning on diffraction, the wave directly behind the breakwater does not impinge against it but rather runs along it without being effected by its properties (i.e. dampened by absorptive materials). In addition to this, it was determined that while the front of the breakwater reflected the wave energy which encountered it, the leeside of the breakwater, which was specified as a separate obstacle, did not reflect any energy. Therefore, it was determined that SWAN was not capable of representing a uniform breakwater with a reflection coefficient. Therefore SWAN was only used to create diffraction diagrams for various wave environments with a fully absorbing breakwater.

SWAN's model outputs for diffraction against a non-reflective breakwater were compared with the model outputs from PHAROS also with a non-reflective breakwater and with the analytical diffraction diagrams produced by Goda whom used a fully reflective breakwater. Comparatively, the model outputs from PHAROS and SWAN matched very well especially for cases which used a broad directional spectrum. The comparison with Goda's analytically produced diffraction diagrams was not as similar. However, this is in part due to the difference in diffraction effects due to reflection.

From this study, it was determined that using SWAN for diffraction purposes is possible. Despite what the SWAN user manual may state, this model can perform diffraction around obstacles with good approximations. However, as the model can not yet replicate all aspects related to diffraction, such as reflection off breakwaters, its use should be limited to feasibility studies.

Diffraction Diagram Comparison
Overall, PHAROS showed close similarity to Goda's diagrams. As with SWAN, the resemblance was greater between broad directionally spread waves than with narrow directionally spread waves. The diffraction contour comparison for narrow swell-type waves against a semi-infinite breakwater did not align. However, the alignment between PHAROS and SWAN model outputs was almost exact. This could indicate a problem with Goda's diagram (as the other diagrams matched up more clearly) or it could just be an indication of comparative equation processes being carried out between PHAROS and SWAN.

Chapter 9. Importance of the Reflection Coefficient

Information on the penetration of waves behind breakwaters is important for the design of harbors and to assess the safety of mooring systems. Therefore, a clear understanding of diffraction patterns and what influences them is beneficial to designers. By recognizing triggers of sources or sinks to diffraction, a designer can effectively design breakwaters and the interior layout to effectively work with the incoming wave energy.

Knowledge that the reflection coefficient of a breakwater most significantly affects the diffracted wave height near the breakwater tip and along the leeside can aid in creating more economical breakwater tips. Additionally, as the wave environment near breakwater tips is of interest and concern for vessel safety, recognizing the reflection coefficient's prominence in this area may be reason enough for reducing breakwater reflectivity.

Farther away from the breakwater, the portion of the diffraction coefficient associated with incident waves becomes much larger than the portion associated with reflected waves and therefore these effects become insignificant. However, dockage and mooring systems placed near the breakwater will be affected by both its interior and exterior reflection coefficients.

Even though the reflection related portion of the diffraction coefficient is rather small, understanding that reflection cause changes to the agitation level within a breakwater's shadow zone is of value.

Chapter 10. Application and Relevance

This study was conducted to better understand the effects of breakwater reflection on diffraction patterns. The aspect of reflection is of interest to breakwater designers as they are frequently used to protect valuable vessels and structures in their shadow zone. Many times, these objects are placed directly behind the breakwater in what is considered a calm area but in actuality, can contain significant agitation.

Some designers think that a way to significantly remove breakwater leeside agitation is to use wave energy absorbing armor, such as rubble and other porous materials. As shown in this study, this does not completely eliminate agitation. The studies of Daemrich showed that, in theory, the second term of the Sommerfeld equation, which is related to the amount of reflection effect, is only weighted and not erased when breakwaters have reduced reflection coefficients. This information is important for the placement of structures or dockage on the leeside of the breakwater.

Breakwaters are typically non-revenue producing structures which constitute a large portion of overall construction costs. A designer whom is well informed on the many aspects of wave structure interactions, including diffraction, can devise breakwater layouts which both fulfill the required specifications while reducing unnecessary costs associated with over design. These qualifications are highly sought after by developers.

Chapter 11. Recommendations

It is the opinion of the author that the subject of reflection coefficient effect in diffraction has been thoroughly covered. However, within the course of this thesis, multiple questions arose about modeling systems, unexplained results, and wave theory.

It was discovered through literature review and modeling that the wave environment near the breakwater tip is very dynamic. Many factors influence this area and the wave interaction with the structure itself also causes unique wave patterns to form. As breakwater tips are more sensitive to extreme events than the breakwater trunk, they are designed more robust and therefore more expensive. Research into the phenomenon in this area is of interest.

From the study of composite breakwaters, it was discovered that in areas further away from the breakwater leeside of breakwater gaps, breakwaters with fully absorbent front faces actually transmitted higher diffracted wave height than fully reflective front faces. Even though this difference is very small, the finding is of interest as it is not immediately explainable by theory. More research into the causes of this are recommended.

As mentioned within the section about the SWAN modeling program, the author was unable to properly represent a uniform breakwater with reflective capability through the given set of codes. This may require additional operational coding. As reflective breakwaters are commonly used in coastal engineering, this option would be very beneficial to the program.

References

Goda, Y., Takayama, T. and Suzuki, Y., “Diffraction diagrams for directional random waves,” *Proc. 16th International Conference Coastal Engineering.* (Hamburg, 1978) pp. 628-650.

Goda, Y., “Random Seas and Design of Maritime Structures,” 2nd Edition, *Advanced Series on Ocean Engineering – Volume 15,* 2000

Mobarek, I. and Wiegel, R.L., “Diffraction of Wind Generated Waves,” *Proc. 10th Conference Coastal Engineering.* (Tokyo, 1966) pp.185-206

Penny, W.G. and Price, A.T., “The Diffraction Theory of Sea Waves by Breakwater and the Shelter Afforded by Breakwaters” *Philos. Transactions of the Royal Society of London,* Series A, No. 882, Vol. 244, March 1952, pp. 253-263

Sommerfield, A., “Mathematische Theorie der Diffraction,” *Mathematische Annalen*, Vol. 47, 1896, pp. 317-374.

Wiegel, R.L., “Diffraction of Waves by Semi-infinite Breakwater,” *Journal Hydraulic Div., Proc. ASCE*, Vol. 88, No. HY1, 1962, pp. 27-44.

Johnson, J.W., “Generalized Wave Diffraction Diagrams,” *Proc. 2nd International Conference Coastal Engineering* (Houston, 1952)

Daemrich, K.F. and Kohlhase, S., “Influence of Breakwater-Reflection on Diffraction,” *Proc. 16th International Conference Coastal Engineering.* (Hamburg, 1978) pp. 651-663.

Silvester, R. and Teck-Kong Lim, “Application of Wave Diffraction Data,” *Proc. 11th International Conference Coastal Engineering.* (London, 1968)

Briggs, M.J., Thompson, E.T. and Vincent, C.L., “Wave Diffraction Around Breakwaters,” *Journal of Waterways, Port, Coastal and Ocean Engineering*, 121 (1995), pp. 23-35.

Enet, F., Nahon, A., van Vledder, G., Hurdle, D., “Evaluation of diffraction behind a semi-infinite breakwater in the swan wave model,” *9th International Workshop on Wave Hindcasting and Forecasting,* (Victoria, 2006)

Holthuijsen, L.H., Herman, A., and Booij, N., “Phase-decoupled refraction-diffraction for spectral wave models,” *Coastal Engineering,* 49 (2003), pp.291-305

Kuik, A.J., van Vledder, G., and Holthuijsen, L.H., “A method for the routine analysis of pitch-and-roll buoy wave data,” *Journal of Physical Oceanography*, 18 (1988), pp. 1020-1034

Battjes, J.A., “Shallow Water Wave Modeling,” *International Symposium: Waves – Physical and Numerical Modelling*. (1994)

APPENDIX A: Sommerfeld Solution for Wave Diffraction

(*as presented in Goda, 1978)

$$F_d(r,\alpha,f,\theta) = F_{id}(r,\alpha,f,\theta) + F_{rd}(r,\alpha,f,\theta)$$

$$F_{id} = \frac{1}{\sqrt{2}}\exp\left[i\left\{kr\cos(\alpha-\theta)+\frac{\pi}{4}\right\}\right]\times\left[\left\{C(\gamma_1)+\frac{1}{2}\right\}-i\left\{S(\gamma_1)+\frac{1}{2}\right\}\right]$$
$$= \exp\left[i\left\{kr\cos(\alpha-\theta)\right\}\right]+\frac{1}{\sqrt{2}}\exp\left[i\left\{kr\cos(\alpha-\theta)+\frac{\pi}{4}\right\}\right]\times\left[\left\{C(\gamma_1)-\frac{1}{2}\right\}-i\left\{S(\gamma_1)-\frac{1}{2}\right\}\right]$$

$$F_{rd} = \frac{1}{\sqrt{2}}\exp\left[i\left\{kr\cos(\alpha+\theta)+\frac{\pi}{4}\right\}\right]\times\left[\left\{C(\gamma_2)+\frac{1}{2}\right\}-i\left\{S(\gamma_2)+\frac{1}{2}\right\}\right]$$
$$= \exp\left[i\left\{kr\cos(\alpha+\theta)\right\}\right]+\frac{1}{\sqrt{2}}\exp\left[i\left\{kr\cos(\alpha+\theta)+\frac{\pi}{4}\right\}\right]\times\left[\left\{C(\gamma_2)-\frac{1}{2}\right\}-i\left\{S(\gamma_2)-\frac{1}{2}\right\}\right]$$

where:

$$\gamma_1 = \sqrt{\frac{4kr}{\pi}}\cos\frac{\alpha-\theta}{2}$$

$$\gamma_2 = \sqrt{\frac{4kr}{\pi}}\cos\frac{\alpha+\theta}{2}$$

$$\left.\begin{aligned} C(\gamma) &= \int_0^{\gamma}\cos\frac{\pi}{2}\chi^2 d\chi \\ S(\gamma) &= \int_0^{\gamma}\sin\frac{\pi}{2}\chi^2 d\chi \end{aligned}\right\}\ \text{Fresnel integrals}$$

F_{id} represents the sum of the incident waves and the associated scattered waves
F_{rd} represents the sum of the reflected waves and the associated scattered waves.

Primary reflected waves only exist in the region I, whereas the region III is primarily occupied by scattered waves.

APPENDIX B: Wiegel Diffraction Diagrams, 1962

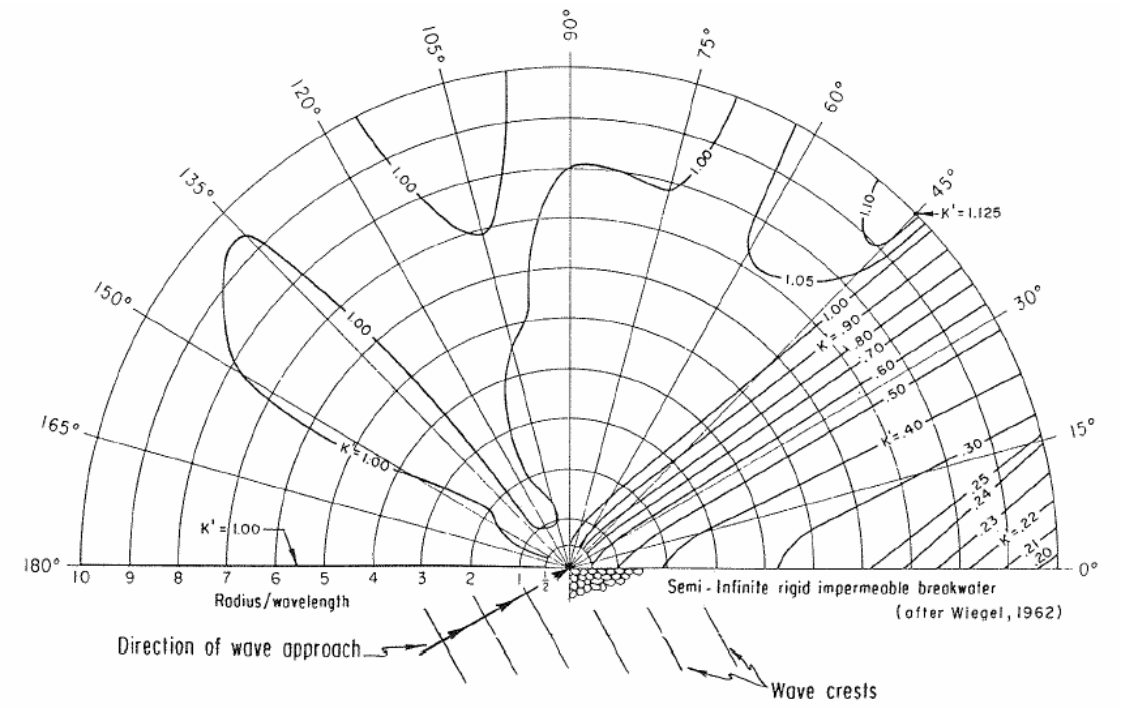

Figure 2-29. Wave diffraction diagram--30° wave angle.

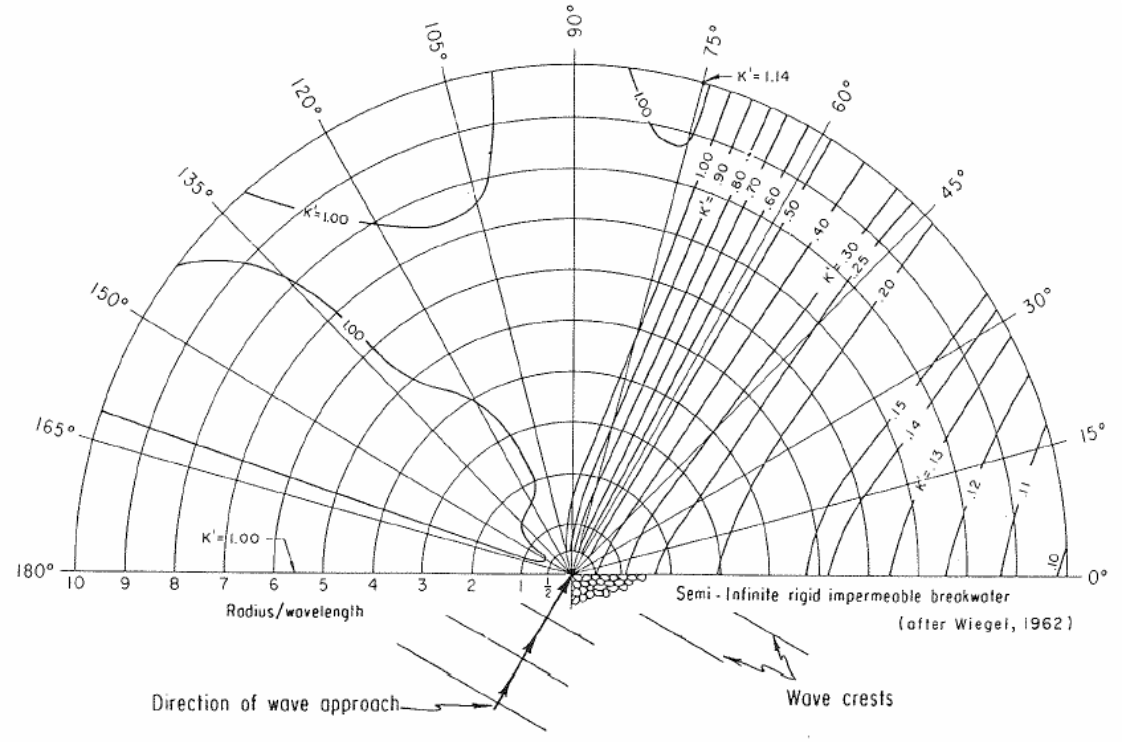

Figure 2-31. Wave diffraction diagram--60° wave angle.

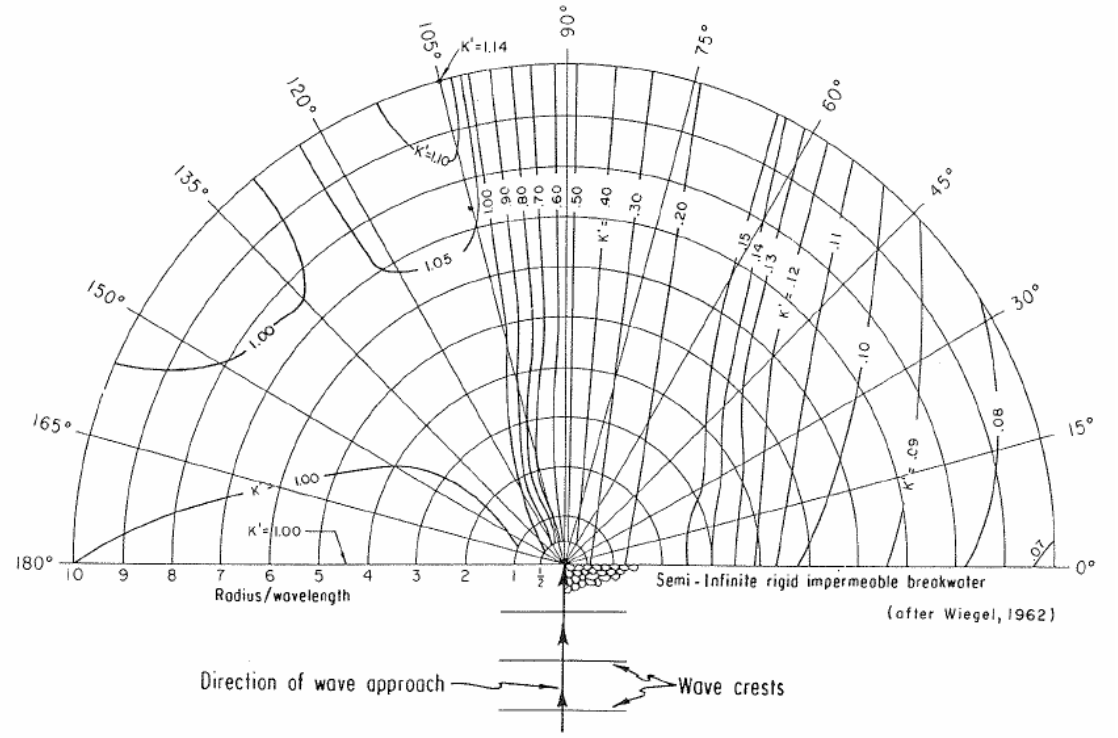

Figure 2-33. Wave diffraction diagram--90° wave angle.

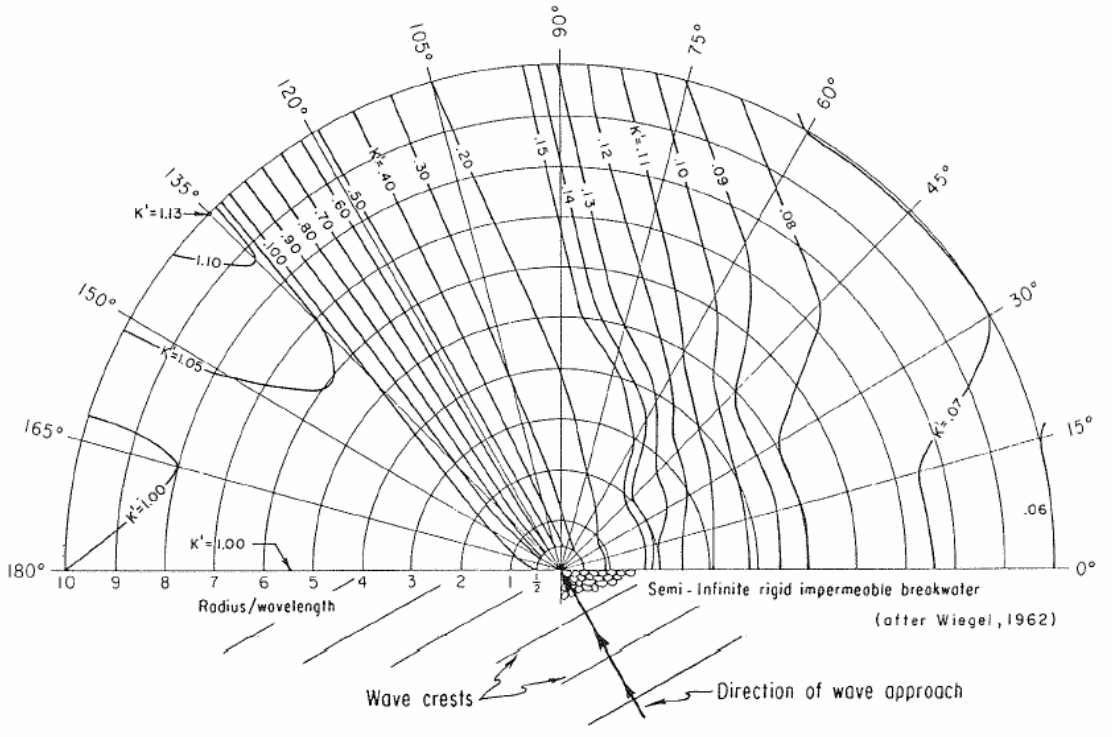

Figure 2-35. Wave diffraction diagram--120° wave angle.

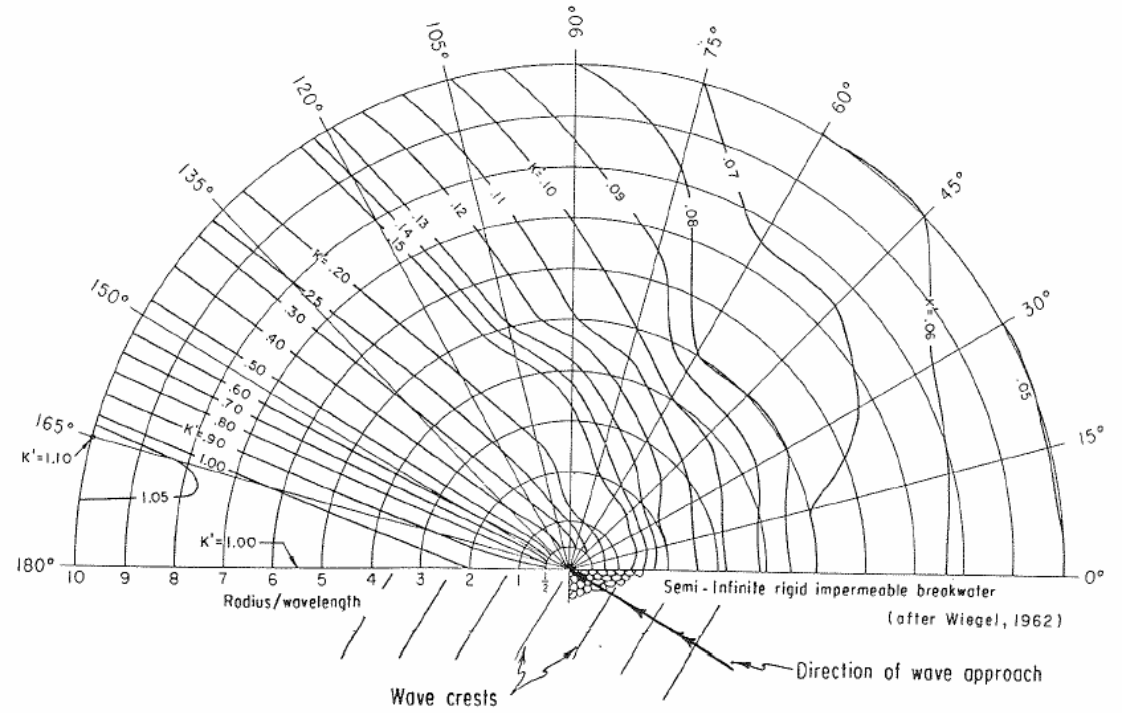

Figure 2-37. Wave diffraction diagram--150° wave angle.

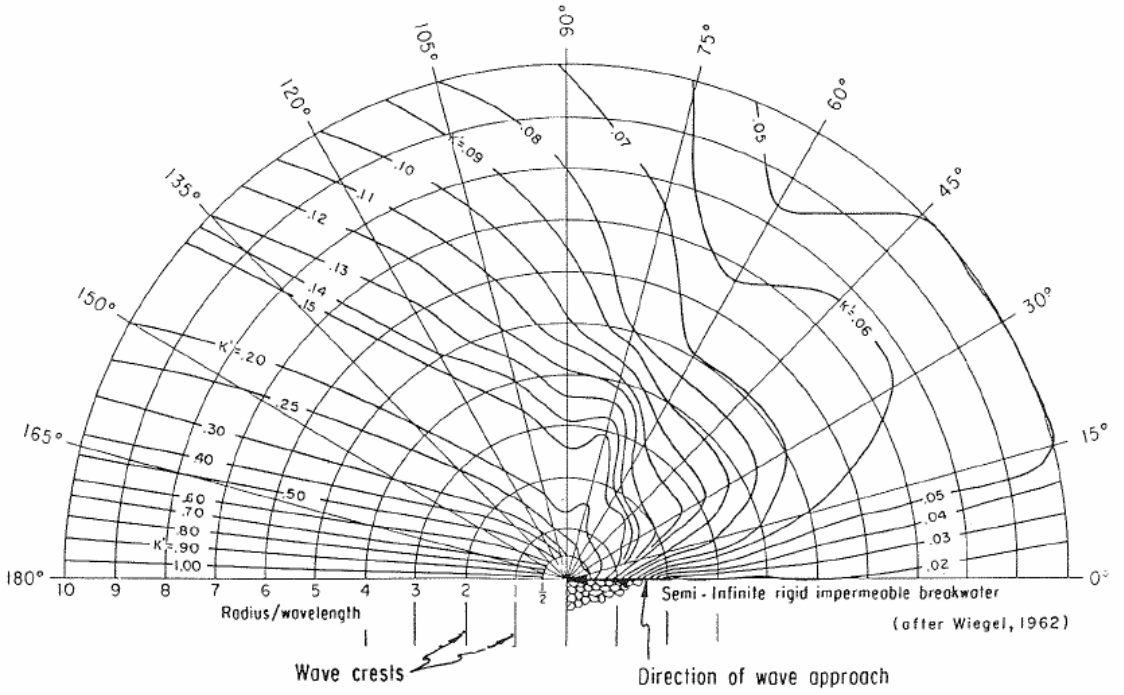

Figure 2-39. Wave diffraction diagram--180° wave angle.

APPENDIX C: Goda Diffraction Diagrams, 1978

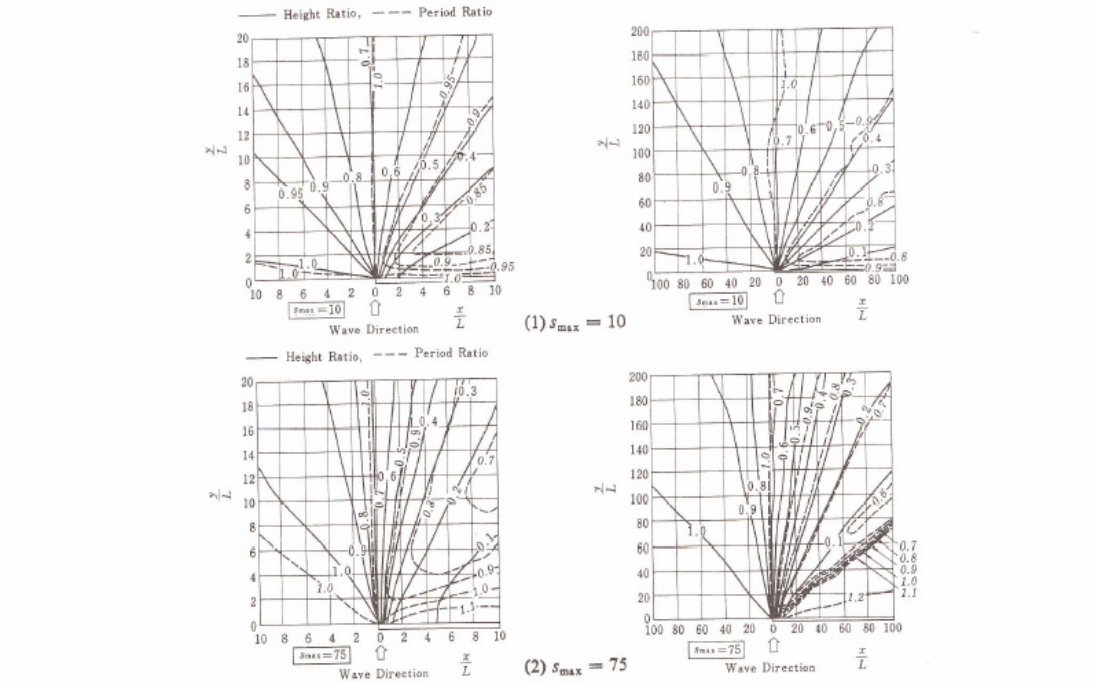

Fig. 3.11. Diffraction diagrams of a semi-infinite breakwater for random sea waves of normal incidence (solid lines for wave height ratio and dash lines for wave period ratio).[16]

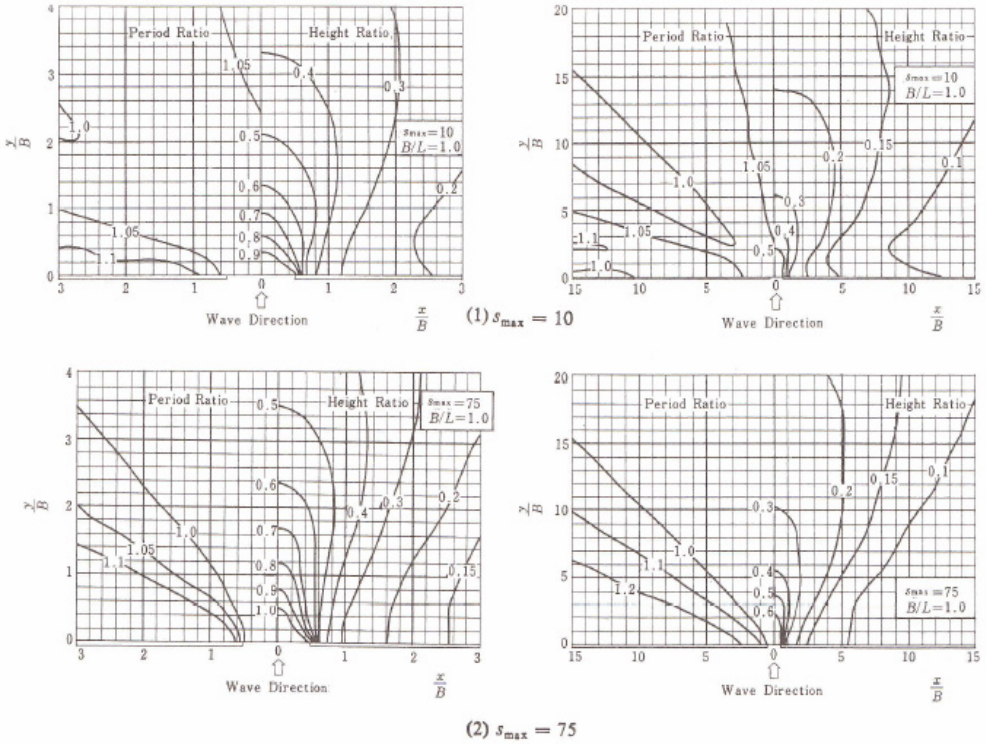

Fig. 3.12. Diffraction diagrams of a breakwater opening with $B/L = 1.0$ for random sea waves of normal incidence.[16]

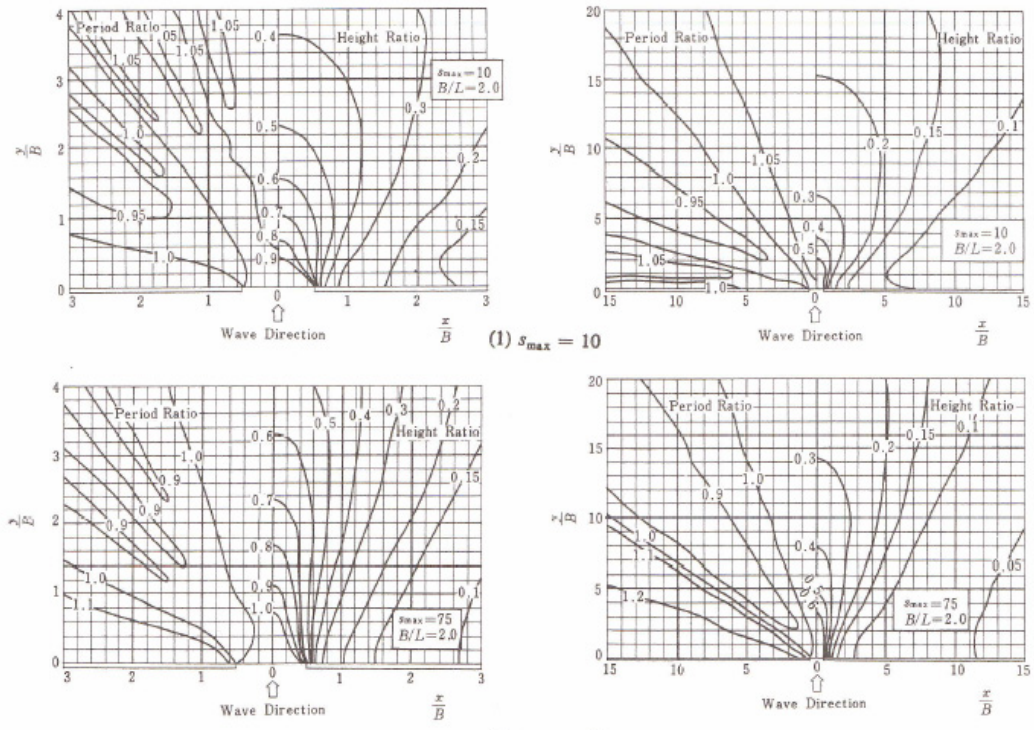

Fig. 3.13. Diffraction diagrams of a breakwater opening with $B/L = 2.0$ for random sea waves of normal incidence.[16]

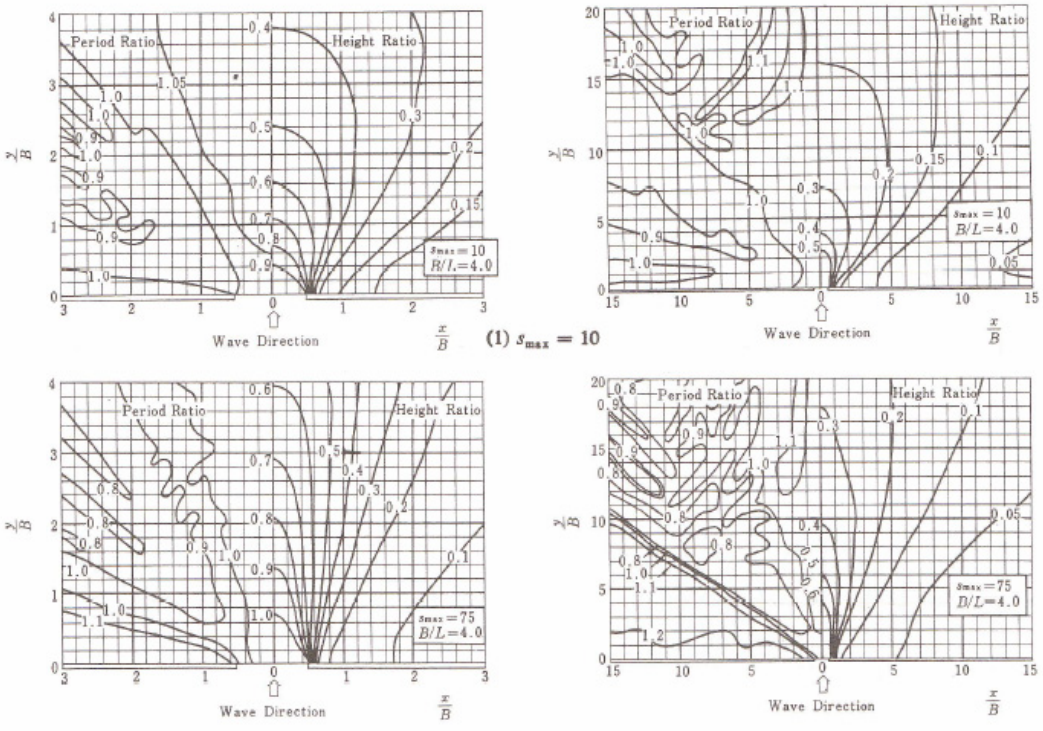

Fig. 3.14. Diffraction diagrams of a breakwater opening with $B/L = 4.0$ for random sea waves of normal incidence.[16]

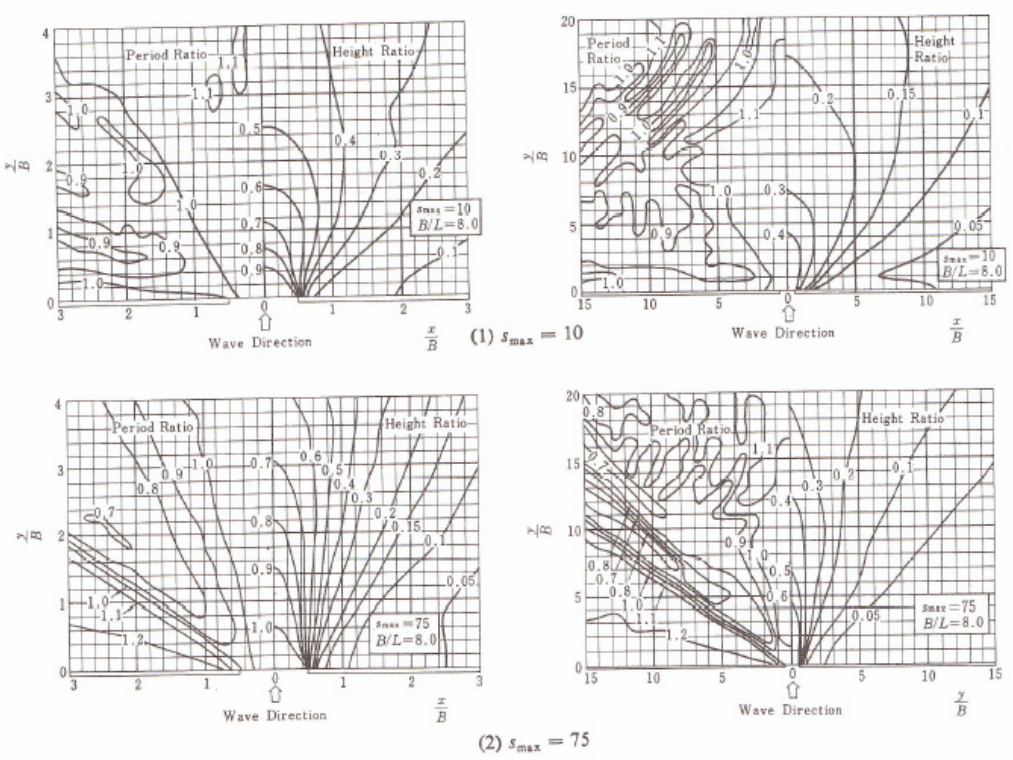

Fig. 3.15. Diffraction diagrams of a breakwater opening with $B/L = 8.0$ for random sea waves of normal incidence.[16]

APPENDIX D: PHAROS Model Results

Semi-Infinite Pharos File Names

					Reflection		Directional		Spectral	
Run	Wave Type	Model Type	Peak Per	Peak Dir	Front	Back	Spread (deg)	Interval (deg)	# frequencies	Notes:
R00	Mono	Long Crest	8	0	100	100				
R10	Mono	Long Crest	8	0	50	50				
R20	Mono	Long Crest	8	0	0	0				
R21	Mono	Long Crest	8	0	0	100				
R110	Swell	Directional	8	0	100	100	-25-25	5		
R111	Swell	Spectral	8	0	100	100	-25-25	5	5	Smallest Mesh: 8/WL
R112	Swell	Directional	8	0	50	50	-25-25	5		
R114	Swell	Directional	8	0	0	0	-25-25	5		
R115	Swell	Directional	8	0	0	100	-25-25	5		
R120	Wind	Directional	8	0	100	100	-80-80	10		
R121	Wind	Spectral	8	0	100	100	-80-80	10	5	Smallest Mesh: 8/WL
R122	Wind	Directional	8	0	50	50	-80-80	10		
R124	Wind	Directional	8	0	0	0	-80-80	10		
R125	Wind	Directional	8	0	0	100	-80-80	10		

R00

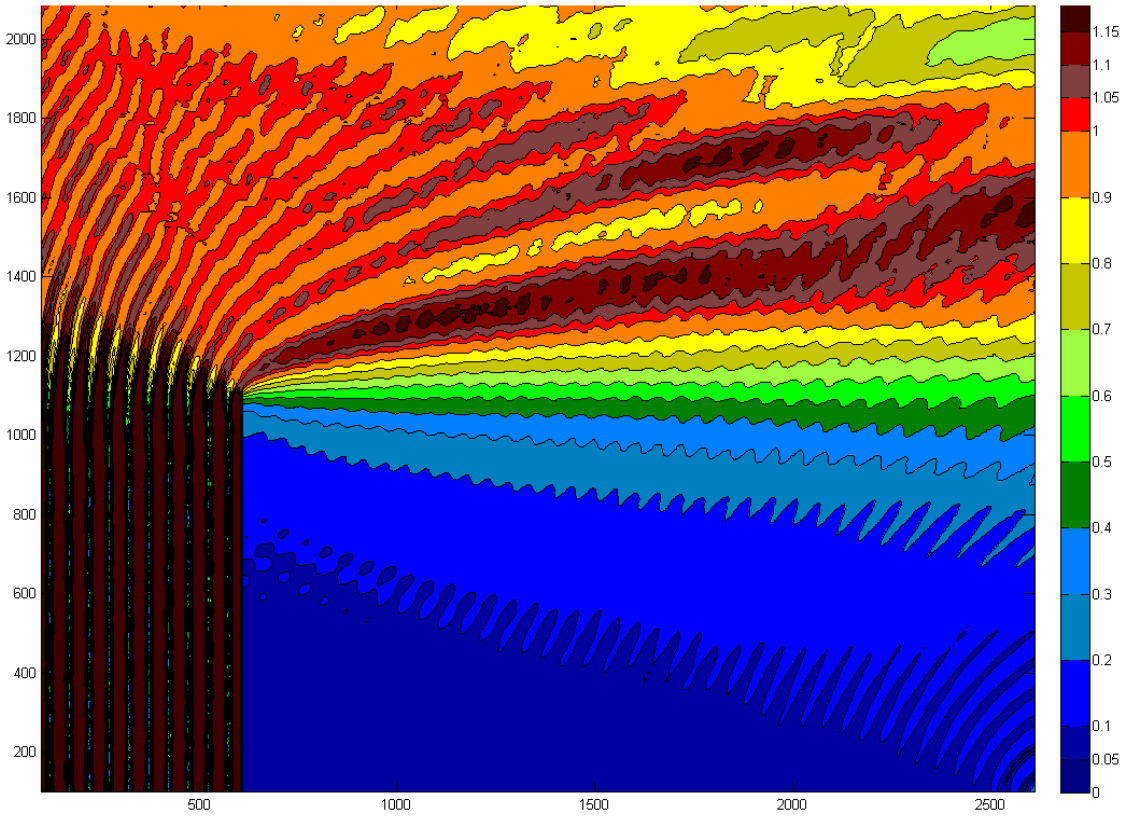
2000
1800
1600
1400
1200
1000
800
600
400
200
500
1000
1500
2000
2500
1.15
1.1
1.05
1
0.9
0.8
0.7
0.6
0.5
0.4
0.3
0.2
0.1
0.05
0

R10

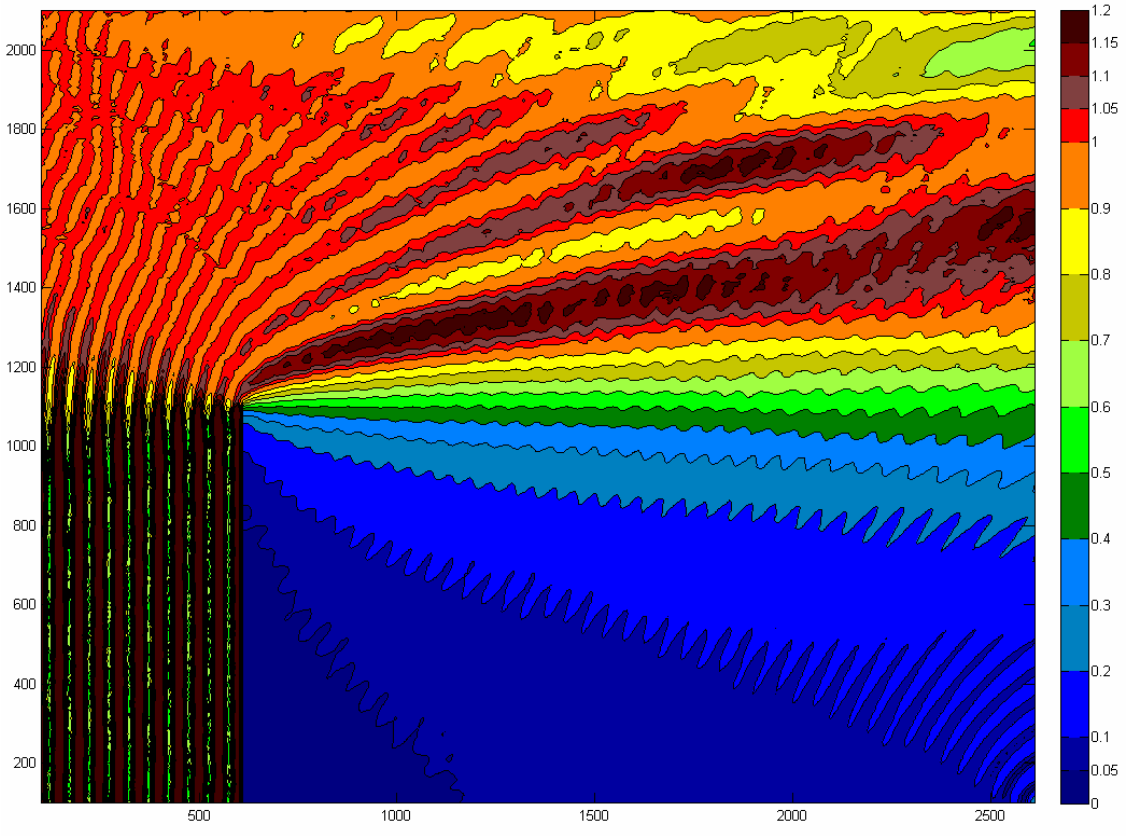
2000
1800
1600
1400
1200
1000
800
600
400
200
500
1000
1500
2000
2500
1.2
1.15
1.1
1.05
1
0.9
0.8
0.7
0.6
0.5
0.4
0.3
0.2
0.1
0.05
0

R20

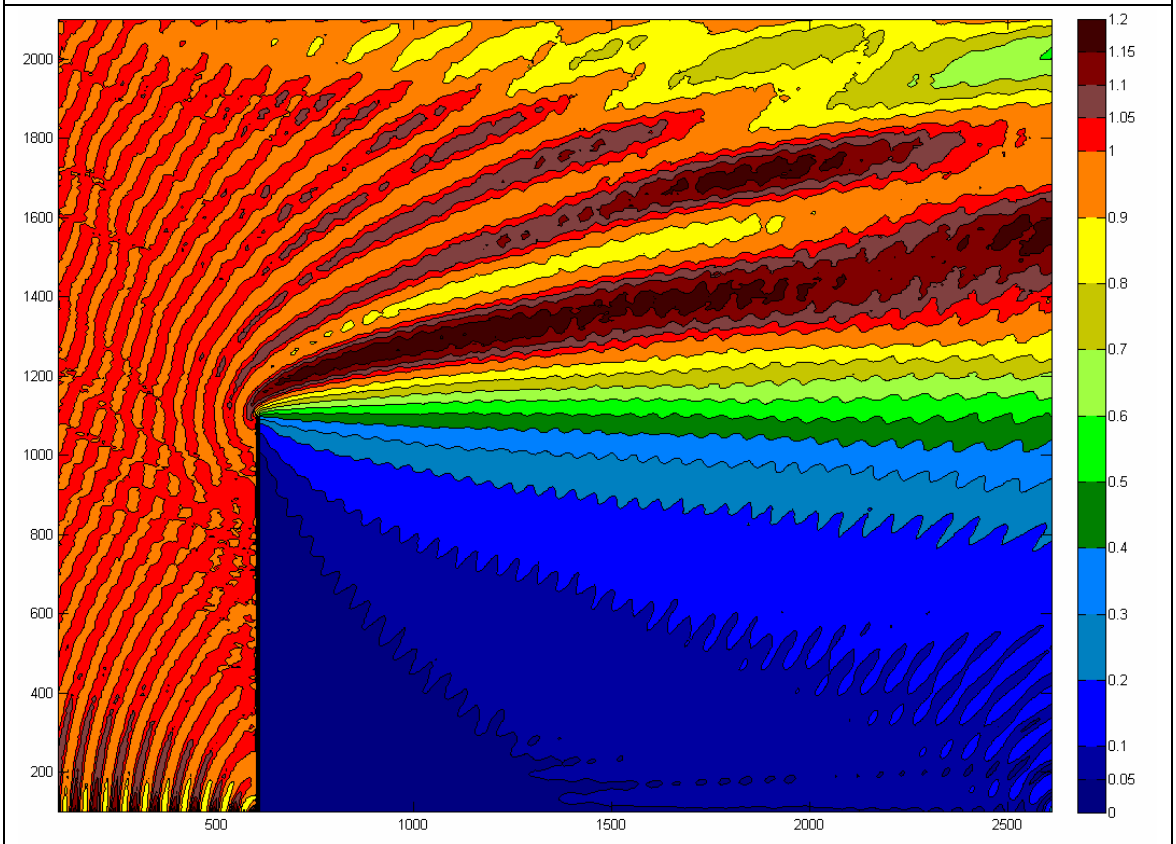
2000
1800
1600
1400
1200
1000
800
600
400
200
500
1000
1500
2000
2500
1.2
1.15
1.1
1.05
1
0.9
0.8
0.7
0.6
0.5
0.4
0.3
0.2
0.1
0.05
0

R21

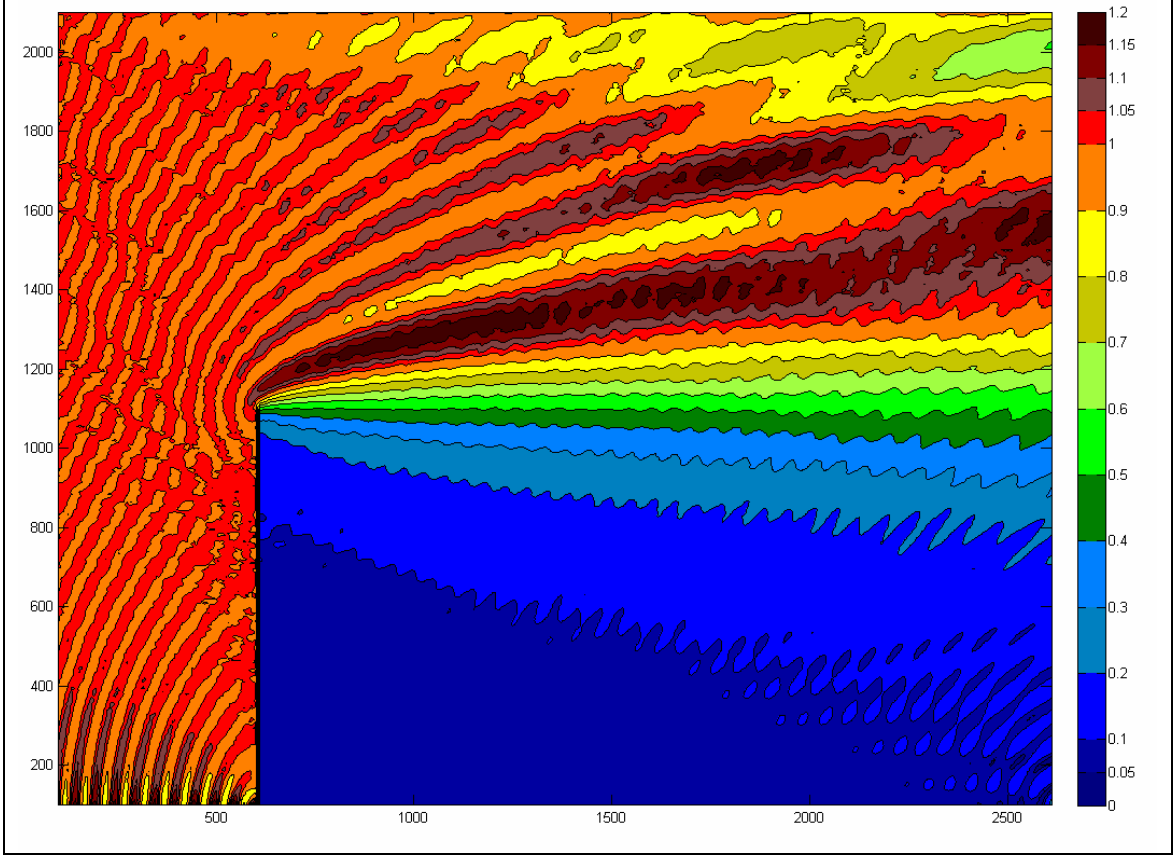
2000
1800
1600
1400
1200
1000
800
600
400
200
500
1000
1500
2000
2500
1.2
1.15
1.1
1.05
1
0.9
0.8
0.7
0.6
0.5
0.4
0.3
0.2
0.1
0.05
0

R110

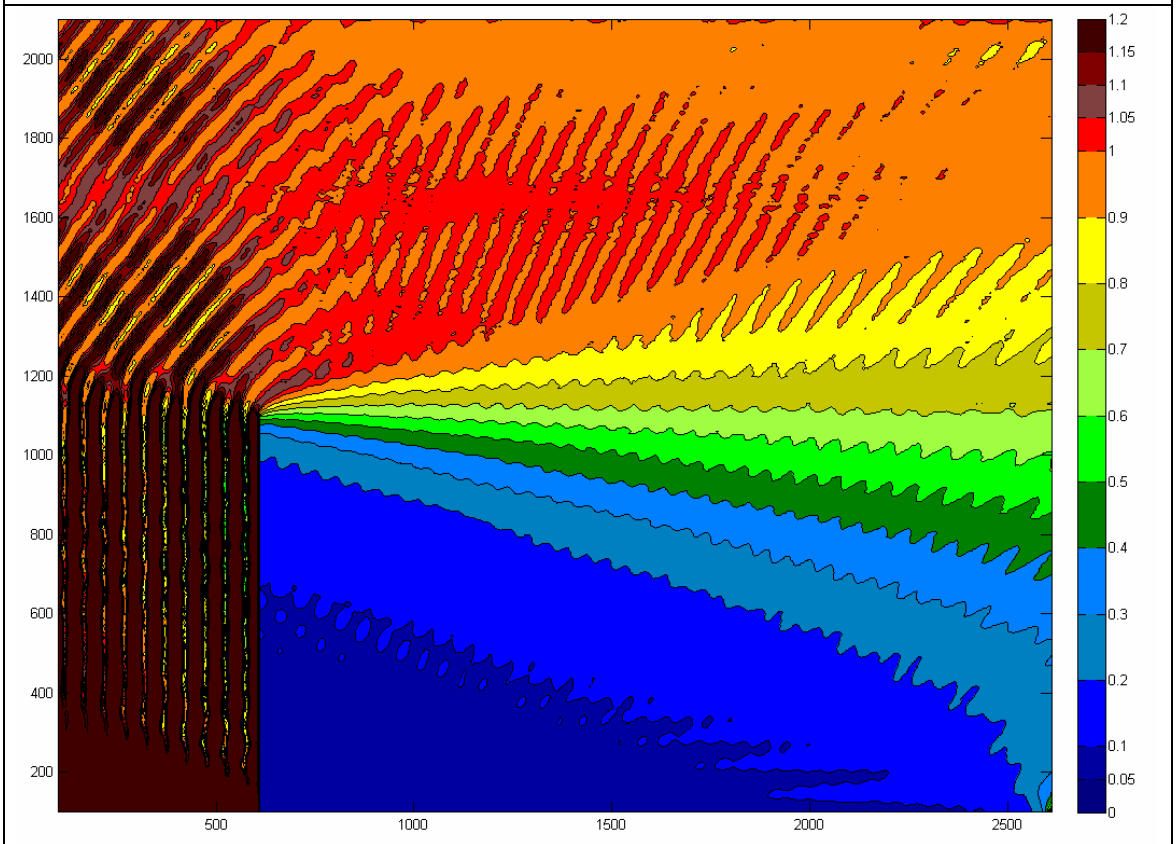
2000
1800
1600
1400
1200
1000
800
600
400
200
500
1000
1500
2000
2500
1.2
1.15
1.1
1.05
1
0.9
0.8
0.7
0.6
0.5
0.4
0.3
0.2
0.1
0.05
0

R111

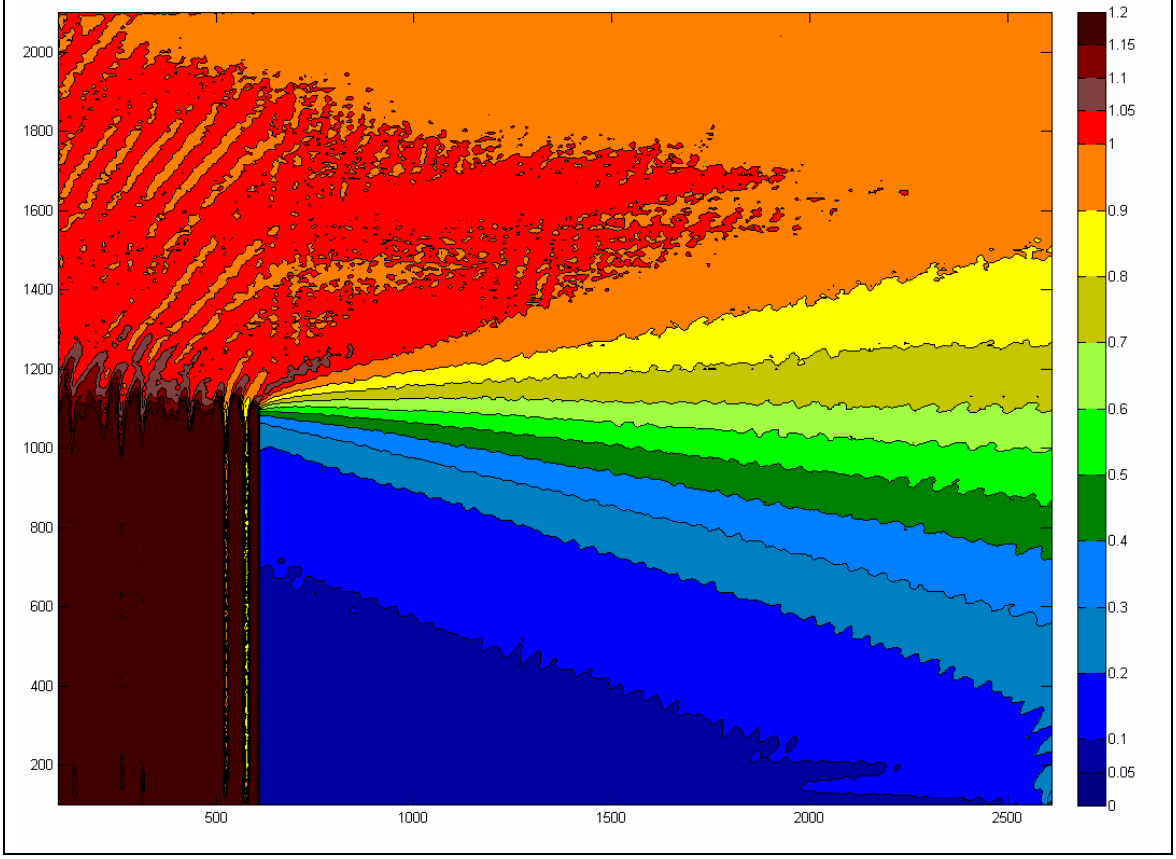
2000
1800
1600
1400
1200
1000
800
600
400
200
500
1000
1500
2000
2500
1.2
1.15
1.1
1.05
1
0.9
0.8
0.7
0.6
0.5
0.4
0.3
0.2
0.1
0.05
0

R112

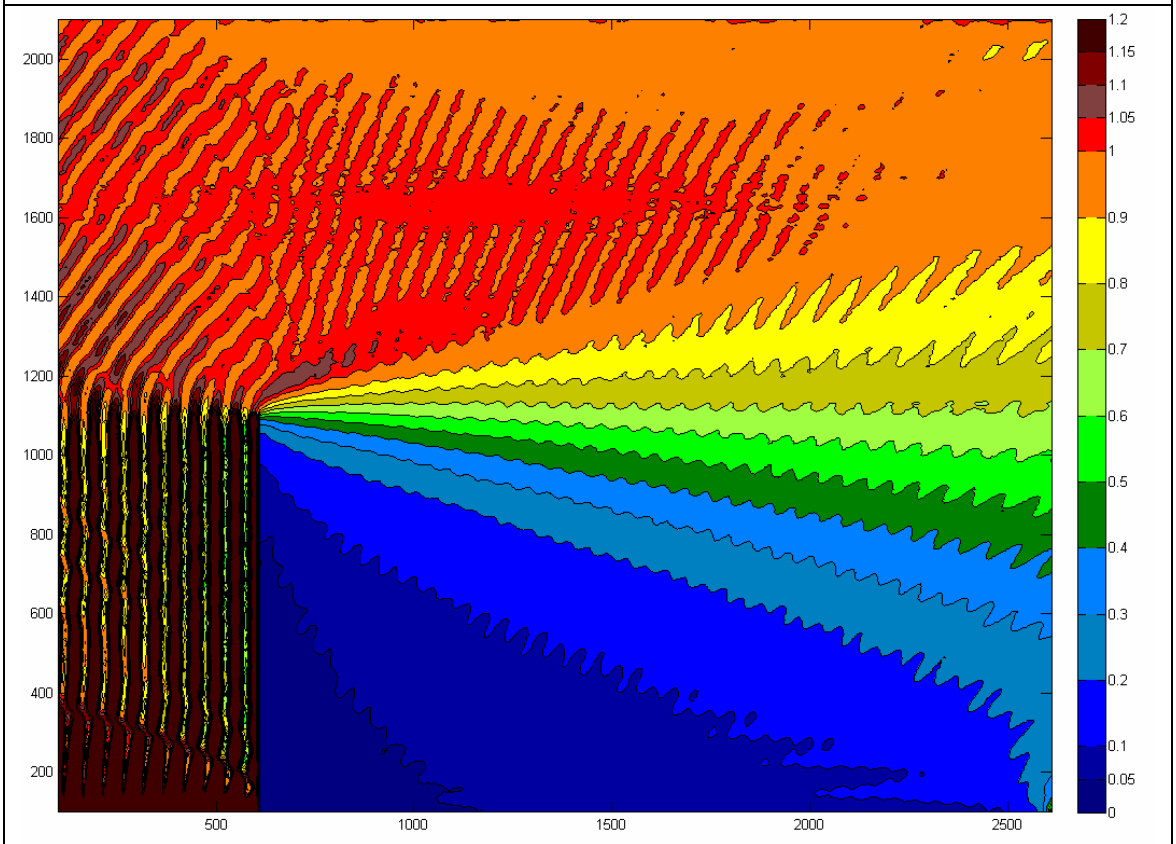
2000
1800
1600
1400
1200
1000
800
600
400
200
500
1000
1500
2000
2500
1.2
1.15
1.1
1.05
1
0.9
0.8
0.7
0.6
0.5
0.4
0.3
0.2
0.1
0.05
0

R114

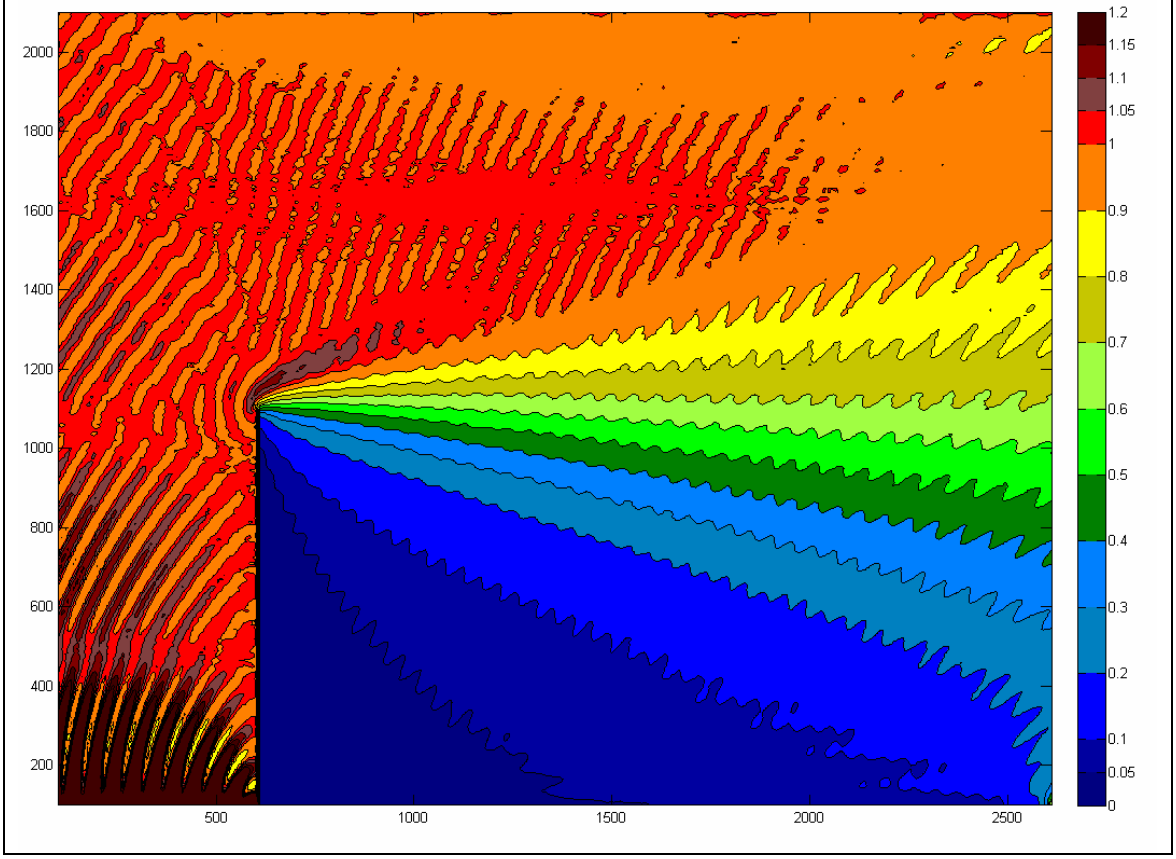
2000
1800
1600
1400
1200
1000
800
600
400
200
500
1000
1500
2000
2500
1.2
1.15
1.1
1.05
1
0.9
0.8
0.7
0.6
0.5
0.4
0.3
0.2
0.1
0.05
0

R115

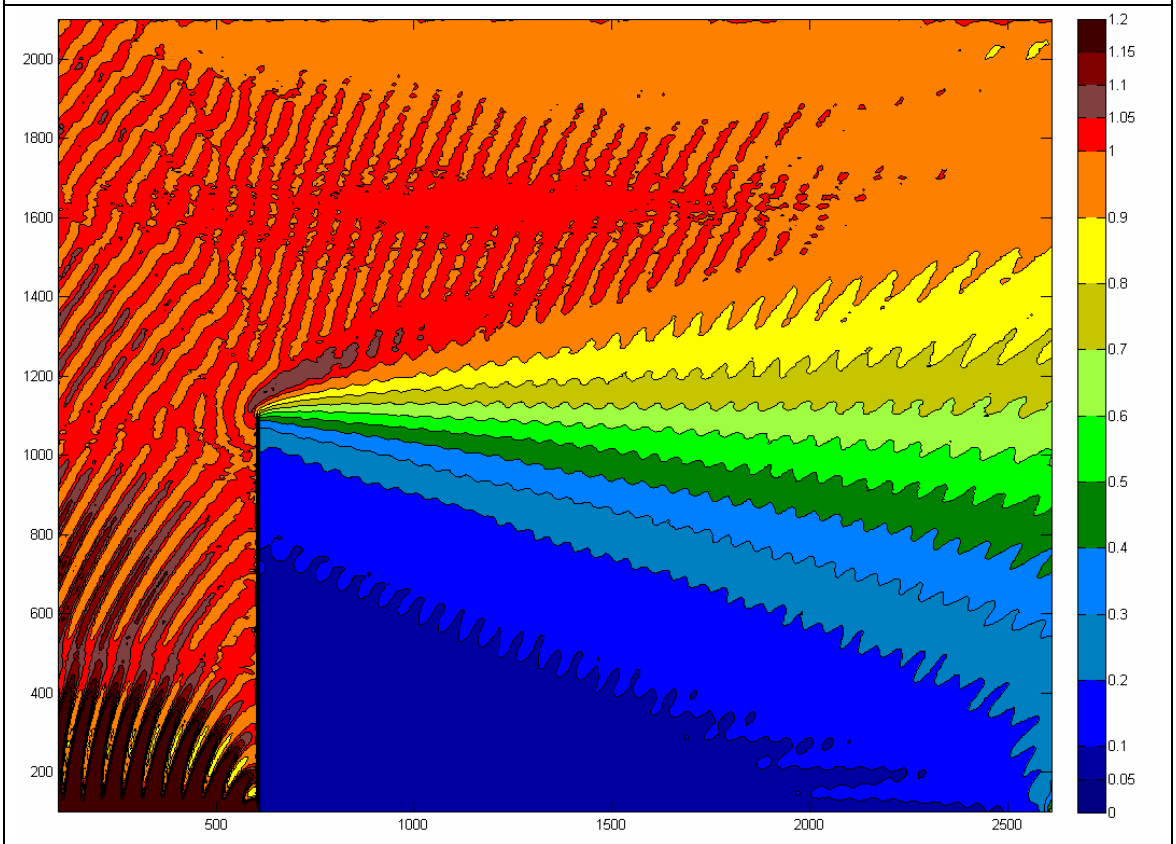
2000
1800
1600
1400
1200
1000
800
600
400
200
500
1000
1500
2000
2500
1.2
1.15
1.1
1.05
1
0.9
0.8
0.7
0.6
0.5
0.4
0.3
0.2
0.1
0.05
0

R120

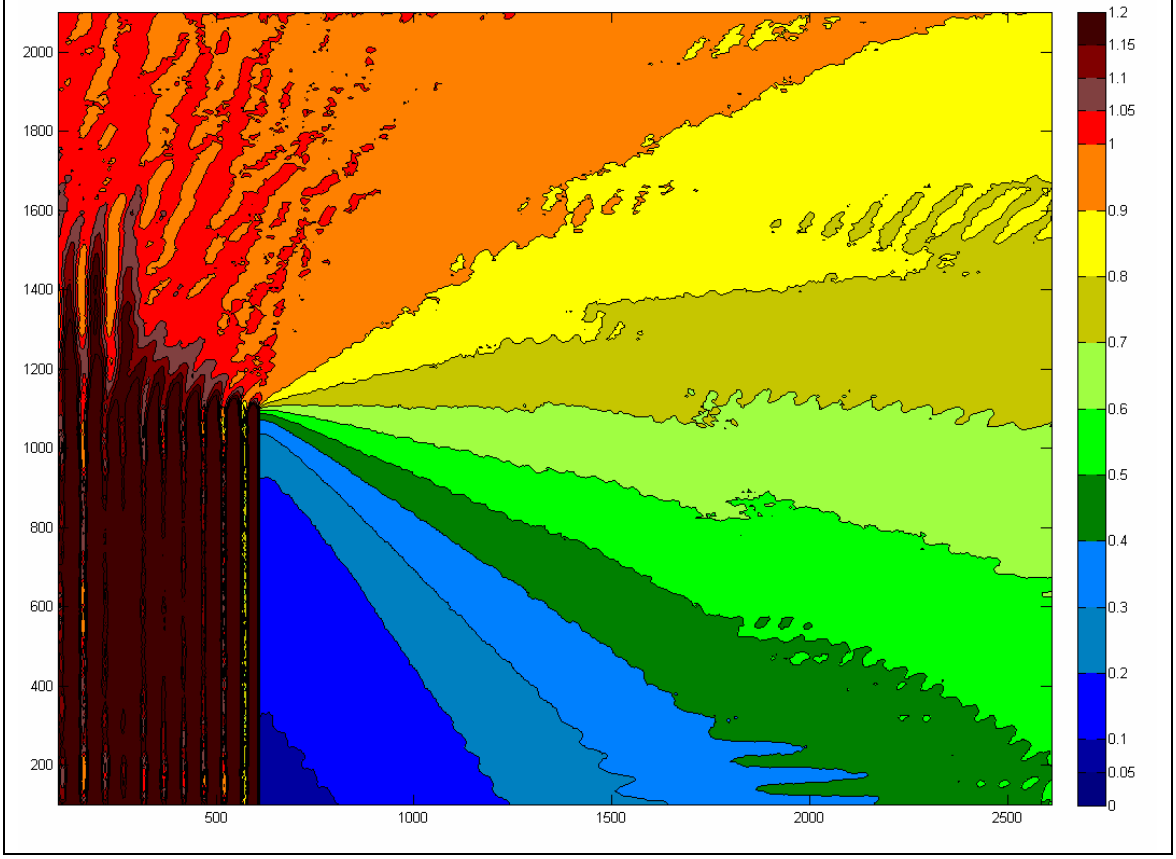
2000
1800
1600
1400
1200
1000
800
600
400
200
500
1000
1500
2000
2500
1.2
1.15
1.1
1.05
1
0.9
0.8
0.7
0.6
0.5
0.4
0.3
0.2
0.1
0.05
0

R121

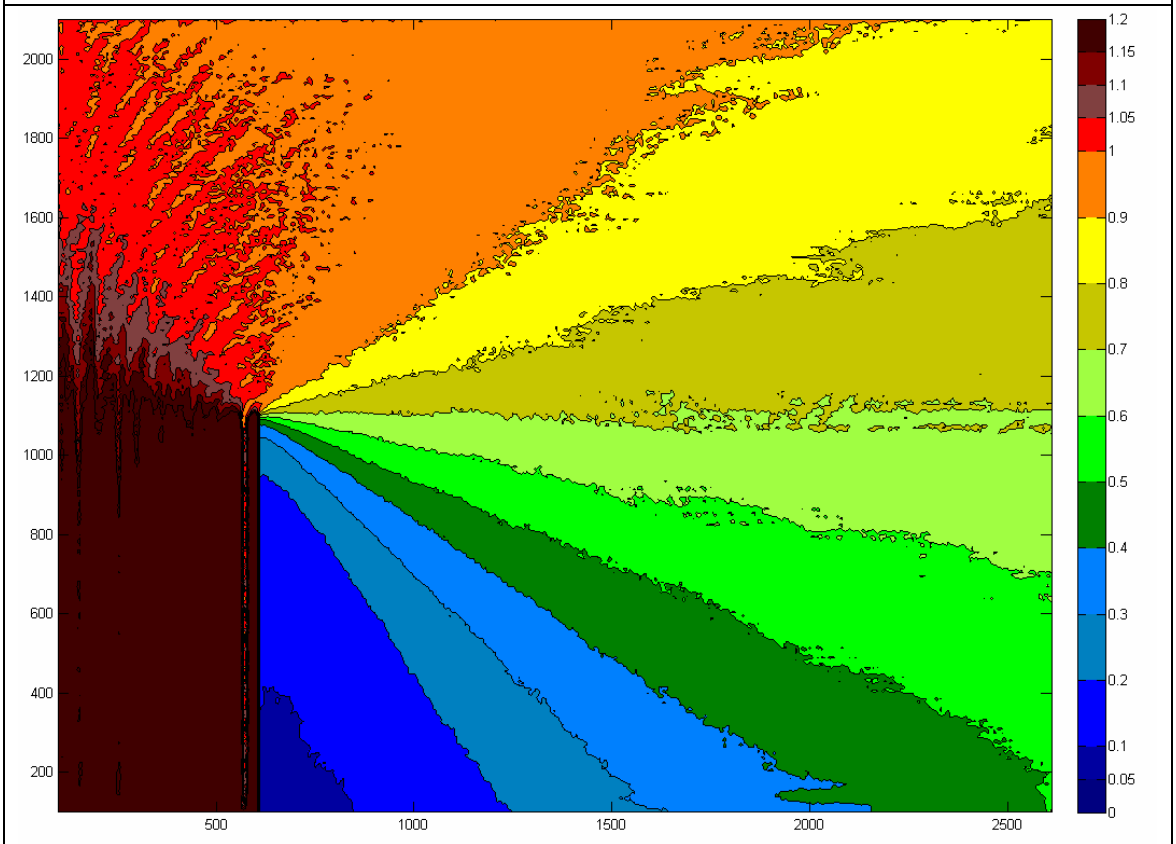
2000
1800
1600
1400
1200
1000
800
600
400
200
500
1000
1500
2000
2500
1.2
1.15
1.1
1.05
1
0.9
0.8
0.7
0.6
0.5
0.4
0.3
0.2
0.1
0.05
0

R122

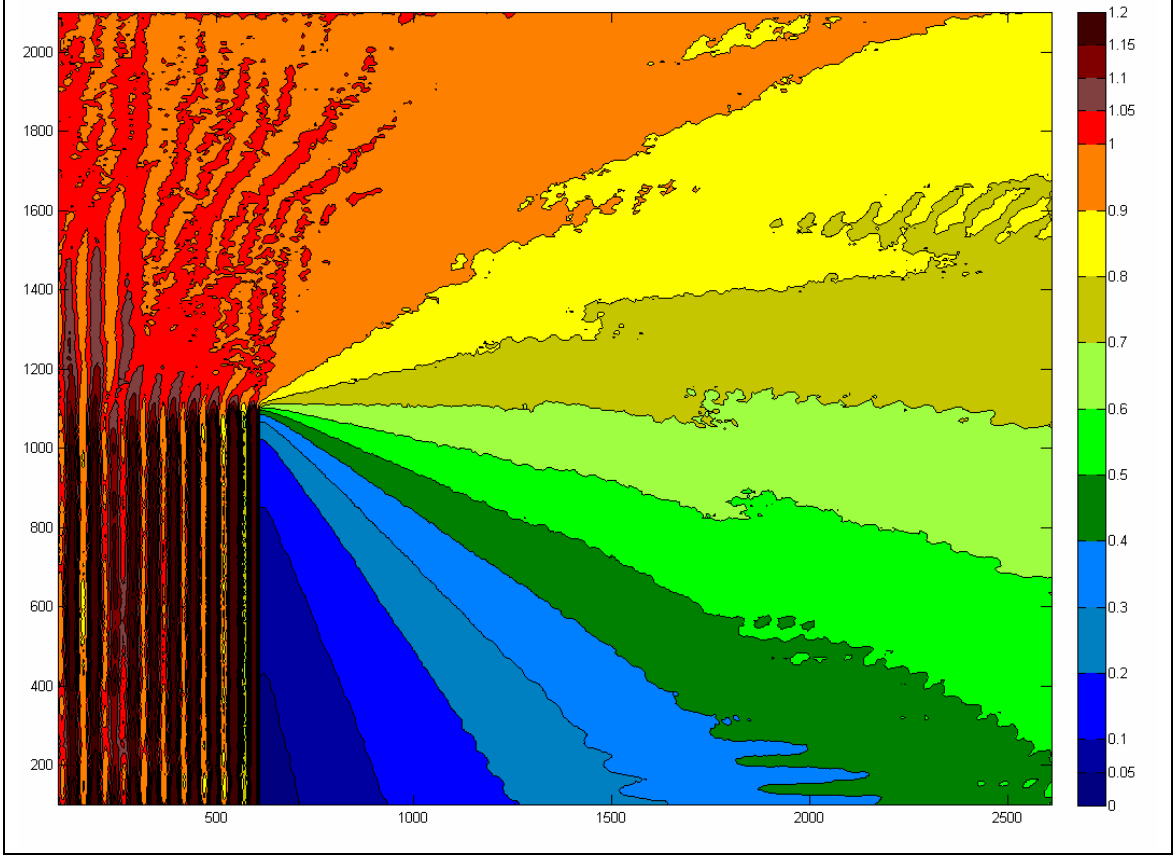
2000
1800
1600
1400
1200
1000
800
600
400
200
500
1000
1500
2000
2500
1.2
1.15
1.1
1.05
1
0.9
0.8
0.7
0.6
0.5
0.4
0.3
0.2
0.1
0.05
0

R124

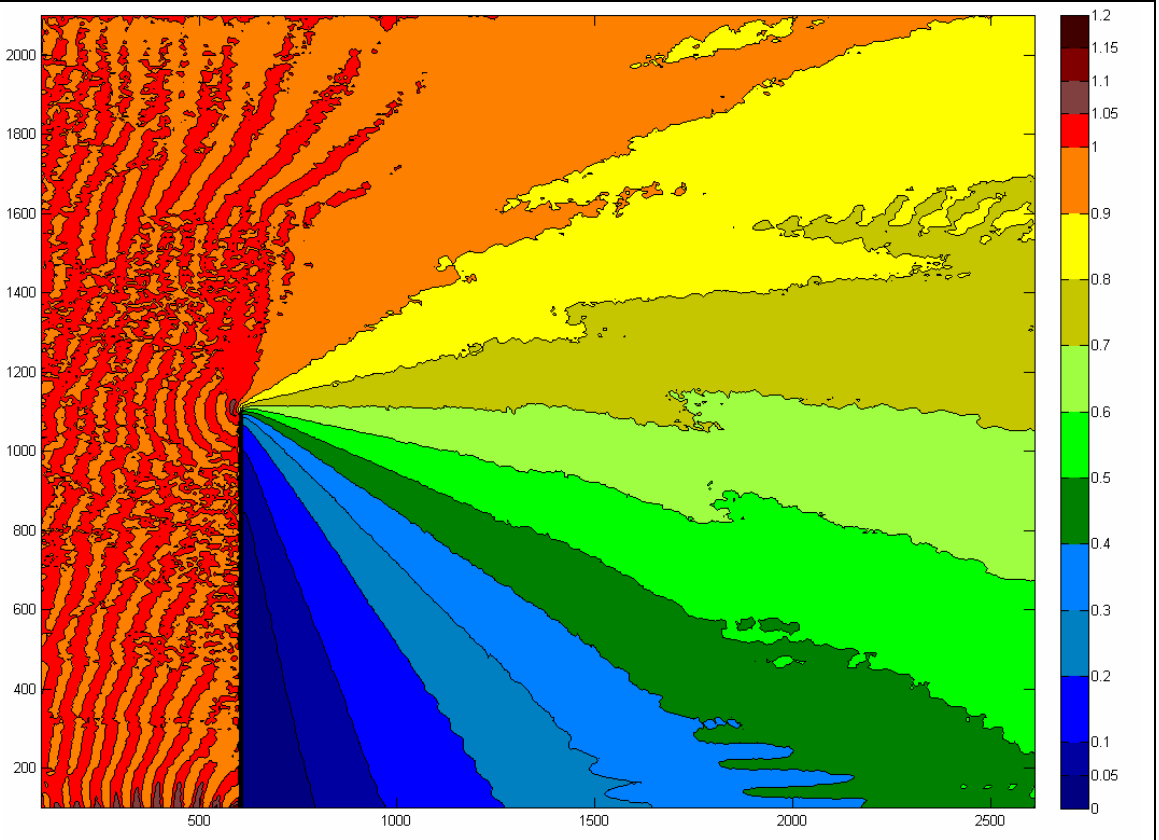
2000
1800
1600
1400
1200
1000
800
600
400
200
500
1000
1500
2000
2500
1.2
1.15
1.1
1.05
1
0.9
0.8
0.7
0.6
0.5
0.4
0.3
0.2
0.1
0.05
0

R125

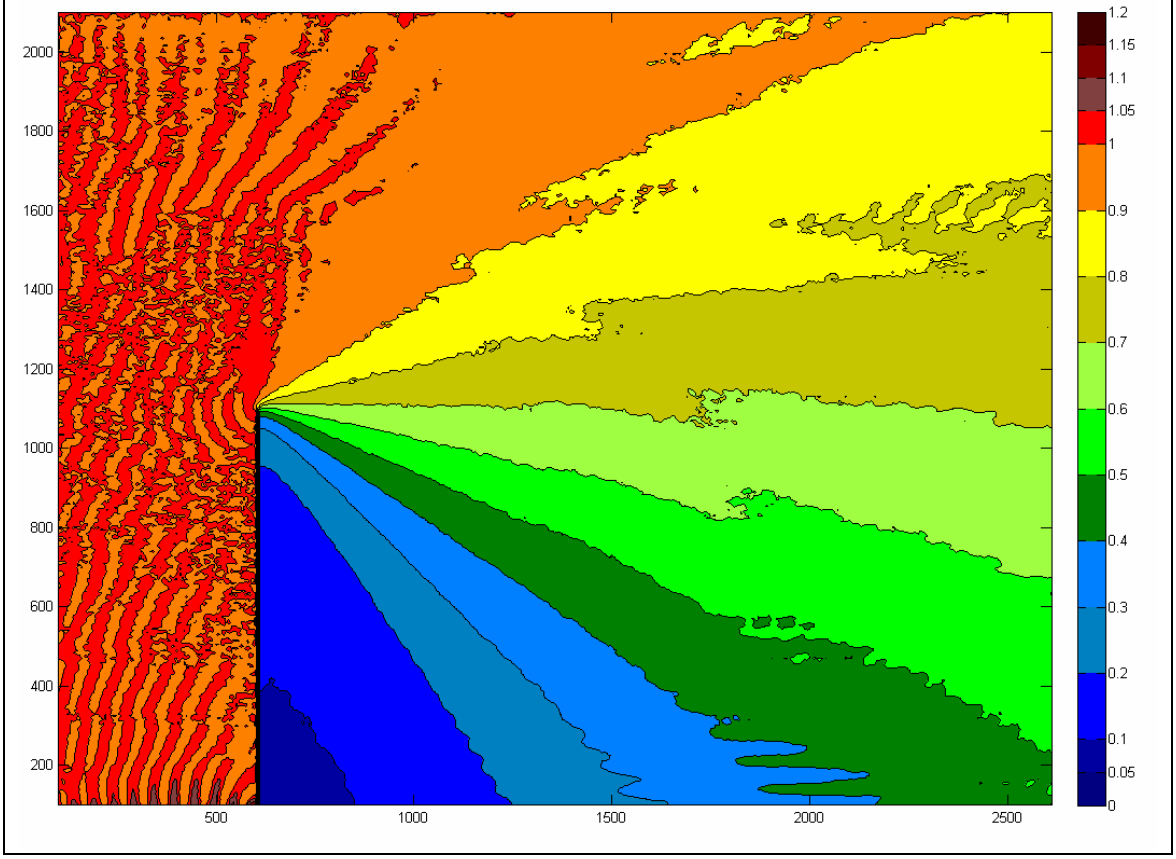
2000
1800
1600
1400
1200
1000
800
600
400
200
500
1000
1500
2000
2500
1.2
1.15
1.1
1.05
1
0.9
0.8
0.7
0.6
0.5
0.4
0.3
0.2
0.1
0.05
0

1WL Gap Pharos File Names

					Reflection		Directional		Spectral	
Run	**Wave Type**	**Model Type**	**Peak Per**	**Peak Dir**	**Front**	**Back**	**Spread (deg)**	**Interval (deg)**	**# frequencies**	**Notes:**
R00	Mono	Long Crest	8	0	100	100				
R01	Mono	Long Crest	8	0	50	50				
R02	Mono	Long Crest	8	0	0	0				
R10	Swell	Directional	8	0	100	100	-25 to 25	5		
R11	Swell	Spectral	8	0	100	100	-25 to 25	5	5	Smallest Mesh: 8/WL
R12	Swell	Directional	8	0	50	50	-25 to 25	5		
R14	Swell	Directional	8	0	0	0	-25 to 25	5		
R20	Wind	Directional	8	0	100	100	-80 to 80	10		
R21	Wind	Spectral	8	0	100	100	-80 to 80	10	5	Smallest Mesh: 8/WL
R22	Wind	Directional	8	0	50	50	-80 to 80	10		
R24	Wind	Directional	8	0	0	0	-80 to 80	10		

R00

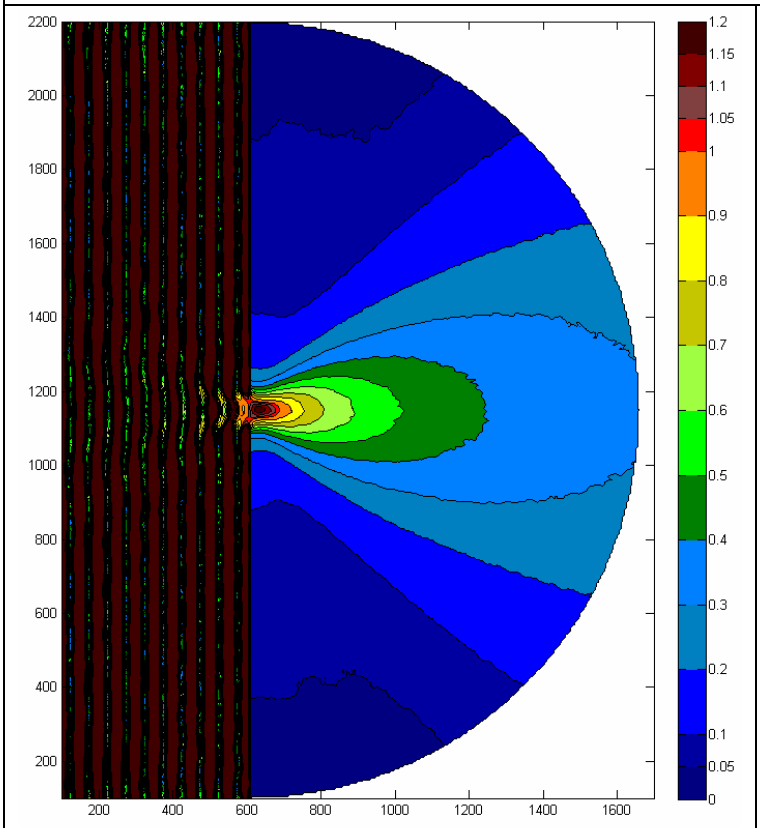
2200
2000
1800
1600
1400
1200
1000
800
600
400
200
200
400
600
800
1000
1200
1400
1600
1.2
1.15
1.1
1.05
1
0.9
0.8
0.7
0.6
0.5
0.4
0.3
0.2
0.1
0.05
0

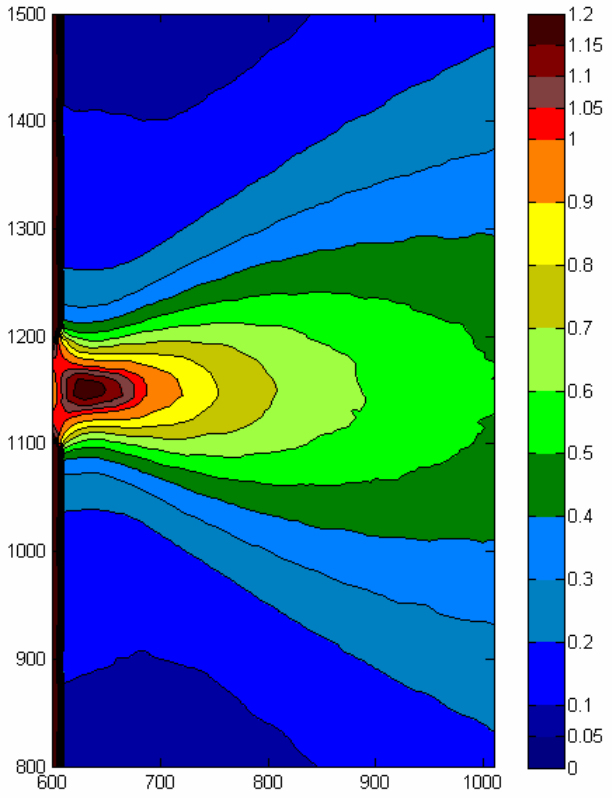
1500
1400
1300
1200
1100
1000
900
800
600
700
800
900
1000
1.2
1.15
1.1
1.05
1
0.9
0.8
0.7
0.6
0.5
0.4
0.3
0.2
0.1
0.05
0

R01

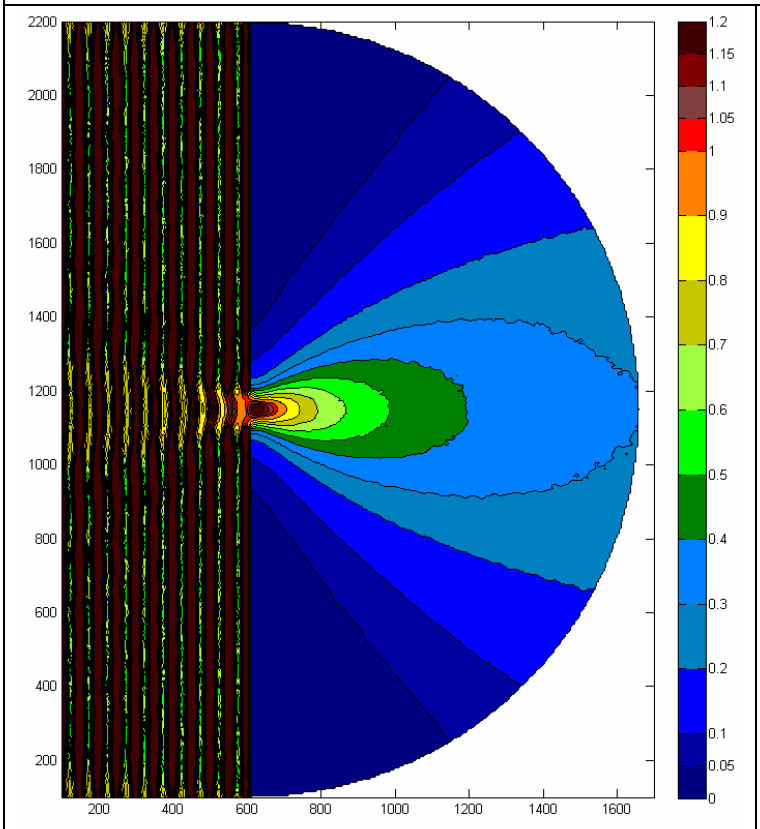
2200
2000
1800
1600
1400
1200
1000
800
600
400
200
200
400
600
800
1000
1200
1400
1600
1.2
1.15
1.1
1.05
1
0.9
0.8
0.7
0.6
0.5
0.4
0.3
0.2
0.1
0.05
0

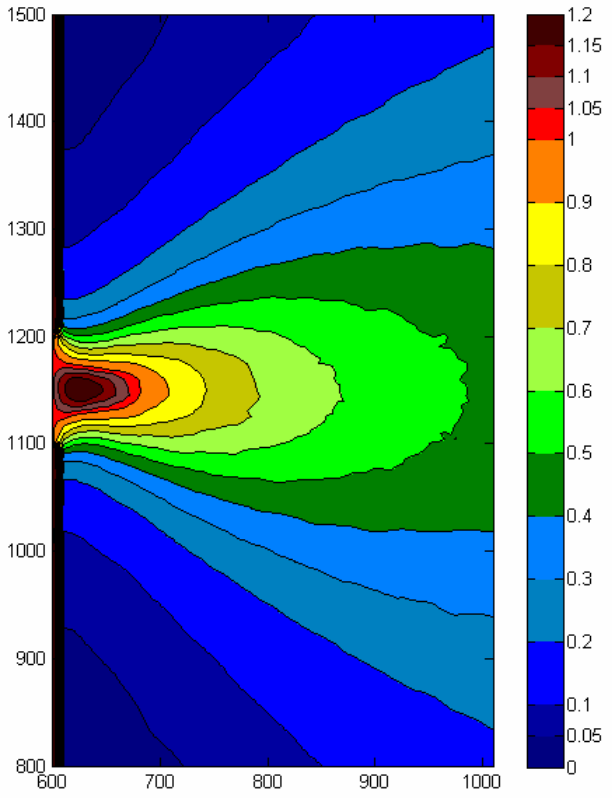
1500
1400
1300
1200
1100
1000
900
800
600
700
800
900
1000
1.2
1.15
1.1
1.05
1
0.9
0.8
0.7
0.6
0.5
0.4
0.3
0.2
0.1
0.05
0

R02

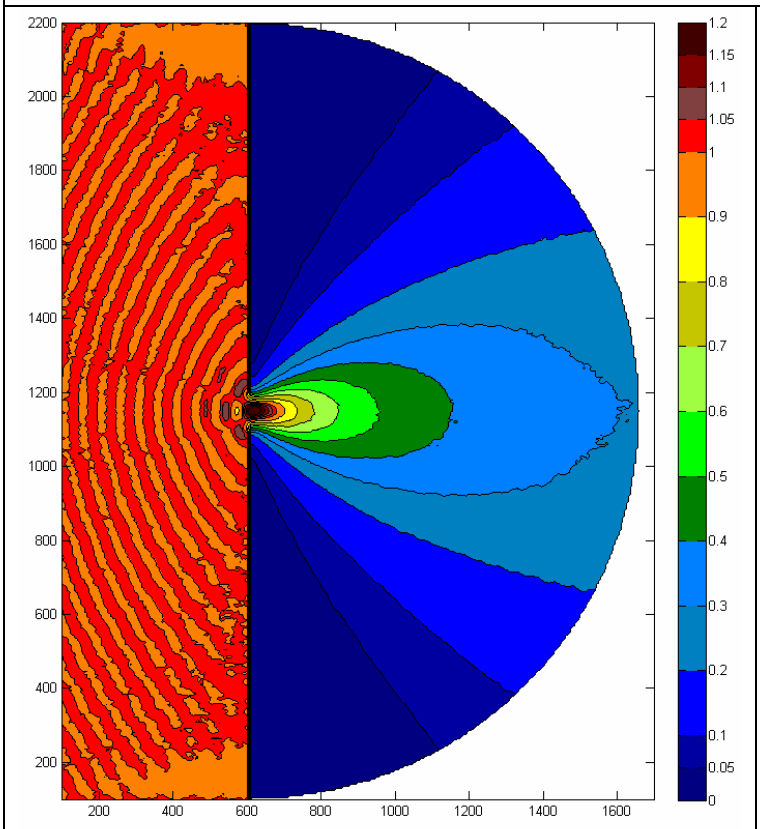
2200
2000
1800
1600
1400
1200
1000
800
600
400
200
200
400
600
800
1000
1200
1400
1600
1.2
1.15
1.1
1.05
1
0.9
0.8
0.7
0.6
0.5
0.4
0.3
0.2
0.1
0.05
0

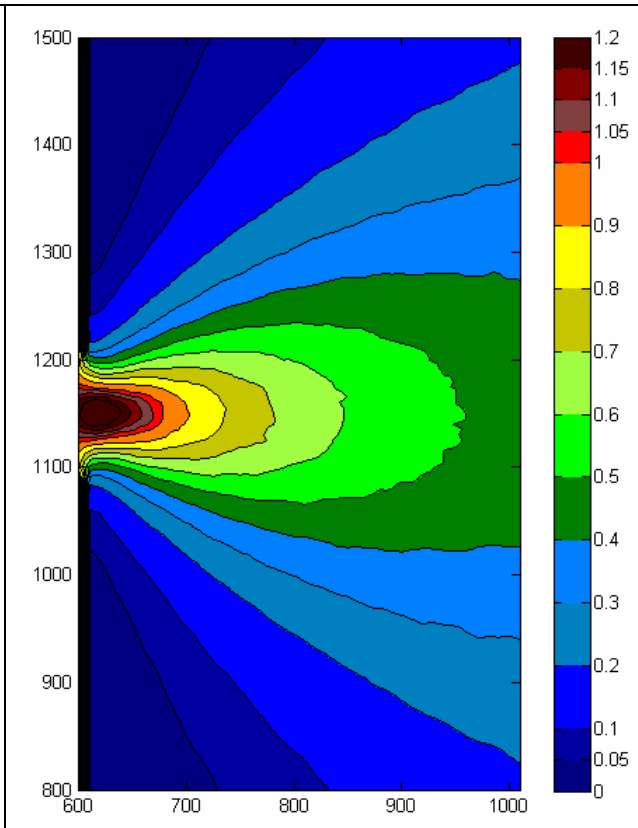
1500
1400
1300
1200
1100
1000
900
800
600
700
800
900
1000
1.2
1.15
1.1
1.05
1
0.9
0.8
0.7
0.6
0.5
0.4
0.3
0.2
0.1
0.05
0

R10

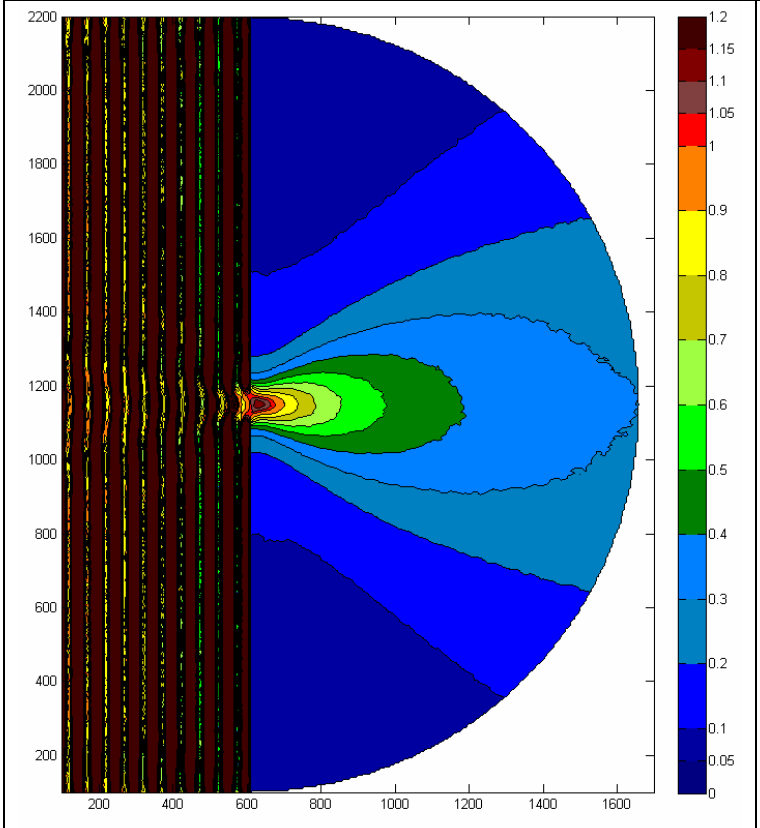
2200
2000
1800
1600
1400
1200
1000
800
600
400
200
200
400
600
800
1000
1200
1400
1600
1.2
1.15
1.1
1.05
1
0.9
0.8
0.7
0.6
0.5
0.4
0.3
0.2
0.1
0.05
0

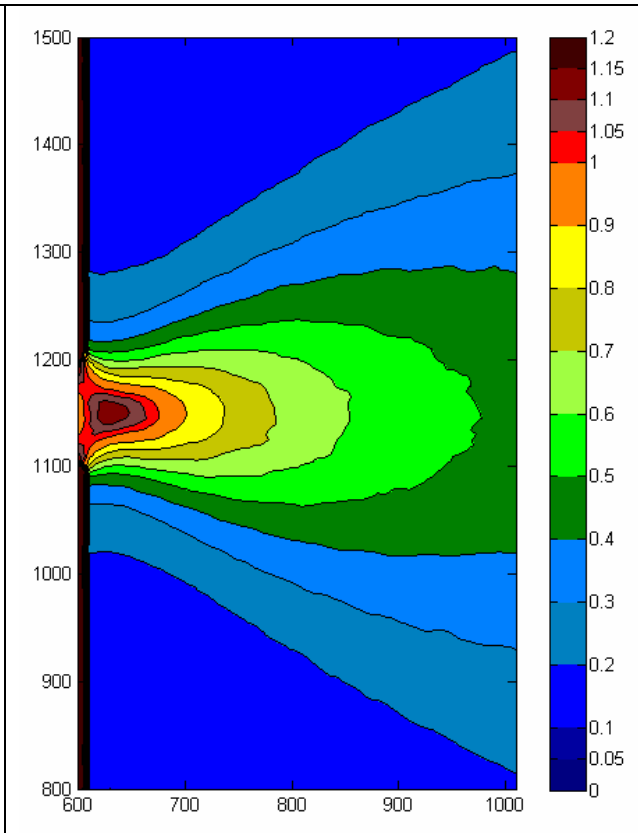
1500
1400
1300
1200
1100
1000
900
800
600
700
800
900
1000
1.2
1.15
1.1
1.05
1
0.9
0.8
0.7
0.6
0.5
0.4
0.3
0.2
0.1
0.05
0

R11

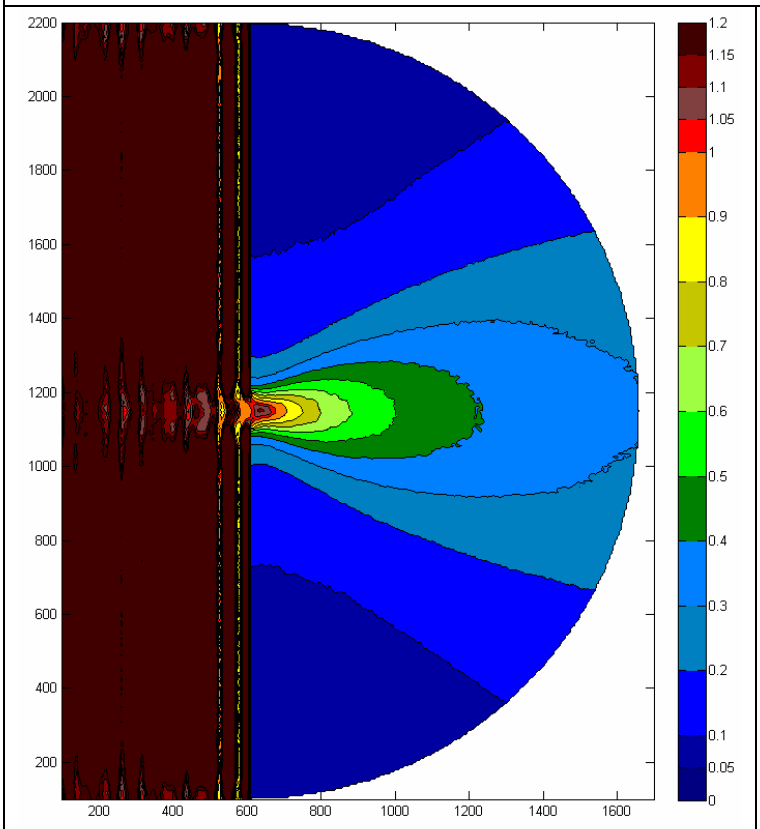
2200
2000
1800
1600
1400
1200
1000
800
600
400
200
200
400
600
800
1000
1200
1400
1600
1.2
1.15
1.1
1.05
1
0.9
0.8
0.7
0.6
0.5
0.4
0.3
0.2
0.1
0.05
0

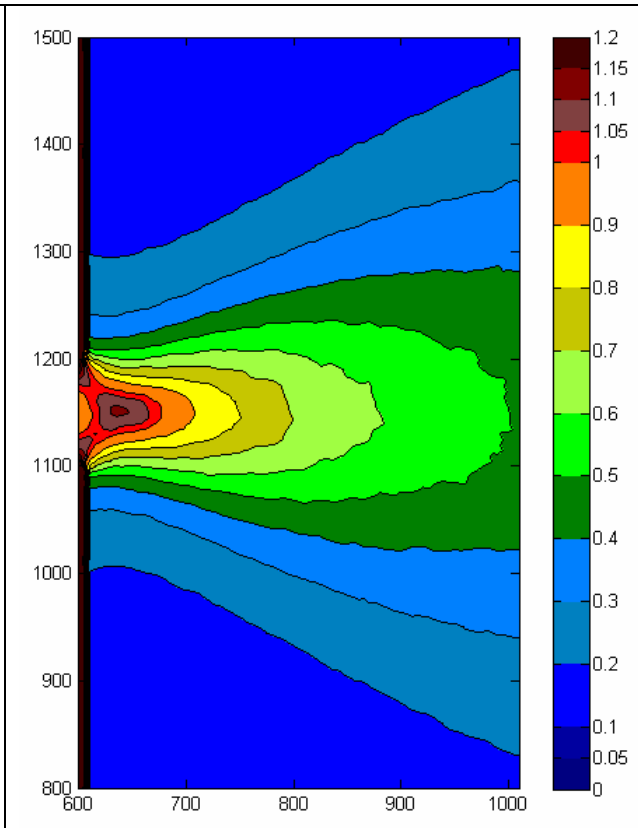
1500
1400
1300
1200
1100
1000
900
800
600
700
800
900
1000
1.2
1.15
1.1
1.05
1
0.9
0.8
0.7
0.6
0.5
0.4
0.3
0.2
0.1
0.05
0

R12

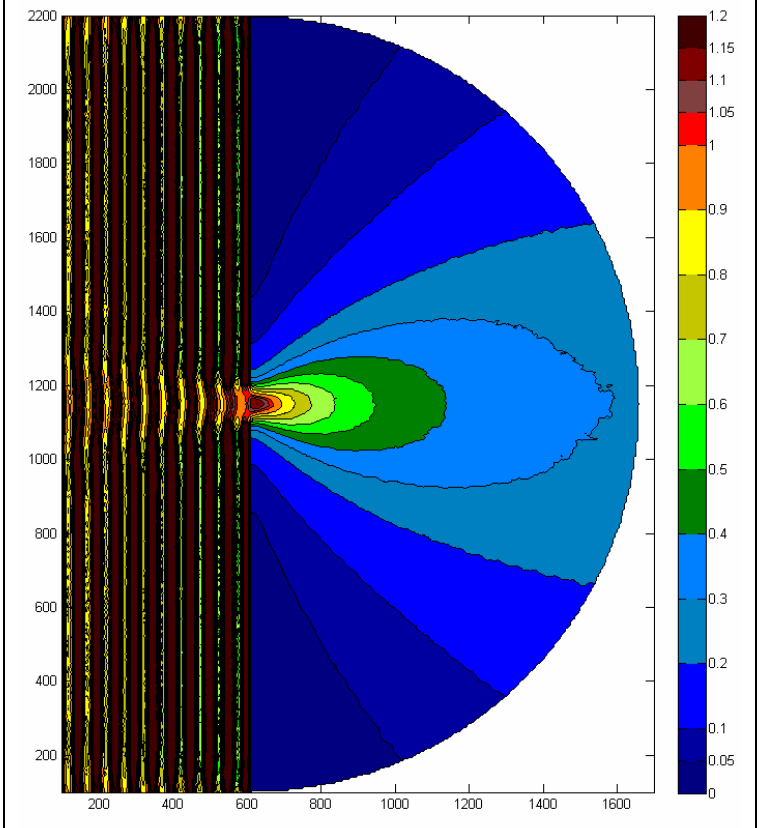
2200
2000
1800
1600
1400
1200
1000
800
600
400
200
200
400
600
800
1000
1200
1400
1600
1.2
1.15
1.1
1.05
1
0.9
0.8
0.7
0.6
0.5
0.4
0.3
0.2
0.1
0.05
0

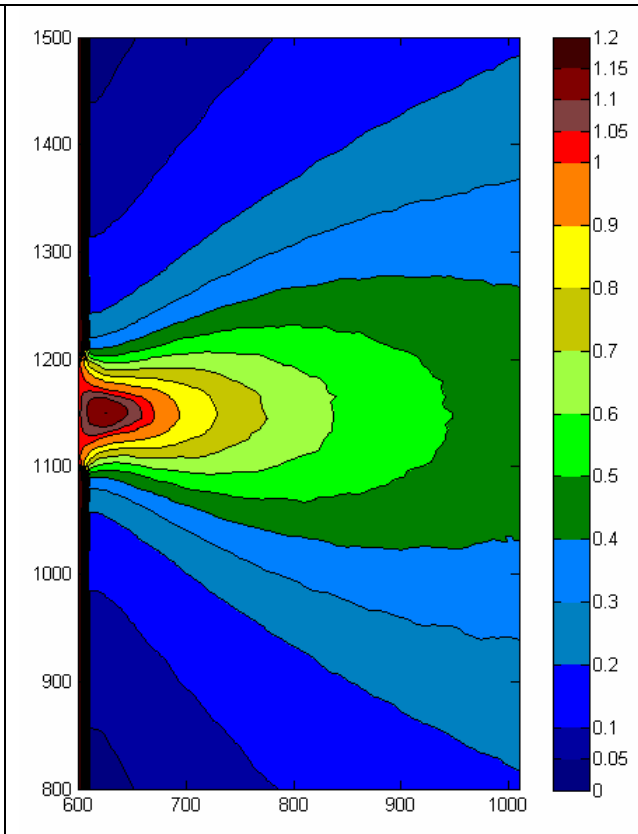
1500
1400
1300
1200
1100
1000
900
800
600
700
800
900
1000
1.2
1.15
1.1
1.05
1
0.9
0.8
0.7
0.6
0.5
0.4
0.3
0.2
0.1
0.05
0

R14

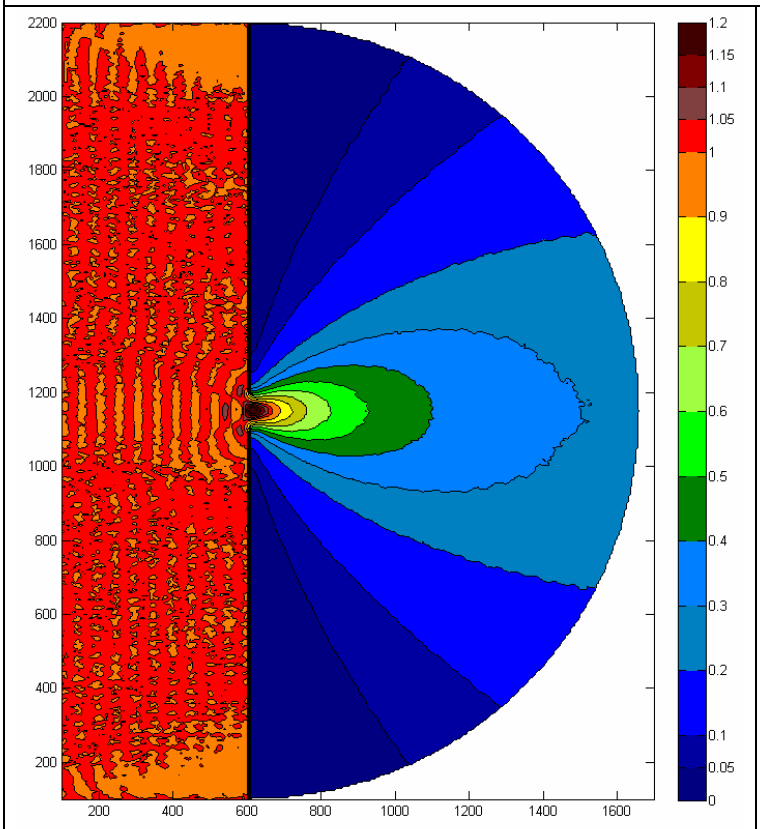
2200
2000
1800
1600
1400
1200
1000
800
600
400
200
200
400
600
800
1000
1200
1400
1600
1.2
1.15
1.1
1.05
1
0.9
0.8
0.7
0.6
0.5
0.4
0.3
0.2
0.1
0.05
0

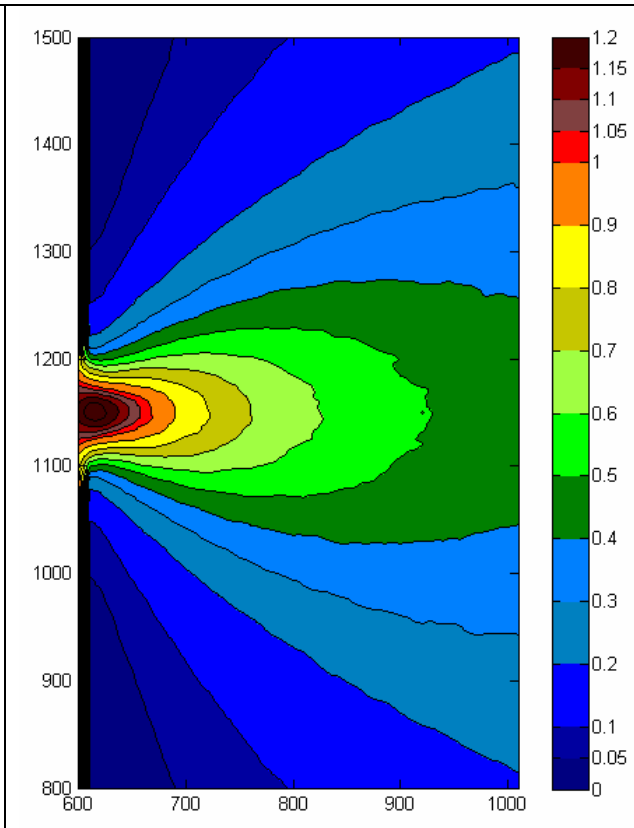
1500
1400
1300
1200
1100
1000
900
800
600
700
800
900
1000
1.2
1.15
1.1
1.05
1
0.9
0.8
0.7
0.6
0.5
0.4
0.3
0.2
0.1
0.05
0

R20

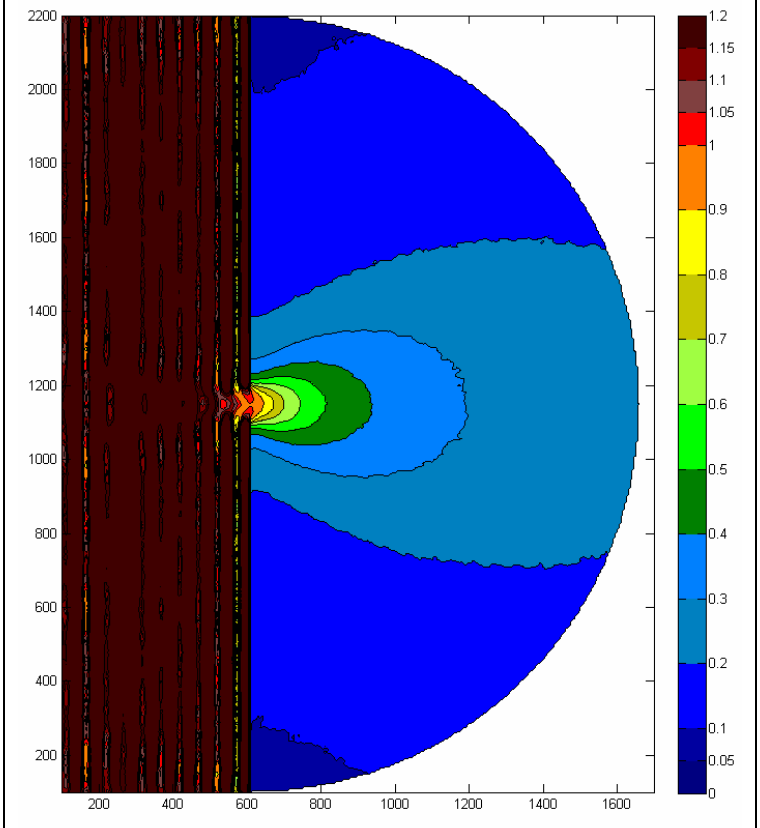
2200
2000
1800
1600
1400
1200
1000
800
600
400
200
200
400
600
800
1000
1200
1400
1600
1.2
1.15
1.1
1.05
1
0.9
0.8
0.7
0.6
0.5
0.4
0.3
0.2
0.1
0.05
0

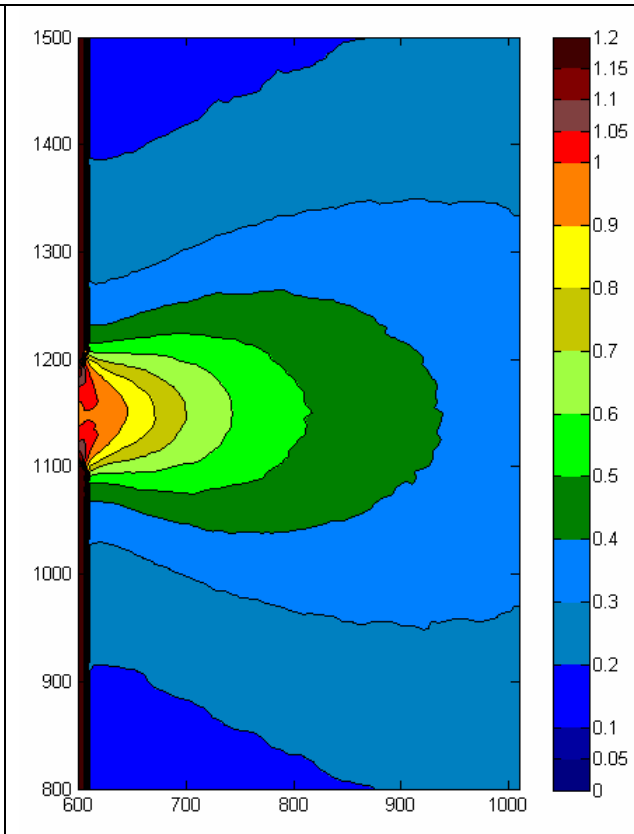
1500
1400
1300
1200
1100
1000
900
800
600
700
800
900
1000
1.2
1.15
1.1
1.05
1
0.9
0.8
0.7
0.6
0.5
0.4
0.3
0.2
0.1
0.05
0

R21

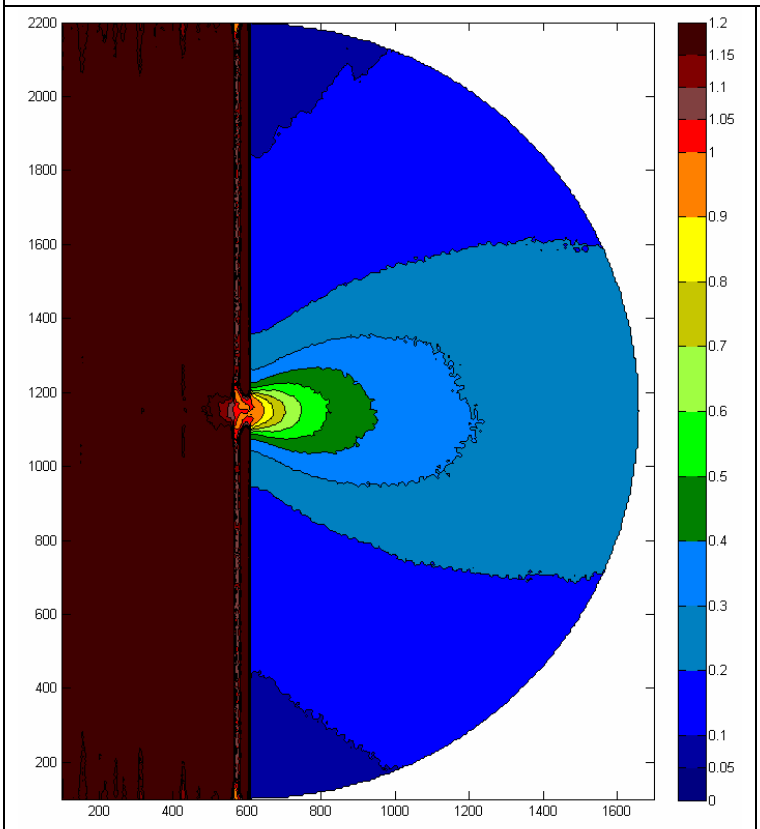
2200
2000
1800
1600
1400
1200
1000
800
600
400
200
200
400
600
800
1000
1200
1400
1600
1.2
1.15
1.1
1.05
1
0.9
0.8
0.7
0.6
0.5
0.4
0.3
0.2
0.1
0.05
0

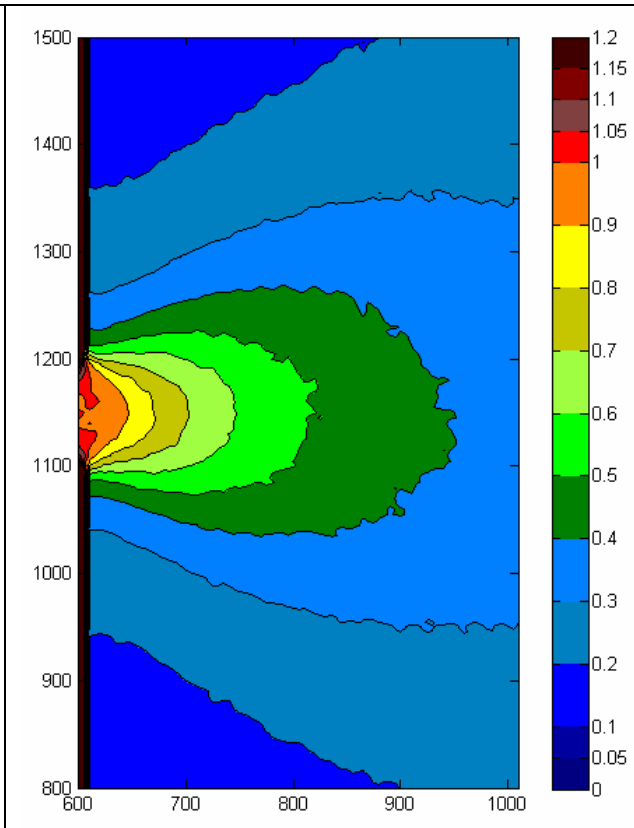
1500
1400
1300
1200
1100
1000
900
800
600
700
800
900
1000
1.2
1.15
1.1
1.05
1
0.9
0.8
0.7
0.6
0.5
0.4
0.3
0.2
0.1
0.05
0

R22

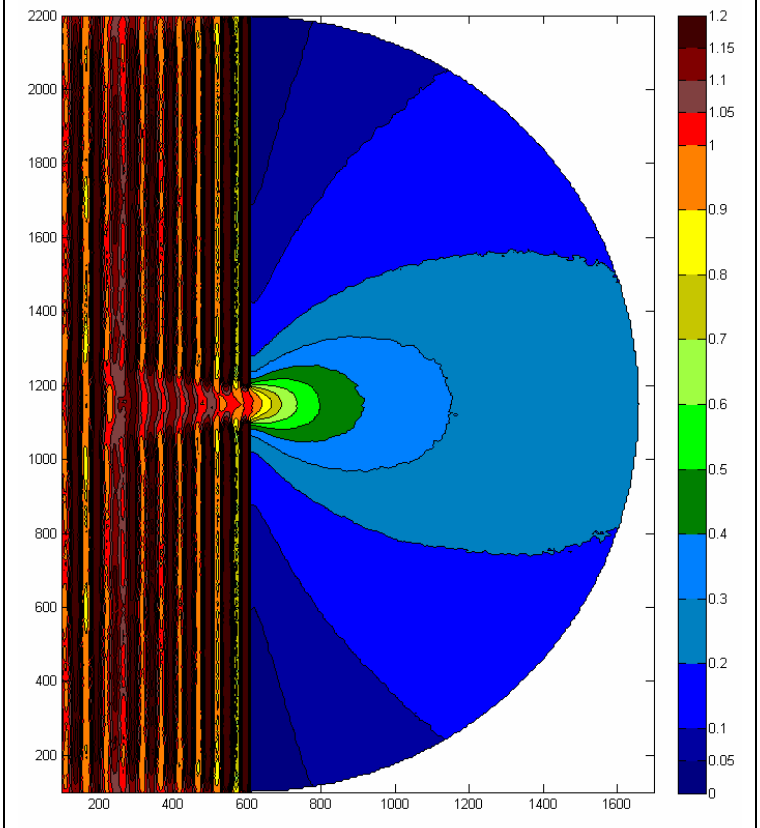
2200
2000
1800
1600
1400
1200
1000
800
600
400
200
200
400
600
800
1000
1200
1400
1600
1.2
1.15
1.1
1.05
1
0.9
0.8
0.7
0.6
0.5
0.4
0.3
0.2
0.1
0.05
0

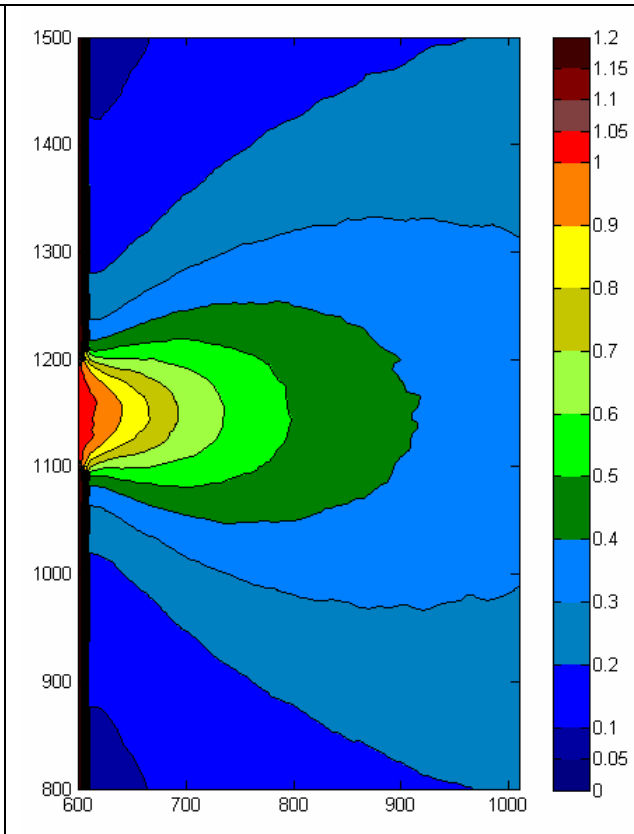
1500
1400
1300
1200
1100
1000
900
800
600
700
800
900
1000
1.2
1.15
1.1
1.05
1
0.9
0.8
0.7
0.6
0.5
0.4
0.3
0.2
0.1
0.05
0

R24

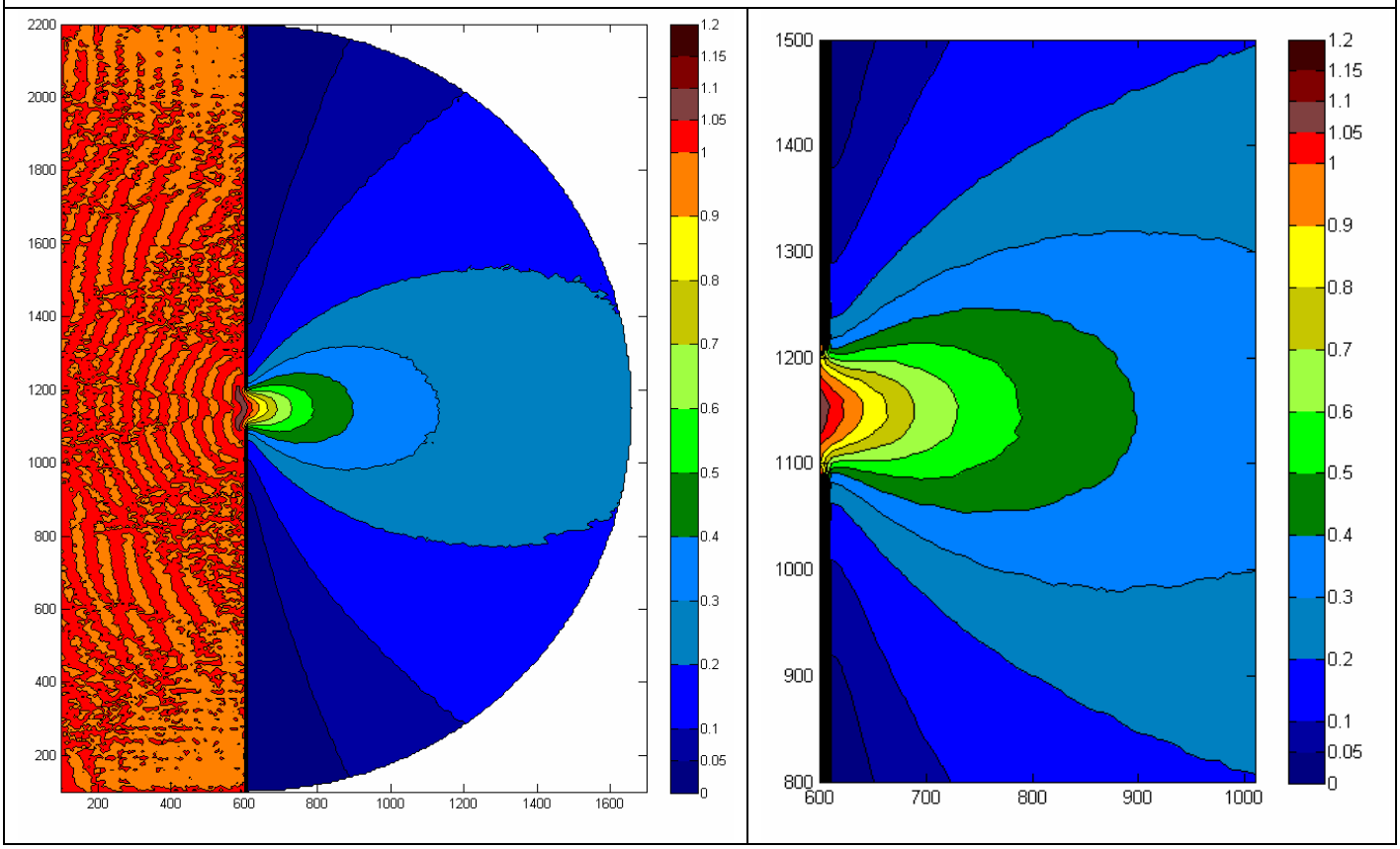
2200
2000
1800
1600
1400
1200
1000
800
600
400
200
200
400
600
800
1000
1200
1400
1600
1.2
1.15
1.1
1.05
1
0.9
0.8
0.7
0.6
0.5
0.4
0.3
0.2
0.1
0.05
0
1500
1400
1300
1200
1100
1000
900
800
600
700
800
900
1000
1.2
1.15
1.1
1.05
1
0.9
0.8
0.7
0.6
0.5
0.4
0.3
0.2
0.1
0.05
0

2WL Gap Pharos File Names

					Reflection		Directional		Spectral	
Run	**Wave Type**	**Model Type**	**Peak Per**	**Peak Dir**	**Front**	**Back**	**Spread (deg)**	**Interval (deg)**	**# frequencies**	**Notes:**
R00	Mono	Long Crest	8	0	100	100				
R01	Mono	Long Crest	8	0	50	50				
R02	Mono	Long Crest	8	0	0	0				
R03	Mono	Long Crest	8	0	0	100				
R10	Swell	Directional	8	0	100	100	-25 to 25	5		
R11	Swell	Spectral	8	0	100	100	-25 to 25	5	5	Smallest Mesh: 8/WL
R12	Swell	Directional	8	0	50	50	-25 to 25	5		
R14	Swell	Directional	8	0	0	0	-25 to 25	5		
R15	Swell	Directional	8	0	0	100	-25 to 25	5		
R20	Wind	Directional	8	0	100	100	-80 to 80	10		
R21	Wind	Spectral	8	0	100	100	-80 to 80	10	5	Smallest Mesh: 8/WL
R22	Wind	Directional	8	0	50	50	-80 to 80	10		
R24	Wind	Directional	8	0	0	0	-80 to 80	10		
R25	Wind	Directional	8	0	0	100	-80 to 80	10		
R121	Wind	Spectral	8	0	100	100	-80 to 80	10	5	Smallest Mesh: 32/WL

R00

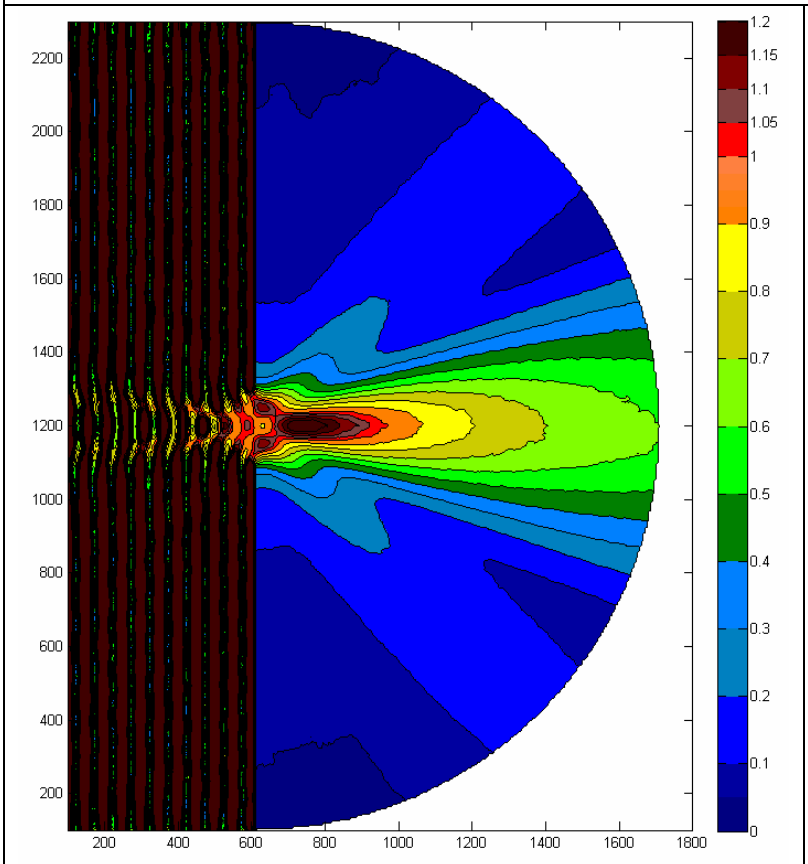
2200
2000
1800
1600
1400
1200
1000
800
600
400
200
200 400 600 800 1000 1200 1400 1600 1800
1.2
1.15
1.1
1.05
1
0.9
0.8
0.7
0.6
0.5
0.4
0.3
0.2
0.1
0

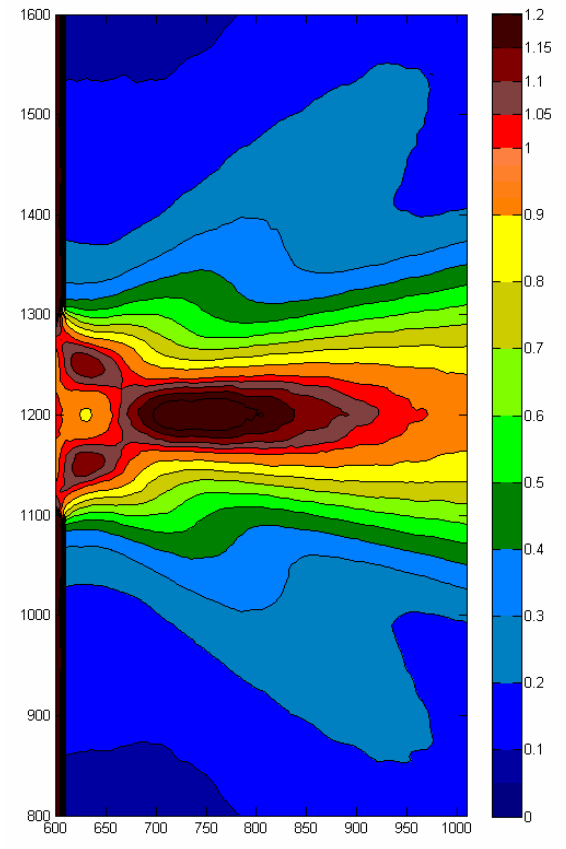
1600
1500
1400
1300
1200
1100
1000
900
800
600 650 700 750 800 850 900 950 1000
1.2
1.15
1.1
1.05
1
0.9
0.8
0.7
0.6
0.5
0.4
0.3
0.2
0.1
0

R01

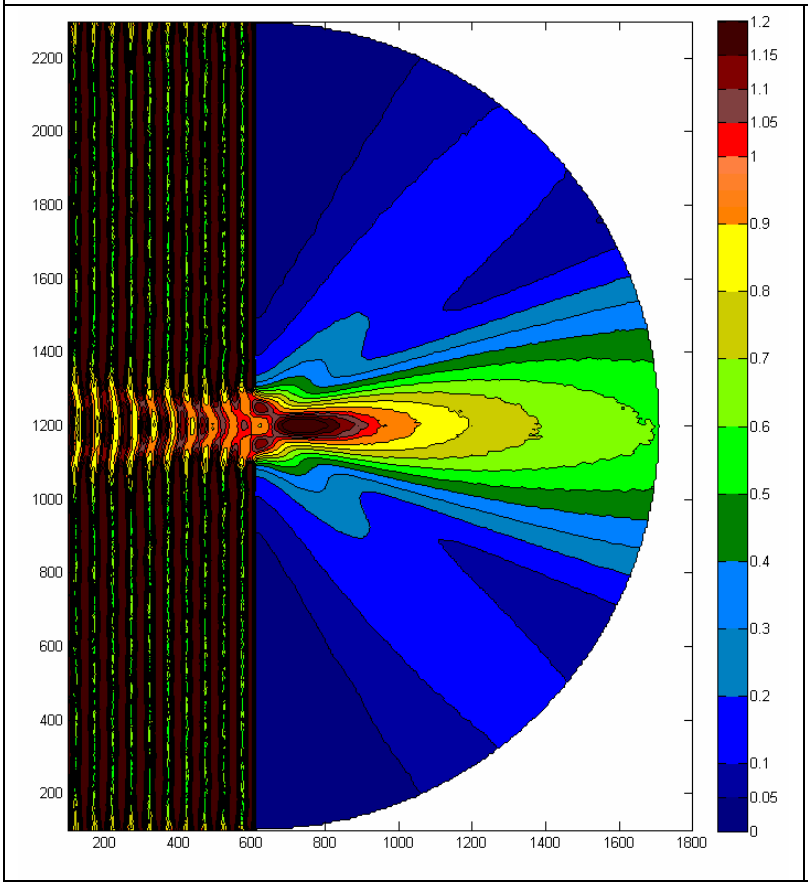
2200
2000
1800
1600
1400
1200
1000
800
600
400
200
200 400 600 800 1000 1200 1400 1600 1800
1.2
1.15
1.1
1.05
1
0.9
0.8
0.7
0.6
0.5
0.4
0.3
0.2
0.1
0.05
0

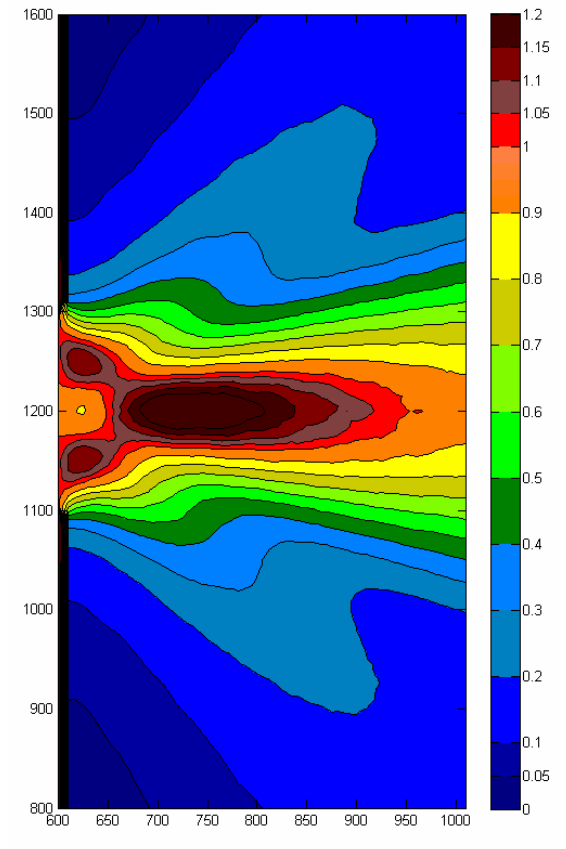
1600
1500
1400
1300
1200
1100
1000
900
800
600 650 700 750 800 850 900 950 1000
1.2
1.15
1.1
1.05
1
0.9
0.8
0.7
0.6
0.5
0.4
0.3
0.2
0.1
0.05
0

R02

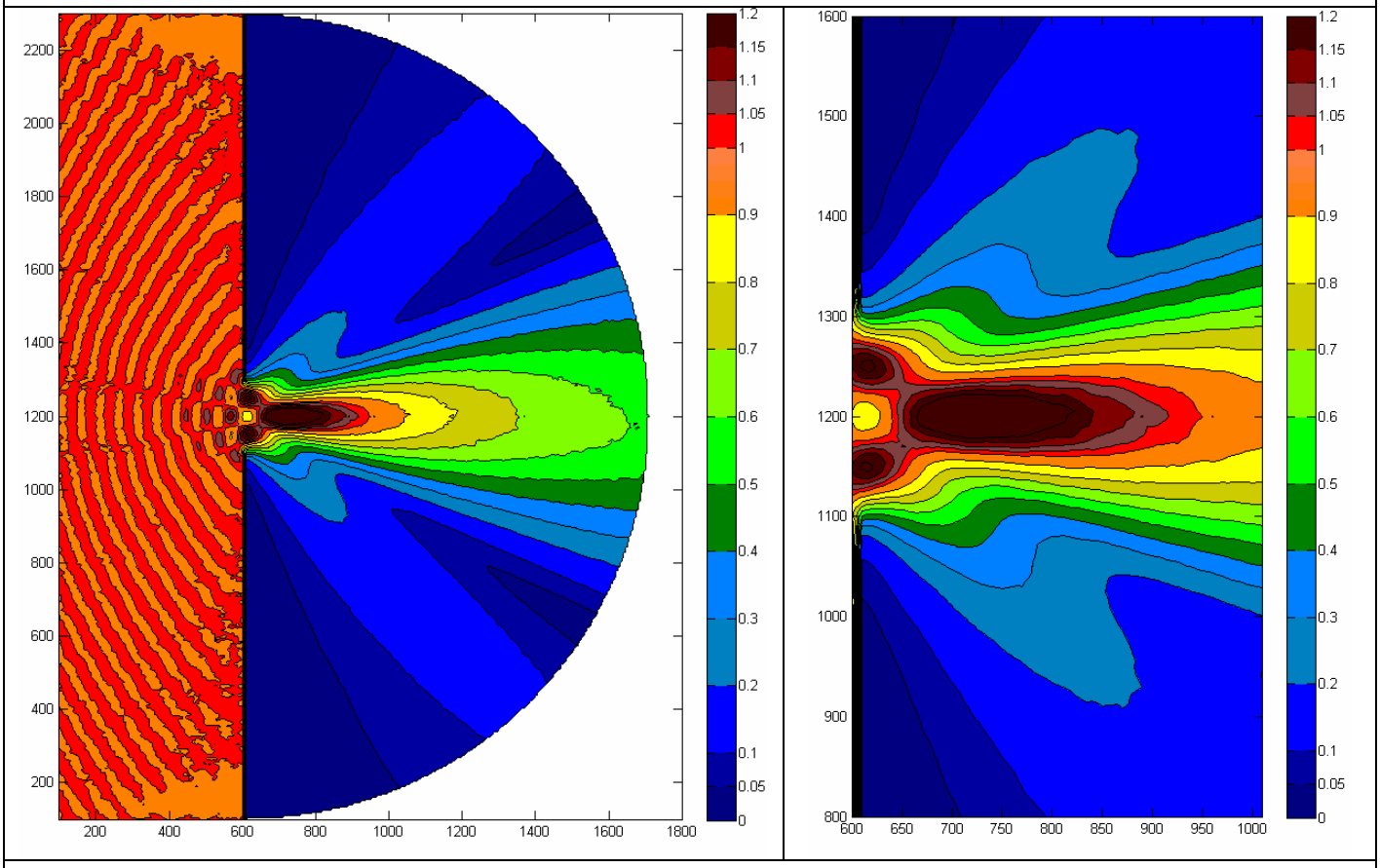
2200
2000
1800
1600
1400
1200
1000
800
600
400
200
200 400 600 800 1000 1200 1400 1600 1800
1.2
1.15
1.1
1.05
1
0.9
0.8
0.7
0.6
0.5
0.4
0.3
0.2
0.1
0.05
0
1600
1500
1400
1300
1200
1100
1000
900
800
600 650 700 750 800 850 900 950 1000

R03

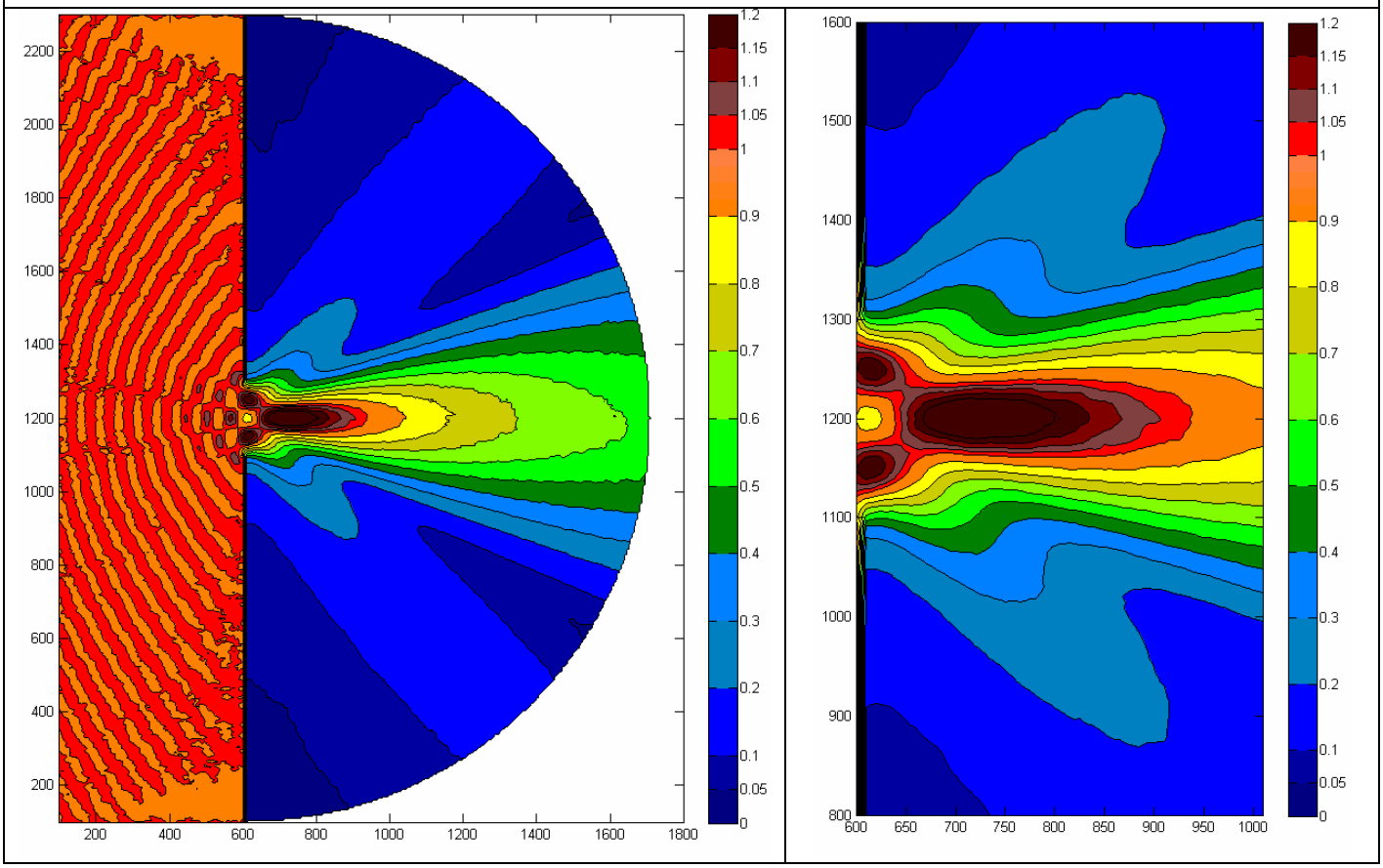
2200
2000
1800
1600
1400
1200
1000
800
600
400
200
200 400 600 800 1000 1200 1400 1600 1800
1.2
1.15
1.1
1.05
1
0.9
0.8
0.7
0.6
0.5
0.4
0.3
0.2
0.1
0.05
0
1600
1500
1400
1300
1200
1100
1000
900
800
600 650 700 750 800 850 900 950 1000

R10

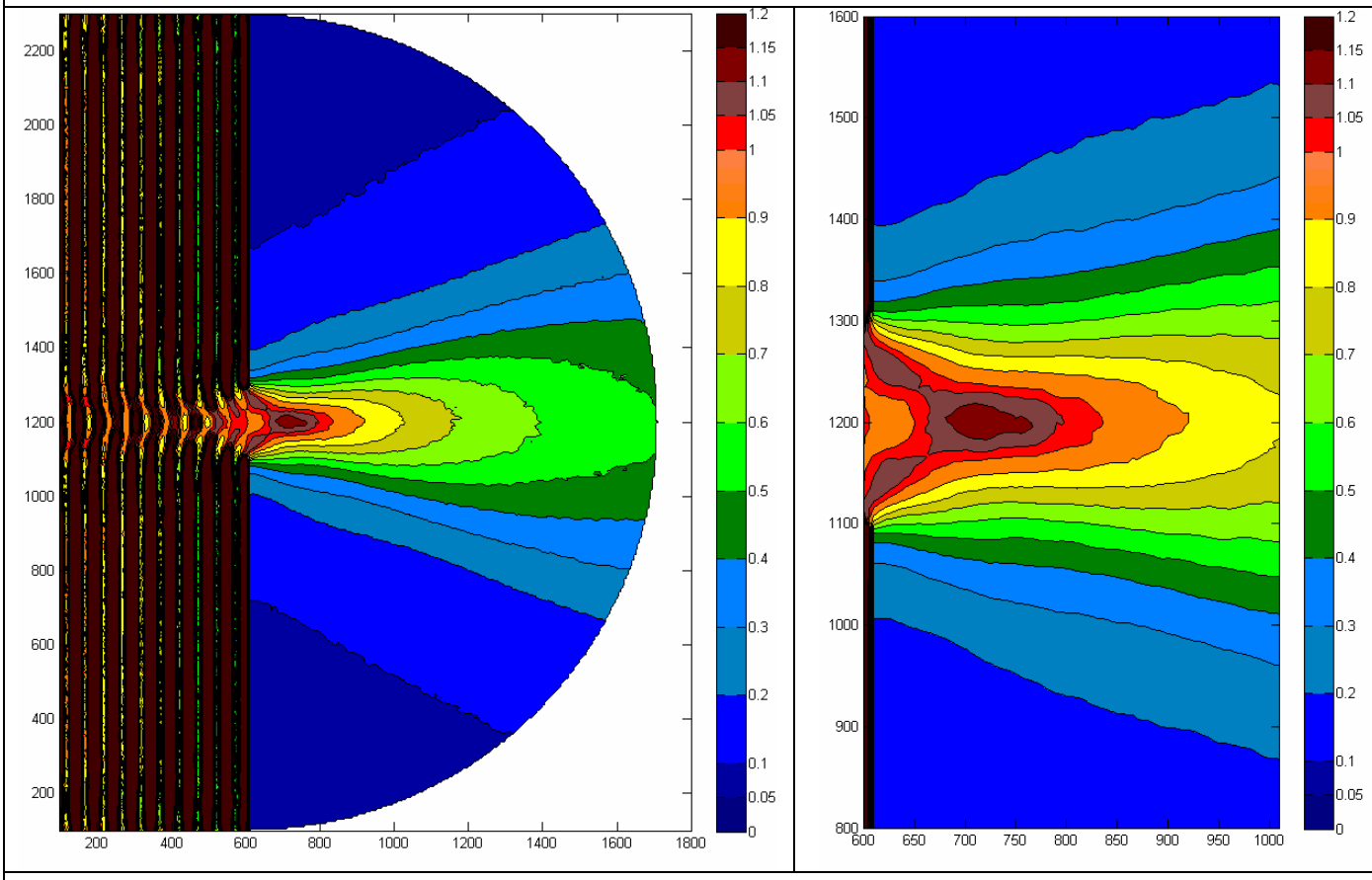
2200
2000
1800
1600
1400
1200
1000
800
600
400
200
200 400 600 800 1000 1200 1400 1600 1800
1.2
1.15
1.1
1.05
1
0.9
0.8
0.7
0.6
0.5
0.4
0.3
0.2
0.1
0.05
0
1600
1500
1400
1300
1200
1100
1000
900
800
600 650 700 750 800 850 900 950 1000

R11

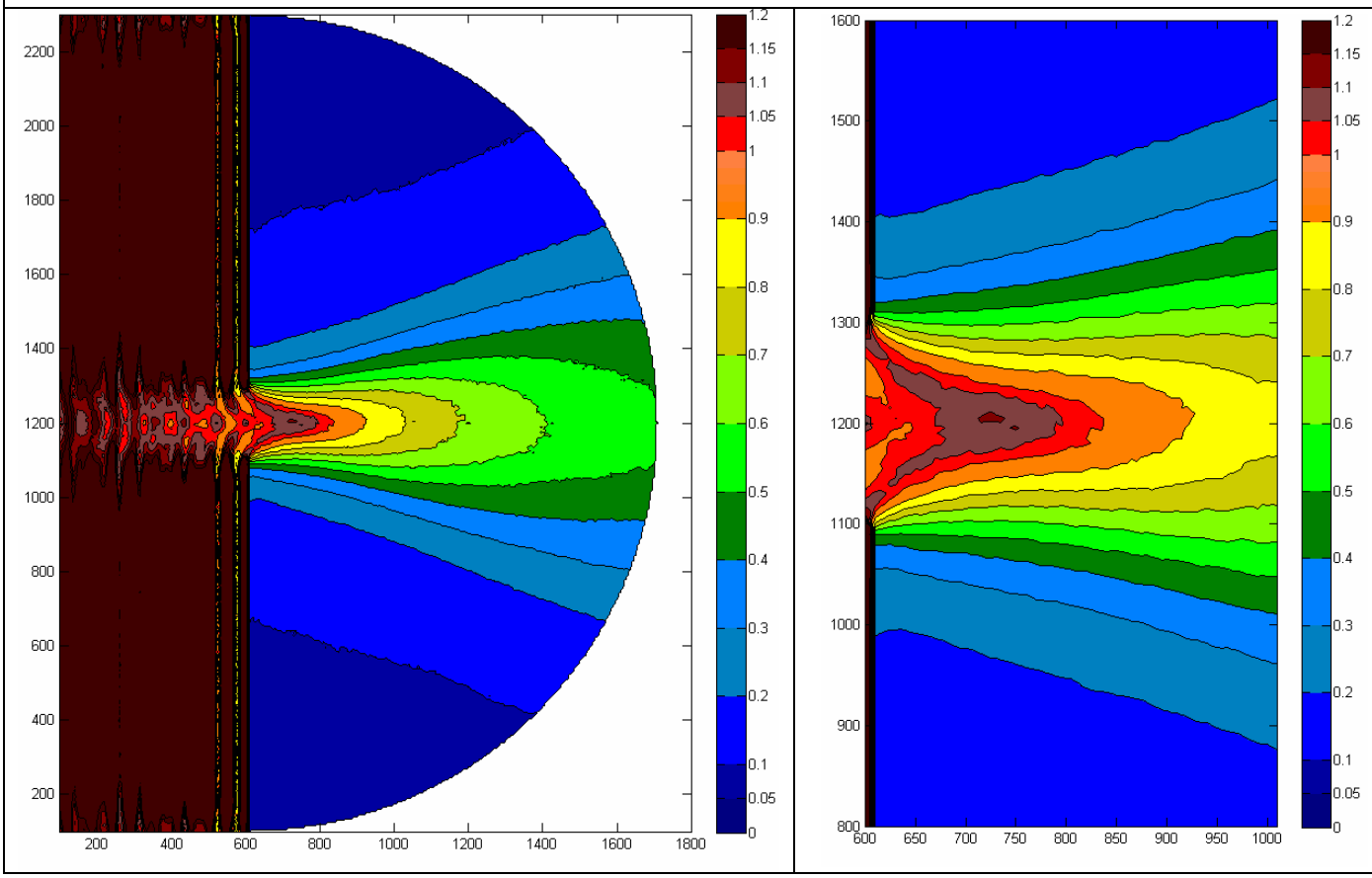
2200
2000
1800
1600
1400
1200
1000
800
600
400
200
200 400 600 800 1000 1200 1400 1600 1800
1.2
1.15
1.1
1.05
1
0.9
0.8
0.7
0.6
0.5
0.4
0.3
0.2
0.1
0.05
0
1600
1500
1400
1300
1200
1100
1000
900
800
600 650 700 750 800 850 900 950 1000

R12

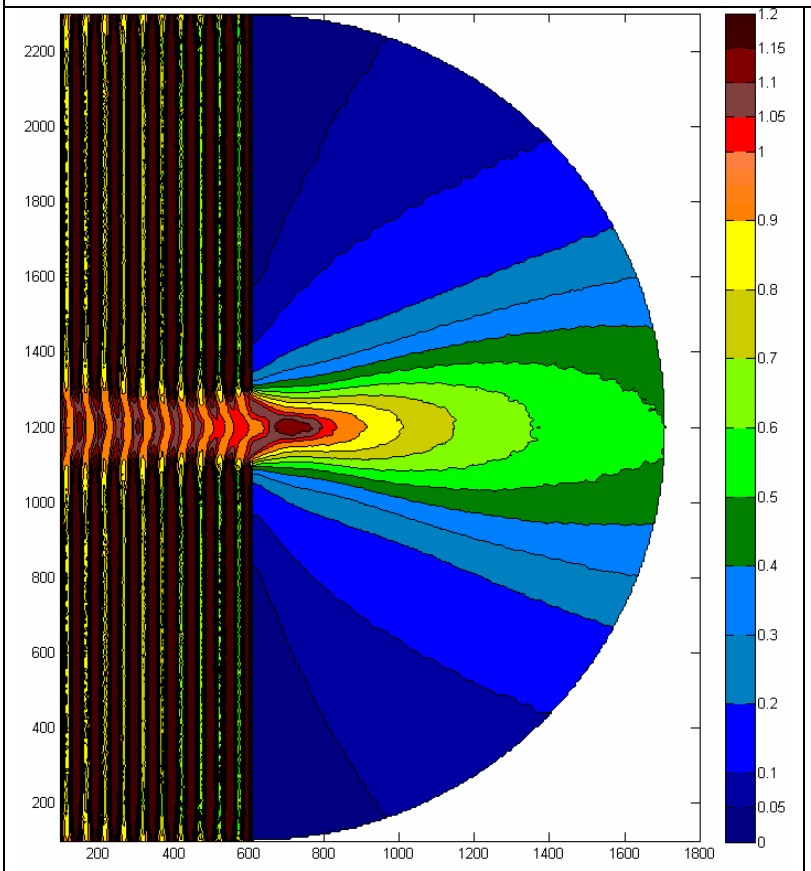
2200
2000
1800
1600
1400
1200
1000
800
600
400
200
200 400 600 800 1000 1200 1400 1600 1800
1.2
1.15
1.1
1.05
1
0.9
0.8
0.7
0.6
0.5
0.4
0.3
0.2
0.1
0.05
0

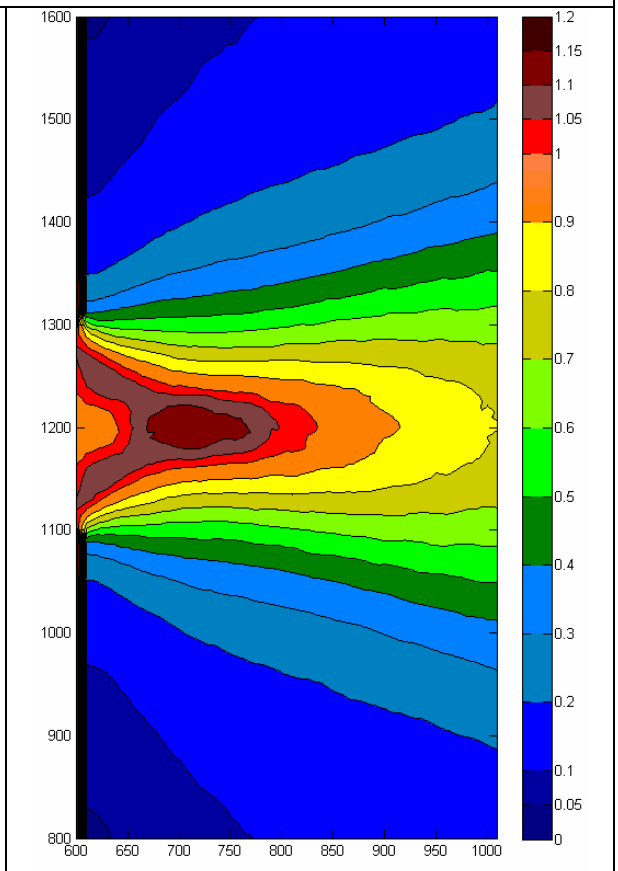
1600
1500
1400
1300
1200
1100
1000
900
800
600 650 700 750 800 850 900 950 1000
1.2
1.15
1.1
1.05
1
0.9
0.8
0.7
0.6
0.5
0.4
0.3
0.2
0.1
0.05
0

R14

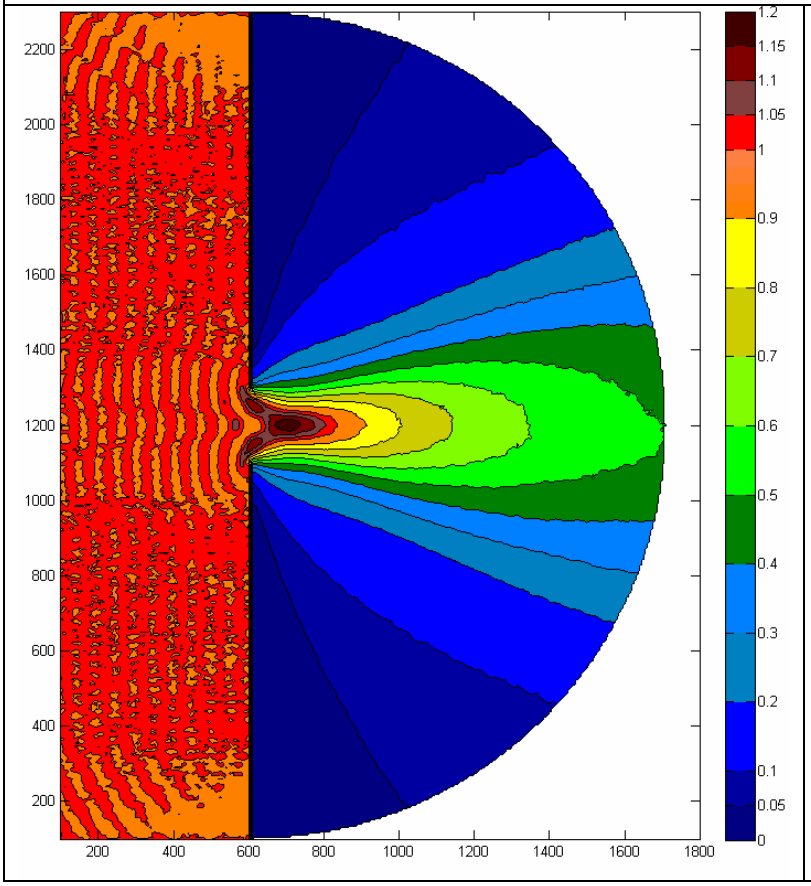
2200
2000
1800
1600
1400
1200
1000
800
600
400
200
200 400 600 800 1000 1200 1400 1600 1800
1.2
1.15
1.1
1.05
1
0.9
0.8
0.7
0.6
0.5
0.4
0.3
0.2
0.1
0.05
0

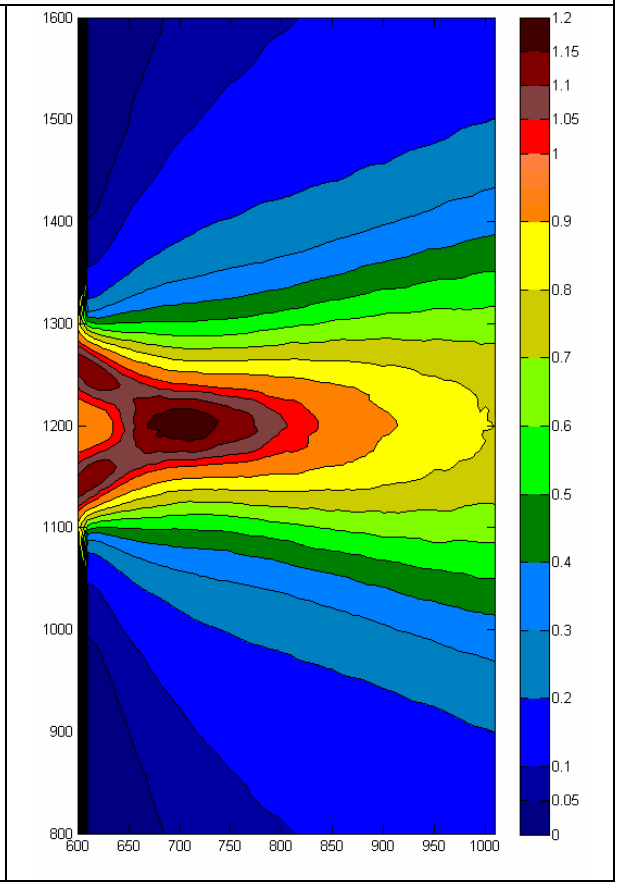
1600
1500
1400
1300
1200
1100
1000
900
800
600 650 700 750 800 850 900 950 1000
1.2
1.15
1.1
1.05
1
0.9
0.8
0.7
0.6
0.5
0.4
0.3
0.2
0.1
0.05
0

R15

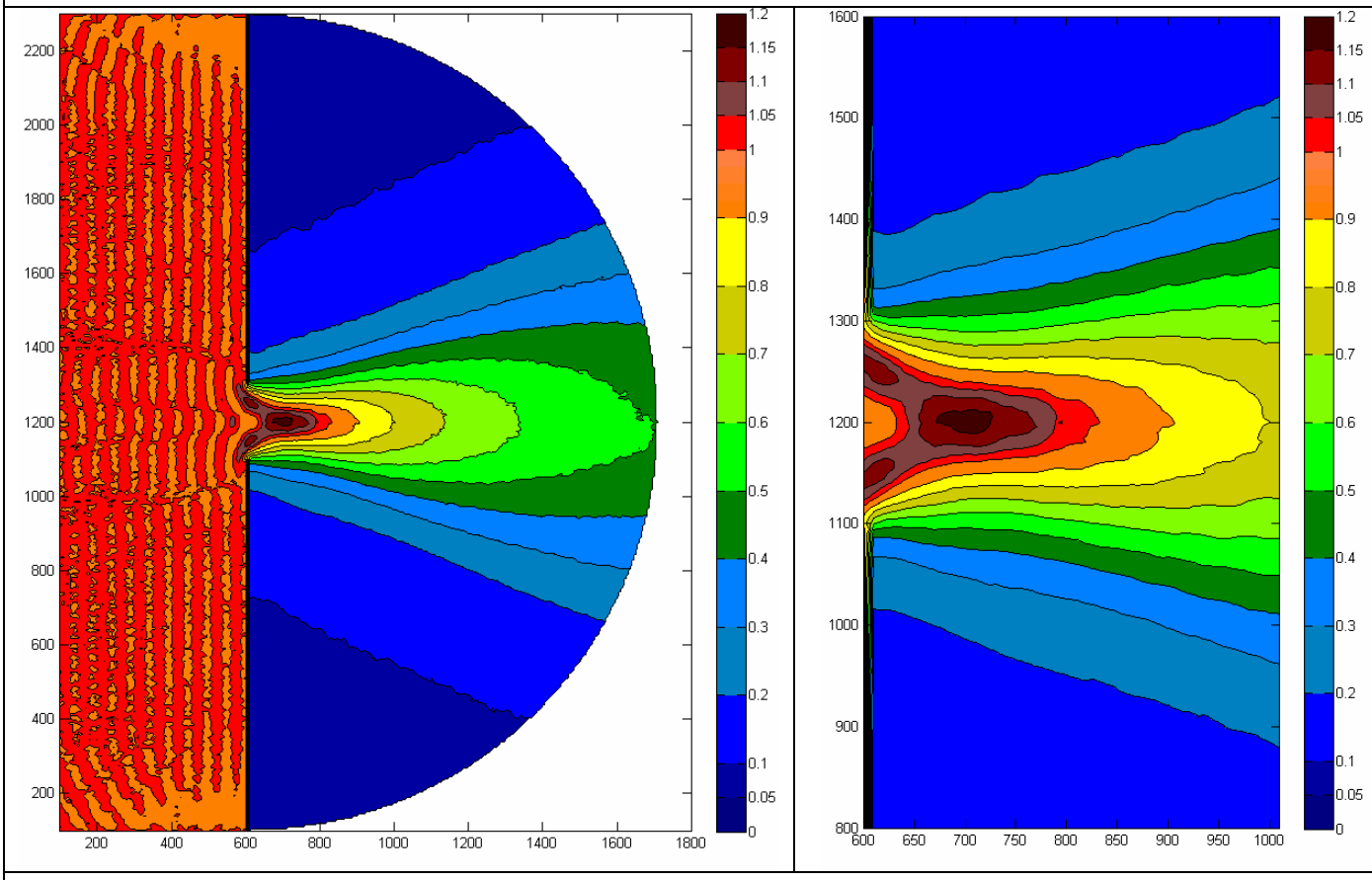
2200
2000
1800
1600
1400
1200
1000
800
600
400
200
200 400 600 800 1000 1200 1400 1600 1800
1.2
1.15
1.1
1.05
1
0.9
0.8
0.7
0.6
0.5
0.4
0.3
0.2
0.1
0.05
0
1600
1500
1400
1300
1200
1100
1000
900
800
600 650 700 750 800 850 900 950 1000

R20

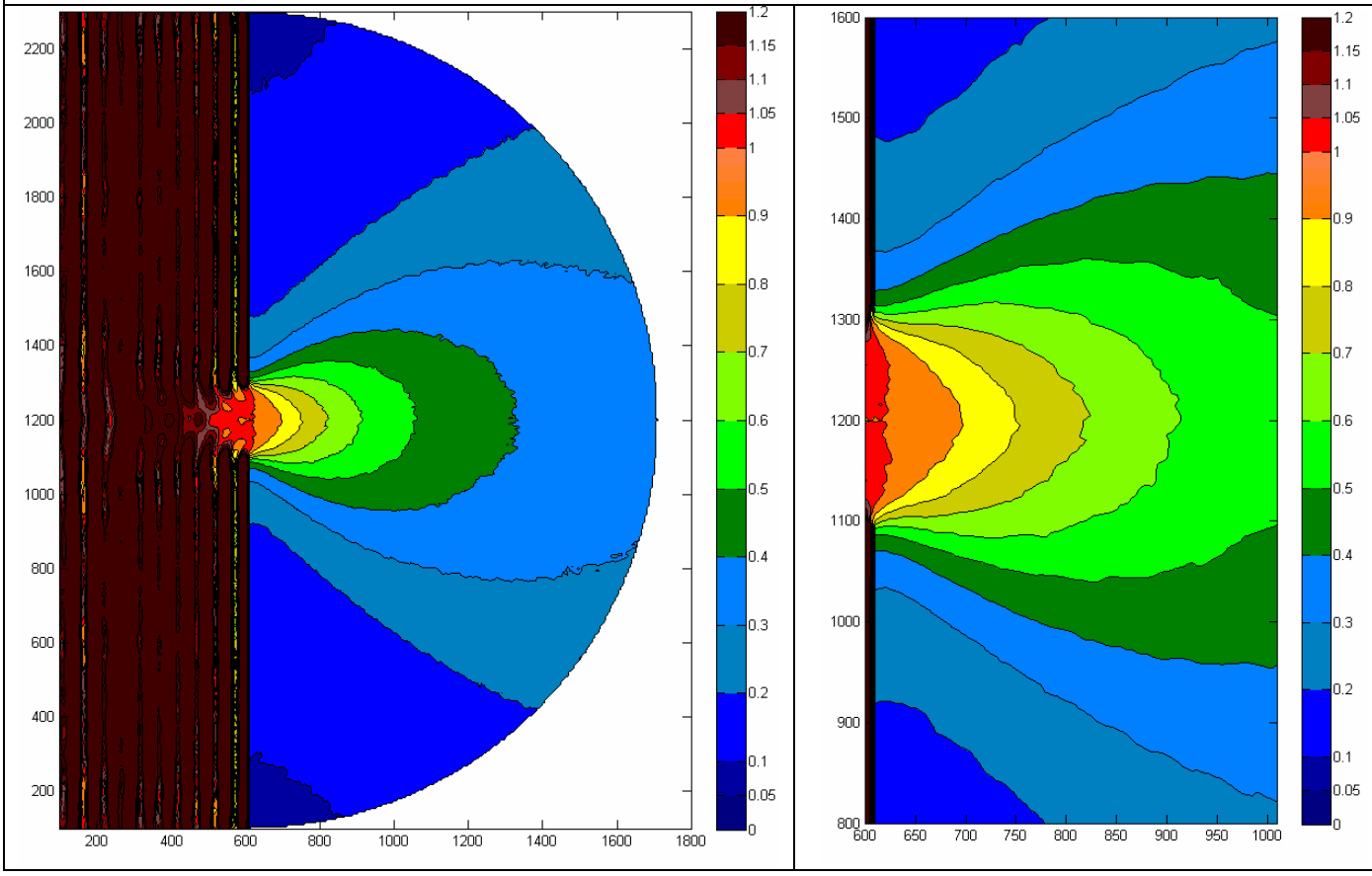
2200
2000
1800
1600
1400
1200
1000
800
600
400
200
200 400 600 800 1000 1200 1400 1600 1800
1.2
1.15
1.1
1.05
1
0.9
0.8
0.7
0.6
0.5
0.4
0.3
0.2
0.1
0.05
0
1600
1500
1400
1300
1200
1100
1000
900
800
600 650 700 750 800 850 900 950 1000

R21

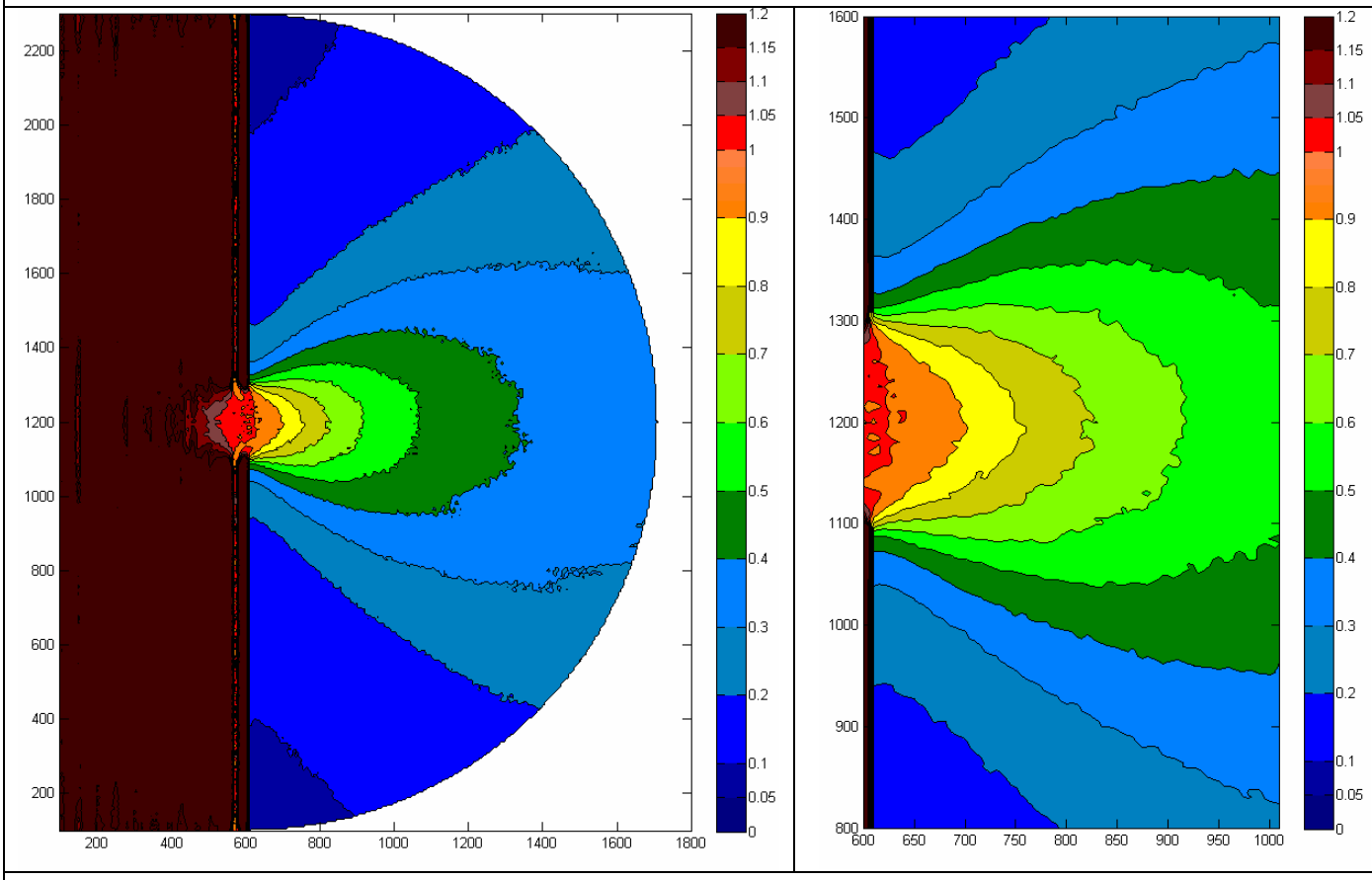
2200
2000
1800
1600
1400
1200
1000
800
600
400
200
200 400 600 800 1000 1200 1400 1600 1800
1.2
1.15
1.1
1.05
1
0.9
0.8
0.7
0.6
0.5
0.4
0.3
0.2
0.1
0.05
0
1600
1500
1400
1300
1200
1100
1000
900
800
600 650 700 750 800 850 900 950 1000

R22

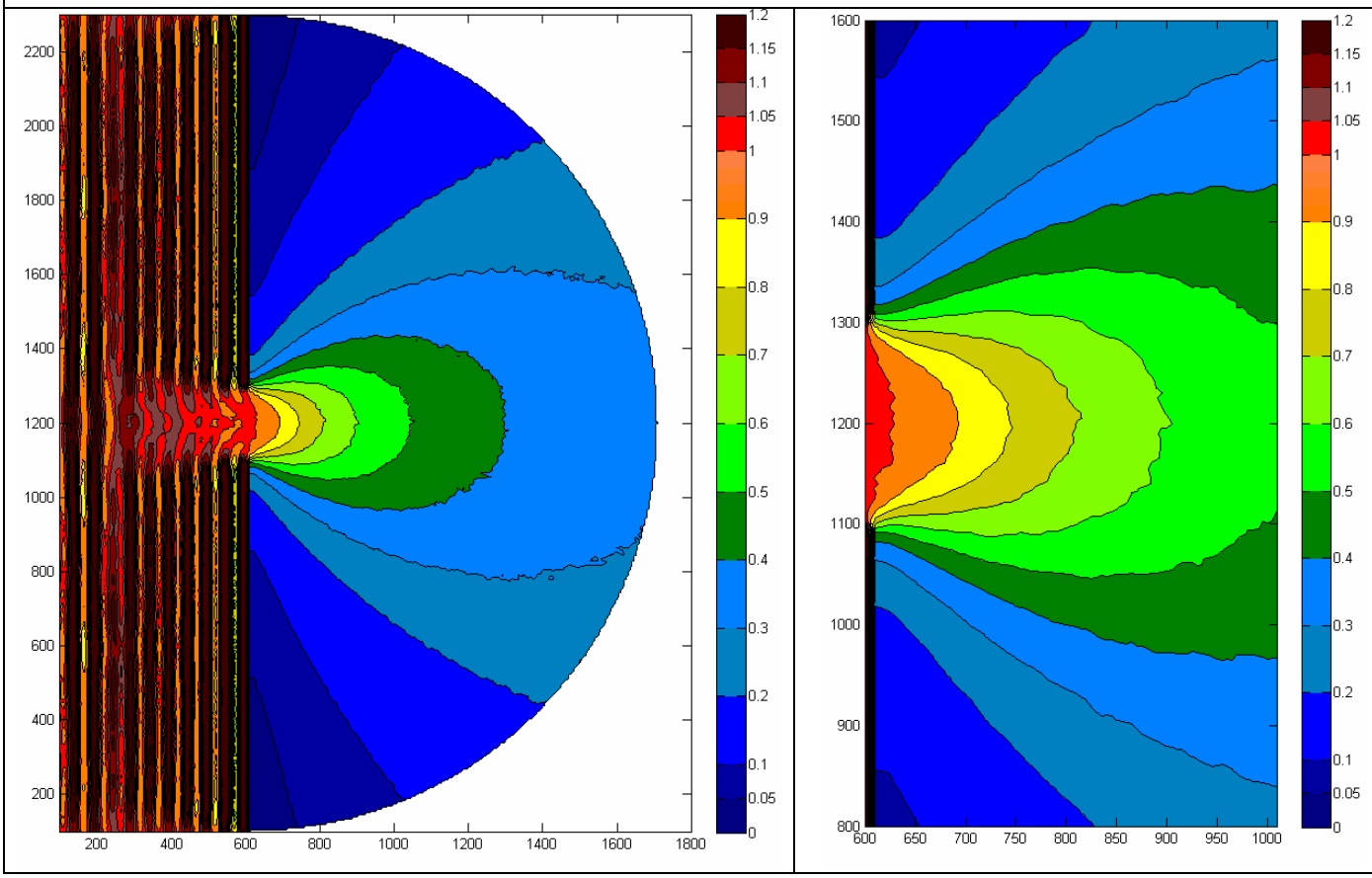
2200
2000
1800
1600
1400
1200
1000
800
600
400
200
200 400 600 800 1000 1200 1400 1600 1800
1.2
1.15
1.1
1.05
1
0.9
0.8
0.7
0.6
0.5
0.4
0.3
0.2
0.1
0.05
0
1600
1500
1400
1300
1200
1100
1000
900
800
600 650 700 750 800 850 900 950 1000

R24

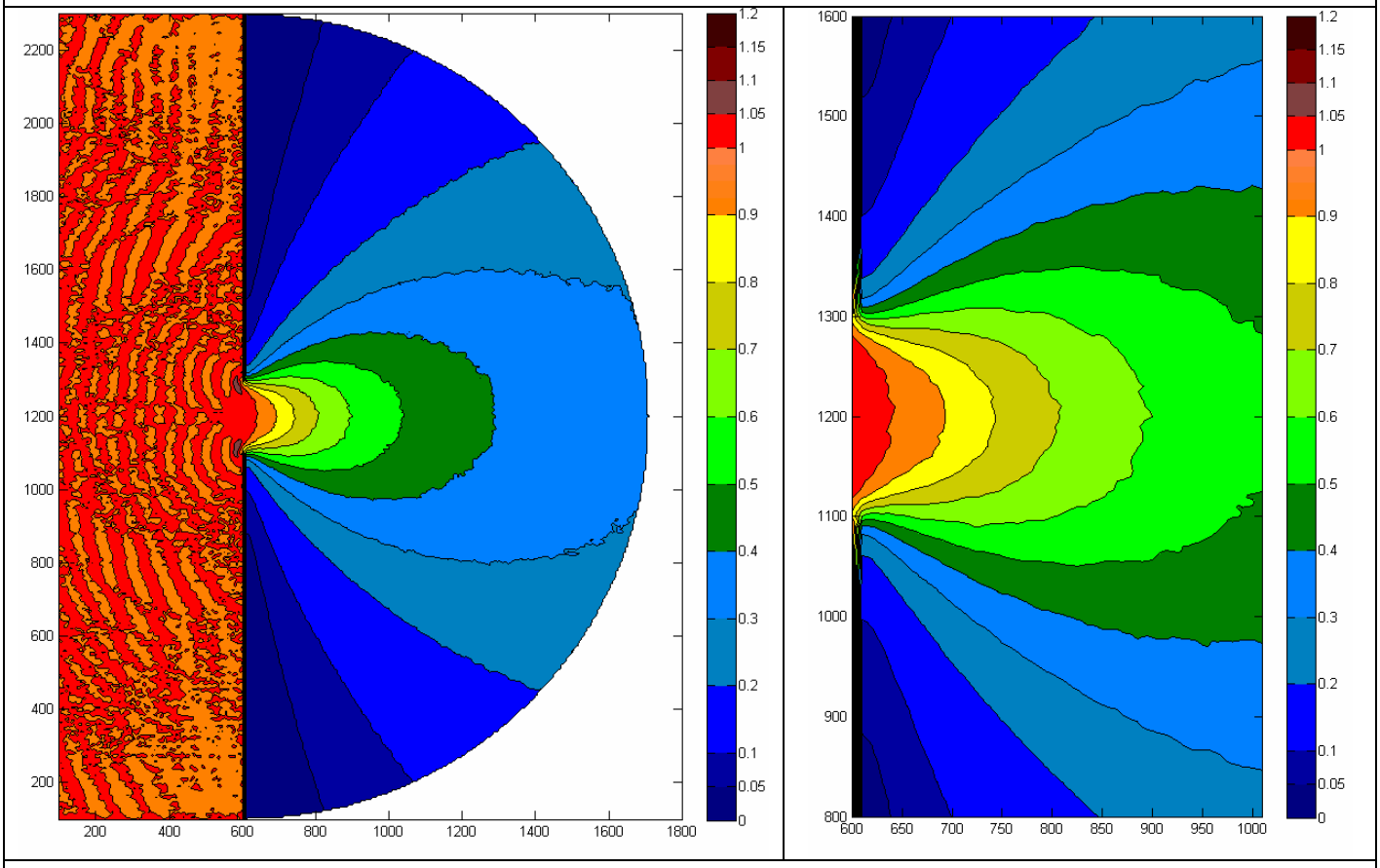
2200
2000
1800
1600
1400
1200
1000
800
600
400
200
200 400 600 800 1000 1200 1400 1600 1800
1.2
1.15
1.1
1.05
1
0.9
0.8
0.7
0.6
0.5
0.4
0.3
0.2
0.1
0.05
0
1600
1500
1400
1300
1200
1100
1000
900
800
600 650 700 750 800 850 900 950 1000

R25

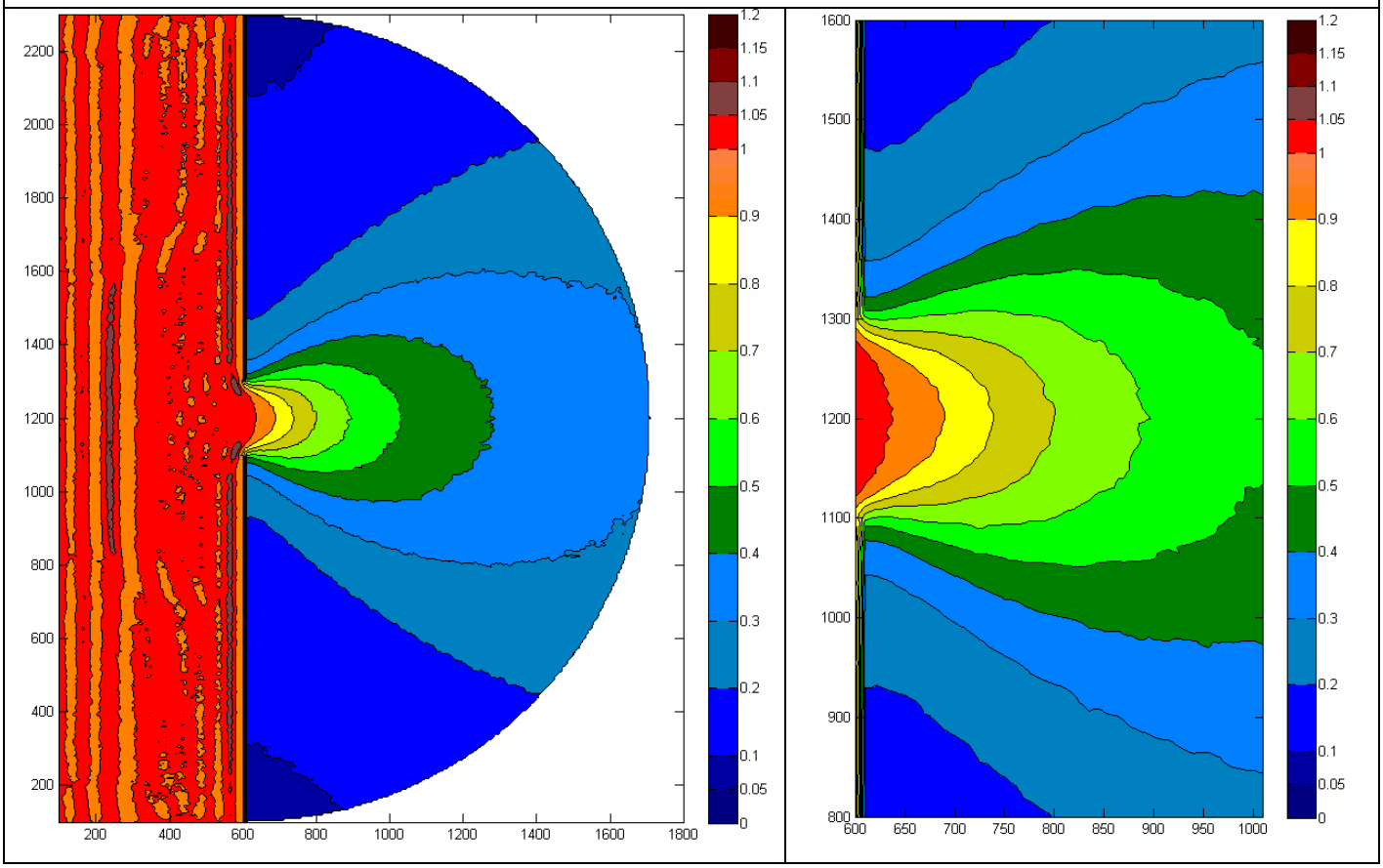
2200
2000
1800
1600
1400
1200
1000
800
600
400
200
200 400 600 800 1000 1200 1400 1600 1800
1.2
1.15
1.1
1.05
1
0.9
0.8
0.7
0.6
0.5
0.4
0.3
0.2
0.1
0.05
0
1600
1500
1400
1300
1200
1100
1000
900
800
600 650 700 750 800 850 900 950 1000

R121

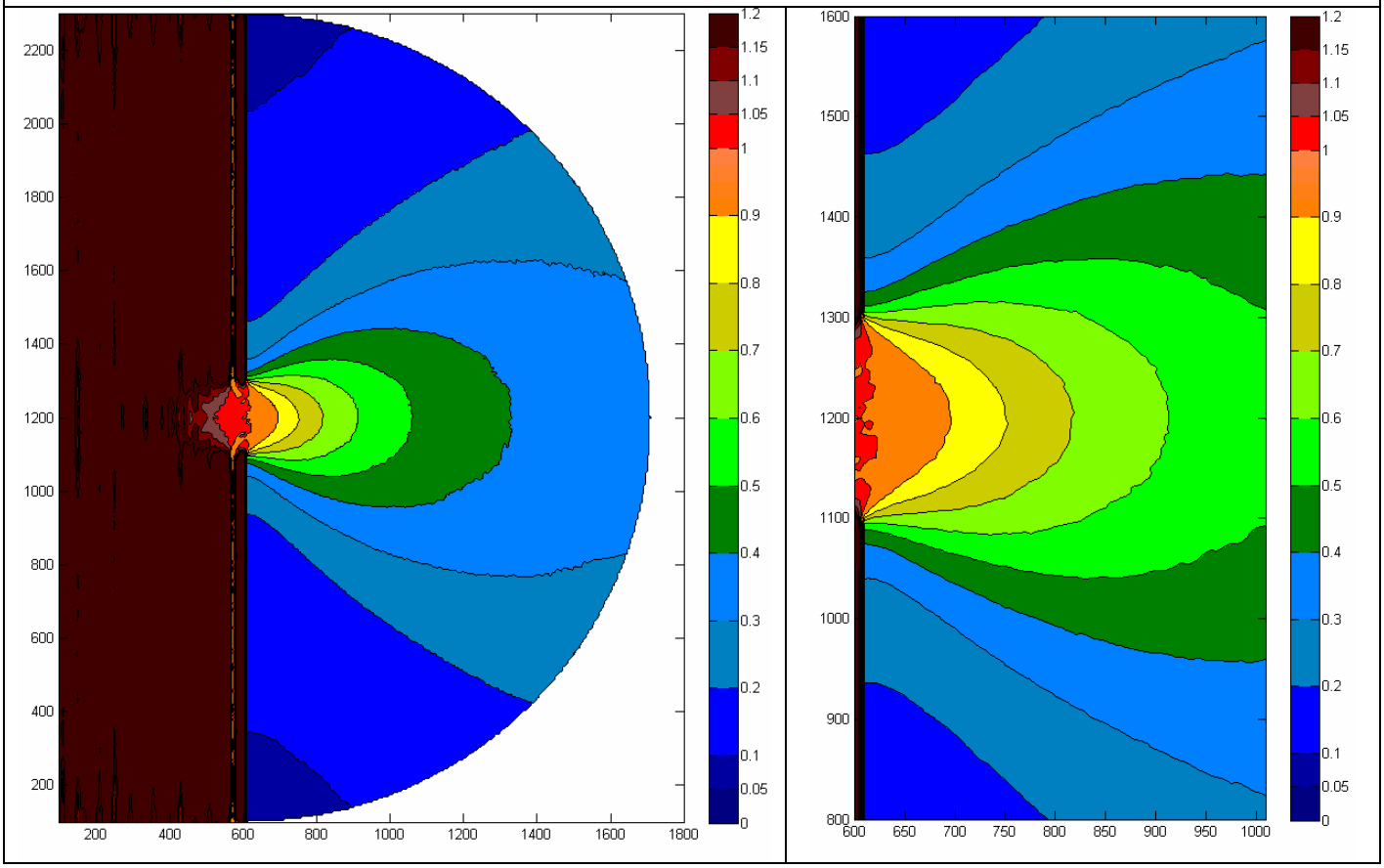
2200
2000
1800
1600
1400
1200
1000
800
600
400
200
200 400 600 800 1000 1200 1400 1600 1800
1.2
1.15
1.1
1.05
1
0.9
0.8
0.7
0.6
0.5
0.4
0.3
0.2
0.1
0.05
0
1600
1500
1400
1300
1200
1100
1000
900
800
600 650 700 750 800 850 900 950 1000
1.2
1.15
1.1
1.05
1
0.9
0.8
0.7
0.6
0.5
0.4
0.3
0.2
0.1
0.05
0

4WL Gap Pharos File Names

					Reflection		Directional		Spectral	
Run	**Wave Type**	**Model Type**	**Peak Per**	**Peak Dir**	**Front**	**Back**	**Spread (deg)**	**Interval (deg)**	**# frequencies**	**Notes:**
R00	Mono	Long Crest	8	0	100	100				
R01	Mono	Long Crest	8	0	50	50				
R02	Mono	Long Crest	8	0	0	0				
R10	Swell	Directional	8	0	100	100	-25 to 25	5		
R11	Swell	Spectral	8	0	100	100	-25 to 25	5	5	Smallest Mesh: 8/WL
R12	Swell	Directional	8	0	50	50	-25 to 25	5		
R14	Swell	Directional	8	0	0	0	-25 to 25	5		
R20	Wind	Directional	8	0	100	100	-80 to 80	10		
R21	Wind	Spectral	8	0	100	100	-80 to 80	10	5	Smallest Mesh: 8/WL
R22	Wind	Directional	8	0	50	50	-80 to 80	10		
R24	Wind	Directional	8	0	0	0	-80 to 80	10		

R00

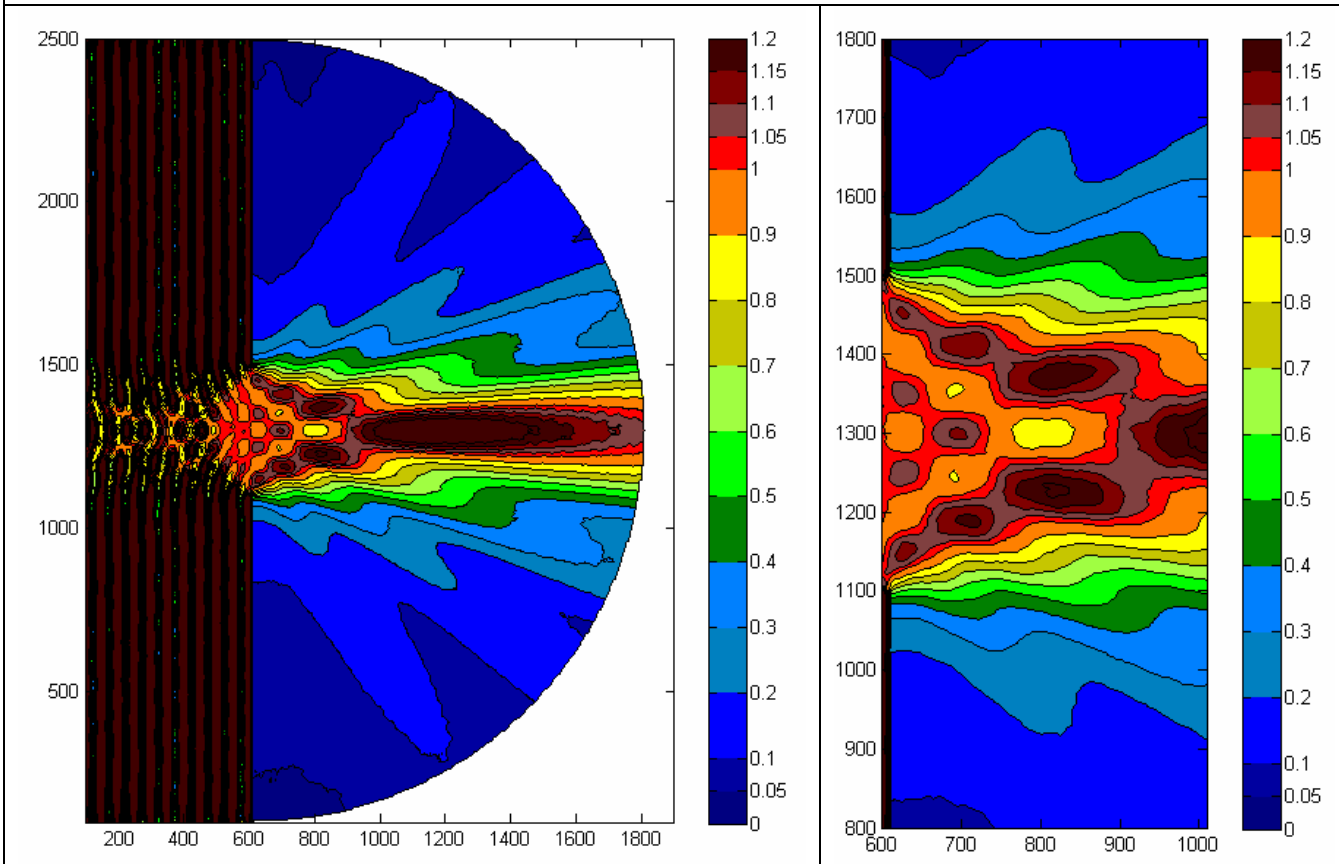
2500
2000
1500
1000
500
200 400 600 800 1000 1200 1400 1600 1800
1.2 1.15 1.1 1.05 1 0.9 0.8 0.7 0.6 0.5 0.4 0.3 0.2 0.1 0.05 0
1800
1700
1600
1500
1400
1300
1200
1100
1000
900
800
600 700 800 900 1000
1.2 1.15 1.1 1.05 1 0.9 0.8 0.7 0.6 0.5 0.4 0.3 0.2 0.1 0.05 0

R01

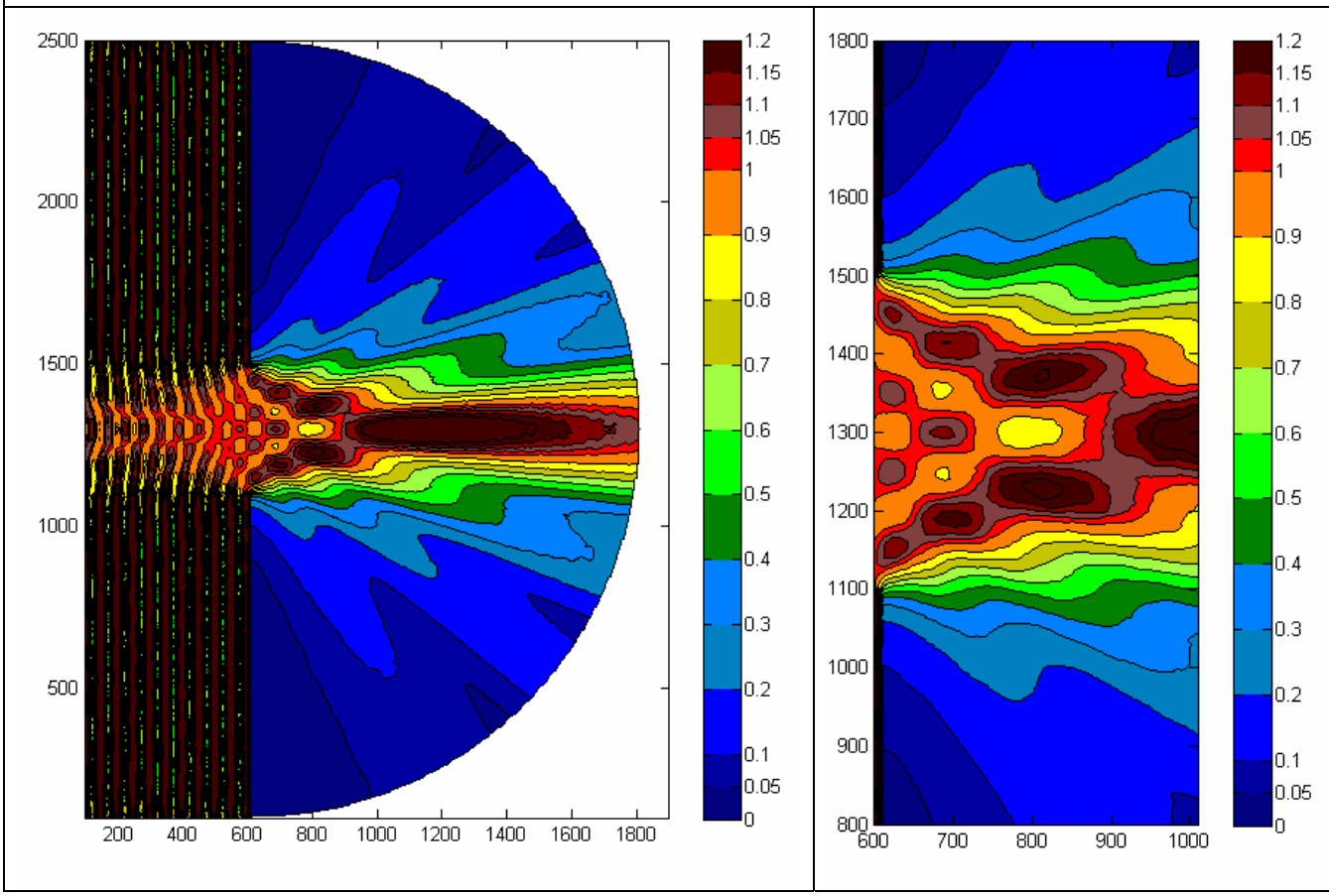
2500
2000
1500
1000
500
200 400 600 800 1000 1200 1400 1600 1800
1.2 1.15 1.1 1.05 1 0.9 0.8 0.7 0.6 0.5 0.4 0.3 0.2 0.1 0.05 0
1800
1700
1600
1500
1400
1300
1200
1100
1000
900
800
600 700 800 900 1000
1.2 1.15 1.1 1.05 1 0.9 0.8 0.7 0.6 0.5 0.4 0.3 0.2 0.1 0.05 0

R02

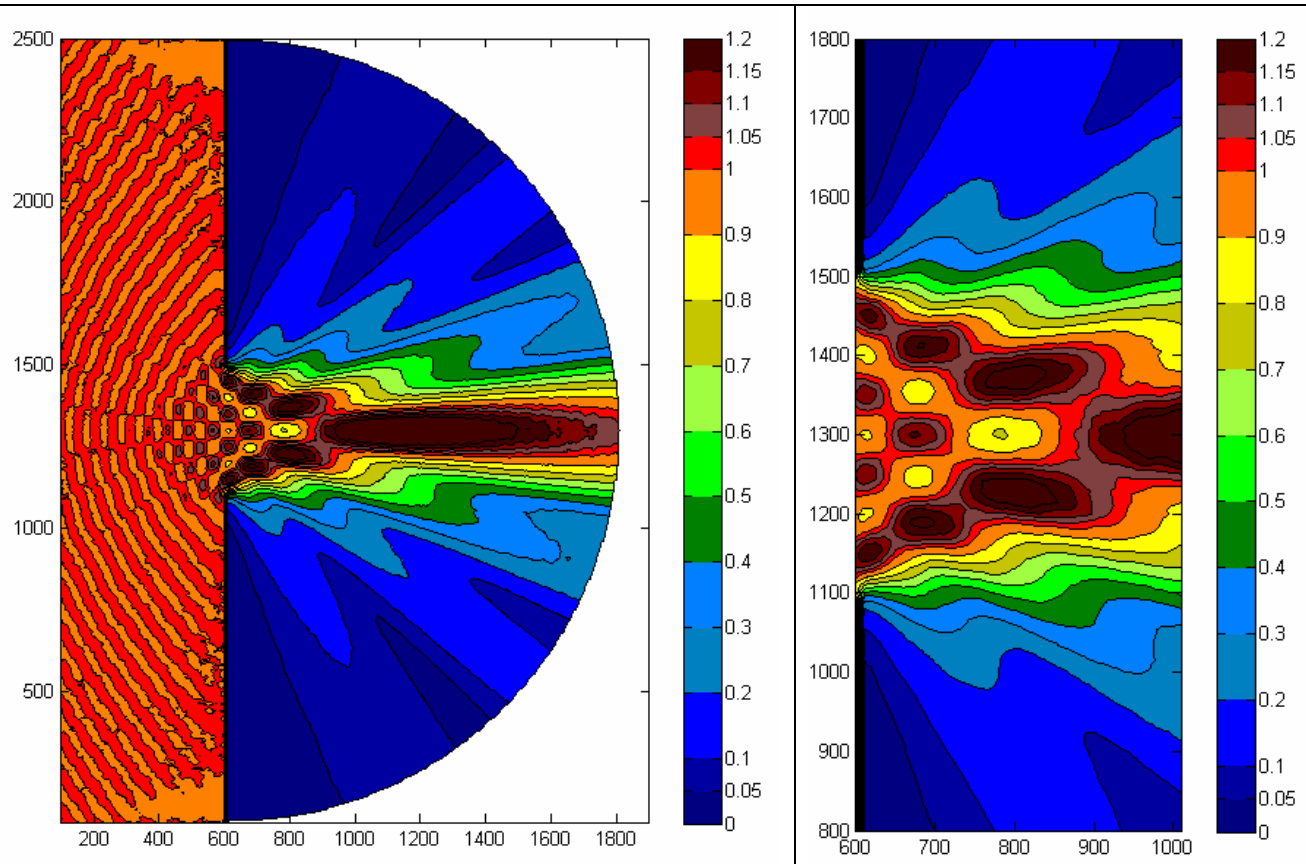
2500
2000
1500
1000
500
200 400 600 800 1000 1200 1400 1600 1800
1.2 1.15 1.1 1.05 1 0.9 0.8 0.7 0.6 0.5 0.4 0.3 0.2 0.1 0.05 0
1800
1700
1600
1500
1400
1300
1200
1100
1000
900
800
600 700 800 900 1000
1.2 1.15 1.1 1.05 1 0.9 0.8 0.7 0.6 0.5 0.4 0.3 0.2 0.1 0.05 0

R10

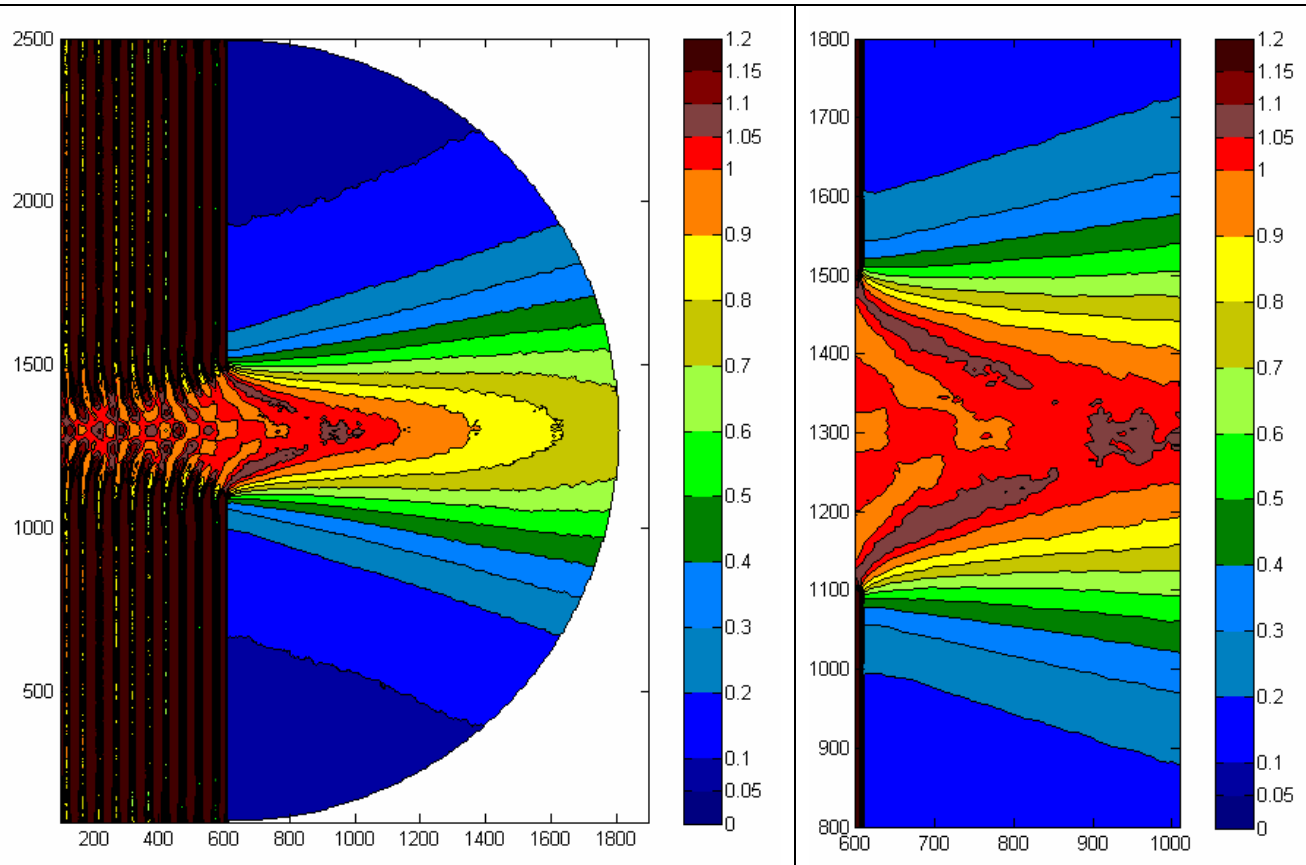
2500
2000
1500
1000
500
200 400 600 800 1000 1200 1400 1600 1800
1.2 1.15 1.1 1.05 1 0.9 0.8 0.7 0.6 0.5 0.4 0.3 0.2 0.1 0.05 0
1800
1700
1600
1500
1400
1300
1200
1100
1000
900
800
600 700 800 900 1000
1.2 1.15 1.1 1.05 1 0.9 0.8 0.7 0.6 0.5 0.4 0.3 0.2 0.1 0.05 0

R11

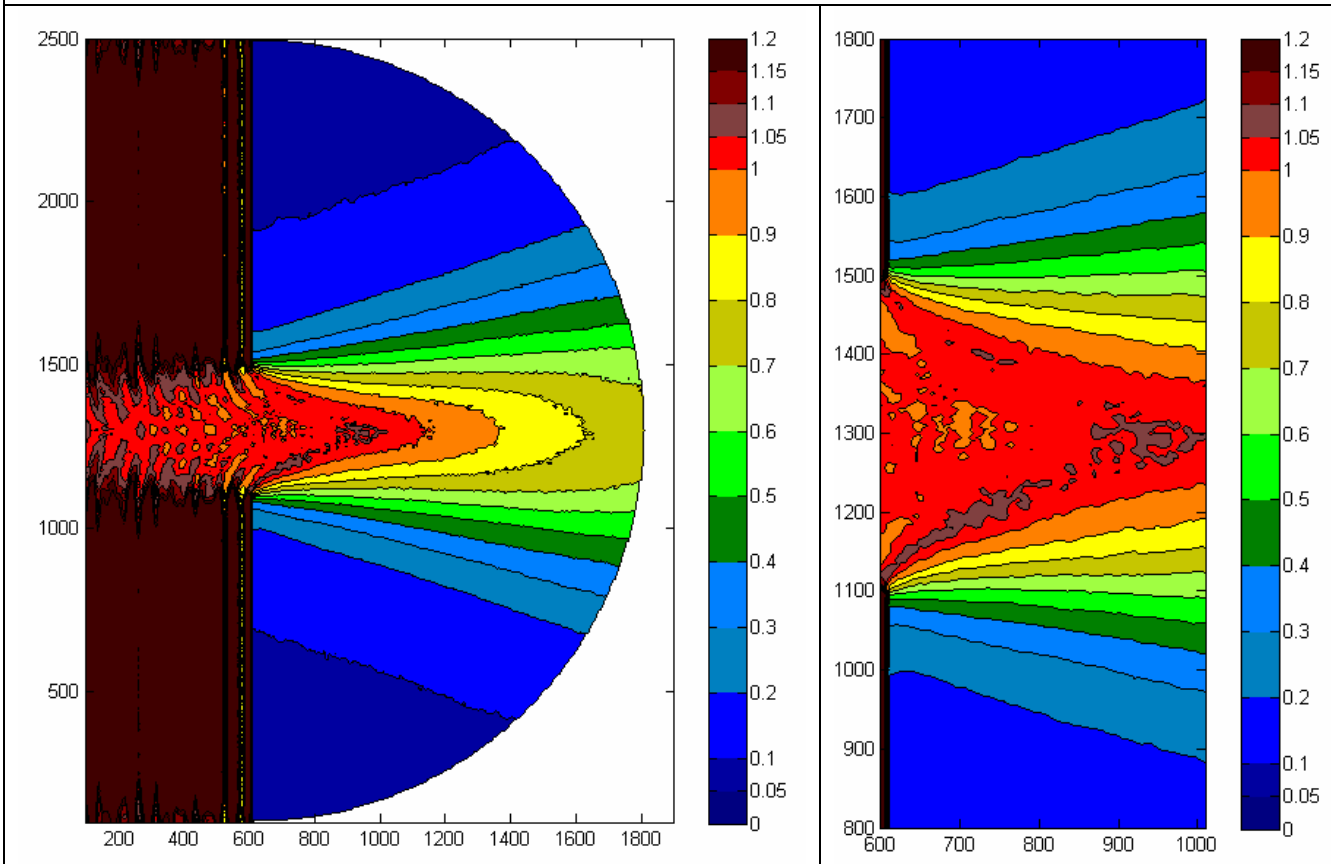
2500
2000
1500
1000
500
200 400 600 800 1000 1200 1400 1600 1800
1.2 1.15 1.1 1.05 1 0.9 0.8 0.7 0.6 0.5 0.4 0.3 0.2 0.1 0.05 0
1800
1700
1600
1500
1400
1300
1200
1100
1000
900
800
600 700 800 900 1000
1.2 1.15 1.1 1.05 1 0.9 0.8 0.7 0.6 0.5 0.4 0.3 0.2 0.1 0.05 0

R12

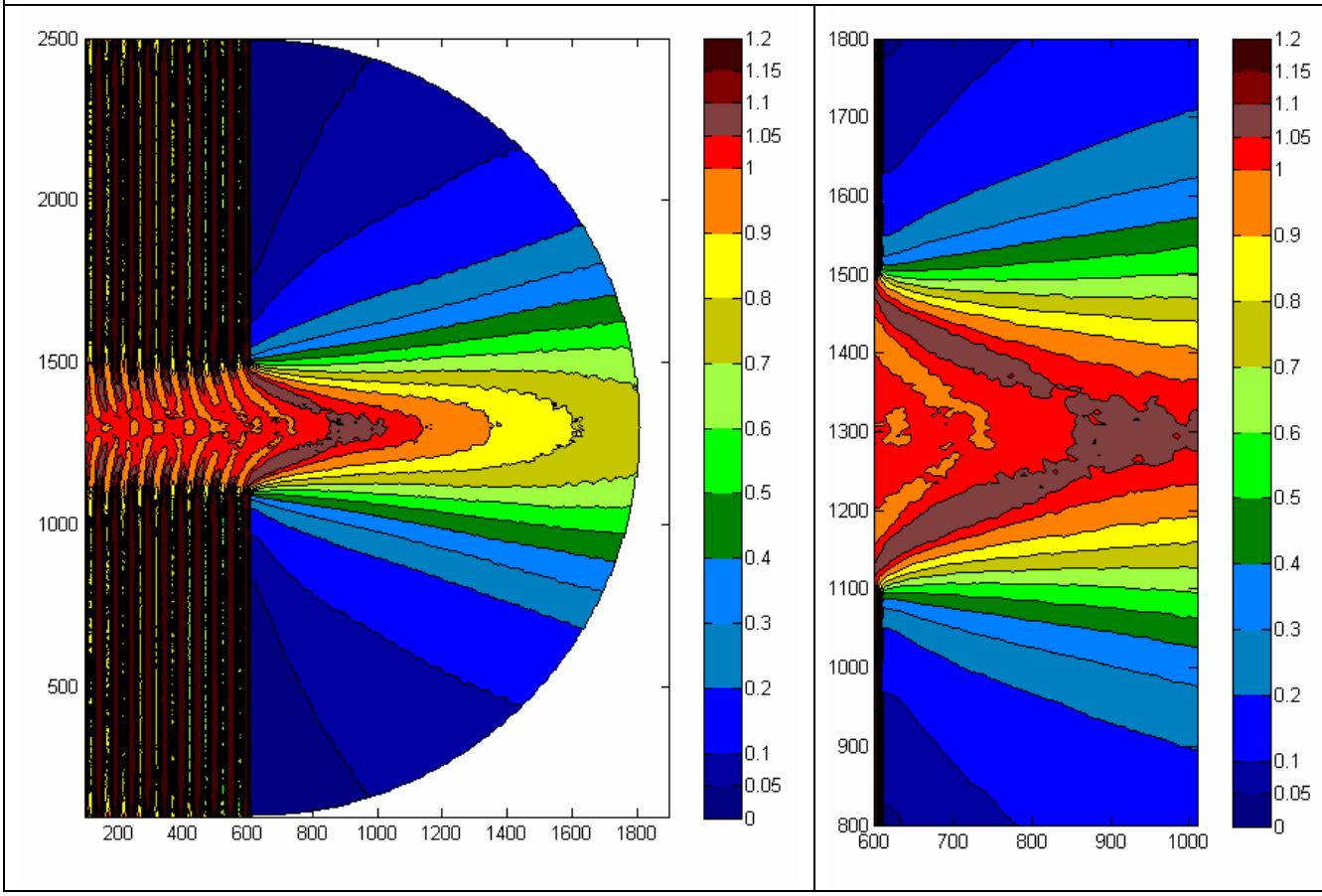
2500
2000
1500
1000
500
200 400 600 800 1000 1200 1400 1600 1800
1.2 1.15 1.1 1.05 1 0.9 0.8 0.7 0.6 0.5 0.4 0.3 0.2 0.1 0.05 0
1800
1700
1600
1500
1400
1300
1200
1100
1000
900
800
600 700 800 900 1000
1.2 1.15 1.1 1.05 1 0.9 0.8 0.7 0.6 0.5 0.4 0.3 0.2 0.1 0.05 0

R14

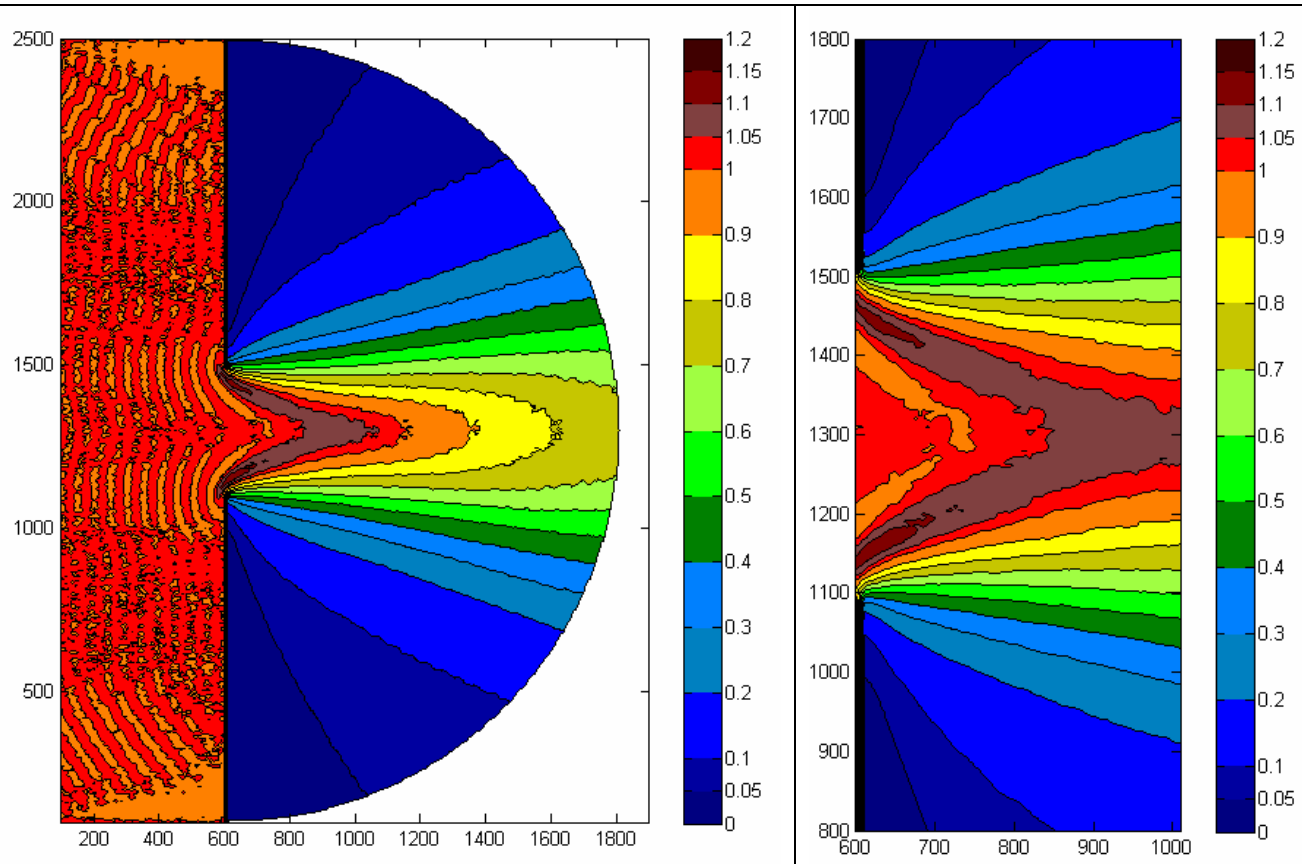
2500
2000
1500
1000
500
200 400 600 800 1000 1200 1400 1600 1800
1.2 1.15 1.1 1.05 1 0.9 0.8 0.7 0.6 0.5 0.4 0.3 0.2 0.1 0.05 0
1800
1700
1600
1500
1400
1300
1200
1100
1000
900
800
600 700 800 900 1000
1.2 1.15 1.1 1.05 1 0.9 0.8 0.7 0.6 0.5 0.4 0.3 0.2 0.1 0.05 0

R20

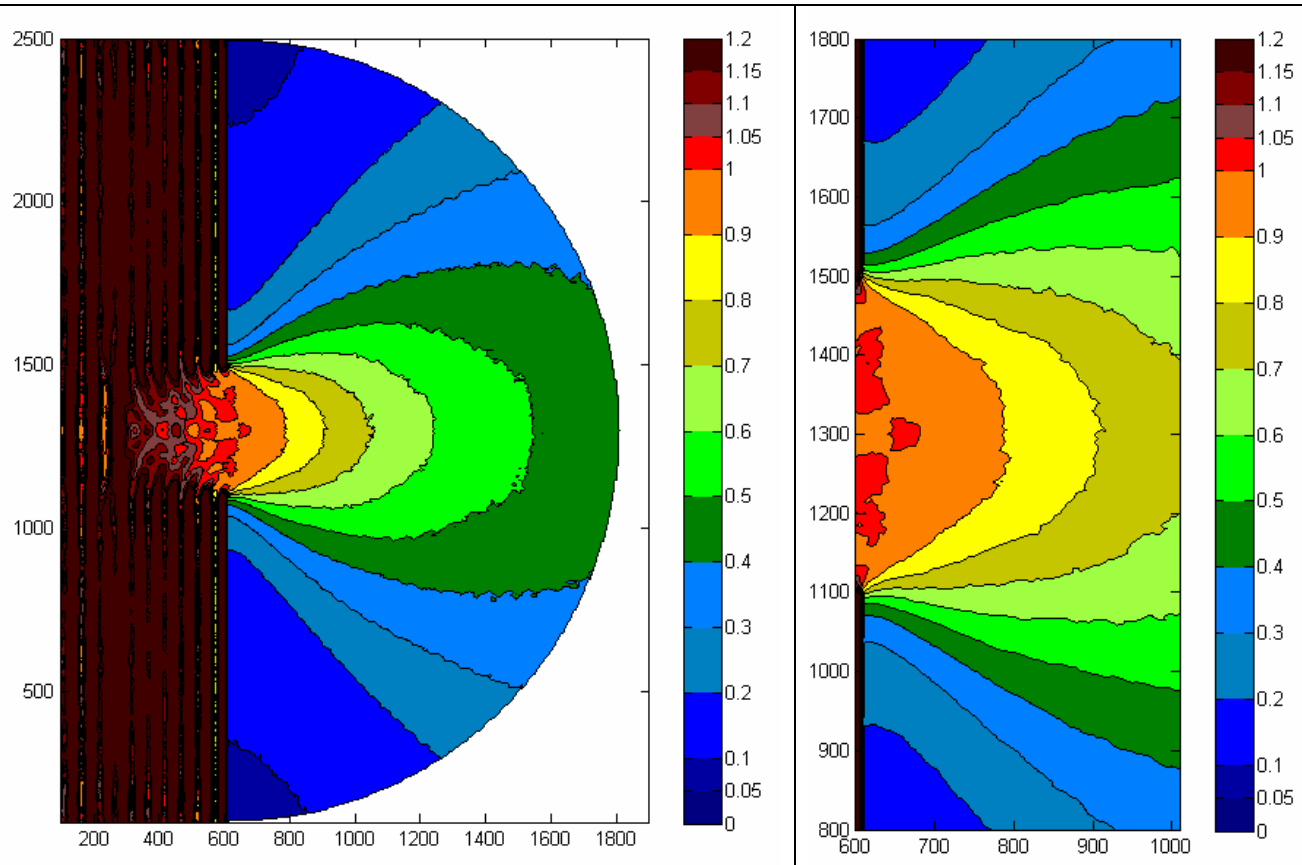
2500
2000
1500
1000
500
200 400 600 800 1000 1200 1400 1600 1800
1.2 1.15 1.1 1.05 1 0.9 0.8 0.7 0.6 0.5 0.4 0.3 0.2 0.1 0.05 0
1800
1700
1600
1500
1400
1300
1200
1100
1000
900
800
600 700 800 900 1000
1.2 1.15 1.1 1.05 1 0.9 0.8 0.7 0.6 0.5 0.4 0.3 0.2 0.1 0.05 0

R21

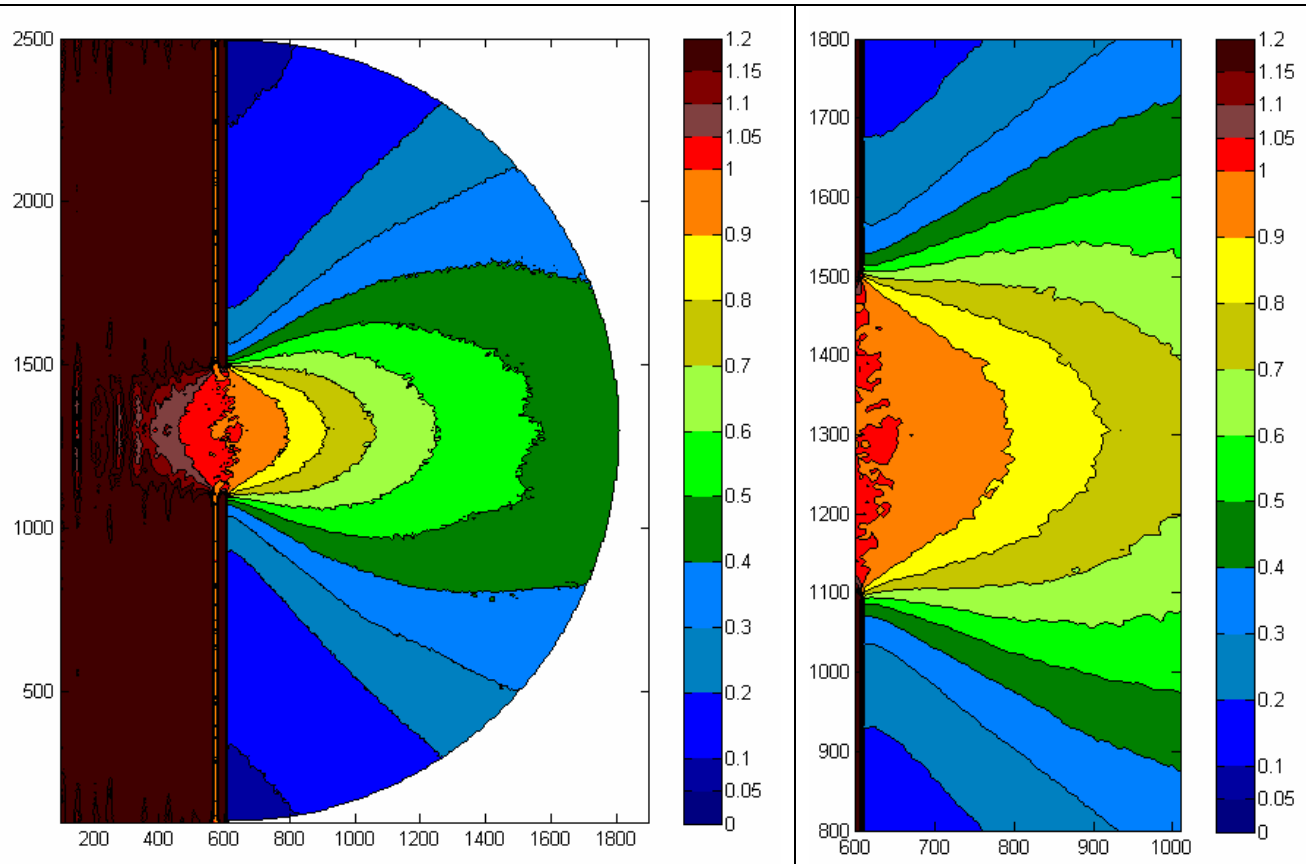
2500
2000
1500
1000
500
200 400 600 800 1000 1200 1400 1600 1800
1.2 1.15 1.1 1.05 1 0.9 0.8 0.7 0.6 0.5 0.4 0.3 0.2 0.1 0.05 0
1800
1700
1600
1500
1400
1300
1200
1100
1000
900
800
600 700 800 900 1000
1.2 1.15 1.1 1.05 1 0.9 0.8 0.7 0.6 0.5 0.4 0.3 0.2 0.1 0.05 0

R22

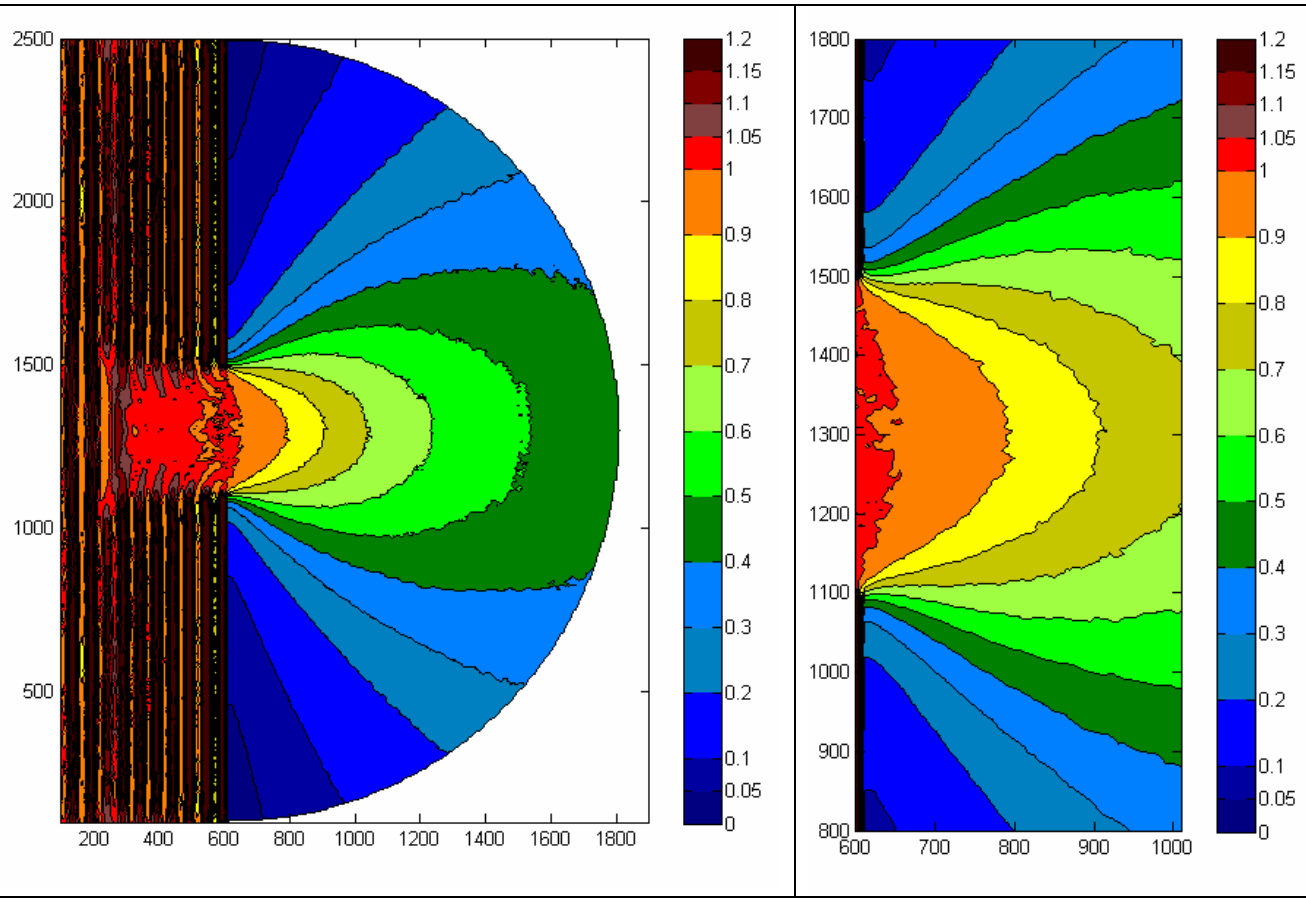
2500
2000
1500
1000
500
200 400 600 800 1000 1200 1400 1600 1800
1.2 1.15 1.1 1.05 1 0.9 0.8 0.7 0.6 0.5 0.4 0.3 0.2 0.1 0.05 0
1800
1700
1600
1500
1400
1300
1200
1100
1000
900
800
600 700 800 900 1000
1.2 1.15 1.1 1.05 1 0.9 0.8 0.7 0.6 0.5 0.4 0.3 0.2 0.1 0.05 0

R24

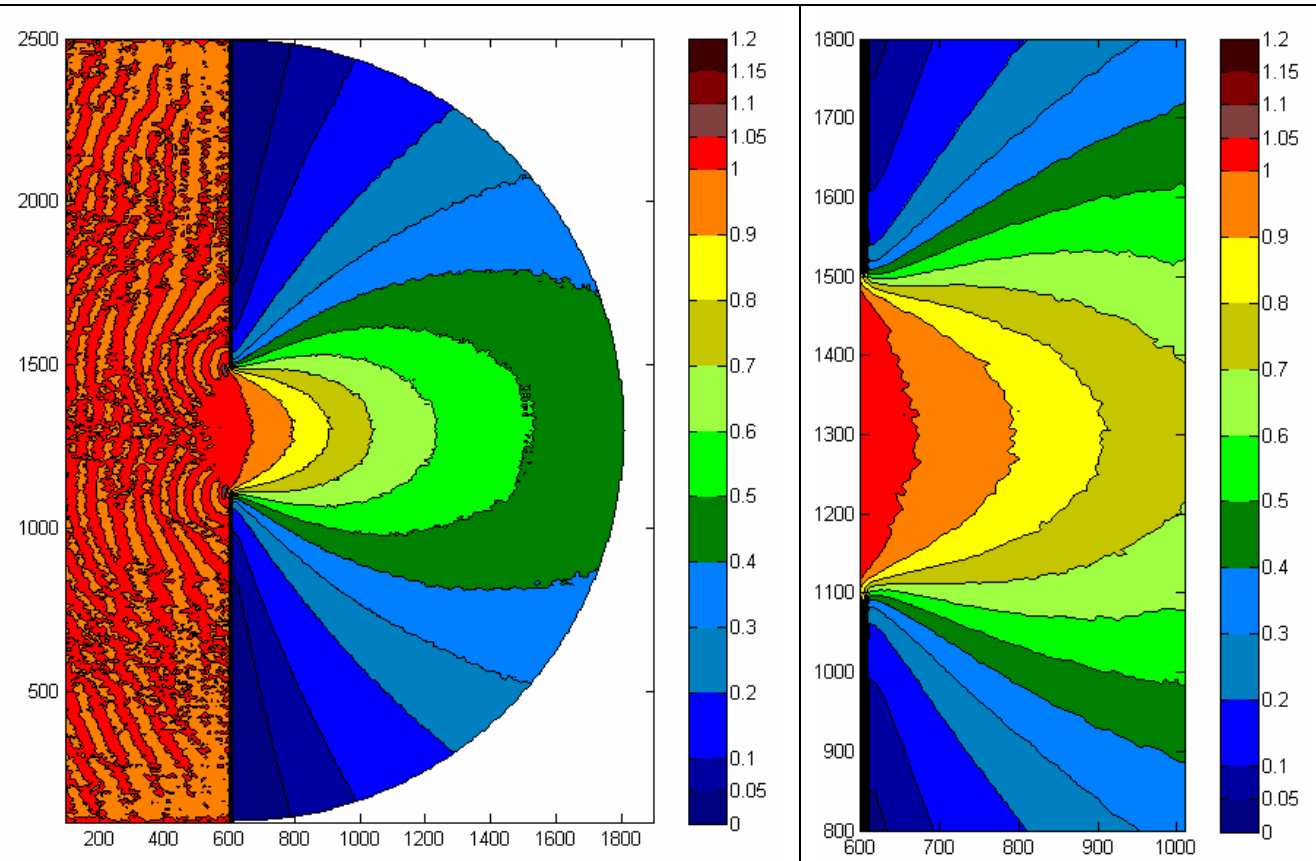
2500
2000
1500
1000
500
200
400
600
800
1000
1200
1400
1600
1800
1.2
1.15
1.1
1.05
1
0.9
0.8
0.7
0.6
0.5
0.4
0.3
0.2
0.1
0.05
0
1800
1700
1600
1500
1400
1300
1200
1100
1000
900
800
600
700
800
900
1000
1.2
1.15
1.1
1.05
1
0.9
0.8
0.7
0.6
0.5
0.4
0.3
0.2
0.1
0.05
0

APPENDIX E: SWAN Model Results

Swell	Wind
Semi - Infinite	
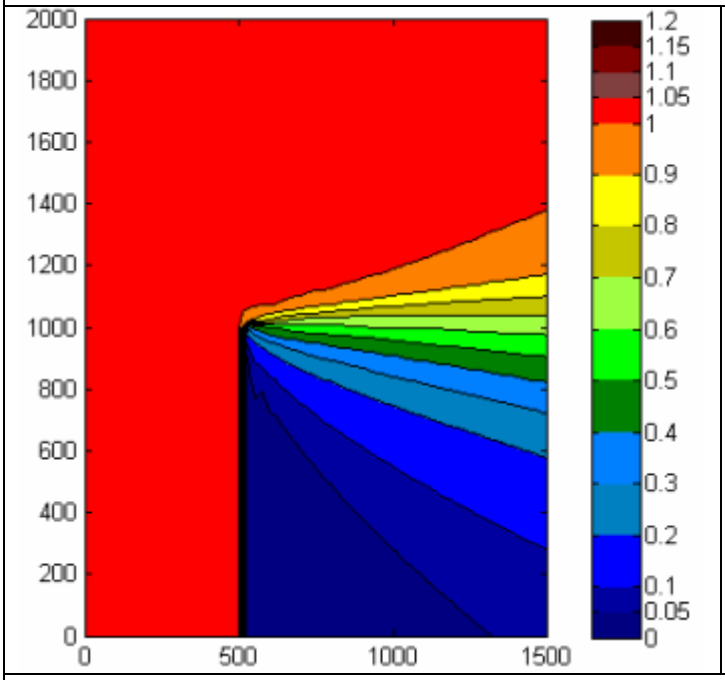	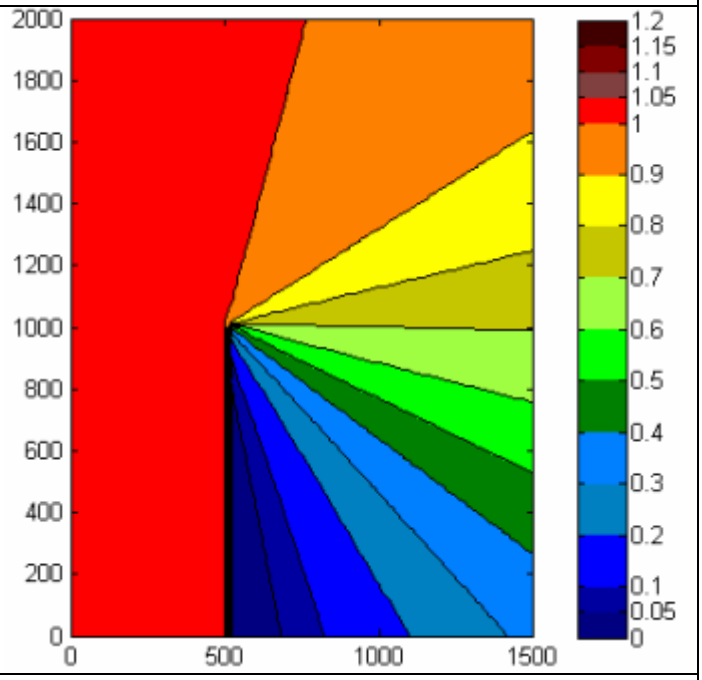
0.5L Gap	
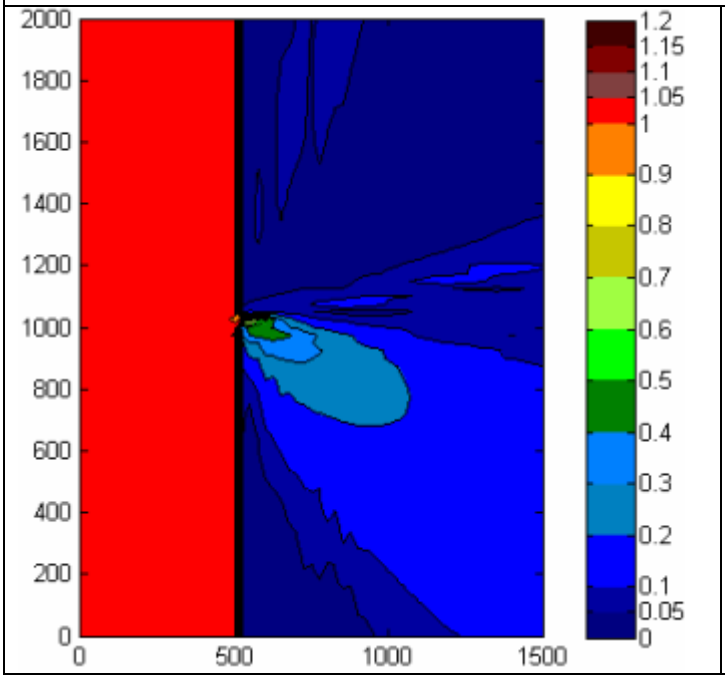	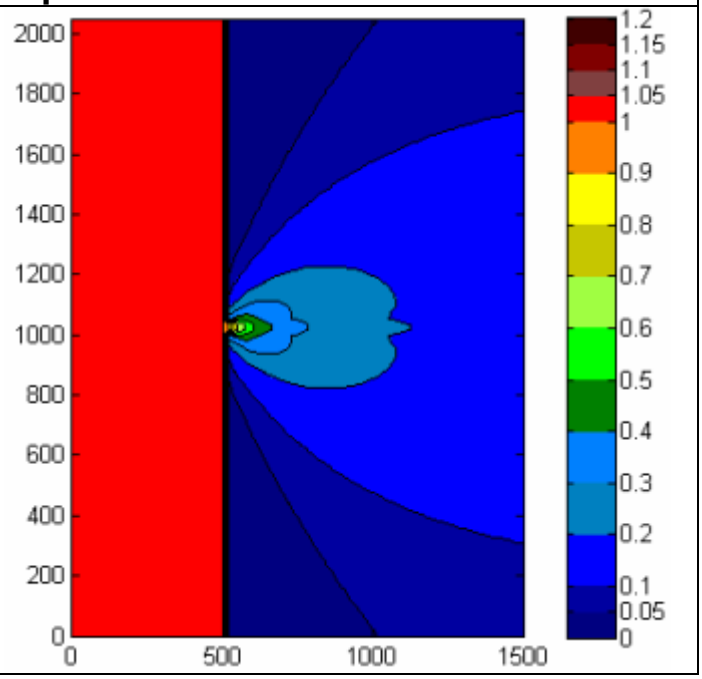

1L Gap

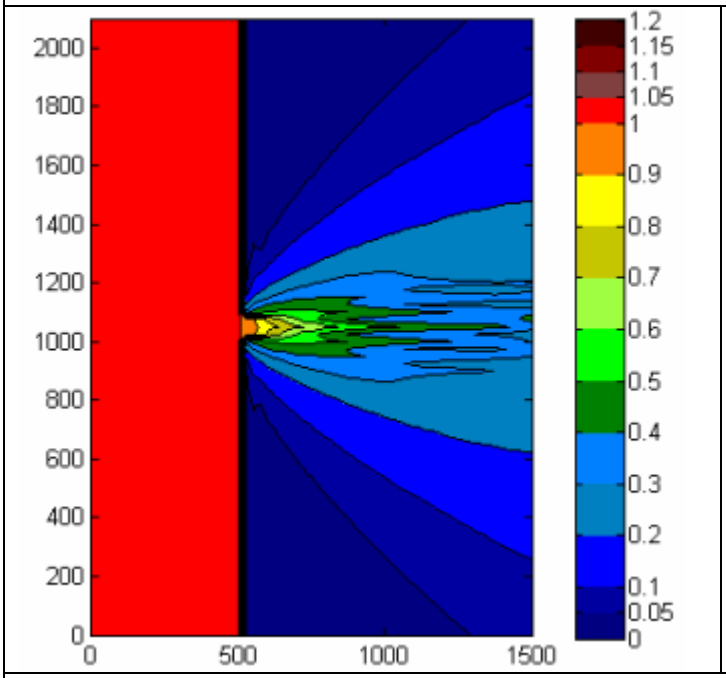
2000
1800
1600
1400
1200
1000
800
600
400
200
0
0
500
1000
1500
1.2
1.15
1.1
1.05
1
0.9
0.8
0.7
0.6
0.5
0.4
0.3
0.2
0.1
0.05
0

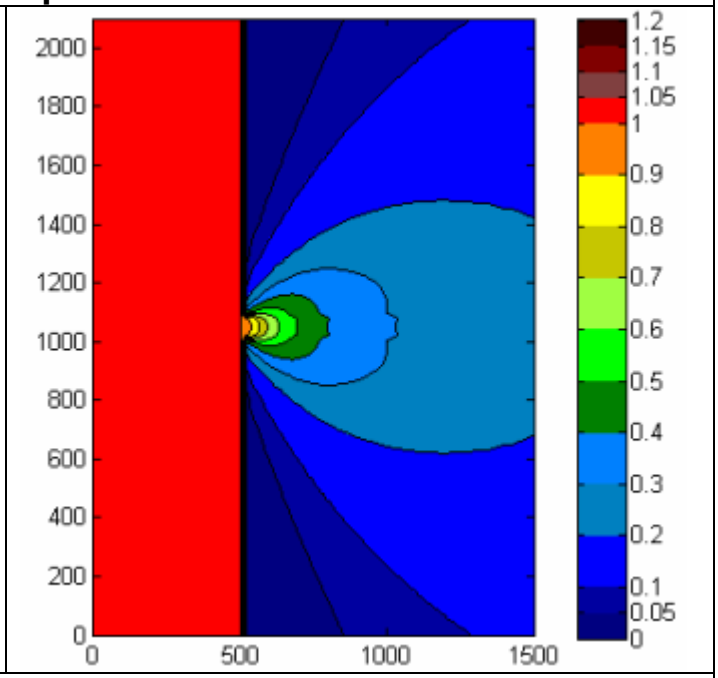
2000
1800
1600
1400
1200
1000
800
600
400
200
0
0
500
1000
1500
1.2
1.15
1.1
1.05
1
0.9
0.8
0.7
0.6
0.5
0.4
0.3
0.2
0.1
0.05
0

2L Gap

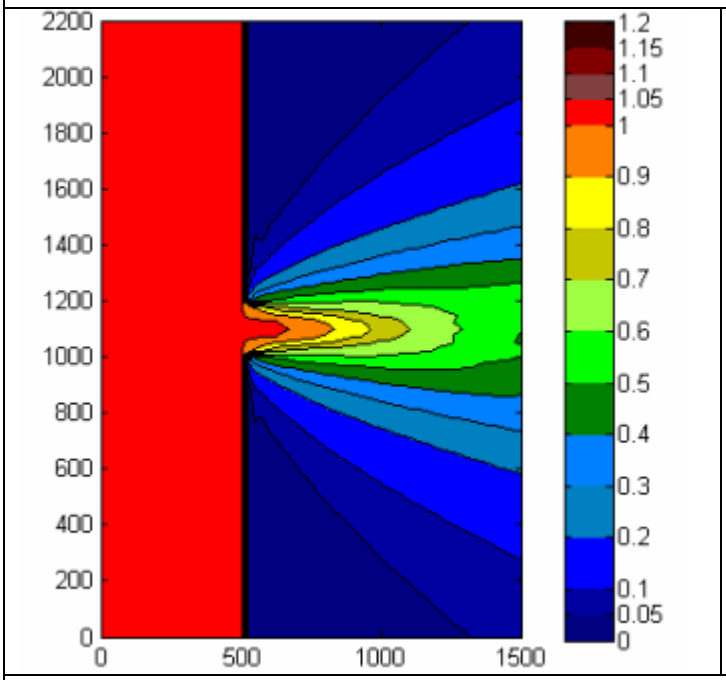
2200
2000
1800
1600
1400
1200
1000
800
600
400
200
0
0
500
1000
1500
1.2
1.15
1.1
1.05
1
0.9
0.8
0.7
0.6
0.5
0.4
0.3
0.2
0.1
0.05
0

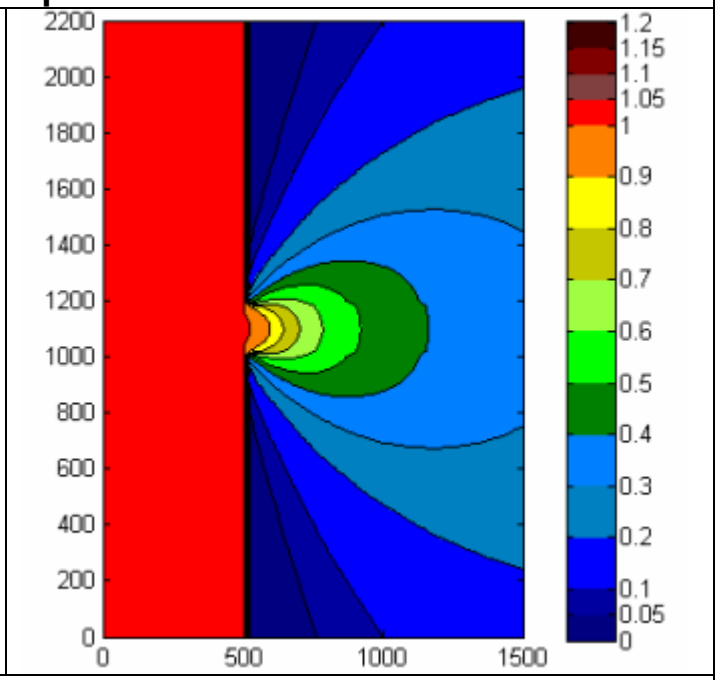
2200
2000
1800
1600
1400
1200
1000
800
600
400
200
0
0
500
1000
1500
1.2
1.15
1.1
1.05
1
0.9
0.8
0.7
0.6
0.5
0.4
0.3
0.2
0.1
0.05
0

3L Gap

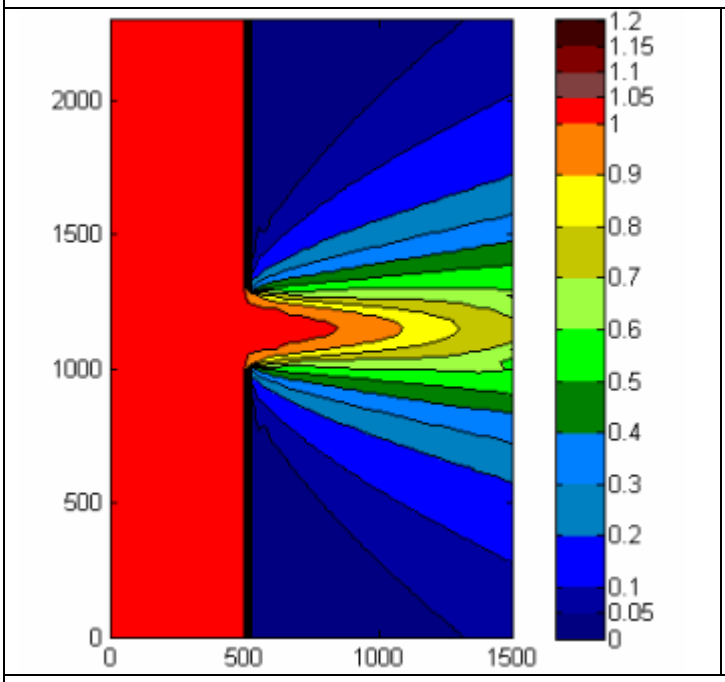
2000
1500
1000
500
0
0
500
1000
1500
1.2
1.15
1.1
1.05
1
0.9
0.8
0.7
0.6
0.5
0.4
0.3
0.2
0.1
0.05
0

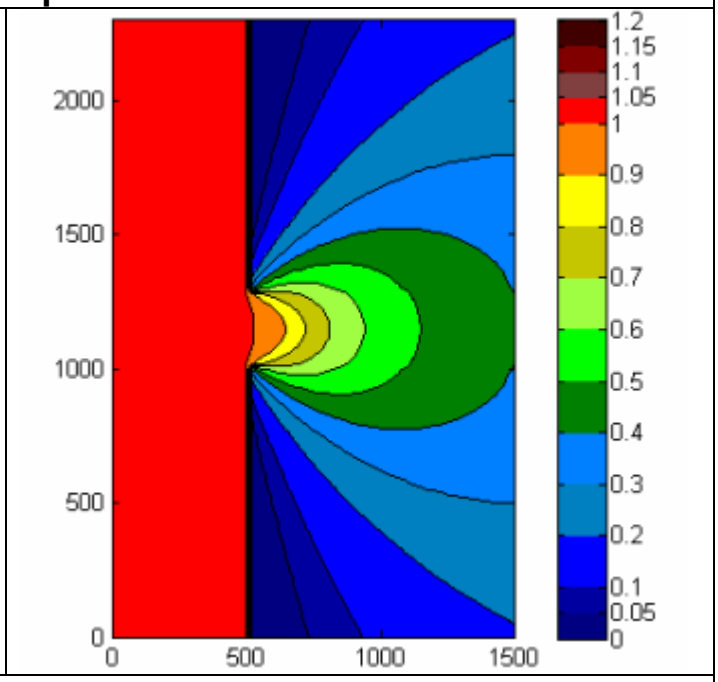
2000
1500
1000
500
0
0
500
1000
1500
1.2
1.15
1.1
1.05
1
0.9
0.8
0.7
0.6
0.5
0.4
0.3
0.2
0.1
0.05
0

4L Gap

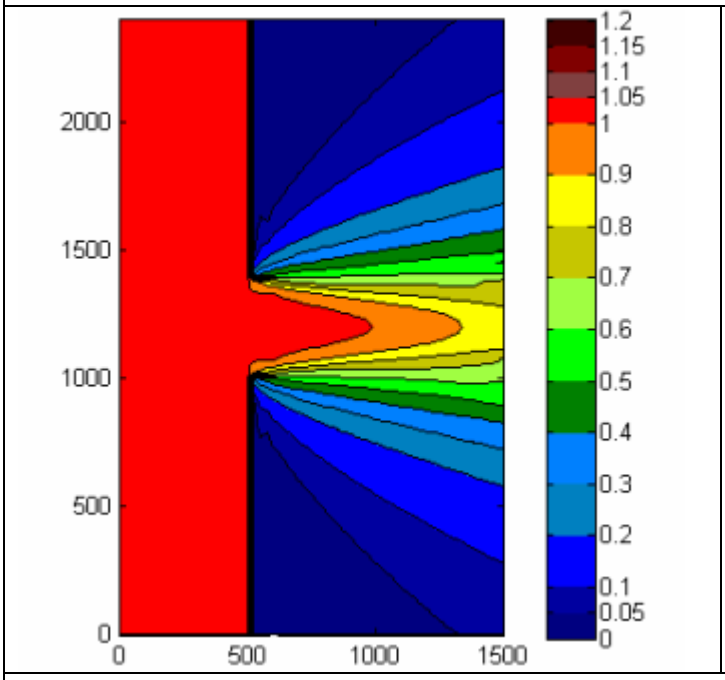
2000
1500
1000
500
0
0
500
1000
1500
1.2
1.15
1.1
1.05
1
0.9
0.8
0.7
0.6
0.5
0.4
0.3
0.2
0.1
0.05
0

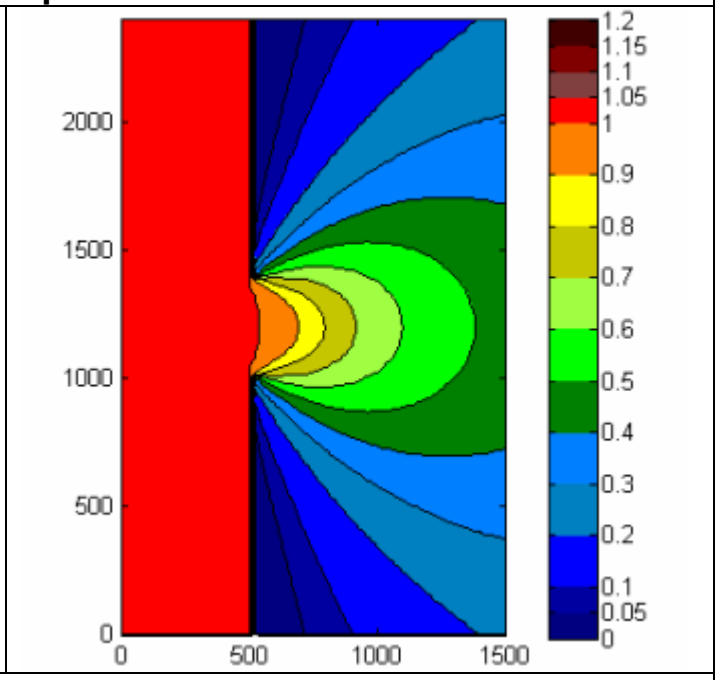
2000
1500
1000
500
0
0
500
1000
1500
1.2
1.15
1.1
1.05
1
0.9
0.8
0.7
0.6
0.5
0.4
0.3
0.2
0.1
0.05
0

5L Gap

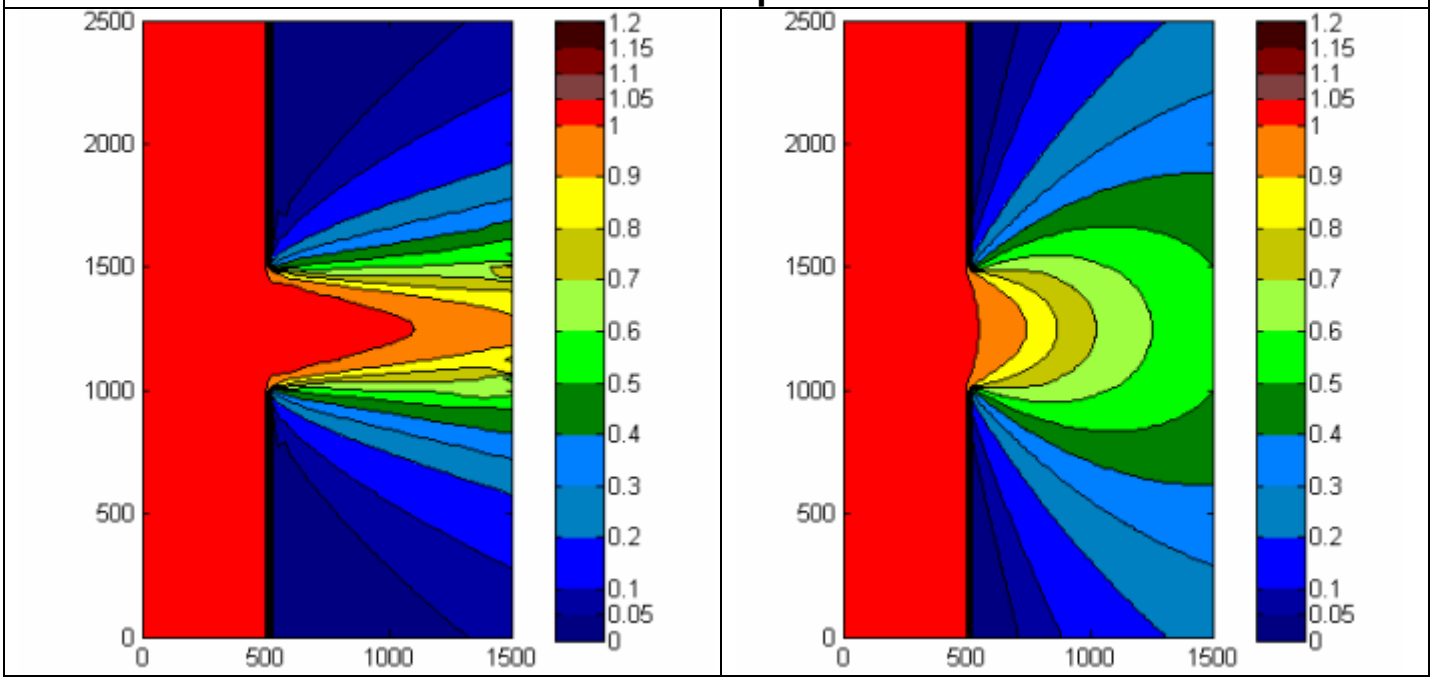
2500
2000
1500
1000
500
0
0
500
1000
1500
1.2
1.15
1.1
1.05
1
0.9
0.8
0.7
0.6
0.5
0.4
0.3
0.2
0.1
0.05
0

APPENDIX F: SWAN Input File

(sample case: Breakwater Gap, B/L = 2, Swell-type waves, 0°, L/Δs = 4)

```
$
$   Template By: ALKYON Hydraulic Consultancy & Research
$
$   Filename: Og2-Ts-D0-R0-G4-N20.SWN
$
$   SWAN input file
$   Date: 2009/06
$

$  Start-up Commands ************************************
$
PROJECT 'diffraction'
       'CASE:  Og2-Ts-D0-R0-G4-N20'
$
SET  LEVEL=  1.00  MAXERR=3
MODE STATIONARY

$  General Commands *************************************

$  Model Discriprion ************************************
$   comp. grid:    xpc      ypc      alpc  xlenc   ylenc    mxc   myc
$                          CIRCLE  mdc  flow  fhigh  msc

CGRID  REGULAR    0  0 0  1500   2200   60   88 &
                           CIRCLE  180   flow=0.04  fhigh=1.0
$   bottom grid:   xpinp      ypinp      alpinp   mxinp   myinp    dxinp     dyinp

INPGRID BOTTOM    0    0     0     1    1   1500   2200
READ BOTTOM  FAC=500 'H1.BOT'  IDLA=3  0  FREE

$   boundary conditions ----------------

BOUNd SHAPespec JONSWAP 10 DSPR DEGRees

$PAR [hs] [per] [dir] [dd]

BOUNdspec  SIDE W &
   CONstant PAR 1 8 0 10

BOUNdspec  SEGMent XY 0 0 499 0 &
   VARiable PAR 499 1 8 0 10
```

```
BOUNdspec  SEGMent XY 0 2200 499 2200 &
   VARiable PAR 499 1 8 0 10

$   obstacle ---------------------------
OBST TRANSM    0   REFL   0   RDIFF 1 LINE   &
  500   -10  &
  500   1000

OBST TRANSM    0   REFL   0   RDIFF 1 LINE   &
  500   1200  &
  500   2210

$   physics ----------------------------

$DIFFRACtion [idiffr] [smpar] [smnum] [cgmod]

DIFFRACtion  1 0 0 1


$   exclusion of processes --------------

OFF QUADrupl
OFF WINDGrowth
OFF WCAPping
OFF BREaking
$OFF REFrac
$OFF FSHift
$OFF BNDCHK

$  accuracy-------------

NUMeric ACCUR drel=0.03 dhoval=0.03 dtoval=0.03 npnts=98. STAT 20

$  Output Commands ************************************
$   write frame/block/table output requests

BLOck 'COMPGRID'  NOHEADer  'Og2-Ts-D0-R0-G4-N20.mat'  LAY-out  idla=3  XP
YP &
DEP HS DIR TM01 TM02 TMM10 DSPR

$PER TM01 TM02 TMM10
$WLEN RTP DIR DSPR  DHSIGN RTM01  DRTM01

$   write table/spectra output requests----------------
```

```
$ test ouput----------

TEST 1 0 &
POINTS XY &
        300.00    300.00 &
        300.00    900.00 &
        300.00    1200.00 &
        300.00    1500.00 &
        1000.00    300.00 &
        1000.00    900.00 &
        1000.00    1200.00 &
        1000.00    1500.00 &
PAR 'Og2-Ts-D0-R0-G4-N20.par' &
S1D 'Og2-Ts-D0-R0-G4-N20.s1d'

$  Compute and stop Commands ******************************
COMPUTE


STOP
```